High resolution Palaeoclimatology of the Holocene Sub Polar North Atlantic

Kathryn Rebecca Miller

Submitted for the Degree of Doctor of Philosophy

University of East Anglia

School of Environmental Sciences

August 2009

Abstract

A high resolution multiproxy investigation of two marine cores from the Gardar Drift in the Sub Polar North Atlantic, cores MD99-2251 and MD99-2252 has been undertaken to examine the extent of Holocene climate variability reflected by changes in diatom floral abundances and ice rafted debris flux. The results from this study provide both an overview of climate variability for the entire Holocene as recorded in the Sub Polar North Atlantic and a detailed high resolution study focussed around the 8.2kyr event. Sea surface temperature (SST) estimates are derived using a weighted average partial least squares (WAPLS) transfer function and a new regionally based diatom transfer function developed as part of this study. Principal component analysis and K-means cluster analysis were undertaken on core MD99-2251 to identify floral groupings within the diatom taxa. The changing composition of diatom assemblages and SST records indicate a highly unstable early Holocene from 11.5 to 9.5kyr with switches in the dominance of cool Sub Arctic floras and warmer North Atlantic floras. The presence of high productivity events in the diatom floras during this interval suggests that the core locations were, at times, in close proximity of the Sub Arctic Front. A broad SST cooling from 9.5 to 7kyr is identified followed by a pronounced warming for 7 to 5kyr and more stable but cooler temperatures during the Late Holocene. Changes in sea surface hydrography, especially the relative strength of the warm Irminger Current, is considered to have had the greatest influence on the composition of diatom floral assemblages. The 8.2kyr event is not recognised as a discrete climate perturbation in either the diatom assemblage data or the IRD record, but is contained within the broad cooling event from 9.5-7kyr. Analysis of sea-ice and cold water flora however does indicate some increase in these species for the interval 8.8 to 7.8kyr.

Acknowledgments

Firstly heartfelt thanks to Mark Chapman for all his patient help, guidance and support for the duration of this PhD. Thanks also to Nalan Koç for all her expertise and generous hospitality, especially during my visits to Tromso and to Julian Andrews for input and encouragement,

I would like to acknowledge fellow scientists from the Norwegian Polar Institute and University of Tromso and the crew of the RV Lance cruise August 2006 for their friendship and good company at sea and hospitality during my stays in Tromso. Thanks also to the diatomists at University College London for their instruction, Geraldine Reid at the Natural History Museum, Ros Boar and Keith Clarke for their generous and patient assistance with taxonomic literature. Karen Haywood for her instruction in oceanography, Hannah Mossman for assistance with ecological statistics and the technicians in the School of Environmental Sciences for continuing their help and support.

To those who walked this path before me, especially Liz, Terry and Sarah. Thank you for your forbearance and faith. To good companions on the way, especially Jenny, James and Tammy, thank you for your company. Not least, my love and thanks to my husband Bill and my children Beth, Jessica and Ethan for patience especially at my absences, for their encouragement and inspiration.

This project was supported by a NERC studentship at the University of East Anglia, School of Environmental Science as part of the RAPID programme.

Contents

List of Figures

List of Tables

Section One

Introduction

Chapter One

Introduction

"*With unspeakable labour the eye of man has forced its way gradually towards the north, over mountains and forests, and tundra onward through the mists along the vacant shores of the polar seas...*"

Fridtjof Nansen 'In Northern Mists'

Chapter One: Introduction

1.1 Introduction

Interglacial climates such as the Holocene have long been considered to be more stable than glacial climates. However more recent studies have indicated that the Holocene has been subject to considerable variability if less pronounced than that of glacial climates. Mayewski *et al.*(2004) examining around fifty Holocene palaeoclimate records recognise six period of significant rapid climate change for the Holocene (Figure 1.1). These intervals of rapid climate change are recognisable in both marine and terrestrial records. Various studies have sought to define the nature and causality of these Holocene fluctuations and whether any cyclicites may be observed.

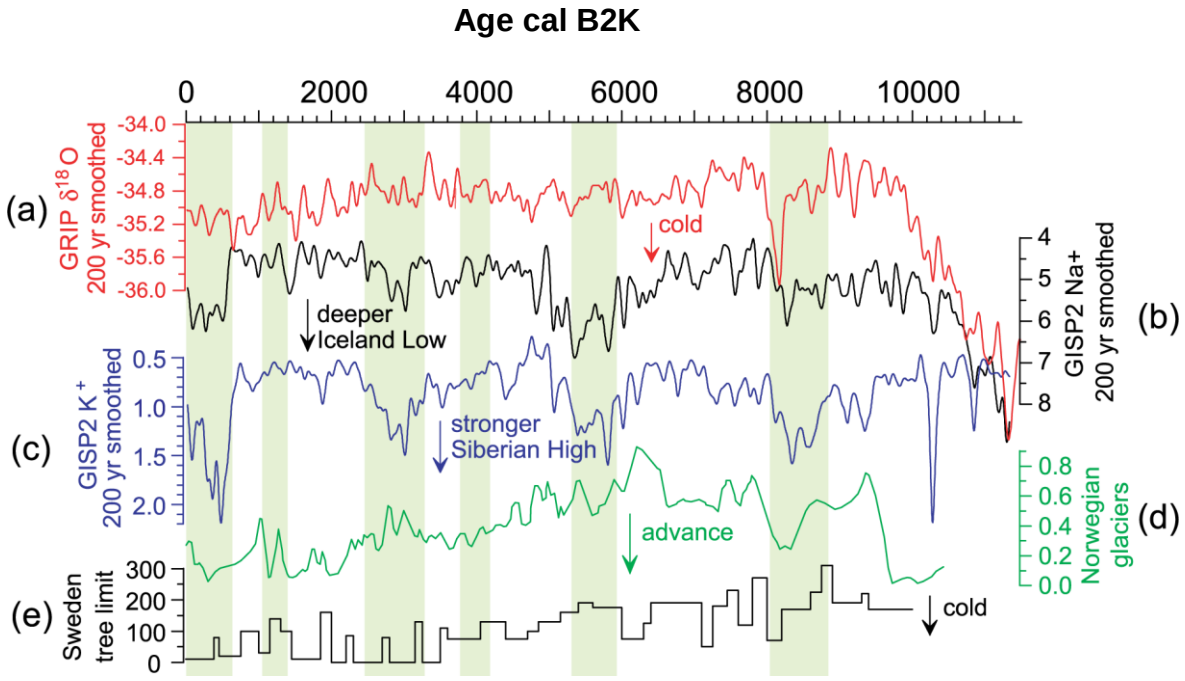

Figure 1.1 Palaeoclimate records indicating Holocene climate variability. a) Gaussian smoothed (200 yr) GRIP $\delta^{18}O$ (‰) proxy for temperature (Johnsen *et al.*, 1992). b) Gaussian smoothed (200 yr) GISP2 sodium Na+ ppb ion proxy for the Icelandic low (Mayewski *et al.*, 1997; Meeker & Mayewski, 2002). c) Gaussian smoothed (200 yr) GISP2 potassium K^+ ppb ion proxy for the Siberian High (Mayewski et al., 1997; Meeker & Mayewski, 2002). d) Norwegian glacier advance (Nesje *et al.*, 2001). e) Treeline limit shifts in Sweden (Karlén & Kuylenstrierna, 1996) The green boxes indicate six intervals of Holocene rapid climate change recognised in this multiproxy review of Holocene climate variability (Mayewski *et*

Particular attention has been given to the 8.2kyr event, the largest climate perturbation during the Holocene. This perturbation has been recognised in a wide range of palaeoclimate records (Rea *et al.*, 1994; Keigwin & Jones, 1995; Lamb *et al.*, 1995; Hughen *et al.*,1996; Alley *et al.*, 1997; Bond *et al.*, 1997; Kleiven *et al.*, 2008). The exact timing of this event however varies between records. Ellison *et al.* (2006) recognise a two stage event at 8490 and 8290 years ago. Rohling & Palike (2005) observe that where the 8.2kyr event is recognised in the North Atlantic it is present with a more broad cooling occurring around 8.6 to 8.0kyr (Figure 1.2).

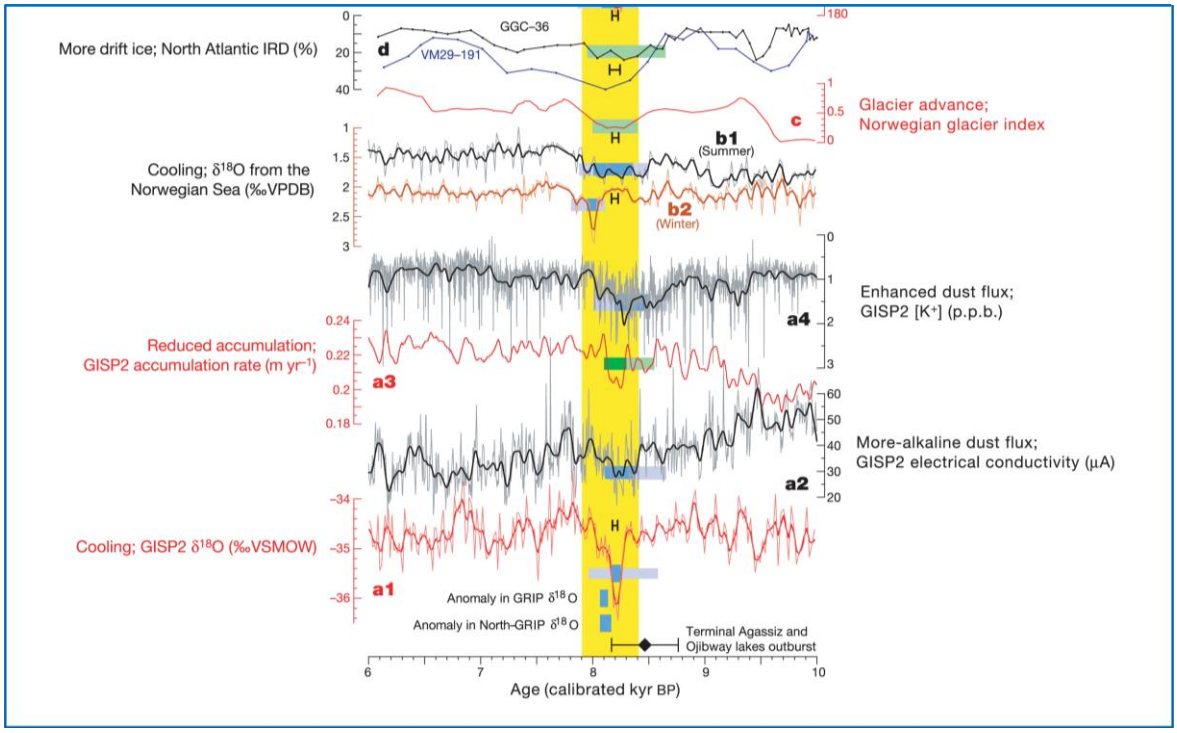

Figure 1.2 Collection of well-dated climate proxy records used to identify anomalies around 8.2 kyr BP indicating a braod cooling form 8.6-8.0kyr may better describe the '8.2kyr event' in North Atlantic palaeoproxies. All smoothed records shown are based on a 50-yr moving gaussian filter. Coloured blocks identify the anomalies recognized in the various records: blue is statistically significant in digital records; green is visually identified in digital records; brown is estimated from published graphs. Heavy coloured blocks indicate peak events; lighter blocks highlight broader anomalies. The yellow band marks an interval spanning three conspicuous maxima in 14C production. The black diamond with error bar alongside the age axis indicates the best age estimate for the meltwater flood from lakes Agassiz and Ojibway **a1** ice-δ^{18}O series45 (GISP2), **a2** electrical conductivity series13,14 (GISP2), **a3** is a 50-yr smoothing of the ice-accumulation data set46 (GISP2) **a4** GISP2 potassium ion series **b1** δ18O of right-coiling *Neogloboquadrina pachyderma*, **b2** δ^{18}O of left-coiling *N. pachyderma*. **c** Norwegian glacier expansion index based on glacial lake cores investigated at a resolution better than 50 yr **d** IRD percentages in North Atlantic sediment cores VM29-191 (548 N, 158 E) & GGC-36 (458 N, 458 E). (Rohling & Palike, 2005).

Various palaeoceanographic proxies have been employed to define this Holocene climate variability within North Atlantic marine cores. These proxies determine past changes in both North Atlantic deep water circulation, especially the pattern of deep water flow and strength of the meridional overturning circulation, and surface conditions, particularly variations in sea surface temperature. Proxies include grain size analysis, sediment lightness, stable isotope and alkenone studies, the relative abundance analysis of zooplankton and phytoplankton communities (Bianchi & McCave, 1999; Oppo *et al*., 2003; Risebrobakken *et al.*, 2003; Hall *et al.*, 2004; Bendle & Rosell-Mele, 2007). In addition patterns of drift ice and past global ice volumes have been used to reconstruct wide scale variations in Holocene climate (Bond *et al*., 1997) (Figure 1.3).

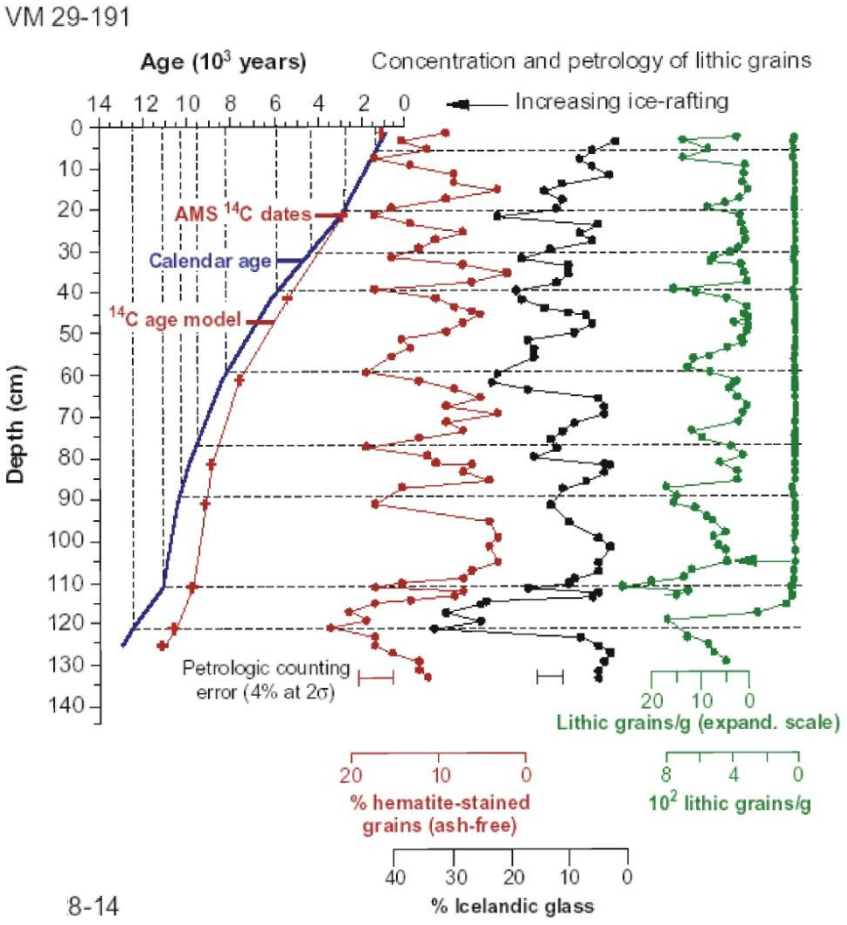

Figure 1.3 Holocene Ice rafted debris flux in North Atlantic in marine core VM 29-191 (54° 16´ N 16° 47´ W) indicating cycles in Holocene ice drift input. Bond *et al*. (1997)

1.2 Research Aims

This study consists of a high resolution multiproxy study of two Holocene marine cores from the Gardar Drift in the Sub Polar North Atlantic; cores MD99-2251 and MD99-2252 (Figure 1.4). The study presents both an overview of climate variability for the entire Holocene as recorded in the Sub Polar North Atlantic and a detailed high resolution study around the 8.2kyr event. Diatom assemblage data, ice rafted debris counts and stable isotope analyses of planktonic foraminifera are used to reconstruct.sea surface temperatures, palaeocurrent patterns and drift ice patterns over the core sites.

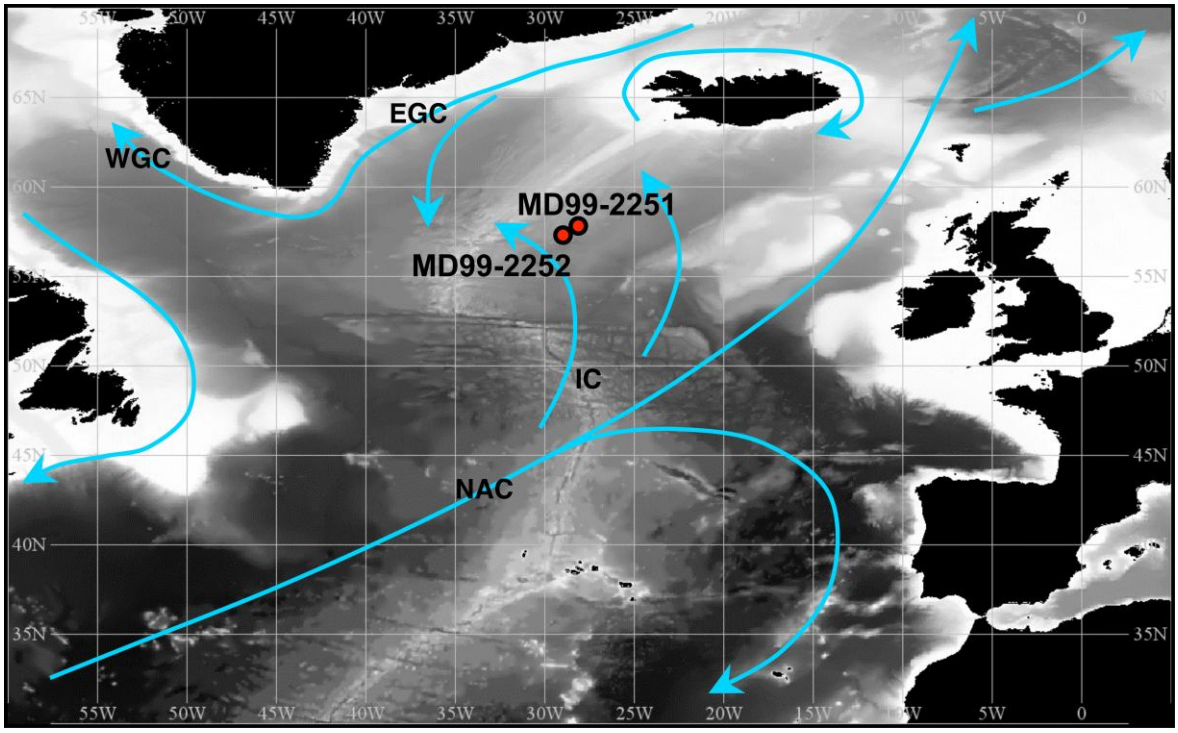

Figure 1.4 The location of cores MD99-2251 and MD99-2252 and the major surface currents influencing the core sites. NAC North Atlantic Current, IC Irminger Current, EGC East Greenland Current and WGC West Greenland Current

The Gardar Drift sites were chosen because of their high sedimentation rates which allow for high resolution sampling of the sores. Sedimentation rates for the Gardar drift at typically 10-20cm ka^{-1} but reaching maximum rate in excess of 100 cm ka^{-1}. Holocene

sedimentation rates are recorded as 5- 40cm ka^{-1} (Bianchii & McCave, 2000). Marine core MD99-2251 was sampled at decadal resolution from 7.8-8.8kyr to attempt to resolve the 8.2kyr event and at approximately every 250 years for the remainder of the Holocene. Marine core MD99-2252 was sampled at a mean resolution of 180 years per sample. In addition to being a site of high sedimentation, the Gardar drift lies under the Irminger current, a branch of the North Atlantic Current, an important component of the thermohaline circulation of the oceans and so of key importance to our understanding of ocean circulation.

Previous analyses of planktonic foraminifera from marine core MD99-2251 (Ellison *et al.*, 2006) show a relatively stable Holocene (Figure 1.5). Planktonic foraminifera derived sea surface temperatures (SSTs) are stable for most of the Holocene apart from the around the 8.2kyr event. Similarly percentage abundances of *N.pachyderma* sinistral which may be used as a proxy for temperature, are stable apart from the around the 8.2kyr event where a two stage event at 8490 and 8290 years ago is recognised (Figure 1.6)

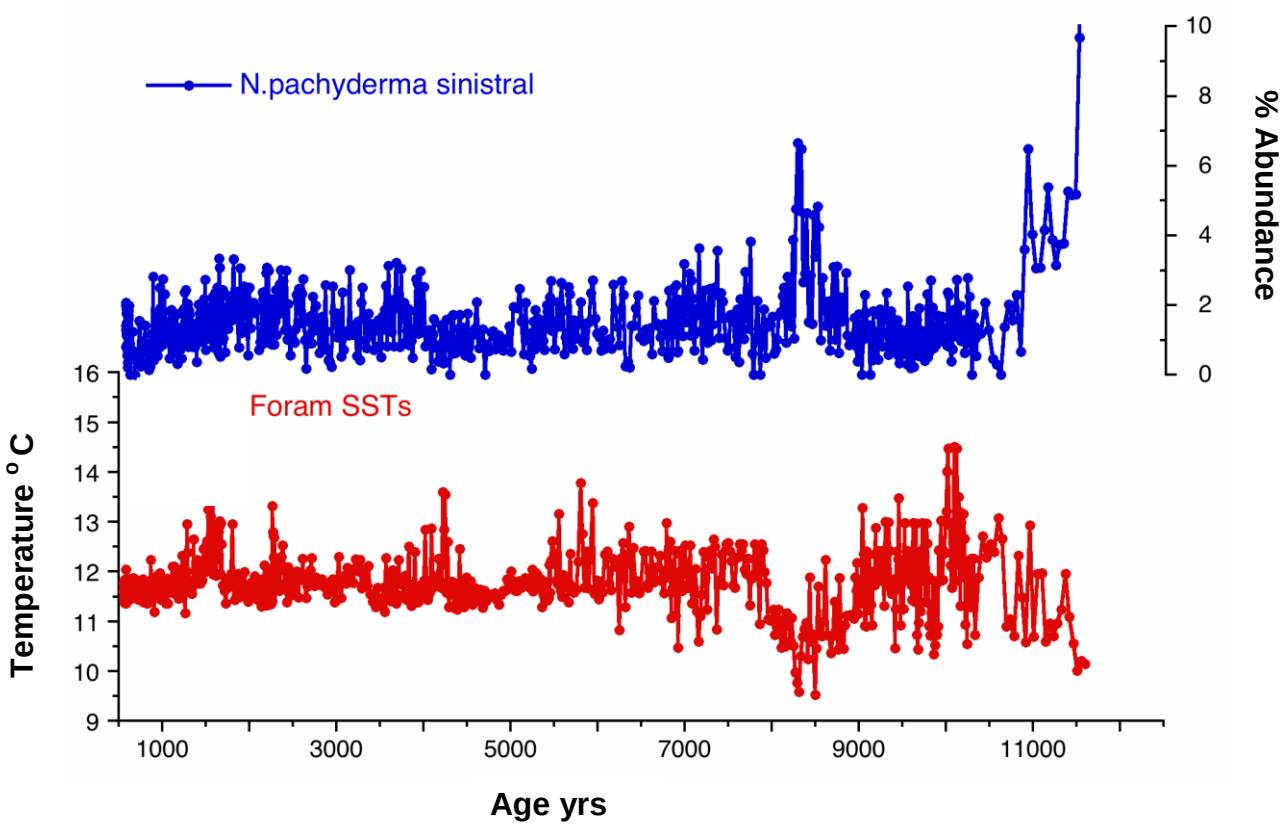

Figure 1.5 Planktonic foraminifera generated SSTs and percentage abundance of the planktonic foraminifera *N.pachyderma* sinistral in marine core MD99-2251 (Ellison *et al.*,2006).

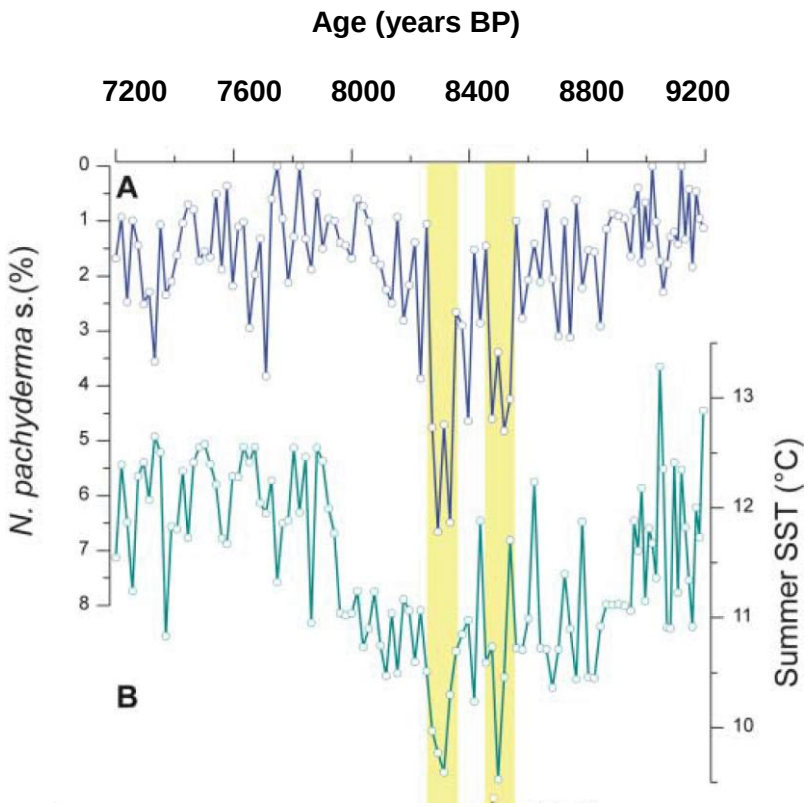

Figure 1.6 Percentage abundance of the planktonic foraminifera *N.pachyderma* and planktonic foraminifera generated SSTs for marine core MD99-2251 indicating a recognise a two stage event around 8200 years BP at 8490 and 8290 years BP. The events are characterised by decrease in SSTs and increase in the percentage abundance of *N.pachyderma* sinistral (Ellison *et al.*,2006)

Diatom flora show a higher diversity of species in high latitudes than planktonic foraminifera, which at low temperatures become dominated by the form *N.pachyderma* sinistral. Species abundance counts of diatom flora were undertaken in this study to determine whether the down core percentage abundance distribution of diatom floral assemblages better resolve the Holocene sea surface temperatures and the palaeoceanography of the Sub Polar North Atlantic. High resolution counts of diatom flora and ice rafted debris abundances were made from 7.8-8.8 kyr to determine if these two palaeoproxies support the idea of a single 8.2kyr event or a broad cooling

Core MD99-2251 (57°26.87' 027°54.47') extends for the entire Holocene and is sampled at decadal resolution for the 8.2kyr event and at least every 250yrs for the remainder of the Holocene. Core MD99-2252 (57°26.84' 027°55.83') provides a record of the last 7200yrs (perhaps 7.2kyr is more consistent) and is sampled at intervals of approximately every 180yr. Both cores are analysed for relative abundance of diatom floras, sea surface temperatures are reconstructed using a transfer function and variations in the distribution of different floral assemblages are assessed. Prinicpal compnent analysis and K-means cluster analysis are undertaken downcore for MD99-2251 and groupings compared with those identified in the published literature. A new regionally based diatom transfer function is developed. In addition, core MD99-2251 is analysed for ice rafted debris input for the high resolution 8.2kyr study and core MD99-2252 for stable isotope analysis of planktonic foraminifera. The study attempts to address a number of research questions.

Research questions

- Do sea surface temperature (SST) reconstructions from diatom abundance counts show a relatively stable Holocene or a more diverse temperatureregime?
- Are the same trends reflected in diatom generated SSTs as in foraminifera generated SSTs and if not, why not?
- Can diatom floral assemblages be used to reconstruct paleocurrent patterns for the Holocene?
- Is the 8.2kyr event recorded in the diatom flora and the ice rafted debris record of the Gardar Drift?
- If the 8.2kyr event is recorded in these proxies, is it seen as a single event or a broad cooling?
- Are these variations found in the diatom flora and ice rafted debris abundances replicated on a regional scale?

1.3 Thesis Structure

The first section of the thesis explores the scientific background to this study. Chapters two and three explore the oceanography and the palaeoceanography of the northern North Atlantic as the setting for the study sites. Chapter two includes an examination of the contemporary ocean floor topography, water masses and currents of the region. Chapter three reviews variations in North Atlantic deep, intermediate and surface water during the Holocene and possible mechanisms proposed for this variability. Chapter four examines ecology of marine planktonic diatoms with particular reference to the taxa considered in this study, those taxa are listed.

The second section of the thesis consists of an examination of the palaeoproxies employed in this study and the results of those analyses. Chapter five reviews the core site, the age models employed and the sampling techniques adopted. In Chapter six the main methodologies for sample preparation and diatom abundance counting are presented as well as the results of diatom abundance counts for cores MD99-2251 and MD99-2252, including the high resolution 8.2kyr study. Chapter six also presents the results of the transfer function generated sea surface temperatures, diatom assemblage data and down ycore multivariant analyses of species groupings found within the data. The stable isotope data for MD99-2252 is also presented in this chapter. Chapter seven explores the development of a new regionally based diatom transfer function using new core top diatom assemblage counts and previously published data (Jiang *et al.* 2001). Chapter eight reviews the use of ice rafted debris (IRD) abundance as a palaeoproxy and presents the IRD data for the high resolution 8.2kyr study.

The third section of the thesis consists of discussions and conclusion. A discussion of the key findings of this study and an examination of their wider significance occurs in Chapter nine. Conclusions are presented in Chapter ten. A bibliography, diatom plates and the raw data counts are included as appendicies. There are two appendices. Appendix one outlines the biology of diatom, frustule morphology and terminology. Appendix two consists of the rationale for the systematic adopted in this study and taxonomic descriptions of each of the species.

Chapter Two

The Oceanography of the Sub Polar North Atlantic

" Among our scientific pursuits may also be mentioned the determining of the temperature of the water and the degree of saltness at varying depth..."

Fridtjof Nansen 'Farthest North'

Chapter Two: The Oceanography of the Sub Polar North Atlantic

2.1 Introduction

The core sites in this study lie in the Icelandic basin in the northern North Atlantic. In this chapter there will be an overview of the importance of the northern North Atlantic to our understanding of the global thermohaline circulation, a study of the ocean floor topography of the northern North Atlantic emphasising the effect ofthat topography on the thermohaline circulation and a review of the main water masses and surface currents effecting the core sites. These water masses include Sub Polar mode water, North Atlantic deep water, Denmark Straits overflow water, Iceland Scotland overflow water and Labrador sea water. The key currents influencing the core sites that are considered are the North Atlantic current, the Irminger current and the East Greenland current.

2.1.1The global thermohaline circulation

The core sites in this study lie in the Icelandic basin. The northern North Atlantic is an area of fundamental importance to our understanding of ocean circulation as it is the region where North Atlantic Deep Water (NADW) is formed, a driver in the thermohaline circulation of the oceans. Broecker (1987) first suggested the concept of the ‘thermohaline conveyor belt’ (Figure 2.1). The thermohaline circulation of the oceans is forced by density differences caused by changes in temperature and salinity. These changes in temperature and salinity are the result of differences in surface heating and cooling, geothermal heating and freshwater flux. Salinity is enhanced by evaporation and the formation of sea-ice and decreased by ice-melt, runoff and precipitation.

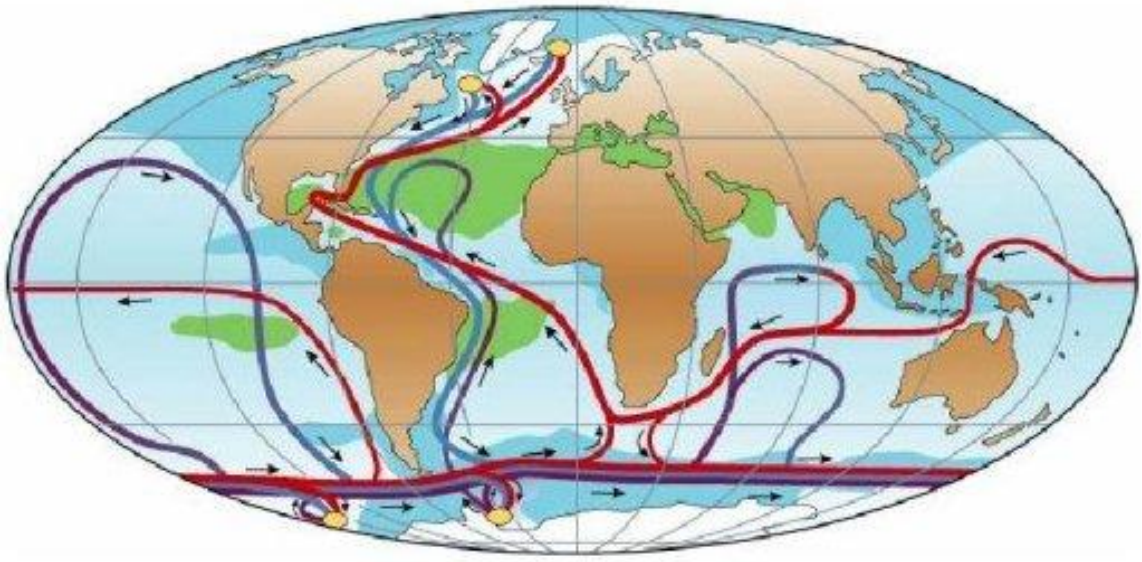

Figure 2.1 Global Thermohaline Circulation. Indicating surface, deep and bottom currents, salinity and locations of deep water formation. After Rahmstorf (2002)

Salinity > 36‰ Surface
Salinity < 34‰ Deep
Deep Water Formation Bottom

2.2 Ocean Floor Topography

The ocean floor topography of the Sub Polar North Atlantic is an important control of ocean circulation, especially as if effects the formation and flow of both deep and bottom waters. Deep water formation occurs in the North Atlantic as a result of both topographic and oceanographic reasons (Brown *et al.*, 2001). The semi enclosed Nordic Seas allow water to accumulate at depth behind the sill of the Greenland-Scotland ridge. It is important to note however that deep water also forms in the Labrador Sea where there are no such topographic constraints and therefore topographic features should not be considered the only significant factor in the formation of deep waters. In order for deep water to form the water column must become unstable due to increased surface densities from cooling and or increased salinity. An increase in surface densities occurs in the northern North Atlantic, Nordic and Labrador Seas due to intense cooling from to the passage of winter storms and the input of warm more saline water from lower latitudes.

The principle feature of the Atlantic Ocean floor is the Mid-Atlantic ridge running north-south approximately midway between the continental margins. The Mid-Atlantic ridge is flanked on either side by the abyssal plains. These in turn are broken up by transverse ridges, (those running perpendicular to the Mid-Ocean ridge), plateaus, hills and seamounts. At the margins of the abyssal plains the escarpments of the continent slope rise to the continental shelf. In the Sub Polar North Atlantic the extension of the Mid-Atlantic Ridge north of the Charlie-Gibbs Fracture Zone and south of Iceland is referred to as the Reykjanes Ridge (Figure 2.2). Litvin (1980) describes the variation in morphology of the Reykjanes ridge along its length. To the north, adjacent to Iceland, the ridge is narrower with steep scarp slopes 600-650m high. The top of the ridge lies at a depth of 900-100m below sea level and is crested by peaks and seamounts. There is no distinct median valley, but deep linear depressions. South of 60^{o} latitude the ridge becomes wider, develops a wider rift zone and south of 58^{o} latitude a distinct median valley. The base of this valley lies at 2500-2900m and the crests at 1600-1800m depth. There are small displacements of the ridge and transverse depressions at 57^{o} and 55^{o}N. The margins of the ridge lie at 220-2800m depth in this southern region. The Reykjanes Ridge divides the sea floor into the Iceland and Irminger Basins.

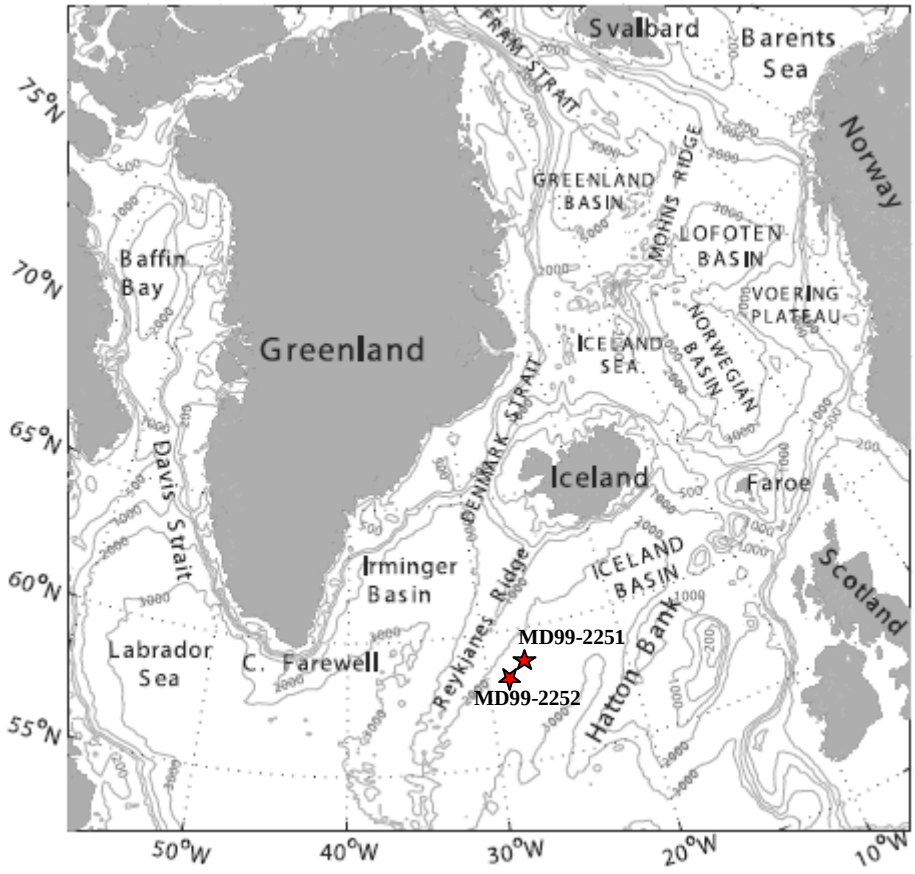

Figure 2.2 Bathymetry of the Sub Polar North Atlantic region. 200, 500, 1000, 2000, and 3000 m isobaths are shown. After Jakobsen *et al.* (2003)

The predominant transverse ridge in the Sub Polar North Atlantic is the Greenland-Iceland-Faeroe-Scotland ridge (Figure 2.3) which extends from the Denmark Strait to the Scottish shelf and divides the Sub Polar North Atlantic from the Nordic Seas. The ridge is 4000km long and, at its widest point on the Iceland plateau, 1500km wide. It may be divided into six distinct regions; the Denmark Straits, the Icelandic Plateau, the Iceland-Faeroe Ridge, the Faeroe Islands, the Faeroe Bank Channel and the submarine banks and ridges lying southwest of the Faeroe Bank Channel (Nilsen, 1983). Of most importance to the circulation of the Sub Polar North Atlantic are the regions of the ridge that allow flow between the Nordic Seas and the North Atlantic, specifically the Denmark Straits, the Iceland-Faeroe Ridge and the Faeroe Bank Channel. The Denmark Strait is 110km wide and at its deepest point, 620m deep. It has a thick layer of sediments at its base derived both from the Greenland shelf and deposition from the deep water flow through the straits from the Nordic Seas. The Iceland-Faeroe Ridge is flat topped feature with a maximum depth of approximately 500m (Wright, 1998). Sediment deposition is thin over the ridge

but increases on the margins towards Iceland and the Faeroe Islands. The Faeroe Bank Channel is the deepest part of the Greenland-Scotland ridge, reaching a maximum depth of 1200m. It has around 400m of sediment at its base.

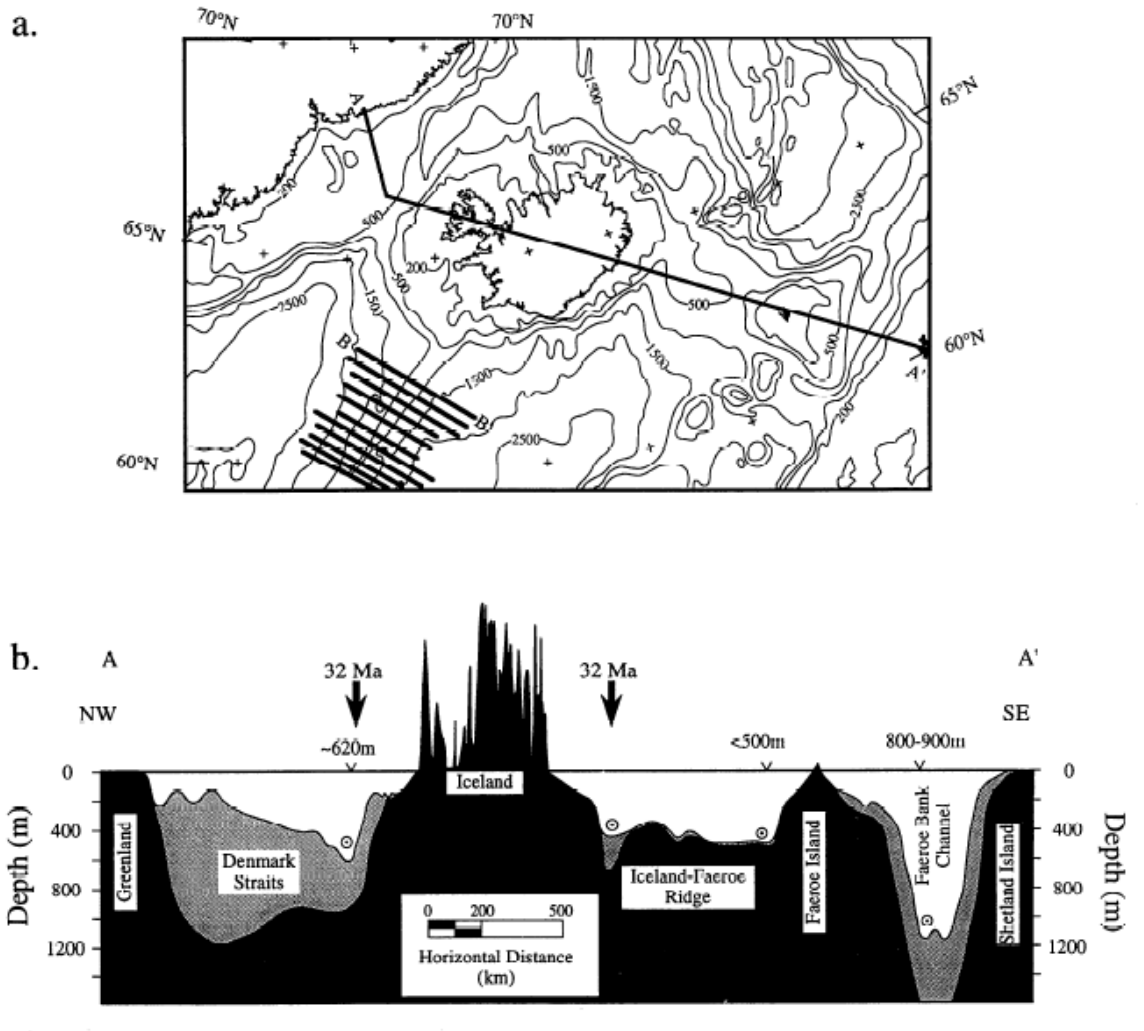

Figure 2.3 a) Bathymetry of the Greenland-Scotland ridge. 200 and 500m contours shown then every subsequent 500m. b) Cross section through the Greenland-Scotland ridge. Sediment coverage is shown in shaded grey. After Wright & Miller (1996)

)

Recent studies (Kuijpers *et al.*, 2003; Belan, *et al.*, 2004; Kristoffersen *et al.*, 2004; Kuijpers & Werner 2007) have emphasised the role of deep-draft icebergs in scouring the seabed and maintaining the flow through these channels. Deep-draft icebergs leave a characteristic scour on sea bed sediments, referred to as an iceberg plough mark (IPM). At the southeast Greenland margin IPMs were found to 700m depth and immediately south of the Davis Strait at 800m and 850m on the northeastern Faeroe margin.

The Greenland- Scotland ridge acts as a barrier between water masses at depth. A cross section of the Greenland-Scotland ridge (Figure 2.4) indicates the temperatures and salinity differentials. To the south of the ridge the temperatures and salinities are high; temperatures are in excess of 5^{o}C and salinities are in excess of 35 psu to depths of great than 1000m, except in a narrow layer adjacent to the ridge where overflow waters affect temperature and salinities. To the north of the ridge temperatures and salinities are low. Intermediate and deep water have temperatures that are less than 0 ^{o}C and salinities in the region of 34.9 psu (Hansen & Osterhus, 2000).

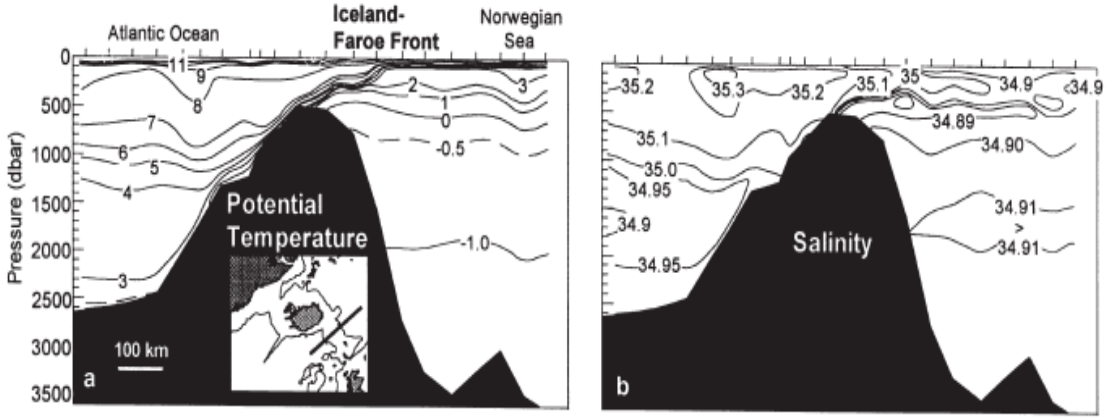

Figure 2.4 Potential a)Temperature and b) Salinity across the Scotland Iceland Ridge. The location of the cross section is indicated on the insert map. After Hansen & Osterhus (2000)

2.3 The Water Masses of the Sub Polar North Atlantic

Water masses are bodies of water that may be defined by identifiable conservative chemical and physical properties such as temperature and salinity (Table 2.). Conservative properties are those which only change at the boundaries of the water mass. Water masses may further be divided into surface, intermediate and deep water masses depending on their position in the water column. One of the complications inherent in discussing the water masses of the subpolar North Atlantic is that a plethora of names have been used to describe these different bodies of water. Where relevant therefore, alternative names are also noted in this discussion.

	Potential Temperature ^{o}C	Salinity psu
Sub Polar Mode Water (SPMW)	8[1]	35.23[1]
North Atlantic Deep Water (NADW)	2-3.5[4]	34.88-34.98[4]
Denmark Straits Overflow Water (DSOW)	0.4-2[3] < 1.5[4]	34.8-34.9[3] ~34.9[4]
Iceland Scotland Overflow Water (ISOW)	2.42[1] 2-3[2] 1.8-3.5[4]	35.00[1] below 34.90[2] ~34.92[4]
Labrador Sea Water (LSW)	3.4[1]	34.885[1]

Table 2.1. A summary of the temperature and salinity properties of the water masses considered in this study .(van Aken & deBoer, 1995[1]; Hansen & Osterhus, 2000[2]; Maurtizen, 1996 [3]; Hunter *et al.*, 2007 [4]).

2.3.1 Sub Polar Mode Water

Water of Atlantic origin in the subpolar North Atlantic has been variously described by different authors as North Atlantic Central Water (NACW) eg Ruddick *et al.*, (1997), Eastern North Atlantic Water (ENAW) eg Harvey (1982), North-East Atlantic Water (NEAW) eg Stocker *et al.*,(1998), Modified North Atlantic Water (MNAW), eg Martin (1986), Hansen & Osterhus (2000) and Sub Polar Mode Water (SPMW) eg McCartney & Talley (1996), Bersch *et al.*,(1999). While these definitions vary slightly; Hansen & Osterhus, (2000) do not for example recognise SPMW as synonymous with MNAW as SPMW includes Labrador Sea Water (LSW). Broadly speaking all these definitions refer to the properties of deep waters of Atlantic origin just prior to it crossing the Greenland-Scotland ridge. The term Sub Polar Mode Water (SPMW) is adopted in this study as it represents the most recent research into the properties and origins of this water (Brambilla *et al.*, 2008; Brambilla & Talley, 2008).

Mode waters are near surface water masses with near uniform properties of density salinity and temperature. Subpolar Mode Water (SPMW) was first described by McCartney & Talley (1982) and later modified by Talley (1999) and Read (2001). SPMW lies between the ocean surface and the permanent pycnocline and has representative potential densities of 27.3-27.5 kmg $^{-3}$. SPMW is significant in the transfer of warm salty

North Atlantic water from the subtropical gyre to the Labrador and Nordic Seas. SPMW is formed during late winter convection. It increases in density due to cooling and transforms into Labrador Sea Water and the dense water masses of the Nordic Seas. Thus SPMW forms the upper limb of the meridional overturning circulation and contributes to the waters that become North Atlantic Deep Water (NADW). SPMW is found in several branches of the North Atlantic Current (NAC) in the eastern subpolar gyre, being recognised by its characteristic density (Brambilla *et al.*, 2008; Brambilla & Talley, 2008). SPMW is also thought to be important in its possible influence on global atmospheric circulation as it represents a large near surface heat source (Hanawa & Talley, 2001).

2.3.2 North Atlantic Deep Water (NADW)

NADW is an important component of the thermohaline circulation of the oceans. The thermohaline circulation is driven by inputs of cold dense water in high latitudes: NADW and Antarctic Bottom Water (AABW) (Dickson & Brown, 1994). Various theories have been expounded as to the origin and transport of NADW. Early studies of the origins and transport of NADW (Worthington, 1970; Swift *et al.*, 1980; McCartney & Talley, 1982; Aargaard *et al.*, 1985b) proposed that warm North Atlantic water becomes cooler and denser in the Greenland and Iceland Seas by atmospheric heat loss, mixing of intermediate water masses, vertical overturning and the formation and melting of sea ice resulting in deep convection. These processes were considered to be the principal means of formation for NADW. There were various objections to these scenarios including the fact that more dense water overflowed the Greenland-Scotland Ridge than was formed in the Greenland and Iceland Seas. Mauritzen (1996a) proposed that the Norwegian Atlantic Current becomes increasingly dense due to atmospheric heat loss and that deep water is transported at shallow and intermediate depths along the boundary currents of the Greenland and Iceland Seas.

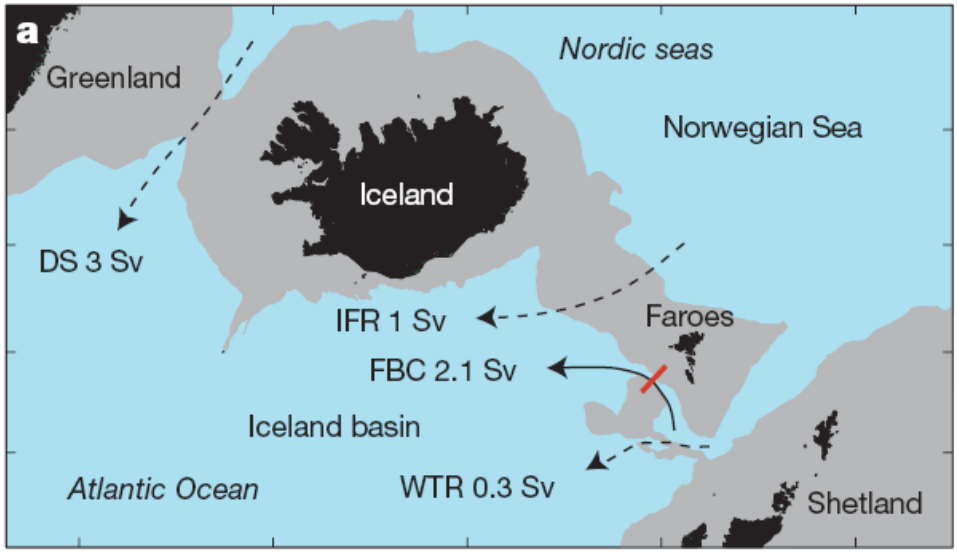

Figure 2.5 Greenland-Scotland Ridge Overflows Denmark Straits (DS), Iceland-Faroe Ridge (IFR), Faroe Bank Channel (FBC), Wyville-Thomson Ridge (WTR). After Olsen *et al.*, (2008)

Dickson & Brown (1994) identified four main constituents to NADW: Denmark Straits Overflow Water (DSOW), Iceland Scotland Overflow Water (ISOW), Labrador Sea Water (LSW) and Antarctic Bottom Water (AABW) also known (McCartney, 1992) as Lower Deep Water (LDW). Of these, the overflow waters across the Greenland-Scotland Ridge DSOW and ISOW (as well as, to a lesser extent, the small overflow of water which passes through the Faroe-Shetland Channel and flows over the Wyville-Thomson Ridge), make up the majority of NADW (Hansen & Osterhus, 2000). Figure 2.5 shows the quantities of water contributing to each of these overflows.

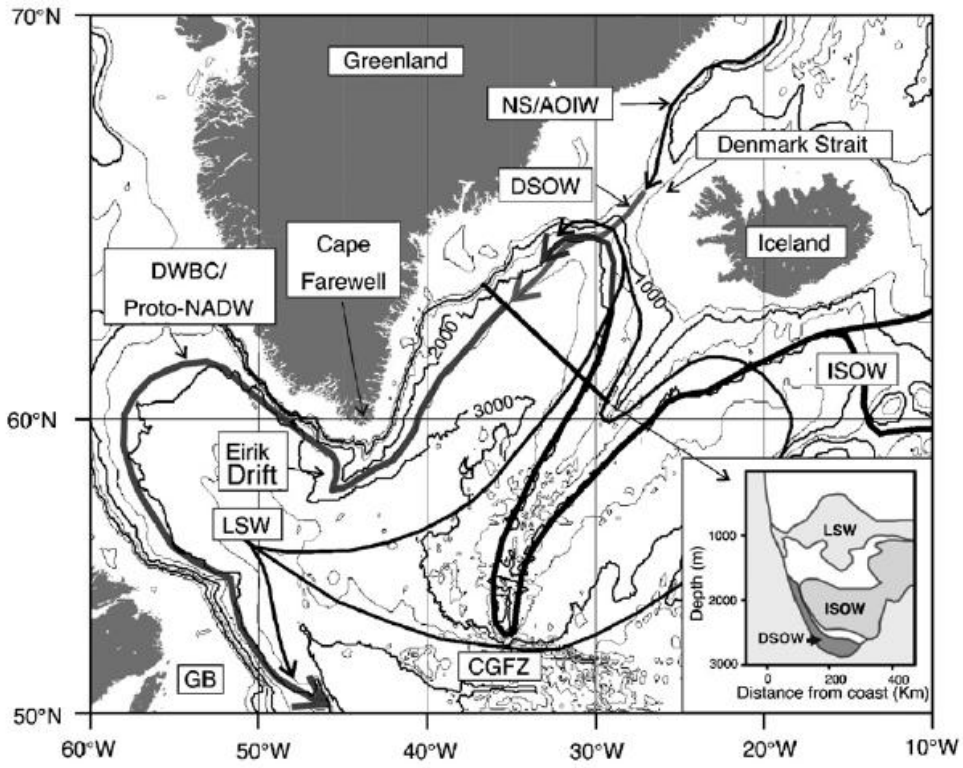

Figure 2.6 The pathways of DSOW and ISOW through the Iceland and Irminger Basins and the entrainment of LSW as part of the formation of NADW. After Hunter *et al*. (2007). Norwegian Sea/Arctic Ocean Intermediate Water (NS/AOIW), Deep Western Boundary Current (DWBC).

After crossing the Greenland Iceland Scotland Ridge, DSOW and ISOW sink and follow pathways defined by the ocean floor topography to join the Deep Western Boundary Current (DWBC) (Figure 2.6) (Hunter *et al.*, 2007). As they pass through the Iceland and Irminger basins they then entrain LSW and Antarctic Bottom Water (AABW). The DWBC is therefore carrying DSOW, ISOW, LSW and AABW when it reaches southern Greenland. This water is considered to be nearly mature NADW (Hunter *et al.*,2007). This proto NADW found off Cape Farewell is also sometimes referred to as lower NADW (Tanhua *et al.*, 2005). Mature NADW is formed when the DWBC reaches the Grand Banks off Newfoundland and has received further inputs of LSW, AABW and ISOW in the Labrador Basin.

2.3.3 Denmark Strait Overflow Water (DSOW)

DSOW is a main contributor to North Atlantic Deep Water (NADW) (Dickson *et al.,* 1990: Dickson & Brown, 1994). There has been much recent debate as to the origins of Denmark Straits Overflow Water (DSOW). The traditional understanding was that these waters were formed in the Icelandic Basin (Swift, 1980). However more recent studies (Rudels *et al.,* 2002; Mauritzen, 1996a, b; Jeansson *et al.,* 2008), based on the properties of water masses in the Arctic and Nordic Seas, have identified the main source of DSOW as the East Greenland Current (EGC) with a minor component formed in the Iceland Sea. The EGC interacts with a number of surface, intermediate and deep water masses on its course from the Fram Strait to the Denmark Strait (Figure 2.10). Rudels *et al.* (2002) recognises the densest portions of DSOW as being formed by isopycnal mixing in the EGC of Re-circulating Atlantic Water (RAW) with Arctic Deep Water (AAW) and of upper Polar Deep Water (uPDW) with Arctic Intermediate Water (AIW). This conclusion is supported by subsequent studies (Olsen *et al.,* 2005; Rudels *et al.,* 2005; Jeansson *et al.,* 2008).

These studies also identify stratification of the DSOW overflow plume. The two water bodies resultant from isopycnal mixing in the ECG mix at the Denmark Strait sill and as the overflow plume descends the sill form the dense component of DSOW. The less saline and dense upper layer of DSOW has properties characteristic of Polar Intermediate Water (PIW) (Rudels *et al.,* 2002). Jeansson *et al.* (2008) identify a three layered structure to the overflow plume: the upper fresher PIW layer, an intermediate layer consisting of RAW and AAW and a dense deep layer of PDW, Greenland Sea Arctic Intermediate Water (GSAIW) and Nordic Seas Deep Water (NSDW).

An important proviso of these studies is that they only claim to have identified the source of DSOW for their particular duration of study and that they are based on the conservative properties of water masses. Jeansson *et al.* (2008) observe that once these different water masses from the Arctic Ocean, the Nordic Seas and the Re-circulating Atlantic Water have mixed in the EGC, it becomes extremely difficult to distinguish them on the basis of temperature and salinity alone. They therefore propose adding additional parameters, such as nutrient, oxygen and CFC content, to identify the separate water masses. Other authors still advocate an Iceland Sea origin for DSOW (Jonsson, 1999;

Jonsson & Valdimarisson, 2004) from studies using current measurements from the Greenland Iceland Seas and across the Denmark Straits.

2.3.4 Iceland Scotland Overflow Water (ISOW)

Warm salty water enters the upper layers of the Norwegian Sea from the North Atlantic Current. This water is then modified in the Nordic and Artic Seas (Swift & Aagaard, 1981; Rudels & Quadfasel, 1991). This modified water then returns to the North Atlantic. The water that overflows across the Iceland-Faroe Ridge and through the Faroe Bank Channel from the Norwegian Sea into the Iceland Basin is referred to as Iceland Scotland Overflow Water (ISOW) (Van Aken & deBoer 1995). Hansen & Osterhus (2000) identify the water masses contributing to ISOW as Modified East Iceland Water (MEIW), Norwegian Sea Deep Water (NSDW) and Norwegian Sea Arctic Intermediate Water (NSAIW). Van Aken & deBoer (1995) argue that diapycnal mixing of these water masses as they flow across the Iceland-Faroe Ridge and through the Faroe Bank Channel causes them to form the homogeneous ISOW. McCartney (1992) observes that this ISOW then mixes with Labrador Sea Water (LSW) and Lower Deep Water (LDW) in the Iceland Basin, the resulatant water mass flowing through the Charlie Gibbs Fracture Zone in the Western North Atlantic where it becomes a main contributor to North Atlantic Deep Water (NADW).

2.3.5 Labrador Sea Water (LSW)

Labrador Sea Water (LSW) is an intermediate water mass formed through deep winter convection in the Labrador Sea (Lazier, 1980; Gascard & Clarke, 1983). In summer, melting sea-ice freshens the surface waters of the Labrador Sea, thus lowering in density. In winter the surface waters experience significant heat loss as a result of dry Arctic air masses from Northern Canada passing over the surface waters and the formation of pack ice. This results in deep convection and the production of LSW (Brown *et al.*, 2001). LSW is fresh, cold and high in dissolved gases. Pickart *et al.* (2003) argued that the Labrador Sea was not the only point of origin for LSW and that water with equivalent properties to LSW is also formed in the Irminger Sea. Kieke *et al.* (2006) distinguished between

classical (LSW) and upper (ULSW) Labrador Sea Water on the basis of density and CFC content. This distinction has not been accepted by all subsequent authors.

Yashayaev *et al.*, (2007) recognise three ways in which LSW is important to North Atlantic circulation: by influencing mid-depth circulation, by controlling the exchanges between the subpolar and subtropical gyres at intermediate depth and by controlling the strength of the lower limb of the MOC as the dense waters that overflow the Greenland-Scotland ridge, DSOW and ISOW, mix with LSW before entering the abyssal reservoirs of the North Atlantic.

2.4 Currents of the Subpolar North Atlantic

	Temperature	Salinity
North Atlantic Current[1]	~8 °C	35.2–35.3
Irminger Current[2]	4°-6°C	34.9-35.0psu
East Greenland Current[3]	Upper 150m (Polar water) between 0 and -1.7°C (freezing point of low salinity sea water)	<30 psu at surface ~ 40psu at 150m
	150-800m > 0°C	34.88 – 35 psu
	>800m < 0°C	34.87 - 34.95 psu.

Table 2.2 Temperatures and salinities of The North Atlantic Current, the Irminger Current and the East Greenland Current
(WOA 98)[1] (Reynaud et al. 1995) [2] (Aagaard and Coachman 1968a)[3].

2.4.1 North Atlantic Current (NAC)

The North Atlantic Current (NAC), also previously known as the North Atlantic Drift, brings warm and saline waters from the subpolar gyre into the eastern North Atlantic and Nordic Seas. (Figure 2.7) There have been many recent studies of the pathways of this current (Krauss, 1986; Sy, 1988; McCartney, 1992; Kase & Krauss, 1996). The NAC divides into a number of branches as it travels northwards. Above the Charlie-Gibbs fracture zone the current divides eastwards into the Irminger Current, discussed below. The remainder of the NAC continues northwards.

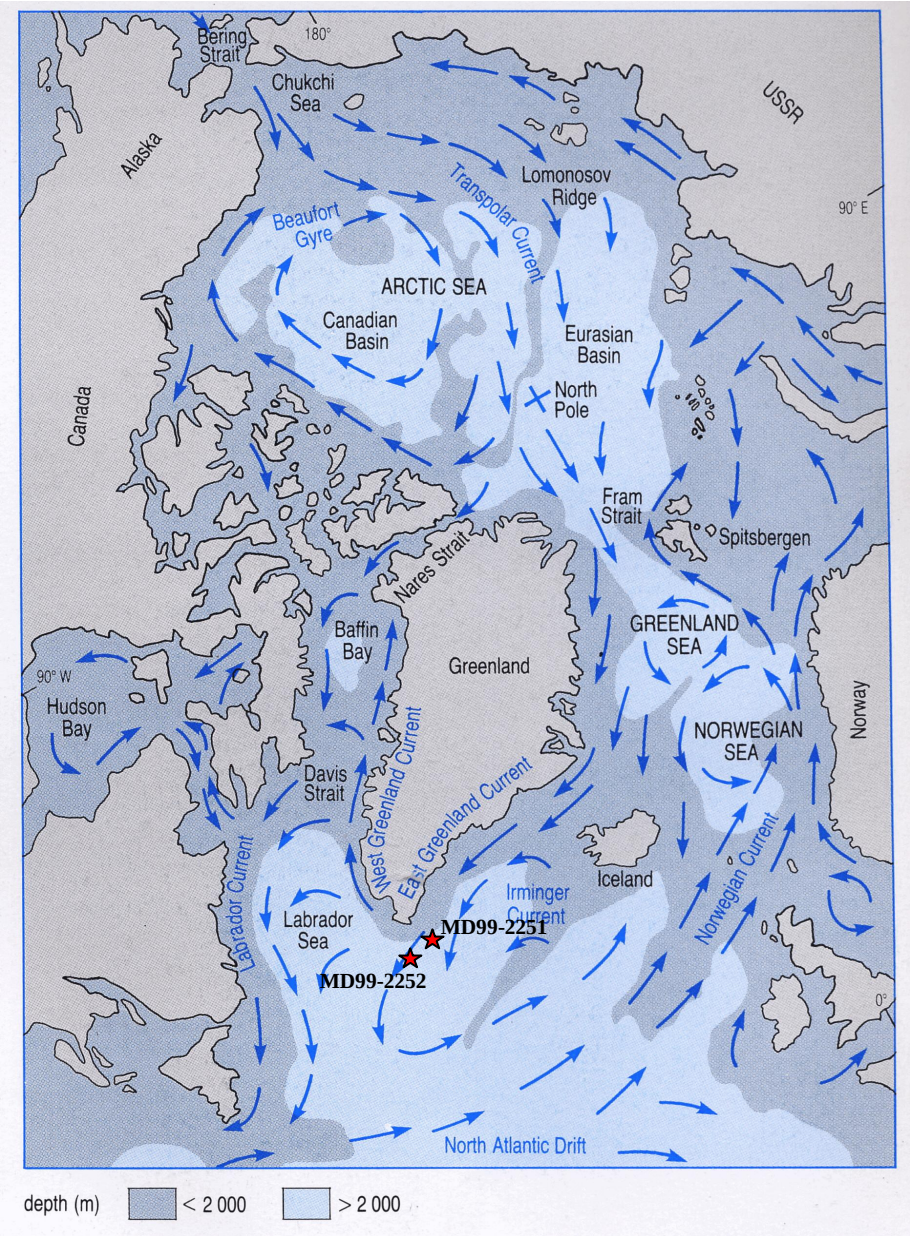

Figure 2.7. The currents of the northern North Atlantic. After Brown *et al.*(2001)

McCartney & Mauritzen (2001) conclude that the NAC warm water enters the Nordic Seas from this northward branch of the NAC which joins the Rockall Slope Current. Together these currents form a thick warm pool of water which envelops the Rockall Trough and Rockall Hatton Plateau. This water then flows northwards through the Faroe-Shetland Channel and north of the Faroe Islands. Hansen & Osterhus (2000) recognise two branches of the NAC crossing the Greenland-Scotland Ridge east of Iceland; one flowing over towards the Iceland Faroe region of the ridge and one through the Faroe-Shetland

Channel. These two flows together with the Irminger Current west of Iceland, make up the branches of water from the Atlantic Ocean flowing into the Nordic Seas as shown in Figure 2.8. Hansen *et al.*(2003). Hansen & Osterhus (2000) observe that the NAC is not the only source of warm saline water crossing the Greenland-Scotland Ridge; the Continental Slope Current which flows along the Norwegian Coast also brings additional warm saline waters onto the Nordic Seas.

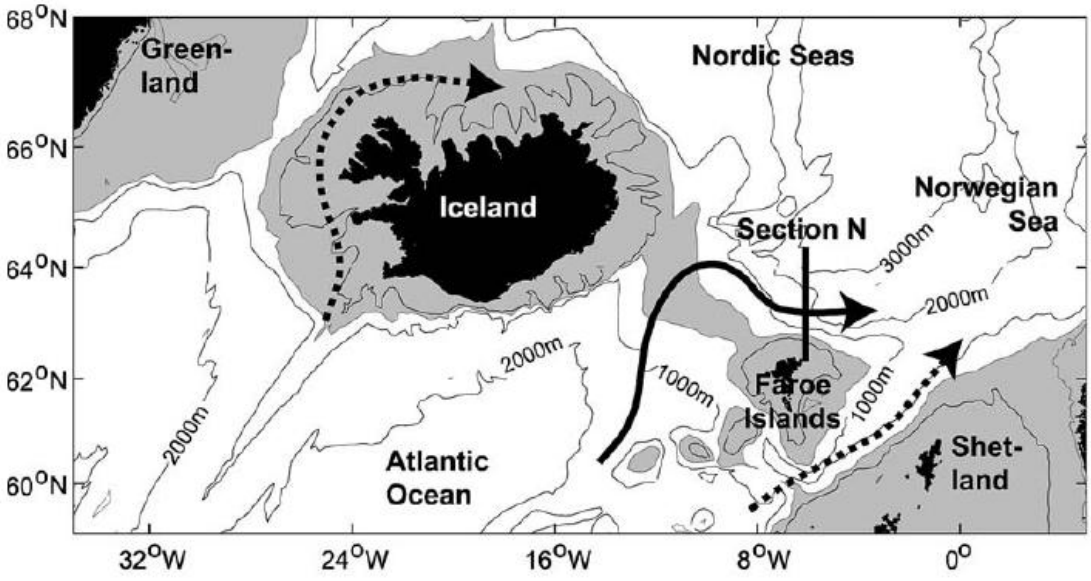

Figure 2.8 The inflow paths of warm, saline water from the Atlantic Ocean into the Nordic Seas. The broken and solid arrows indicate the pathways of the flow across the Greenland–Scotland Ridge. The shaded areas indicate regions shallower than 500m. After Hansen *et al.* (2003).

2.4.2 The Irminger Current

The North Atlantic Current divides into branches shortly after it crosses the Mid Atlantic Ridge between 50° and 52 °N above the Charlie-Gibbs fracture zone (Sy *et al.*, 1992). Bersch *et al.* (1999) indicates that the Irminger Current separates from the North Atlantic Current at 26 °W transporting warm, saline, less dense Sub Polar Mode Water. West of the Rekyjanes Ridge, the current flows in a north to north-easterly direction through the Irminger Basin to the Scotland-Greenland Ridge. Bersch (1995) also recognises a southerly deflected flow of the Irminger Current east of the Rekyjanes Ridge.

When it reaches the Greenland-Scotland Ridge just west of Iceland, the Irminger Current splits again into branches (Figure 2.9). One branch is deflected west and then south where it joins the East Greenland Current as a narrow 130m band of flow (Bersch, 1999). The other branch is deflected eastward, north of Iceland where it forms the North Iceland Irminger Current. As the current travels eastward it gradually looses it characteristic higher salinities and temperatures (Hansen & Osterhus, 2000) so that northeast of Iceland where it encounters the East Icelandic Current the percentage of Atlantic water is less than 30%.

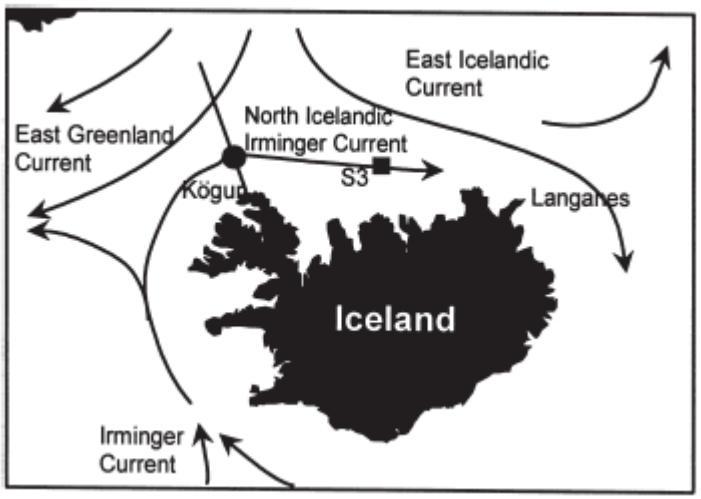

Figure 2.9 The bifurcation of the Irminger Current west of Iceland. After Kristmannsson (1998)

2.4.3 The East Greenland Current

The East Greenland Current (EGC) extends southward from the Fram Strait 79^{o}N to Cape Farewell 60^{o}N along the east coast of Greenland. The EGC may be considered in two sections: north of the Denmark Straits where it interacts and mixes with surface, intermediate and deep water from the Polar and Nordic Seas and south of the Denmark Straits where it is joined by the warmer more saline water of the Irminger Current (IR). The EGC transports both low salinity Polar Surface Water (PSW) and sea ice as well as deep and intermediate water from the Arctic Ocean and Nordic Seas southward into the North Atlantic (Rudels *et al.*, 2002; Maurtitzen, 1996a b). Figure 2.10 indicates the waters

masses that interact with the East Greenland Current. These have been discussed in detail when considering the contribution of the EGC to DSOW.

Sutherland & Pickart (2008) recognise as third current that joins the ECG and the IR south of the Denmark Straits; the East Greenland Coastal Current (EGCC). The EGCC runs along the continental shelf inshore of the EGC and the IR as is a wedge of low salinity water. They argue that the EGCC is an inner branch of the EGC formed from the bifurcation of the EGC at the Denmark Straits.

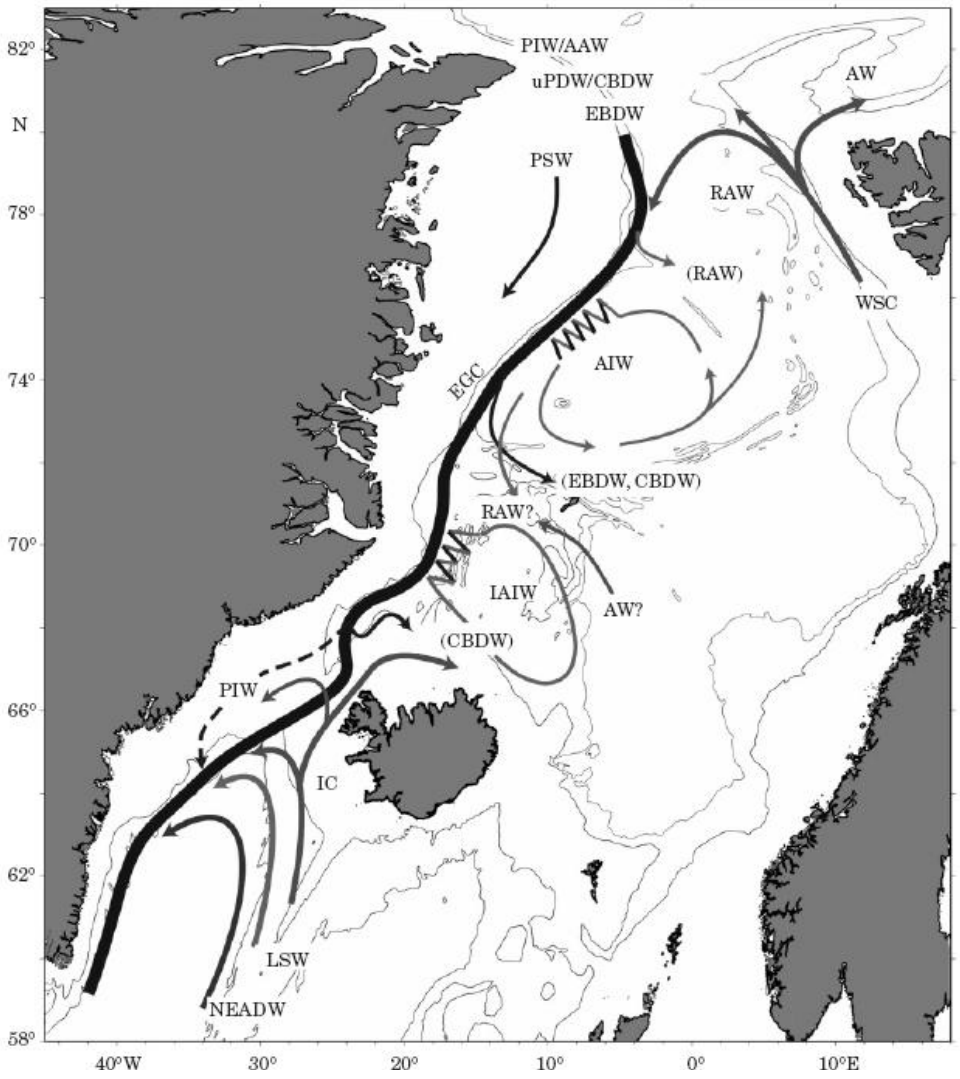

Figure 2.10 The East Greenland Current (EGC), Irminger Current (IC), West Spitbergen Current (WSC), Polar Surface Water (PSW), Re-circulating Atlantic Water (RAW), Arctic Atlantic Water (AAW), Labrador Sea Water (LSW), Arctic Intermediate Water (AIW), Polar Intermediate Water (PIW), Iceland Sea Arctic Intermediate Water (IAIW), Canadian Basin Deep Water (CBDW), Eurasian Basin Deep Water (EBDW), Nordic Deep Water (NDB), Northeast Atlantic Deep Water (NEADW), Upper Polar Deep Water (uPDW). After Rudels *et al.* (2002).

Chapter Three

The Palaeoceanography of the Sub Polar North Atlantic

"I could with a little imagination make every walk seem different.... an occasion the path led back down the eons while I watch the slow pulsations of the Ice Age...by speeding up the centuries I could visualise a tidal wave of ice flooding down from the Arctic forming towering barriers on the margins of the sea. For centuries nothing but obliterating ice...but finally the ice imperceptibly sinking, the oceans rising as the ice melted and the land resurrecting under the sun..."

Richard E Byrd 'Alone'

Chapter Three: The Palaeoceanography of the Sub Polar North Atlantic

3.1 Introduction

Glacial climates are known to experience extreme quasi-cyclic fluctuations such as the approximately 1500 year Dansgaard Oeschger cycles recognised in the Greenland ice cores from the last glacial period (Dansgaard *et al.*, 1993) (Figure 3.1). It was long considered that unlike glacial climates, interglacial climates such as the Holocene (11,500 cal yr BP to present) were relatively stable. More recent studies have however shown that the Holocene has been subject to climate variability, if at a more muted amplitude to the fluctuations of the glacial periods. Pertinent to the study of these Holocene climate variations has been the question of whether or not these fluctuations show any pattern or cyclicity and what factors are forcing the changes.

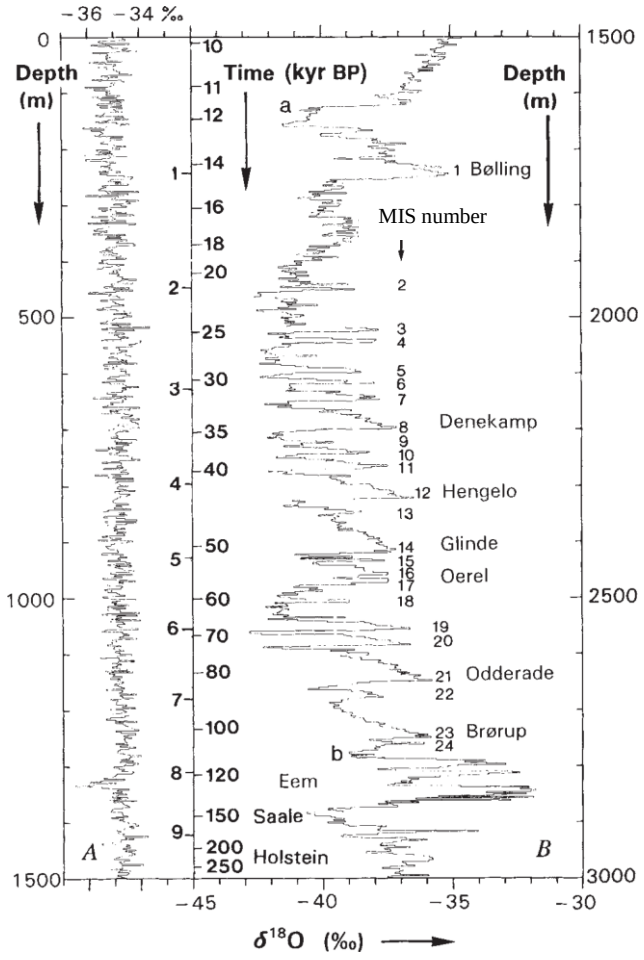

Figure 3.1 Continuous GRIP summit ice core $\delta^{18}O$ record with numbered interstadials showing a ~1500yr cyclicity. MIS (Marine isotope stage). After Dansgaard *et al.* (1993).

3.2 Cyclicities in Holocene Climate variation

As climate variability in glacial cycles has been identified as exhibiting 1500 year cycle, the question was raised as to whether a similar cyclicity may be identified for interglacial periods. A study of Ice Rafted Debris (IRD) from two marine cores from the North Atlantic VM 28-14 (64°47´N, 29°34´W) and VM 29-191 (54°16´N, 16°47´W) by Bond *et al.* (1997) identified such a cycle. Millennial scale peaks in IRD were found at 11.1, 10.3, 9.4, 8.1, 5.9, 2.8 and 1.4kyr. This cycle may be summarised as 1370±500 yrs. Variations in ice rafted debris (IRD) input through the Holocene is discussed more fully in Chapter eight of this study. Similarly paced climate cycles have been recognised in subsequent studies of North Atlantic Holocene sediments (Bianchi & McCave, 1999; deMenocal *et al.,* 2000) and from terrestrial records (Campbell *et al.,* 1998; Yu *et al.,* 2003). Bianchi & McCave (1999) using a sediment grain size proxy, sortable silt mean size, for flow of Iceland Scotland Overflow water (ISOW), recognise a quasi-periodicity of 1500 years for the Holocene (Figure 3.2).

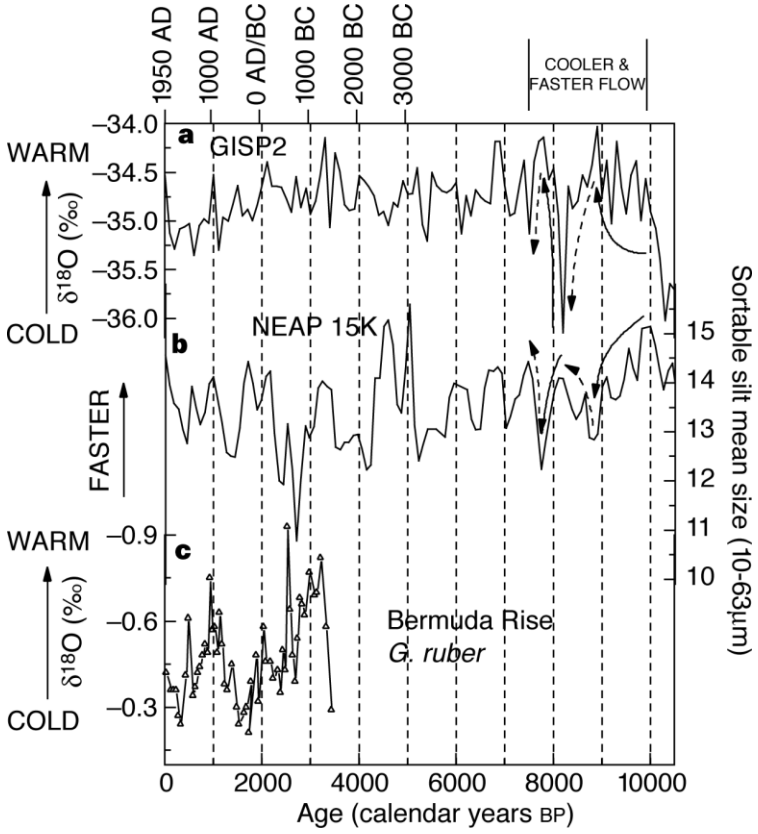

Figure 3.2 a) GISP 2 ice core $\delta^{18}O$ b) mean sortable silt record from NEAP 15K c) Planktonic foraminfera $\delta^{18}O$ from the Sargasso Sea, indicating evidence of a quasi 1500 periodicity through the Holocene (Bianchi & McCave, 1999)

Notably this cyclicity was not recognised in the Greenland ice cores for the Holocene. Instead a 900 year cyclicity is recognised (Grootes & Stuiver, 1997). Chapman & Shackleton (2000) also recognise this 900-1000 year and a 550 year cyclicity in North Atlantic marine cores (Figure 3.2). Schultz & Paul (2002) argue in a review of a number of marine and terrestrial records that the 900 year cycle is prevalent in the Holocene. They further propose that the IRD cycles of Bond *et al.* (1997) with their cyclicity of 1370±500 yrs may be considered to reflect the 900 year cycle.

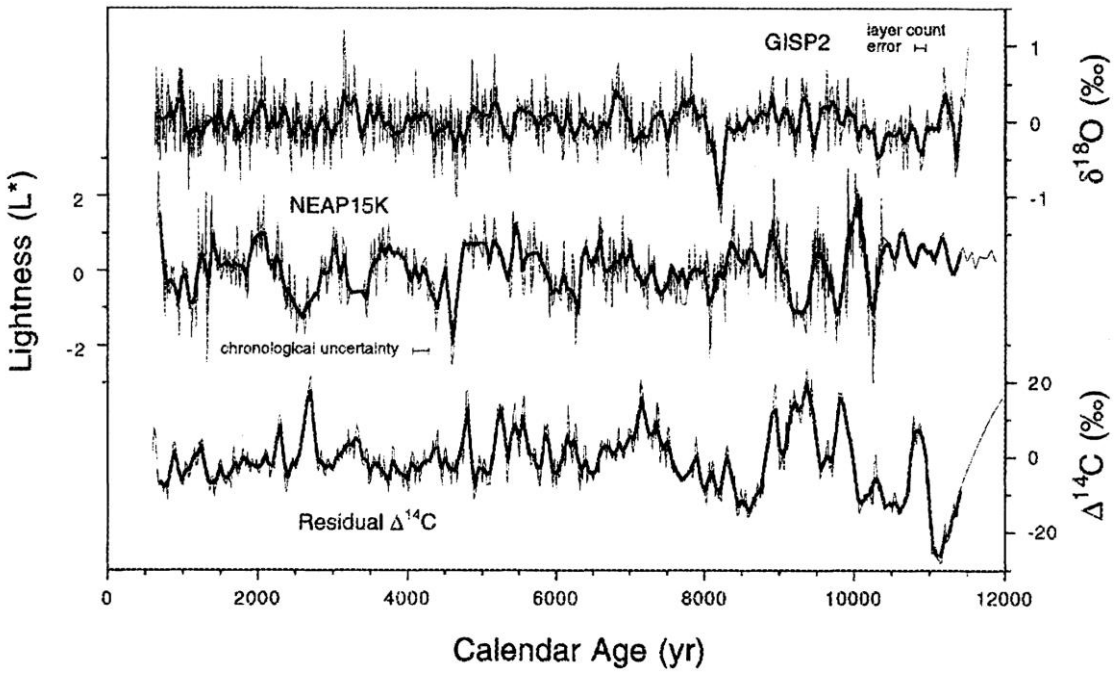

Figure 3.3 A comparison of sediment lightness record NEAP 15K, residual atmospheric ^{14}C (Stuiver & Braziunas, 1993) and GISP2 (Grootes *et al.,* 1993) indicating evidence of 900 year cyclicities for the Holocene. From Chapman & Shackleton (2000)

Other authors identify no millennial or centennial scale cyclicity in Holocene sea surface temperatures. Risebrobrakken *et al.* (2003), in a study of foraminifera from the Nordic Sea, marine core MD95-2011 (66°58´N, 07°38´E), identifies no millennial or centennial scale cyclicity in Holocene sea surface temperatures, but a consistent, multidecadal variability superimposed on a long term warming. A more recent overview of approximately fifty palaeoclimate records for the Holocene (Mayewski *et al.*, 2004), rather than identifying specific periodicities of climate variation for the Holocene, recognises six

intervals of polar cooling and major changes in atmospheric circulation. These intervals are identified as occurring at 9000-8000, 6000-5000, 4200-3800, 3500-2500, 1200-1000 and 600-150 cal yr BP (Figure 3.4). With the exception of the most recent of these fluctuations, which shows an increase in moisture in some tropical regions, these periods also represent increased aridity at the tropics. Possible forcing mechanisms for these cyclicities are discussed at the end of this chapter.

Figure 3.4 Northern hemisphere paleoclimate proxies. a) Gaussian smoothed (200 yr) GRIP δ^{18}O (‰) proxy for temperature (Johnsen *et al.*, 1992.) b) Gaussian smoothed (200 yr) GISP2 sodium Na+ ppb ion proxy for the Icelandic low (Mayewski *et al*., 1997; Meeker & Mayewski, 2002). c) Gaussian smoothed (200 yr) GISP2 potassium K^+ ppb ion proxy for the Siberian High (Mayewski et al., 1997; Meeker & Mayewski, 2002). d) Norwegian glacier advance (Nesje *et al.*, 2001). e) Treeline limit shifts in Sweden (Karlén & Kuylenstrierna, 1996). f) X-ray density measurements for Lake Vuolep Alaskasjaure sediments Northern Sweden (Karlén & Larsson, in review) g) Northeast Atlantic overflow recorded in sortable silt particles for NEAP 15K (Bianchi & McCave, 1999). h) Summer Sea Surface Temperatures SSTs for the Irminger Sea from planktonic foraminifera modern analogue transfer function (Mayewski *et al.*, 2004). i) Abundance of volcanic glass and haematite stained IRD grains in sediment core GGC-36 45°N 45°W(Bond *et al.*, 1997). j) Abundance of volcanic glass and haematite stained IRD grains in sediment core VM29-191 54°N 15°W (Bond *et al.*, 1997). k) Gaussian smoothed (200 yr) varve thickness Elk Lake MN USA (Bradbury *et al.*, 1993). l) Temperature based on δ^{18}O (‰) from lake carbonates Hongshui River China (Zang *et al.*, 2000). m) Relative abundance of warm-water foraminifera Aegean Core LC21 (Rohling *et al.*, 2002). n) δ^{18}O (‰) for Soreq Cave speleothem Israel (Bar-Matthews *et al.*, 1999). o) δ^{13}C for Soreq Cave speleothem Israel (Bar-Matthews *et al.*, 1999). p) Arid episodes in Lake Tigalmanmmine Morocco (van Campo & Gasse, 1993). The green bars indicate periods of Holocene rapid climate change. After Mayewski *et al.*, (2004)

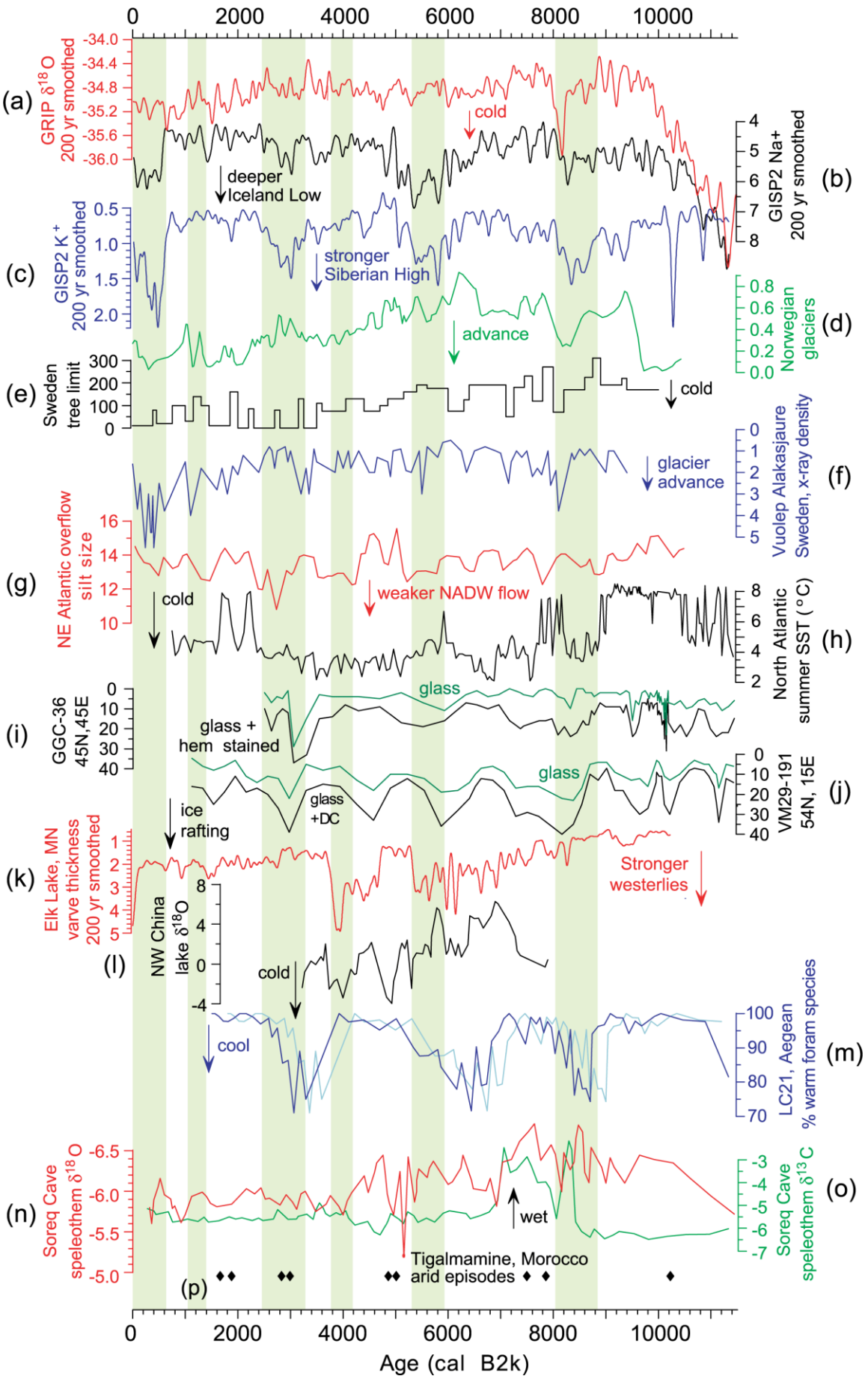
0
2000
4000
6000
8000
10000
(a)
GRIP δ18O 200 yr smoothed
-34.0
-34.4
-34.8
-35.2
-35.6
-36.0
cold
deeper Iceland Low
(b)
GISP2 Na+ 200 yr smoothed
4
5
6
7
8
(c)
GISP2 K+ 200 yr smoothed
0.5
1.0
1.5
2.0
stronger Siberian High
(d)
Norwegian glaciers
0.8
0.6
0.4
0.2
0.0
advance
(e)
Sweden tree limit
300
200
100
0
cold
(f)
Vuolep Alakasjaure Sweden, x-ray density
0
1
2
3
4
5
glacier advance
(g)
NE Atlantic overflow silt size
16
14
12
10
cold
weaker NADW flow
(h)
North Atlantic summer SST (°C)
8
6
4
2
(i)
GGC-36 45N,45E
0
10
20
30
40
glass
glass + hem stained
(j)
VM29-191 54N, 15E
0
10
20
30
40
glass
glass +DC
ice rafting
(k)
Elk Lake, MN varve thickness 200 yr smoothed
1
2
3
4
5
Stronger westerlies
(l)
NW China lake δ18O
8
4
0
-4
cold
cool
(m)
LC21, Aegean % warm foram species
100
90
80
70
(n)
Soreq Cave speleothem δ18O
-6.5
-6.0
-5.5
-5.0
wet
(o)
Soreq Cave speleothem δ13C
-3
-4
-5
-6
-7
(p)
Tigalmamine, Morocco arid episodes
0
2000
4000
6000
8000
10000
Age (cal B2k)

3.3 The 8.2kyr event

The most significant climate event in the Holocene has been widely recognised as the 8.2kyr event. Present as the most prominent event in the Greenland ice cores (Figure 3.5), Alley *et al.* (1997) note that the 8.2kyr event is recognised in palaeoclimate proxies from the northern polar regions to the tropics; glacier advances (Karlen, 1976), cool fresh surface waters in the North Atlantic (Keigwin & Jones 1995), dry windy conditions in the Laurentide Great Lake regions (Rea *et al.*, 1994), dry conditions in monsoonal regions (Lamb *et al.*, 1995), and windy conditions in Caricao Basin (Hughen *et al.*,1996).

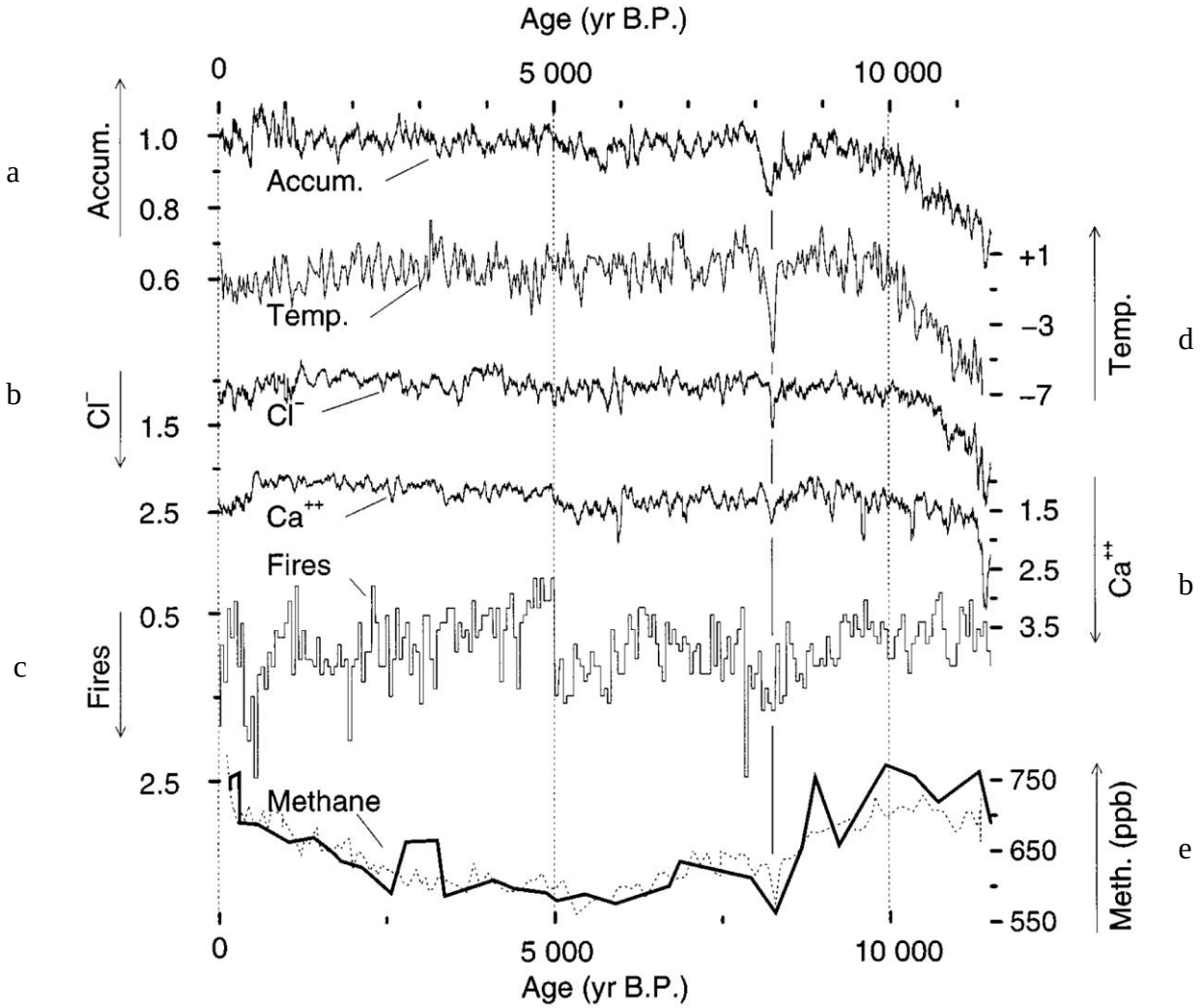

Figure 3.5 Proxies showing evidence of the 8.2kyr event; GISP2 climate data a) approximately 50yr running means of accumulation (Alley *et al.*, 1993; Spinelli, 1996). b) chloride and calcium fluctuations in GISP2. (Chlorine, primarily from sea salt, represents vigor of atmospheric circulation or distance from ocean source. Calcium primarily from continental dust is a proxy for dryness.) (O'Brien *et al.*, 1995). c) 50 yr histogram of frequency of fall out from fires (Taylor *et al.*, 1996). d) Temperature ^{o}C calculated from $\delta^{18}O_{ice}$ (Stuiver *et al*, 1995). e) Methane concentrations in GRIP ice core (Chapallaz *et al.*, 1993; Blunier *et al.*, 1995). After Alley *et al.* (1997)

A number of causes were proposed for the 8.2 kyr event such as underlying periodicity in the climate system (Bond *et al.*, 1995). It is now widely accepted that the event was caused by catastrophic discharges of meltwater from proglacial lakes Agassiz and Ojibway, associated with the decaying of the Laurentide Ice Sheet (Alley & Agustsdottir, 2005; Ellison *et al.,* 2006). These meltwater pulses caused cooling and freshening of surface water, a significant reduction in North Atlantic Deepwater formation causing a slow down of the meridional over turning circulation (Rohling & Palike, 2005, Alley & Agustsdottir, 2005; Ellison *et al.,* 2006). Ellison *et al.* (2006) from a study of the foraminifera and sortable silt from marine core MD99-2251 (one of the same cores analysed in this study), recognise a two pulsed drainage of the proglacial lakes (Figure 3.6). A high resolution analysis is undertaken in this study to determine whether the 8.2kyr event is distinguishable in the North Atlantic Holocene diatom floras and ice rafted debris of MD99-2251.

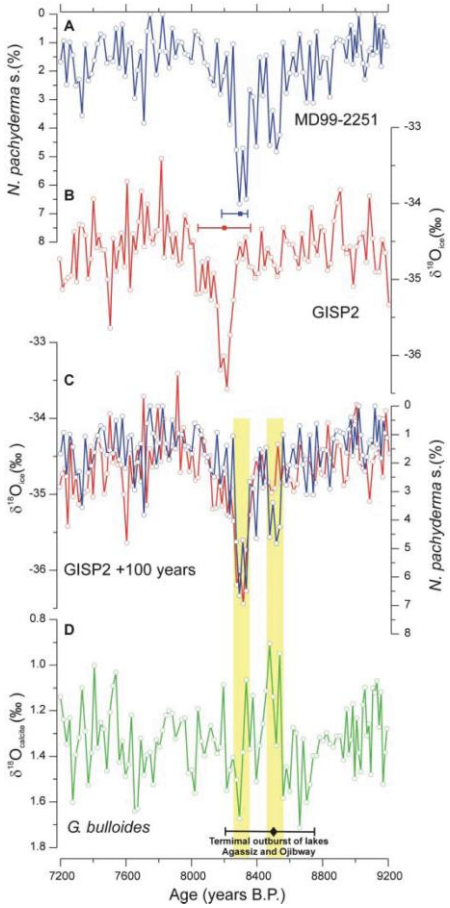

Figure 3.6 Percentage abundance of the planktonic foraminfera *N.pachyderma* sinistral coiling and $\delta^{18}O$ data for planktonic foraminifera *G.bulloides* $\delta^{18}O$ from marine core MD99-2251 compared to GISP2 ice core temperature ($\delta^{18}O$). Dating errors around the 8.2 ky event are shown for each time series. From Ellison *et al.* (2006).

The main characteristics of the present day ocean floor topography, circulation, currents and water masses of the subpolar North Atlantic have been discussed previously in sections 2.1-2.4 of this study. A large number of studies have been undertaken to determine the variation of these systems within the Holocene and what factors may be forcing these changes. These studies have employed a variety of palaeoceoanographic proxies for both deepwater and surface conditions. This review will concentrate on those with greatest relevance to the data later presented in this study. A number of these proxies are also discussed in greater detail in subsequent chapters, notably the use of diatom assemblage counts to reconstruct sea surface temperatures in chapter seven and the use of IRD in chapter nine.

3.4.1 Palaeoproxies of Deep and Intermediate Water Variability

The principal palaeoproxies adopted to determine variability in the strength of deep water circulation include grain size analyses, sediment lightness and carbon isotopes in benthic foraminifera. Mean sortable silt size, a grain size analysis, is a proxy for palaeocurrent speed (Bianchi & McCave 1999). Sediment lightness may be seen as reflecting the variations in deposition of silt and clay particles by bottom currents (Chapman & Shackleton 2000). The $\delta^{13}C$ signal in benthic foraminifera is considered to be an indicator, in the Sub Polar North Atlantic, of the relative proportions of nutrient-depleted North Atlantic Deep Water and nutrient-rich Southern South Water (Duplessy *et al.*, 1992; Austin & Kroon, 2001; Oppo *et al*., 2003; Hall *et al.*, 2004) (Figure 3.7). Other proxies for deepwater flow include coccolith and benthic foraminiferal assemblage data and the concentration of magnetic minerals in ocean floor sediments (Rousse *et al.*, 2006; Giraudeau *et al.*, 2004).

Sediment lightness analysis of marine core NEAP 15K from the Gardar drift found that when atmospheric temperatures, indicated by negative $\delta^{18}O$ values in Greenland ice cores, are lower there is a reduction in North Atlantic Deep Water (NADW) circulation, as indicated by lighter sediments. The core is situated under the flow of Iceland Scotland

Overflow Water (ISOW) an important component of NADW. Mean sortable silt analyses for the same core also indicated a slowing in NADW circulation during cooler intervals (Bianchi & McCave, 1999; Chapman & Shackleton 2000). Hall *et al.* (2004) carried out a mean sortable silt size and benthic foraminifera study of the strength of ISOW flow for marine core NEAP 4K from the Gardar Drift, showed extreme variability of ISOW flow throughout the Holocene (Figure 3.7). The palaeocurrent proxy data did not correlate with the data derived from the $\delta^{13}C$ composition of the benthic foraminifera *Cibiciboides wullerstorfii* from the same site. However, a better correlation was found with the $\delta^{13}C$ data from ODP Site 980, which lies further south and in deeper water (Oppo *et al.*, 2003), and the paleocurrent data from NEAP 4K (62°30´N, 24°19´W) (Figure 3.8).

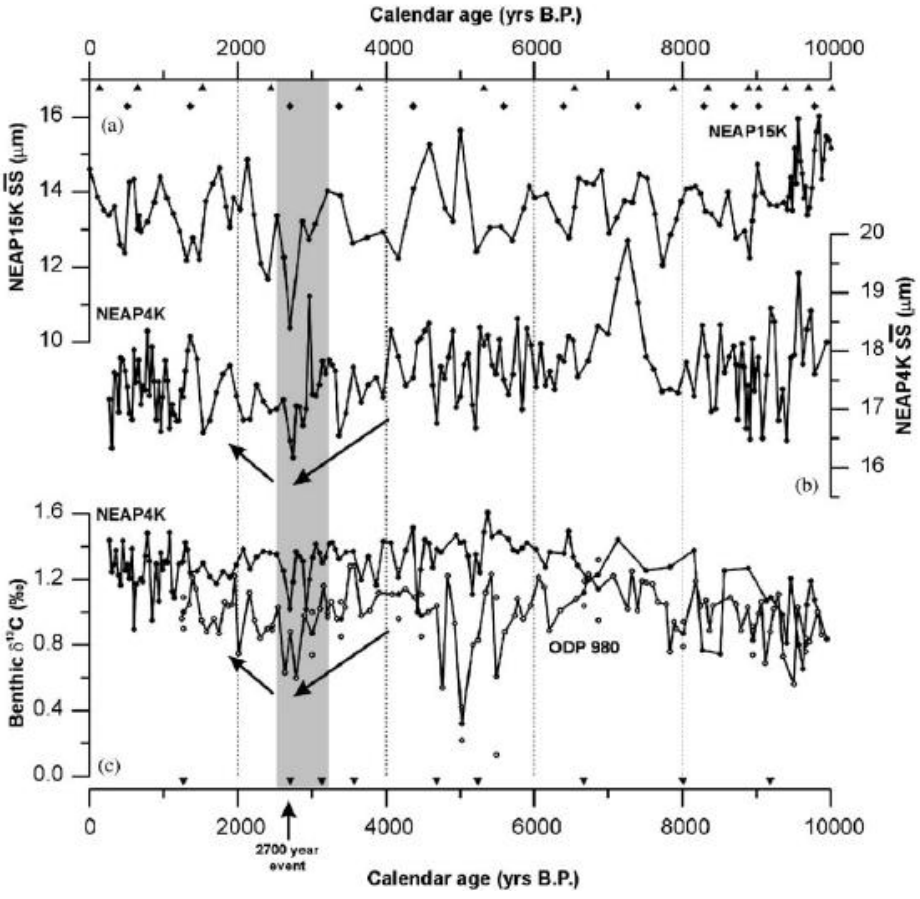

Figure 3.7. Paleoproxies for fluctuations in paleocurrent; mean sortable silt and the $\delta^{13}C$ values of the benthic foraminifera *Cibiciboides wullerstorfii* for marine cores NEAP 4K, NEAP 15K and ODP 980. After Hall *et al.* (2004).

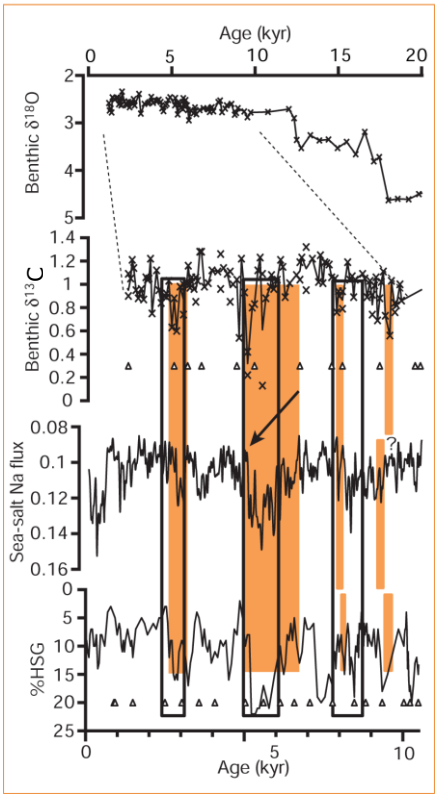

Figure 3.8 Holocene fluctuations in the benthic $\delta^{13}C$ and $\delta^{18}O$ values of *C. wuellerstorfii*, GISP2 sea salt sodium flux, and percentage of haematite stained IRD grains for marine core ODP 980. After Oppo *et al.* (2003).

3.4.2 Palaeoproxies of Surface Water Variability

Variations in sea surface temperatures have been studied using relatively abundance studies of zooplankton and phytoplankton populations. These studies have been undertaken for both foraminifera (Bond *et al.*, 1997; Chapman & Shackleton, 1998; deMenocal *et al.*, 2000, Sarnthein *et al.*, 2003; Knudsen *et al.*, 2008) and diatoms (Andersen *et al.*, 2004; Jiang *et al.*, 2007; Berner *et al.*, 2008; Justwan *et al.*, 2008a). The alkenone ratios in the cell membranes of coccolithophores have also been analysed as a proxy for sea surface temperature, (Chapman *et al.*, 1996; Rimbu *et al.*, 2004; Bendle & Rosell-Mele, 2007). The relative abundance oxygen isotopes in planktonic foraminiferal tests also may be used as a proxy for paleotemperature and ice volume (Sarnthein *et al.*, 1995; Risebrobakken *et al.*, 2003; Ellison *et al.*, 2006). Recent research has examined the magnesium:calcium (Mg/Ca) ratios in planktonic foraminiferal tests, a technique which enables the temperature

and ice volume signatures to be distinguished (Elderfield *et al.*, 2006; Came *et al.*, 2007; Farmer *et al.*, 2008; Thornalley *et al.*, 2009) (Figure 3.9). Other proxies consider the degree of stratification in the water column as a proxy for particular current flows (Ganssen & Kroon , 2000; Hall *et al.*, 2004).

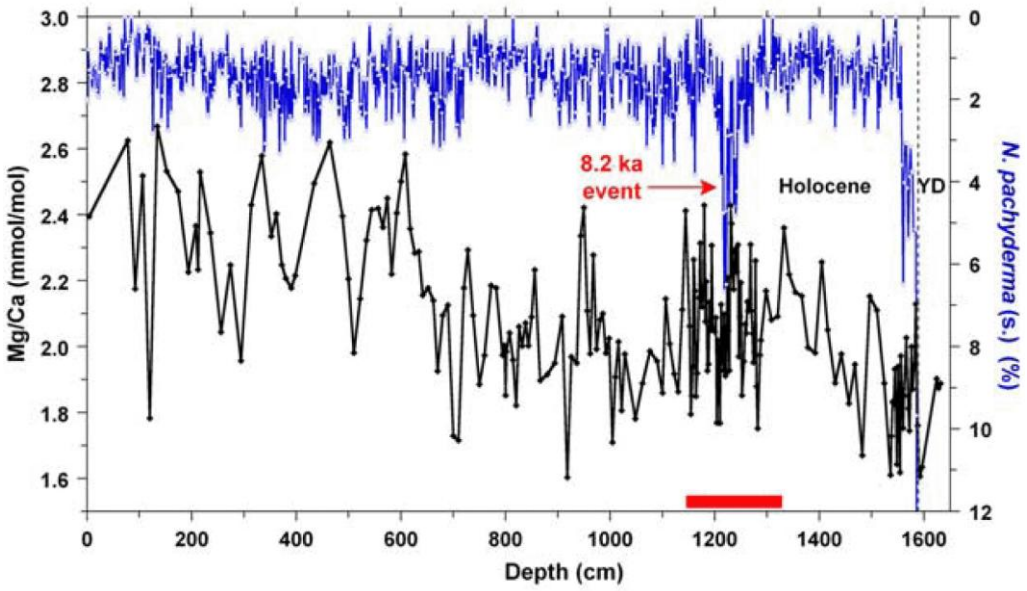

Figure 3.9 Mg/Ca ratios used as palaeoproxy for sea surface temperatures. Here Holocene variations in the relative abundance of the planktonic foraminifera *Neogloboquadrina pachyderma* sinistral are compared to Mg/Ca ratios of planktonic foraminifera *Globigerina bulloides* for marine core MD99-2251. After Farmer *et al.* (2008).

Significantly, the results of these studies do not all identify the same trends in Holocene sea surface temperatures. Mg/Ca analyses of the foraminifera *Globigerina bulloides* for marine core MD99-2251 (57°27´N, 27°54´W) and the foraminifera *Neogloboquadrina pachyderma* (dextral coiling) for marine core ODP site 984 (61°26′N 24°05′W) both indicate a long term warming trend for Holocene sea surface temperatures (Came *et al.*, 2007; Farmer *et al.*, 2008). Other authors identify an early Holocene thermal optimum followed by a long term cooling trend. An alkenone-derived sea surface temperature record from the North Icelandic Shelf, marine core JR51-GC35 (Bendle & Rosell-Melé, 2007) identifies this cooling trend superimposed on millennial-scale oscillations which correlate with glacier advances in northern Iceland. Similarly alkenone derived sea surface temperatures from marine core MD95-2011 (66°58´N, 07°38´E) in the Norwegian Sea show a cooling trend in the Holocene (Moros *et al.*, 2004). Marchal *et al.*

(2002) studied seven alkenone derived paleotempertaure records from the northeast Atlantic and the Mediterranean which all show this same trend.

These differences between the foraminferal and alkenone/diatom proxy data may be explained by the sea surface temperatures being recorded at different depths and/or in different seasons by the different proxies. It is proposed that the diatom and alkenone derived SSTs represent summer temperatures in the euphotic zone which is strongly influenced by levels of summer insolation. Denton *et al.* (2002) argue, in their study of radiolarian derived SSTs for core MD95-2011, that the difference between the diatom and radiolarian derived SSTs may be explained by their position in the water column. Radiolarians and foraminifera may live at greater depths than the phytoplankton, in subsurface waters and to the depth of the thermocline (the upper 50m). At these depths the temperatures are influenced by winter ventilation and less affected by seasonal surface variations. Liu *et al.* (2003) support this hypothesis in their study using different climate models. They conclude that at high latitudes sea surface temperatures are strongly influenced by summer insolation and will therefore decrease through the Holocene with decreasing levels of summer insolation. Whereas thermocline derived temperatures are influenced by winter ventilation and so will increase through the Holocene with increasing levels of winter insolation.

Changes in sea surface temperature have also been noted for studies at higher and lower latitudes than the subpolar North Atlantic, suggesting this is a global rather than a regional climate signal. Sarnthein *et al.* (2003) in a study of foraminifera and ice rafted debris from the Barents Sea, divide the Holocene into an early thermal optimum from 10700-7700 yr BP with a short cooling from 8800 to 8200 yr BP and a general cooling in the middle and late Holocene with two warmer periods at 2200 and 1600 yr BP (Figure 3.10). They identify cycles of 400-650 and 1000-1350 years throughout the Holocene. deMenocal *et al.* (2000) identify similar cyclicity in sea surface temperatures reconstructed for foraminiferal faunal counts for marine core ODP 658C off the coast of West Africa ($20^{o}45´N\ 18^{o}35´W$). They defined six Holocene cooling events centred at 10.2, 8.0, 6.0, 4.6, 3.0 and 1.9kyr.

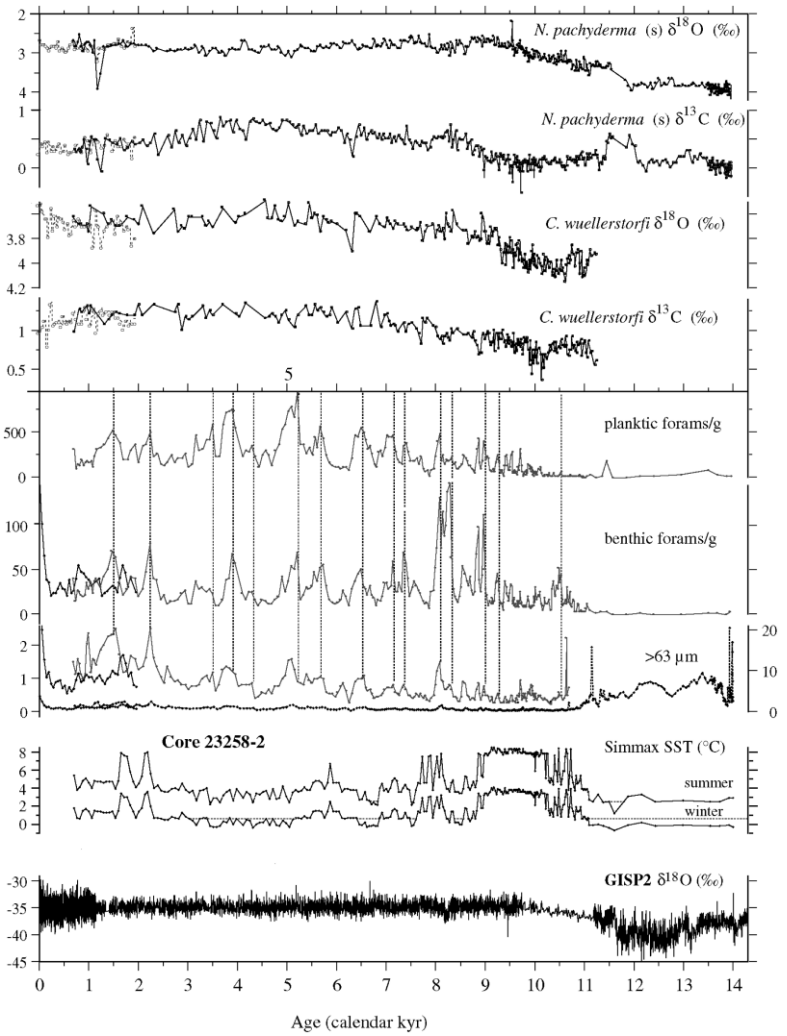

Figure 3.10 Planktonic and benthic foraminifera stable isotope records, sediment and grain size composition for the last 14kyr from a Barent Sea core showing a an early Holocene thermal optimum from 10700-7700 yr BP with a short cooling from 8800 to 8200 yr BP and a general cooling in the middle and late Holocene with two warmer periods at 2200 and 1600 yr BP After Sarnthein *et al.* (2003).

Ganssen & Kroon (2000) use a proxy for the amount of upper ocean stratification in the water column to identify the strength of the North Atlantic Current. They calculate the difference between the $\delta^{18}O$ values in *Globigerina bulloides* and *Globorotalia inflata* (expressed as $\Delta\delta^{18}O_{G.\ bulloides\ -\ G.\ inflata}$). *G.bulloides* is a surface dwelling form and *G.inflata* lives at the thermocline. A $\Delta\delta^{18}O_{G.\ bulloides\ -\ G.\ inflata}$ value of around zero indicates well mixed surface waters, whereas a more negative value indicates increased stratification and is associated with presence the North Atlantic Current. Hall *et al.* (2004) from their study of marine core NEAP 4K (62°30´N, 24°19´W) identify increasing sea surface temperatures and stratification for the early Holocene with a thermal maximum from

around 8.0 to 4.8kyr BP. The influence of the North Atlantic Current then decreases from 4.5 to 2.1kyr BP indicated by increased mixing of the upper water column.

3.5 Proposed Mechanisms of Holocene Climate Variability

A number of possible mechanisms have been proposed for climate variability in the Holocene. These forcing mechanisms include variations in atmospheric and ocean circulation and the input of solar radiation. The input of solar radiation may vary due to earth orbital cycles, changes in sunspot activity, the input of volcanic aerosols and greenhouse gases. Some authors recognise a clear causal link between specific periodicities and forcing mechanisms, while others identify a correlation between particular climate proxies, but consider the causes of these correlations as yet uncertain. It is also recognised that local conditions and feedback mechanisms may amplify or dampen global climate signals at individual sites and for particular proxies. For this reason a synthesis of climate data from a wide range of sites and using multiple climate proxies is considered the most robust means of identifying mechanisms of Holocene climate variability. Mayewski *et al*., (2004) attempt to correlate the Holocene climate fluctuation considered in their review with potential forcing mechanisms including volcanic aerosols, winter and summer insolation at 60^{o}N and 60^{o}S, greenhouse gases CO_2 and CH_4 and ^{10}Be and ^{14}C as proxies of solar variation (Figure 3.11).Mayewski *et al*., (2004) conclude that for the six episodes of rapid climate change that they identify for the Holocene solar variability superimposed on long term changes in insolation is the most probable forcing mechanism for four of the episodes. The 9000-8000yr event is considered to be influenced by solar forcing combined with feedbacks from the break up of the Laurentide ice sheet. A forcing mechanism for the 4200-3800 event is less easy to define.

Figure 3.11 . a) Gaussian smoothed (220 yr) GISP2 Na^{+} (ppb) ion proxy for the Icelandic Low (Mayewski *et al.*,1997; Meeker & Mayewski, 2002). b) Gaussian smoothed (220 yr) GISP2 K^{+} (ppb) ion proxy for the Seberian Low (Mayewski *et al.*,1997; Meeker & Mayewski, 2002). c) Episodes of distinct glacier advance (Denton & Karlen, 1973; Haug *et al.*,2001). d) Emerging tree-stumps from retreating Swiss glaciers (Hormes *et al.*,2001). e) The meltwater outburst of Lake Agissiz (Barber *et al.*,1999). f) Winter insolation values at 60^{o}N (black line) and 60^{o}S (blue line). g) Summer insolation values at 60^{o}N (black line) and 60^{o}S (blue line) (Berger & Loutre, 1991). h) Δ^{14}C residuals (Stuiver *et al.*,1998). i) ^{10}Be concentrations in the GISP2 ice core (Finkel & Nishiizumi, 1997). j) Atmospheric CH_4 (ppbv) concentrations in the GRIP ice core (Chappellaz *et al*., 1993). k) Atmospheric CO_2 (ppmv) concentrations in the GRIP ice core in Taylor Dome Ice Core Antarctica (Indermuhle *et al.*,1999). l) SO_4^{2-} residuals (ppb) from the GISP2 ice core Greenland (Zielinski *et al.*,1996). The green bands represent the timings of rapid climate change. After Mayewski *et al.* (2004).

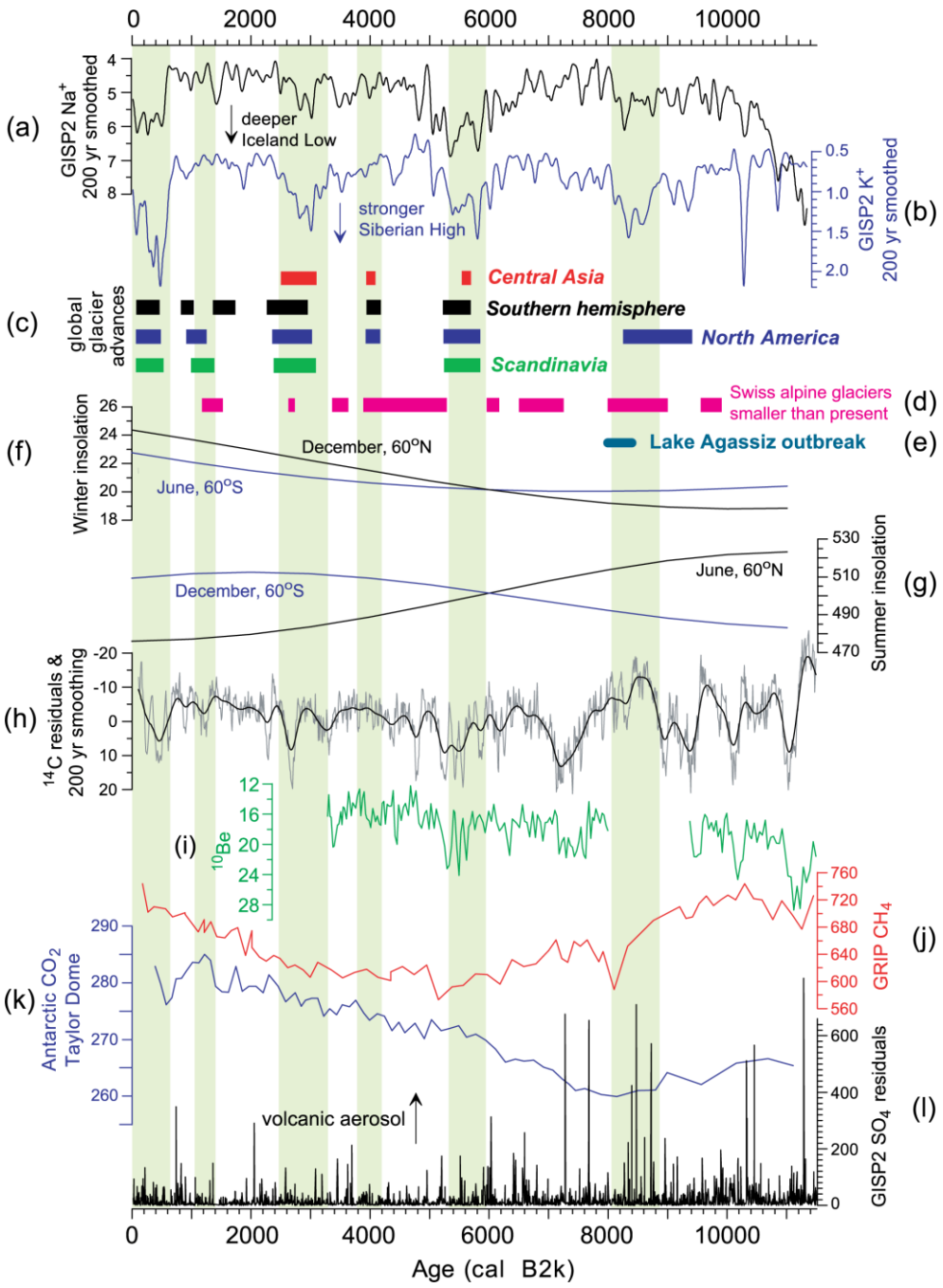

3.5.1 Variations in the Input of Solar Radiation

Bond *et al.* (2001) correlate IRD cycles in the North Atlantic with the flux in cosmogenic nuclides ^{10}Be and ^{14}C. Drift ice events of 200-500 years correlate closely with large changes in nuclide production. They therefore conclude that variations in solar output have influenced changes surface ocean hydrography and surface winds for the subpolar North Atlantic through the Holocene. While the study accepts that the magnitude of this

forcing is small, they argue that climate models suggest a decrease in solar activity of as little as 0.1% can produce a change in surface temperatures through the dynamic response of the atmosphere. Not all studies of drift-ice flux however identify this correlation. Moros *et al.* (2006) argue that variations in iceberg rafting were not uniform across the North Atlantic during the Holocene. From their study of four marine cores off Iceland, they record a long term increases in drift-ice input from 6-5kyr BP to the present in sites influenced by the East Greenland Current, but a decrease in those underlying the North Atlantic Drift. Andrews *et al.* (2009) confirm this regional variability in drift-ice flux. They do not identify a 1500 year periodicity in IRD signal but a multicentennial periodicity of around 670 years.

Other authors (Bianchi & McCave, 1999; deMenocal *et al.,* 2000; Sarnthein *et al.,* 2003) have correlated their sea surface temperature results with the ice rafting records of Bond *et al.* (2001). While Bendle & Rosell-Melé, (2007) note that their alkenone-derived sea surface temperature record from the North Iceland shelf does not correlate with the Bond record through the Holocene. Mayewski *et al*. (2004) in their multiproxy review consider the 6000-5000, 4200-3800, 3500-2500 and 1200-1000 cal yr BP climate variations in the Holocene to have been most probably caused by orbital variations in solar radiation as there is no indication of increased volcanic aerosols, meltwater forcing events or strong variations in sunspots for these time intervals.

3.5.2 Variations in Ocean Circulation

Some authors have argued that changes in North Atlantic ocean circulation may be correlated with climate fluctuations in the Holocene (Stuiver & Braziunas, 1993; Bjorck *et al.,* 1996; Hughen *et al.,*1998; Stocker & Wright, 1996). They argue that changes in the rate of NADW production would influence the distribution of ^{14}C between atmosphere and ocean. Sediment lightness studies from the Gardar drift (Chapman & Shackleton, 2000) identified periodicities of 550 and 1000 years in North Atlantic circulation during the Holocene. These periodicities correspond to those found on the GISP2 Greenland Ice core record (Stuiver *et al.,* 1995) and the authors note that it also corresponds to the $\Delta^{14}C$ flux in

the atmosphere, suggesting that changes in $\Delta^{14}C$ may be related to changes in NADW flow.

Alkenone derived sea surface temperatures from the North Iceland shelf (Bendle & Rosell-Melé, 2007) correlate with data for the strength of NADW (Bianchi & McCave 1999; Oppo *et al.*, 2003) for the later half of the Holocene. Thornalley *et al.* (2009) in their foraminiferal Mg/Ca study from marine core RAPID 12-1K (62°5´N, 49°18´W) identify millennial-scale variations in the inflow of warm saline water into the subpolar North Atlantic which they correlate with Arctic freshwater fluxes.

Mayewski *et al*. (2004) conclude that the 9000-8000 cal yr BP Holocene climate event must be considered as unique, as large ice sheets still existed in the Northern Hemisphere which influenced ocean and atmospheric circulation. This time interval includes the 8.2kyr event (Barber *et al.*, 1999; Ellison *et al.*, 2006; Kleiven *et al.*, 2008). Changes in ^{10}Be which would indicate variation in solar activity (Stuiver *et al.*, 1997) are not indicated during this interval. There is however an increase in the input of volcanic aerosols which would have also resulted in significant cooling (Zielinski *et al.*, 1996). However the most probable cause for this cooling event is changes in ocean circulation.

3.5.3 The North Atlantic Oscillation

Another important atmospheric variation which may drive Holocene climate variability is the North Atlantic Oscillation (Hurrell, 1995; Marshall *et al.*, 2001; Visbek *et al.*, 2003; Hurrell *et al.*, 2003). The North Atlantic winter index is defined as the average pressure difference between the Azores and Iceland in the winter. A positive NAO winter index means that there is a strong pressure gradient between the two regions, a strong atmospheric low over Iceland and strong mid-latitude westerlies (Rousse *et al.*, 2004). It is uncertain how the NAO interacts with ocean circulation as the records of this index only extend back 500-600 years (Cook *et al.*, 2002). However some authors have suggested that the strength of the NAO enhances or weakens the North Atlantic Drift (Taylor & Stephens, 1998; Wanner *et al.*, 2001) (Figure 3.12). Over this time scale the NAO may be identified as exhibiting decadal cycles of stability. Andersen *et al.* (2004) suggest that a persistent

positive NAO state could explain the warm and stable surface conditions during the Holocene climate optimum over the Vøring Plateau.

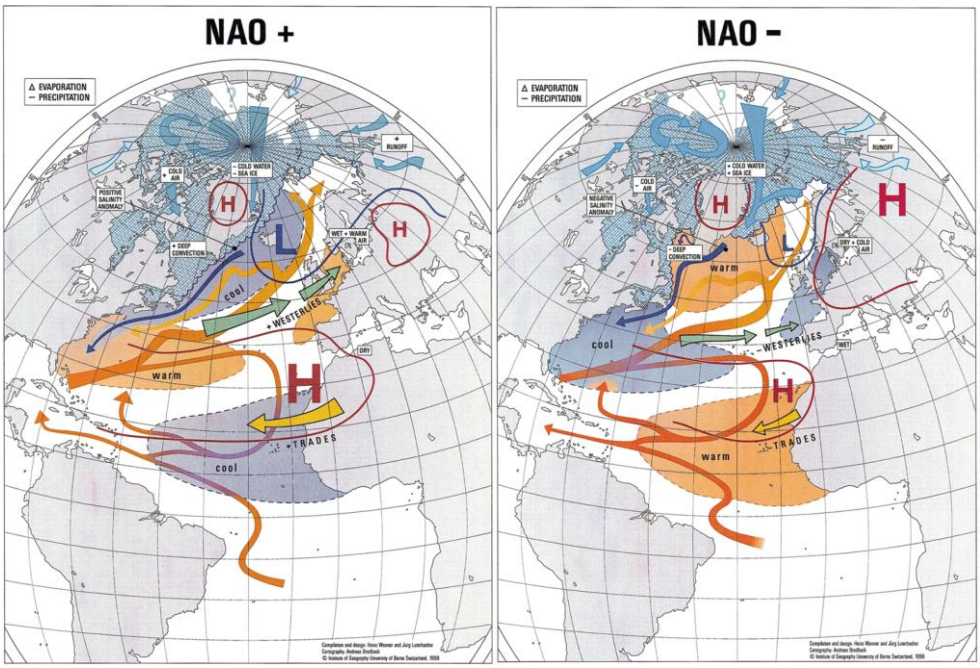

Figure 3.12 Graphical representation of NAO positive and negative modes, indicating the Sea Surface Temperatures (marked as cool in blue shading and warm in orange shading), ice extent, ocean and atmosphere flow (marked with red, orange, green and blue arrows) and high (H) and low (L) pressure zones. White rectangles describe characteristic climate conditions or important processes. After Wanner *et al.* (2001).

Chapter Four

Diatom Taxonomy and Ecology

"Clark finds that with returning daylight the diatoms are again appearing. His nets and line are stained a pale yellow and much of the newly formed ice has also a faint brown and yellow tinge. The diatoms cannot multiply without light..."

Ernest Shackleton 'South'

4.1 Diatom taxa

The following diatom taxa were identified in this study (Table 4.1). Full taxonomic descriptions and discussion of the systematic adopted in this study are found in Appendix Two. A summary of recorded ecological tolerances for each taxa, where known, is also recorded in Table 4.1.

Coscinodiscus asteromphalus	Ehrenberg	
Coscinodiscus linearis	Ehrenberg	
Coscinodiscus marginatus	Ehrenberg	Temperate to subtropical Temperature optimum 27°C Salinity optimum 36‰ Depth optimum 0 to 60m (Canadian diatom database)
Coscinodiscus radiatus	Ehrenberg	Oceanic, temperate species Temperature optimum 25°C Salinity optimum 36‰ Depth optimum 80 to 100m (Canadian diatom database)
Coscinodiscus occulus-iridis	Ehrenberg	
Stellarmina stellaris	Roper	Temperature optimum 24°C, Salinity optimum 36‰ Depth optimum 60m (Canadian diatom database)
Actinocyclus curvatulus	Janisch	Distribution imperfectly known, but fairly widespread (Canadian diatom database) Cosmopolitan (Hasle & Syvertsen, 1997)
Actinocyclus kutzingii	A.Schmidt	Temperature optimum 25°C Salinity maximum 36‰ Maximum depth 0 to 150 (Canadian diatom database)
Actinocyclus octinarius	Ehrenberg	World wide distribution in temperate seas. Temperature optimum 26°C Salinity optimum 36‰ Depth range 20 to 130m (Canadian diatom database)
Azpeitia Africana	Janisch ex A. Schmidt	Temperature optimum 25-27°C, salinity optimum 36‰ Depth optimum 100-150m (Canadian diatom database)

Azpeitia neocrenulata	VanLandingham	Warm water region (Hasle & Syvertsen, 1997)
Azpeitia nodulifera	A.Schmidt G.Fryxell & P Sims in Fryxell *et al.*	Temperature maximum 26°C Salinity maximum 36‰ (Canadian diatom database) Warm water region (Hasle & Syvertsen, 1997)
Hemidiscus cuneiformis	Wallich	Oceanic species, with a wide distribution in tropical and sub-tropical waters Depth range 0 - 200m, optimally 40 to 100m Temperatures range 12 - 29°C Optimum at 25°C Salinity from 34 - 36‰ (Canadian diatom database) Warm water region (Hasle & Syvertsen, 1997)
Roperia tesselata	(Roper) Grunow	Cosmopolitan Found up to 66^{o}N in Norwegian sea and as far south as 57 ^{o}S (Hasle 1976a)
Proboscia alata	Brightwell (Sündstrom)	Temperature range 7 -29°C Temperature optimum 25°C Salinity was from 33 - 37‰ Salinity optimum 36‰ Optimum depth 0 to 90m (Canadian diatom database)
Rhizosolenia bergonii	Peragallo	Relatively uncommon oceanic species, but is widely spread throughout warmer waters Temperature optimum 27°C, Salinity optimum 36‰ Optimum depth 80m (Canadian diatom database)
Rhizosolenia styliformis	Brightwell	Most common in temperate waters Temperature optimum 26°C Salinity optimum 36‰ Optimum depth 0 to 110m (Canadian diatom database)
Rhizosolenia hebetata hebetata	Bailey	Temperature optimum 24°C, salinity optimum 36 ‰ Depth 0 to 200m (Canadian diatom database)
Rhizosolenia hebetata semispina	(Hensen) Gran	Oceanic, boreal-Arctic form. Distribution: Arctic seas, E. Greenland Sea, all parts of the North Sea Also observed in in the waters of

		the tropical and subtropical zones (Canadian diatom database)
Asteromphalus robustus	Castracane	
Bacteriastrum hyalinum		Temperature optimum 26°C Depth optimum 0 to 20m (Canadian diatom database)
Bacteriosira fragilis	Gran	Marine planktonic cold water species from the Northern hemisphere. Temperature mean of 1.4° C (Canadian diatom database)
Porosira glacialis	Grunow (Jorgensen)	Cryoplanktonic diatom, common and often abundant in sea ice Marine planktonic cold water, bipolar species (Canadian diatom database)
Thalassiosira angulata	(Gregory) Hasle	North Atlantic Ocean (Hasle 1978a)
Thalassiosira auguste-lineata	(S.Schmidt) Hasle & Fryxell	
Thalassiosira eccentrica	(Gregory) Hasle	Recorded as cosmopolitan species and as having an Arctic ice association (Canadian diatom database)
Thalassiosira ferelineata	Hasle & Fryxell	Mainly warm water region (Hasle & Syvertsen, 1997)
Thalassiosira gravida	Cleve	Common in neritic plankton in all northern seas. Recorded as temperate to sub polar distribution and as Arctic-boreal-neritic species Temperature range -1.9-28.6°C. Temperature optimum 20°C, Salinity range is from 7-38.8‰ Salinity optimum 36‰ Maximum depth 20 to 120m (Canadian diatom database)
Thalassiosira hyalina	Grunow (Gran)	Recorded as marine planktonic cold water species from the Northern hemisphere Boreal-Arctic-neritic and an Arctic species, common in the North Atlantic. Observed only in waters with a salinity above 31 ‰ with a mean being 33.88‰. This mean value reflects the effect of melting ice and verifies its predominance in polar oceanic water masses (Canadian diatom database)

Thalassiosira lineata	Jouse	Warm-water species (Canadian diatom database) Warm water region (Hasle & Syvertsen, 1997)
Thalassiosira nodulineata	(Hendey) Hasle & Fryxell	
Thalassiosira nordenskioeldii	Cleve	Northern cold water region to temperate (Hasle & Syvertsen, 1997)
Thalassiosira oestrupii	(Ostenfeld) Hasle	Temperature maximum 29°C, salinity maximum 36‰ (Canadian diatom database)
Thalassiosira pacifica	Angst & Gran	Cosmopolitan except for polar regions (Hasle & Syvertsen, 1997)
Thalassiosira trifulta	G.Fryxell in Hasle & Fryxell	
Alveus marina	Kaczmarska & Fryxell	Reported as both marine neritic species inhabiting cold to warm waters, with a preference for cold waters and marine planktonic, warm-water species (Canadian diatom database)
Fragilariopsis atlantica	Paasche	Wide distribution in the Norwegian Sea and recorded at numerous localities in Arctic and Polar water. A second centre of distribution n the warm Atlantic water masses in the south-eastern part of the Norwegian Sea. (Canadian diatom database)
Fragilariopsis cylindrus	Grunow Kreiger in Helmcke & Kreiger	Cryoplanktonic diatom, abundant in some sea ice samples (Canadian diatom database)
Fragilariopsis doliolus	(Wallich) Medlin & Sims	Marine planktonic, warm-water species. Most common in warmer seas Temperature 14 to 27°C Temperature optimum 26°C salinity 35-36‰ Salinity optimum 36‰ Depth 40 to 110m (Canadian diatom database)
Fragilariopsis rhombica	(O'Meara) Hustedt	Ice association: Arctic (Canadian diatom database)
Fragilariopsis oceanica	(Cleve) Hasle	Marine planktonic cold water species Ice association:Arctic. (Canadian diatom database)

Nitzschia braarudii	Heiden & Kolbe	
Nitzschia bicapitata	Cleve emend. G.Fryxell	Marine planktonic, cosmopolitan species (Canadian diatom database)
Nitzschia kolazczekii	Grunow	Marine planktonic, warm-water species (Canadian diatom database)
Synedra spp	Ehrenberg	
Thalassionema nitzschioides	Grunow	Neritic, Reported as North temperate and cosmopolitan species. A pronounced euryhaline species occurring at salinitites down to 4.13 o/oo in Portuguese Guinea and 3.60 o/oo in Tscheskaja Bay in the Barents Sea. (Canadian diatom database)
Thalassionema nitzscihoides var. *parva*	Heiden	
Thalassiothrix longissima		Reported as Boreal-Arctic oceanic and oceanic temperate species Temperature 13-29°C Temperature optimum 25°C, Salinity from 34-36‰ Salinity optimum 36‰ Depth 70 to 90m (Canadian diatom database)

Table 4.1 Marine planktonic diatom taxa identified in marine cores MD99-2251 and MD99-2252 and their ecological tolerances where known

4.2 Ecology

4.2.1 Introduction

.

Diatoms are primary producers requiring light for photosynthesis, nutrients and available silica to produce frustules. They can tolerate a wide range of temperatures and salinities and in certain species, even long periods of desiccation. As a result of these tolerances, diatoms are found in wide range of physical environments as both attached and free floating forms. These include subaerial environments attached to rock, plant, dry mosses and animal, soils and in all but the most hypersaline and hottest water (Round *et al.*, 1990). The diatoms in this study are marine planktonic forms. The particular ecological considerations for these forms are the need to remain buoyant within the marine photic zone, responses to changing nutrient supply within the oceans, tolerances to water turbulence, considerations regarding predation by other organisms and the availability of silica (Lee, 1999).

4.2.2 Light

Diatoms require light for photosynthesis. For marine planktonic forms this means that they must maintain buoyancy within the photic zone. The density of seawater ranges from 1021 to 1028 kg/m^3. The density of the diatom silica frustule is around 2.600 and of the cytoplasm 1030 to 1100 kg/m^3 (Smayda, 1970). Various strategies are therefore adopted by these diatoms in order to achieve neutral or positive buoyancy. These include small size, valve morphology, ionic variation of the cell sap and encasing frustules in low density mucilage sheaths. Adaptations of valve morphology that increase the ratio of surface area to volume and slow sinking rates include, the addition of setae, elongate and disc shaped cells and ribbon shaped colonies. In addition to these morphological adaptations, marine diatoms are able to adopt ionic mechanisms of buoyancy by varying the composition of the vacuolar sap. The concentration of lighter Na^+ ions in relation to heavier K^+ ions is higher in the vacuole than in the surrounding seawater. The concentrations of light NH_4^+ ions also are greater and heavy divalent ions such as SO_4^{2-} are absent. This ionic buoyancy is probably only significant in larger forms where the vacuole is of a sufficient size (Lee, 1999).

Moore & Villareal (1996) observed an inverse relationship between light levels and positive buoyancy in nutrient rich conditions for three species of *Rhizosolenia*. They concluded that at very high light intensities *Rhizosolenia* could undergo physiological changes resulting in negative buoyancy. They proposed that this negative buoyancy was the result of carbohydrate ballasting, a process documented in buoyant cynobacteria. Cells are also capable of exhibiting positive buoyancy and vertical migration around an optimum preferred depth or light level where maximum growth also occurs. Cell buoyancy is also able to respond to nutrient depletion. The *Rhizosolenia* species studied appear to be part of the 'shade flora' which occurs at around 100m depth near the nutricline.

Waite *et al.* (1997) in a study of nine diatom species identified two controls on sinking rates. The first control is related to cell volume. Larger cells sink faster then smaller cells in accordance with Stokes' Law. This control was found to apply to dead or severely metabolically distressed cells. Metabolically active cells however, showed no relationship between cell volume and sinking rate but were rather controlled by vacuole and protoplast modification. The study further suggests a minimum cell volume of 200μm^3 as necessary for active sinking rate control.

The photic zone is frequently turbulent as a result of winds currents and convection. This turbulence acts to keep diatoms in suspension (Round *et al.,* 1990). In addition to the effects of turbulence on diatom buoyancy, population dynamics of diatoms are influenced by stratification in the water column. The spring bloom in phytoplankton in the North Atlantic is associated with vertical stratification of the water column (Ducklow & Harris,1993). Studies of diatom populations around the Antarctic Polar Front show that an increase in phytoplankton occurs with stratification at the Polar Front in early November (Landry *et al,* 2002). The predominance of diatoms in the phytoplankton appears to be related to the extent of stratification, with diatoms dominating in stratified waters (Alvain *et al.,* 2008). At the onset of the spring bloom diatoms dominate the phytoplankton with maximum stratification (Savidge *et al.,*1995). The limiting factor on diatom populations then becomes nutrient availability (which is discussed further in section 4.4.4 of this chapter).

4.2.3 Nutrient Supply and Silica Limitation

Diatoms play and important role in carbon fixation and therefore in the global carbon cycle. They are a major constituent of the ocean's phytoplankton, contributing 40% of the total primary production (Sarthou *et al.* 2005). As a result there has been an increase in the number of studies attempting to define the temporal and special patterns of diatoms in the world's oceans and the environmental constraints on those patterns, in order to better constrain global carbon models. These studies have been based largely on the culture of diatoms in laboratory in seawater with a range of different nutrient concentrations and on satellite data of phytoplankton concentrations under different oceanic conditions.

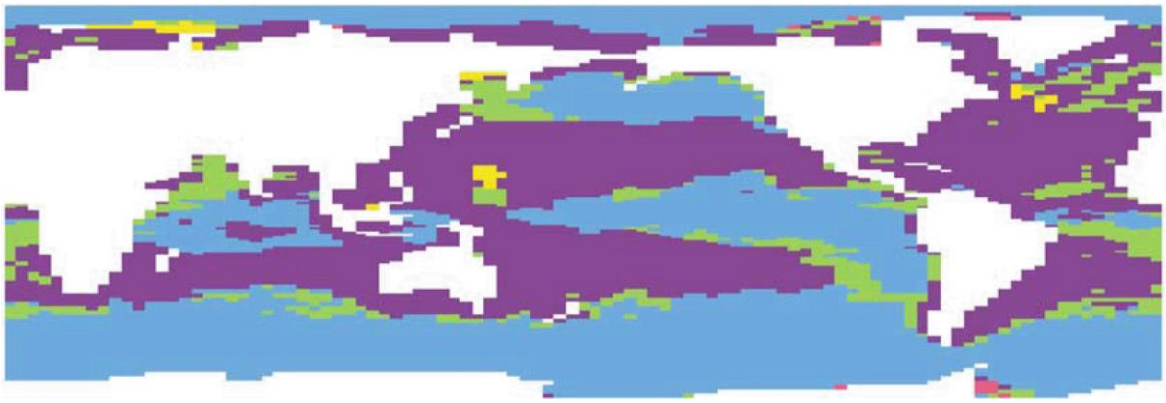

Figure 4.1Diatom nutrient limitation modelled for the world oceans indicating the regional distribultion and the total percentage of the oceans nutrient-limited for diatoms with respect to iron, nitrogen, silica and phosphorus and 'nutrient replete' regions ie those with over 97% of maximum cell quota for all nutrients (Moore *et al.*,2002).

Diatoms dominate the ocean's phytoplankton where nutrient levels are high. Moore *et al.* (2002) modelled the nutrient limitation on diatoms of various elements based on the half saturation level of the particular nutrient in the diatom cell (Figure 4.11). The authors demonstrate that the mid ocean gyres are nitrogen limited for diatoms. The high-nutrient low-chlorophyll (HNLC) regions of the Southern Ocean, equatorial Pacific and subarctic

are iron limited and well as parts of the North Atlantic the Equatorial Indian and Atlantic Oceans during the summer months. The northern Sub Antarctic waters, parts of the North and equatorial Atlantic and the equatorial Pacific are silica limited. Small isolated regions of the ocean are phosphorus restricted with respect to diatom growth. Less than 1% of the world's oceans are nutrient replete with respect to diatoms. These are areas of permanent heavy sea ice cover.

Silica is required not only for frustule growth but also for certain physiological functions in all diatoms. The relationship between silica availability and diatom growth has been extensively studied (Nelson & Treguer, 1992; Dugdale *et al*., 1995; Martin-Jezequel *et al.,* 2000; Shipe *et al.,* 2007). In the North Atlantic, unlike the HNLC regions, the spring plankton bloom depletes the macronutrients. Martin-Jezequel *et al.* (2000) propose that the surface silica pool by diatom production limits diatom growth rates and leads to the collapse of the spring bloom. Brown *et al.*(2003) in a study of ten sites in the Northeastern Atlantic Ocean, used a ^{32}Si radiotracer to track the silica uptake through the spring bloom. The authors conclude that high surface silica availability (above 2µmol L^{-1}) and high absolute and specific silica uptake rates, suggest that dissolved silica availability is the primary control on the diatom spring bloom evolution.

In addition to the modelling studies (Moore *et al.* 2002), iron concentrations in seawater have been demonstrated to have an effect on nearly all the biogeochemical properties of diatoms in laboratory experiments (Sarthou *et al* 2005; Timmermans *et al.*,2004). Timmermans *et al.* (2004) undertook diatom culture studies on four large marine planktonic species under different concentrations of dissolved iron and the effect on both the growth rate and uptake of silicate, nitrate and phosphate. Growth rates increased three to six fold with increased iron concentrations, depending on the size of the diatom cell. Smaller species showed the greatest growth rate increase with additional iron concentrations. With a decrease in iron, nitrate consumption decreased, silicate consumption increased and phosphate consumption showed no clear relationship to iron concentration.

4.2.4 Monospecific diatom blooms

Diatom blooms have been identified in the contemporary strongly stratified surface waters of the equatorial Pacific (Yoder *et al.,* 1994). The authors recognise high concentrations of *Rhizosolenia* spp at the convergence of warm and cold waters. Water mass boundaries in coastal waters had long been identified as associated with increased biological activity and so it was assumed that the same could be true of open ocean frontal systems. Archer *et al.* (1997) concluded that the diatoms were imported from the cooler South Equatorial Current waters and made up a surface layer on the warm side of the ocean front. Localised upwelling was thought to contribute iron which stimulated enhanced productions (Friedrichs & Hoffman, 2001). A number of different diatom genera have been recognised as exhibiting elevated production in the Southern ocean at the Antarctic Polar Front including *Pseudo-nitzschia, Chaetoceros* and *Thalassiothrix* (Smetacek *et al.*, 2002). In the fossil record, monospecific blooms of *Thalassiothrix* have been found in Eemian North Atlantic sediments (Boden & Backman,1996) , Neogene eastern equatorial Pacific (Kemp & Baldauf, 1993) and southern ocean sediments (Grigorov *et al.* 2002). Kemp *et al.* (2006) conclude that giant diatom genera such as *Thalassiothrix, Rhizosolenia* and *Ethmodiscus* may become concentrated at major open ocean fronts. Although they may not be the dominant species when approaching the front they concentrate and then massively sediment.

4.3 Floral Assemblages and water masses

A number of authors have linked diatom floral assemblages to water masses by factor analysis of core top data. Koç Karpuz and Schrader (1990) used the GINT2 transfer function, an Imbrie-Kipp Q-mode factor analysis, based on diatom assemblage data from 104 core top samples from the Greenland Iceland Norwegian (GIN) Seas to identify six different assemblages each strongly reflecting surface water conditions; a Norwegian-Atlantic current assemblage, an Arctic water assemblage, a Sea Ice assemblage, an Arctic-Norwegian waters assemblage, an Atlantic assemblage and a Norwegian-Arctic water assemblage. These six assemblages together accounted for 91.7% of the recorded variance.

Andersen *et al.* (2004a), using an expanded core top data base andI&K analysis, identify eight specific diatom assemblages; an Arctic Greenland Assemblage, a North Atlantic Assemblage, a Sub-Arctic assemblage, a Norwegian Atlantic Current assemblage, a Sea ice Assemblage, an Arctic Assemblage, and East and West Greenland Current Assemblage and a Mixed Water Mass Assemblage. Figure 4.2 indicates the distribution of these floral assemblages. The key species identified as characteristic of each assemblage are indicated in Table 4.2. Based on the factor loading matrix the authors indentify both species which strongly reflect the assemblage (recorded here as Primary assemblage species) and species which also contribute to the assemblage (recorded here as Additional assemblage species).

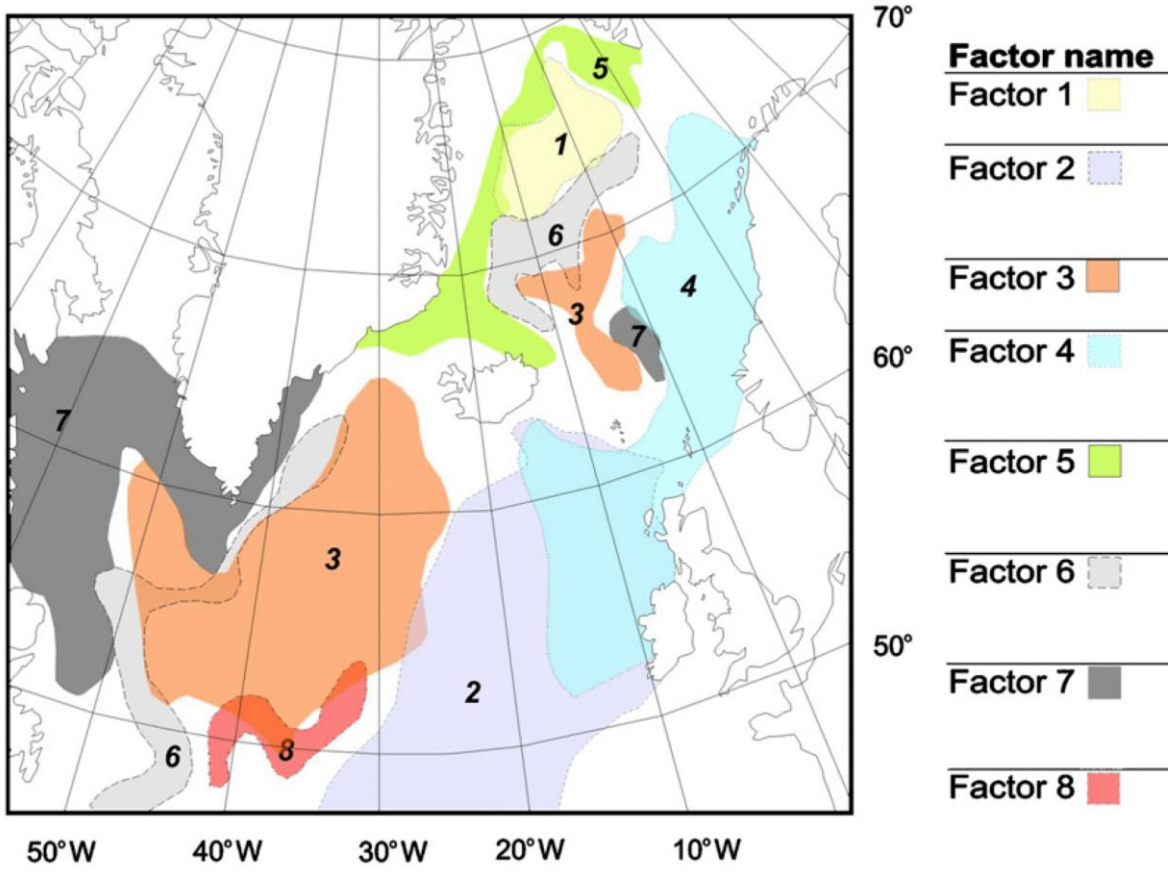

Figure 4.2 The modern distribution of the floral assemblage factors of Andersen *et al.* (2004a) (redrawn Justwan *et al.*,2008). Factor 1 Arctic Greenland Assemblage, Factor 2 North Atlantic Assemblage, Factor 3 Sub Arctic Assemblage, Factor 4 Norwegian Atlantic Current Assemblage, Factor 5 Sea-Ice Assemblage, Factor 6 Arctic Assemblage ,Factor 7 East and West Greenland Current Assemblage, Factor 8 Mixed Water Mass Assemblage.

Factor Number	Factor Name	Primary assemblage species	Additional assemblage species
1	Arctic Greenland Assemblage	*Thalassiosira auguste-lineata, Thalassiosira trifulta*	
2	North Atlantic Assemblage	*Thalassiosira oestrupii*	*Thalassiosira nitzschioides, Nitzschia bicapitata, Rhizosolenia bergonii, Roperia tesselata, Alveus marina*[*]
3	Sub-Arctic Assemblage	*Rhizosolenia hebetata* f. *semispina*	*Rhizosolenia borealis Thalssiosthrix longissima*
4	Norwegian Atlantic Current Assemblage	*Thalassionema nitzschioides*	*Proboscia alata Thalassiosira angulata*
5	Sea Ice Assemblage	*Fragilariopsis oceanica**	*Thalassiosira hyalina Thalassiosira gravida* resting spores *Thalassiosira nordenskioeldii Bacterosira fragilis Fragilariopsis cylindrus**
6	Arctic Assemblage	*Thalassiosira gravida* resting spores	*Thalassiosira gravida* vegetative cells *Actinocyclus curvatulus Rhizosolenia hebetata* f. *semispina Rhizosolenia hebetata* f. *hebetata*
7	East and West Greenland Current Assemblage	*Thalassiosira gravida* vegetative cells	
8	Mixed Water Mass Assemblage	*Rhizosolenia borealis*	

Table 4.2 Primary and additional species for the flora assemblages of Andersen *et al.* (2004a). (* taxonomic nomenclature employed in this study has been adopted. Andersen *et al.* (2004a) refers to *Alveus marina* as *Nitzschia marina, Fragilariopsis oceanica* as *Nitzschia grunowii* and *Fragilariopsis cylindrus and Nitzschia cylindra*)

Table 4.3 presents a simplified version of the factor score matrix produced by Berner *et al.* (2008) Down core mulitvariant analyses (principal component anlaysis and K-means cluster analysis) of the diatom floral counts in marine core MD99-2251 are presented in section 8.6.2 of this study. The groupings identified by these analyses are compared with the floral assemblages identified by Andersen *et al.* (2004a) and Berner *et al.* (2008)

	Factor 1 Arctic Greenland	Factor 2 North Atlantic Current	Factor 3 Sub Arctic	Factor 4 Norwegian Atlantic Current	Factor 5 Sea Ice	Factor 6 Arctic	Factor 7 E & W Greenland Current
T.longissima	0.0542	0.0544	0.1632	0.0272	-0.0068	-0.0011	-0.0020
T.nitzschioides	-0.0424	0.1752	-0.1045	0.8029	0.0173	-0.0083	-0.1515
R.h.hebetata	0.0489	-0.0080	0.0401	0.0158	-0.0203	0.0679	-0.0224
R.h.semispina	-0.0112	-0.290	0.8861	-0.0016	0.0278	0.0764	-0.1574
R.borealis	-0.0375	0.0118	0.3720	0.1865	0.0263	-0.858	-0.0908
P.alata	0.0392	-0.0370	-0.0066	0.3943	0.0008	-0.0463	-0.0738
B.fragilis	0.0172	0.0014	-0.0040	-0.0041	0.0718	0.0113	0.0006
R.tesselata	0.0002	0.0822	-0.0153	0.0495	0.0019	-0.0007	-0.0070
A.curvatulus	0.1236	0.0102	-0.0107	0.0476	-0.0144	0.1322	-0.1135
T.gravida resting spore	0.0118	0.0308	-0.0836	-0.0267	0.1018	0.9384	-0.2259
T.gravida veg	0.1752	-0.0580	0.1464	0.2055	-0.0217	0.2475	0.9118
T.auguste-lineata	0.8742	0.0031	-0.0131	-0.0163	-0.0575	-0.0541	-0.1457
T.trifulta	0.3740	0.0041	-0.0056	0.0155	-0.0575	-0.0233	-0.0656
T.nordenskioeldii	0.0028	-0.0233	0.0362	0.0943	0.1006	0.0369	-0.0415
T.oestrupii	0.0086	0.9550	0.0447	-0.1045	-0.0074	-0.0111	0.0815
T.hyalina	0.1103	-0.0005	-0.0080	-0.0034	0.2090	-0.0402	-0.0032
T.angulata	-0.0225	-0.631	-0.0435	0.2154	0.0288	0.0038	-0.0164
A.marina	0.0023	0.0592	0.0120	-0.0136	-0.0001	-0.0055	0.0045
N.bicapitata	0.0035	0.1159	-0.0087	0.0055	-0.0003	0.0030	-0.0083
F.cylindrus	0.1141	0.0011	-0.0130	-0.0114	0.2647	-0.0730	-0.0038

Table 4.3 The factor score matrix for key species from factor analysis of surface sediments. After Berner *et al.* (2008). All positive scores over 0.1 are highlighted.

Section Two

Methodologies and Results

Chapter Five	*Introduction to Results*
Chapter Six	*Diatom Assemblage Data*
Chapter Seven	*Regional Analysis of Diatom Core Top Floras*
Chapter Eight	*Ice Rafted Debris Data*

Chapter Five

Introduction to Results

"To these various employments was presently added, as the most important of all, the taking of scientific observation, which gave many of us constant occupation..."

Fridjof Nansen 'Farthest North'

Chapter Five: Introduction to Results

5.1 The Core sites

The two marine cores analysed in this study are situated on the Gardar Drift, a sedimentary drift deposit lying on the eastern side of the Rekyjanes Ridge in the Icelandic Basin (Figure 5.1). There are a number of sedimentary drifts in the North Atlantic. Deep water flows provide fine silt and clays which make up the majority of the drift sediment. Keigwin & Jones (1989) assert that there is at least one drift deposit associated with every deep water flow of the North Atlantic. Larger than silt sized particles in drift deposits consist mostly of microfossil skeletons deposited *in situ* and augmented by ice rafted debris during glacial episodes. Drift deposits are particularly useful for palaeoceanographic studies as they have high sedimentation rates, up to 200cm/1000yrs during the last glacial period, allowing high resolution analysis of past climate events. Unlike near shore continental sediments, which also have high sedimentation rates, drift deposits exhibit low rates of bioturbation, are not disrupted by down slope coarse sediment flows and better reflect open ocean conditions (Keigwin & Jones,1989).

Marine cores from sediment drift deposits may be analysed for number of different palaeoceanographic proxies. As deep water flows are considered to be the source of the silt and clay components of a drift deposit, their study may be used to infer provenance of these sediments and the strength of deep water flows, using mean sortable silt, the mean size of the 10-63μm terrigenous fraction, as a proxy for palaeocurrent strength, (Manighetti & McCave, 1995, McCave *et al.*, 1995b; Hall *et al.*, 1998; Bianchi *et al.*, 1999; McCave & Hall, 2006; McCave *et al.*, 2006). The microfossils components of drift sediments are deposited *in situ* and therefore may be used to infer deep and surface ocean conditions at the time of deposition. Studies have been undertaken on analysis of the silt sized diatom flora (Andersen *et al.*, 2004; Berner *et al.*, 2008) and the larger foraminifera fauna (Ellison *et al.*, 2006) of Gardar Drift deposits. Ice rafted debris (IRD), material deposited by drift ice passing over the core site, makes up an additional terrigneous component of drift deposits. Analysis of IRD, usually at the >63μm or >150μm size fraction, may be used to infer variations in drift ice patterns.

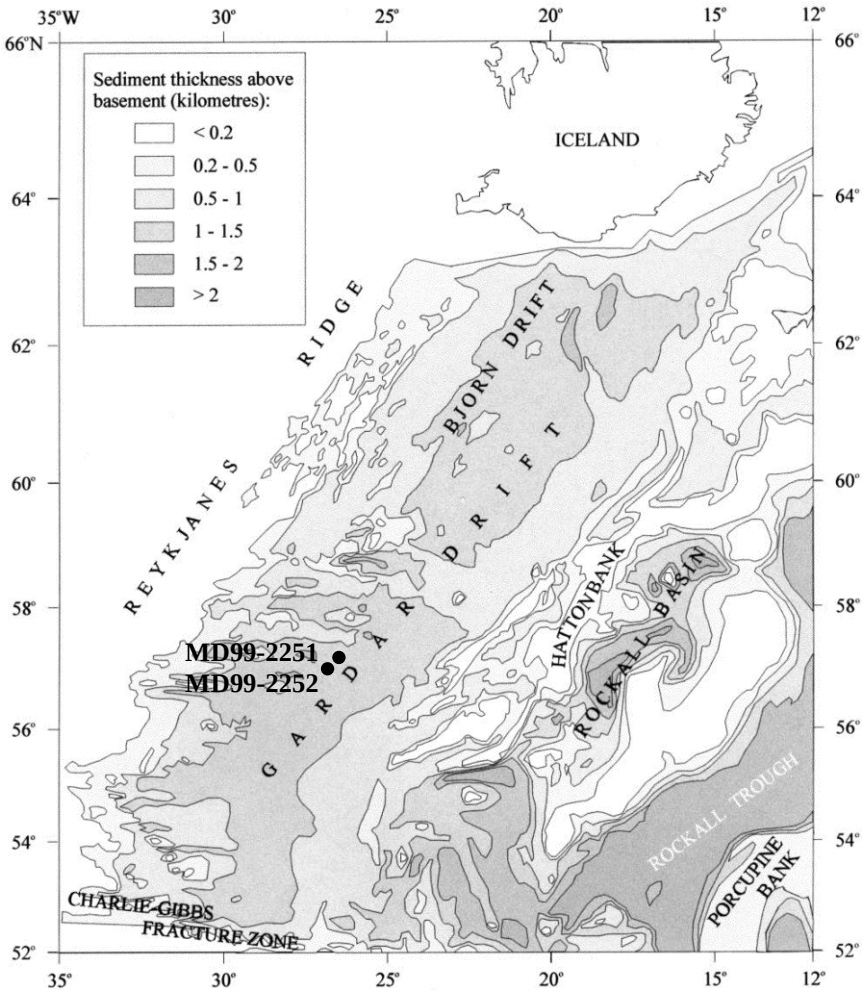

Figure 5.1 Sediment thickness in the Eastern Icelandic basin. (Bianchii & McCave, 2000 modified from Tucholke, 1989). MD99-2251 (57°26.87' 027°54.47') MD99-2252 (57°26.84' 027°55.83').

The Gardar drift is over 1000km in length and stretches from the Icelandic margin to the Charles Gibbs Fracture Zone. It is 1300-1600m thick with an undulating crest. At its northern extent it is broken by abyssal hills and seamounts, which reflect the underlying topography not yet masked by sediment deposition. The drift exhibits large wave like bed forms of irregular size and shape; average heights of 10m and lengths of 1500m (Figure 6.1). Sonar readings taken as part of DSDP Leg 94 indicate that these wave forms may reflect basement morphology. There is no evidence from this DSDP study (Kidd & Hill, 1979) that the wave forms reflect current bottom water flow or have exhibited wave migration.

Bianchi and McCave (2000) however, in a study of 20 box and 18 Karsten cores across the Gardar and Bjorn drifts, identify different types of sediment wave occurring on

the Gardar drift. In the northern portion of the drift; regular migratory waves which form adjacent to the fast-flowing core of the ISOW and migrate down current and upslope, and non-migratory regular and irregular waves on the flanks of the drift. Migratory sediment waves are also observed to the south and at the base of the eastern Gardar drift. These waves are thought to be associated with strong baroclinic flow of the ISOW aligned subparallel to the bathymetric contours. In addition to wave forms they also identify areas of featureless flat seabed at the drift crest (Figure 5.2)

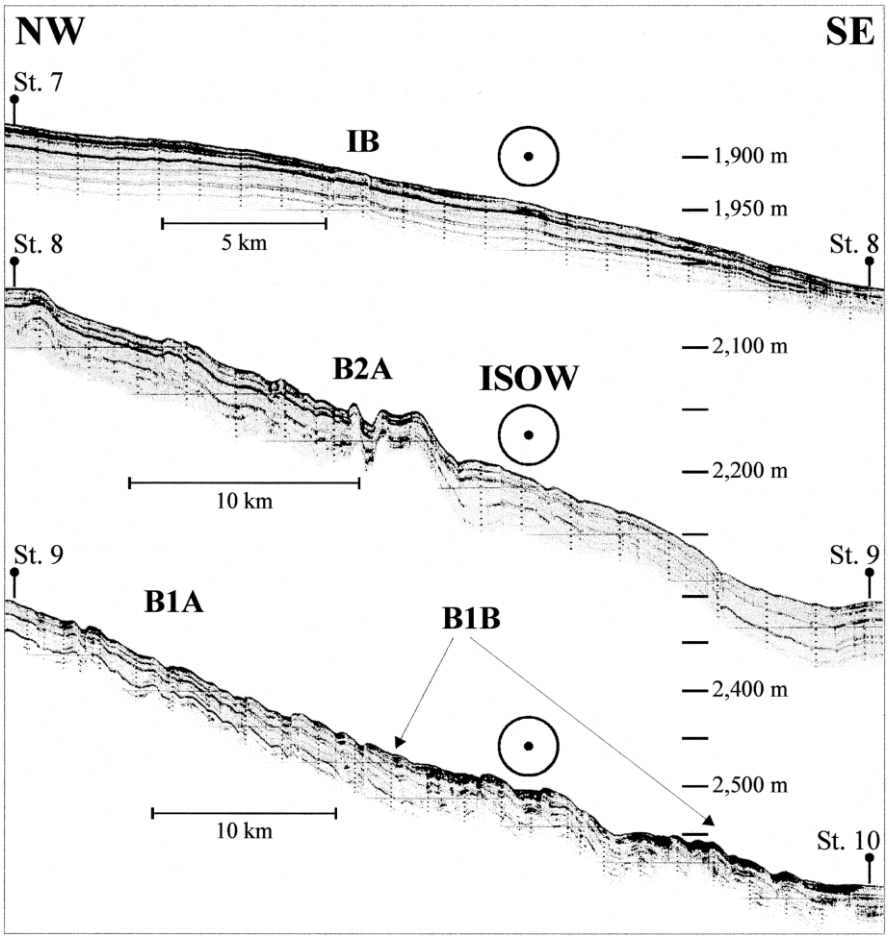

Figure 5.2 A transect of echo-types of the Gardar drift showing different sedimentary forms. (BIB) regular migratory sediment waves. (BIA) regular non migratory sediment waves. (B2A) irregular non migratory sediment waves. (IB) flat sea bed. ISOW (Iceland Scotland Overflow Water). From Bianchi & McCave (2000)

Sedimentation rates for the Gardar drift at typically 10-20cm ka^{-1} but reaching maximum rate in excess of 100 cm ka^{-1}. Holocene sedimentation rates are recorded as

5- 40cm ka^{-1} (Bianchii & McCave, 2000). As previously discussed, sedimentation is dominated by material transported by the Iceland Scotland Overflow Water (ISOW) principally from Iceland and Northwest Europe. Jansen *et al.* (1996) from reports of ODP Leg 162 from the Gardar drift, record that the sediments contain laterally continuous reflectors throughout. These reflectors are thought to be the result of alternate glacial and interglacial conditions. Bianchi and McCave (2000) report that the eastern flank of the drift, which lies under the most intensive flow of the ISOW, exhibits stronger and more closely spaced subsurface and surface reflectors than the western flank.

The maximum sedimentation rates, as inferred from the spacing of internal reflectors, occur a few kilometres west of the ridge crest. They further divide the sediment regimes on the Gardar Drift into two areas; north and south of 58º30'N. The sediments to the north are highly terrigenous, with high levels of sortable silt. This is attributed to the strength of the near bottom current flow in this region and the proximity to the sediment source. The sediments south of 58º30'N have lower levels of terrigenous material and sortable silt attributed to a slower near-bottom current. The main flow of the ISOW current runs over the Björnsson Drift at these latitudes. The southern section of the Gardar drift also lacks the differences in sedimentation between the east and west sides of the ridge exhibited in the northern section.

Two marine sediment cores were analysed in this study, MD99-2251 (57°26.87' 027°54.47') and MD99-2252 (57°26.84' 027°55.83') (Figure 5.3). Both cores were collected as part of Leg 2 of the IMAGES V cruise on July 21st 1999. Marine sediment core MD99-2252 is a Karsten core recovered in 2610m water depth. The core consists of a slab from which 10 sections were recovered to be processed in Cambridge. MD99-2251 is a 36.58 m Calypso core recovered in 2620m water depth. On recovery it was cut into 1.5m sections onboard and labelled but not described. Twenty-five sections were recovered, twenty-four of 1.5m and the final section of 58cm. All sections were reported to be in good condition. Both archive and working halves were sent to Gif-sur-Yvette. U-channel sections were made on all working half sections, also to be processed at Gif-sur-Yvette. In addition, several bags of sediment were recovered for core MD99-22521 2 tops, 1 core cutter and 1 core catcher (Images V Leg 2 cruise report, 1999).

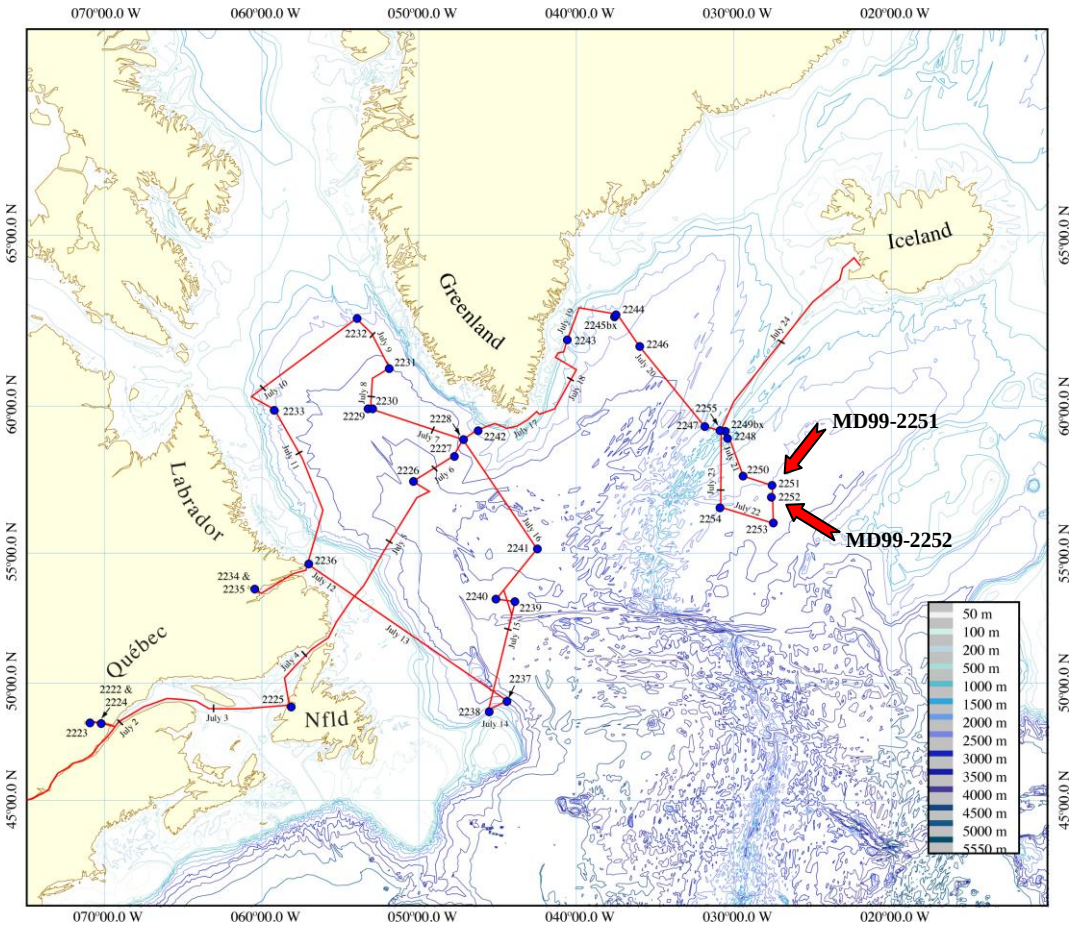

Figure 5.3 The route and core sites of RV Marion Dufresne IMAGES V Leg 2 (June 20th – July 24th 1999). Blue circles indicate the core sites. (Cruise report Images V Leg 2 1999)

Measurements of whole core physical properties for marine core MD99-2251 were undertaken in 1.5m core sections onboard using a Geotek MultiSensor Track (MST) at a down core resolution of 2cm. These measurements include magnetic susceptibility, gamma ray attenuation and p-wave measurements (Figure 5.4). Magnetic susceptibility values varied from 50 to 250 x 10^{-5}SI. Gamma ray attenuation is used to measure the bulk density of the sediment. Bulk density values varied from about 1.35 to 1.55 Mg/m^3 P-wave travel time is measured to calculate the thickness of the sediment, p-wave velocities values ranged from 1475 to 1500 m/sec. In addition split core sections were measured with a spectrophotometer. Spectral reflectance can be used to identify detrital carbonate. Split sections were also logged with respect to sediment texture, biogenic sediment components, laminations and other sedimentary structures (Cruise report Images V Leg 2, 1999).

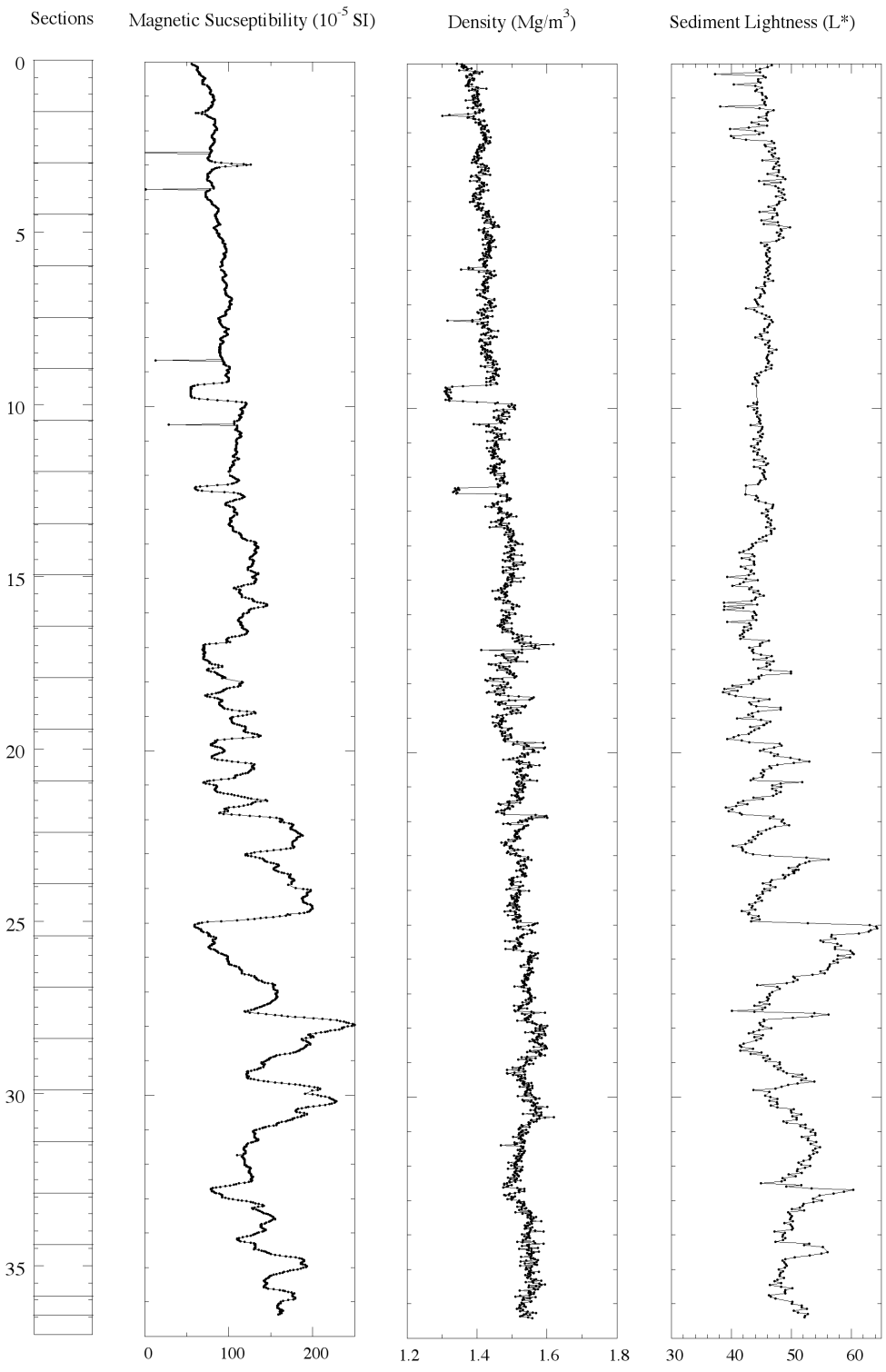

Figure 5.4 Whole core physical properties of MD99-2251 including magnetic susceptibility, density (Mg/m^3) and sediment lightness. (Cruise report Images V Leg 2, 1999).

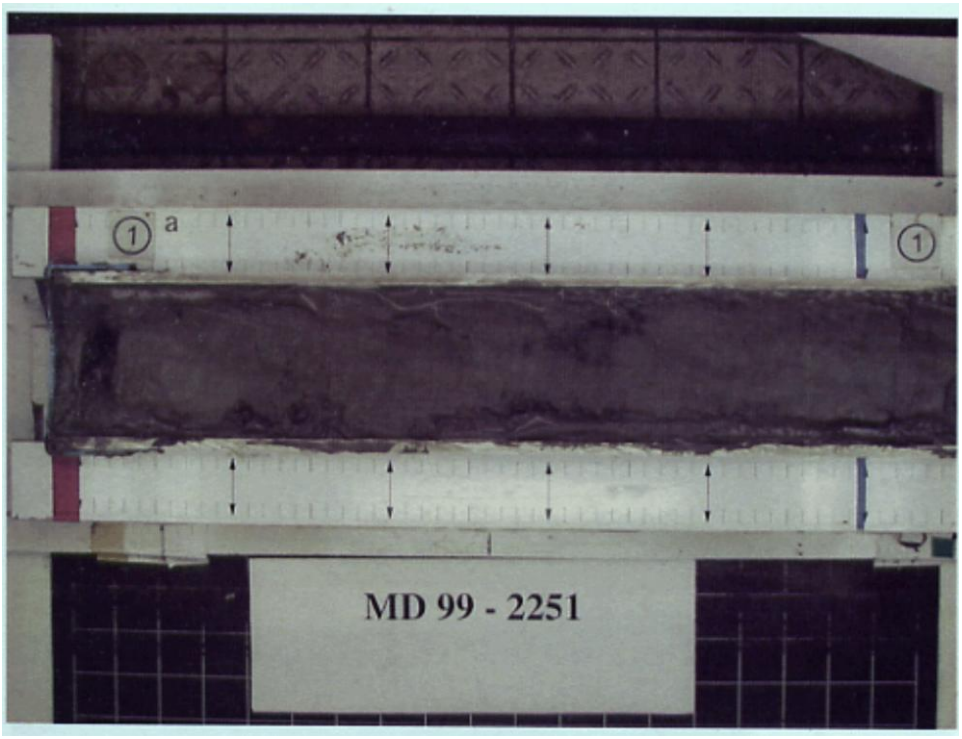

Figure 5.5 On board photograph of core top section 1a of core MD99-2251 (Ellison, 2006)

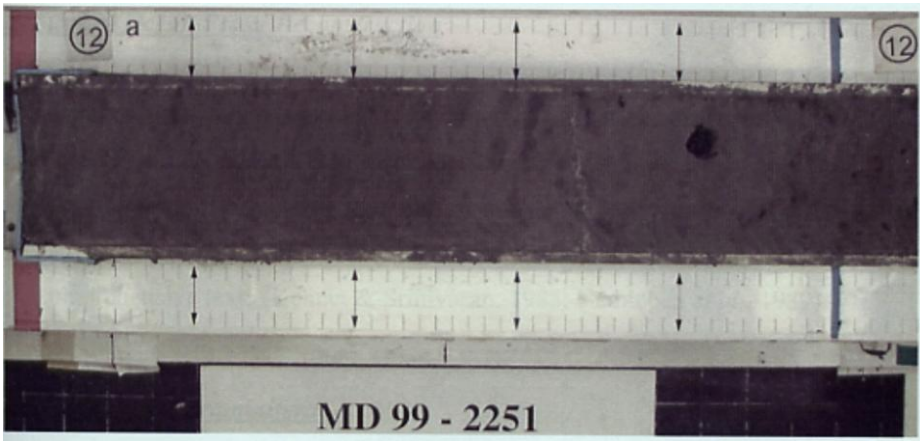

Figure 5.6 Shipboard photograph of section 12a from 1644-1649cm (left to right) indicating colour change across the Holocene-deglacial boundary (Ellison, 2006)

Two core breaks were identified in marine core MD99-2251 during sampling for foraminferal anaylsis at around 940cm and 1230cm. The breaks occurred during core recovery and polystyrene blocks were used to fill the gaps to prevent slippage of the sediment (Ellison *et al.*, 2006). Both breaks are sharp, showing no apparent disturbance in the sedimentation or loss of core material. These breaks may be identified in the magnetic susceptibly, bulk density and p-wave data (Figure 5.4). Sediment sampled for diatom analysis was taken from the U-channels. The U channels are samples taken from the centre of the core with a $2cm^2$ cross section. Breaks in sediment were recorded at 936-984cm and at 1934-1954cm. For the purpose of presentation on of the data in this study, composite depth is recorded. That is depth excluding the breaks. Ellison *et al.*, (2006) notes that there is a robust linear correlation of the AMS ^{14}C dates show either side of the core break, indicating no significant in flow or disruption to the sediment at the point of breaking. However samples were not taken for diatom analysis directly adjacent to the core breaks as a further precaution against contamination.

Sediment breaks in Calypso cores are not uncommon. The Calypso corer is a simple non recoilless piston corer, particularly used for recovering very long cores. These corers maintain a piston inside the core barrel in order to counteract the frictional drag between the sediment core and the core barrel with relatively low pressure above the sediment column (Skinner & McCave, 2003). These corers can suffer from negative pressure anomalies inside the core barrel due to cable recoil when pressure on the cable is suddenly released, such as when the corer hits the sea bed. This usually results in sediments being over sampled as the net upward negative pressure causes suction on the sediments being sampled (Figure 5.7). Magnetic susceptibility analysis may be used to detect this over sampling (Thouveny *et al.*, 2000). Negative pressure anomalies can also cause breakages within the sediment in the core barrel as seen in MD99-2251. The Kasten coring process such as for MD99-2252 may cause sediments to be subject sediment thinning (Figure 5.5).

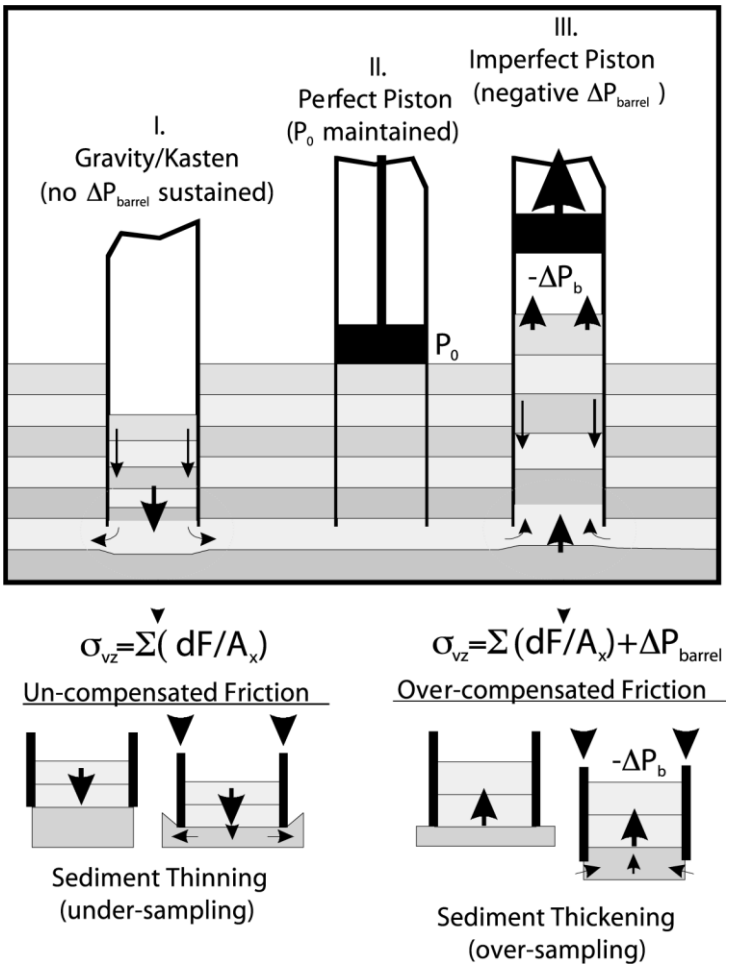

Figure 5.7 Possible over sampling and under sampling scenarios due to coring (Skinner & McCave, 2003)

5.2 Age Models for MD99-2251 and MD99-2252

Marine cores MD99-2251 and MD99-2252 were both dated using Accelerator Mass Spectrometry (AMS) radiocarbon (^{14}C) dates. Thirty monospecific samples of marine calcium carbonate were analysed for MD99-2251. Twenty-eight samples of *Globigerina bulloides* were analysed and two samples of *Neogloboquadrina pachyderma (*sinistral*)* (Ellison *et al.*, 2006). AMS radiocarbon ages obtained using marine calcium carbonate must be calibrated with respect to variations in the ^{14}C content of the ocean reservoir. When carbon dioxide is absorbed into the oceans, fractionation occurs leading to a $15^{o}/_{oo}$ enrichment in ^{14}C activity with respect to the atmosphere. This is the equivalent of approximately 120 years in the age of the sample (Bradley, 1999).

In addition to the effects of fractionation, corrections must be made for marine carbonate-derived radiocarbon dates with respect to geographic location. ^{14}C in the surface ocean varies with the extent of mixing of ^{14}C depleted water with surface waters (Bard *et al.*, 1988). At low latitudes around 400 years must be added to the age of radiocarbon dates derived from marine calcium carbonate to account for this effect of mixing with ^{14}C-depleted waters. At high latitudes the correction may be greater due to the effects of upwelling and sea ice. Sea ice restricts the ocean atmosphere exchanges. The North Atlantic however differs from other high latitude sites as relatively ^{14}C-enriched warm water and deepwater formation restrict the extent of the upwelling of ^{14}C-depleted waters. This gives the modern North Atlantic a reservoir correction similar to that of low latitude surface waters of around 400 yrs. Due to this influence of deepwater formation on ^{14}C radiocarbon ages in the North Atlantic, palaeoceanographic studies must also take into account variations in deepwater formation over time. Bard *et al.*(1994) and Austin *et al.* (1995) compared marine and terrestrial ^{14}C-derived dates associated with the Vedde ash, a definable layer of volcanic ash resulting from a volcanic eruption in Iceland at approximately 10,300 ^{14}C yr BP. They discovered that the marine ^{14}C ages indicated a reservoir effect of 700 yrs which they conclude is the result of reduced deepwater formation at the time of the Vedde ash deposition, or increased sea ice cover.

Given the above consideration in marine calcium carbonate derived AMS ages, radiocarbon dates still need to be calibrated to give calendar ages. This is due to the fact

that levels of atmospheric ^{14}C have varied over time (deVries, 1958). This variation is a result of variation in cosmic ray flux. Cosmic ray flux varies as a result of interstellar modulation, cosmic ray bursts from super novae and other stellar phenomenon, variations on solar activity, changes in the earth's geomagnetic field and nuclear weapons testing. Calibrations sets have therefore been developed to take into account these atmospheric variations (Reimer *et al*., 2002; Reimer *et al*., 2004; Hughen et al. 2004) based on tree ring chronologies, coral and varved sediments. The calendar ages in this study have been calibrated using CALIB5.

Radiocarbon ages are statements of probability (Bradley, 1999) as they reflect the fact that a particular number of radioactive disintegrations will occur in a given time period. As a result radiocarbon dates are given as midpoints on a Poisson distribution probability curve with error bars of plus or minus one or two standard deviations from the mean. The calibrated calendar ages plus of minus two standard deviations (σ) are indicated for MD99-2251 (Table 5.1and Figure 5.8) and MD99-2252 (Table 5.2 and Figure 5.9)

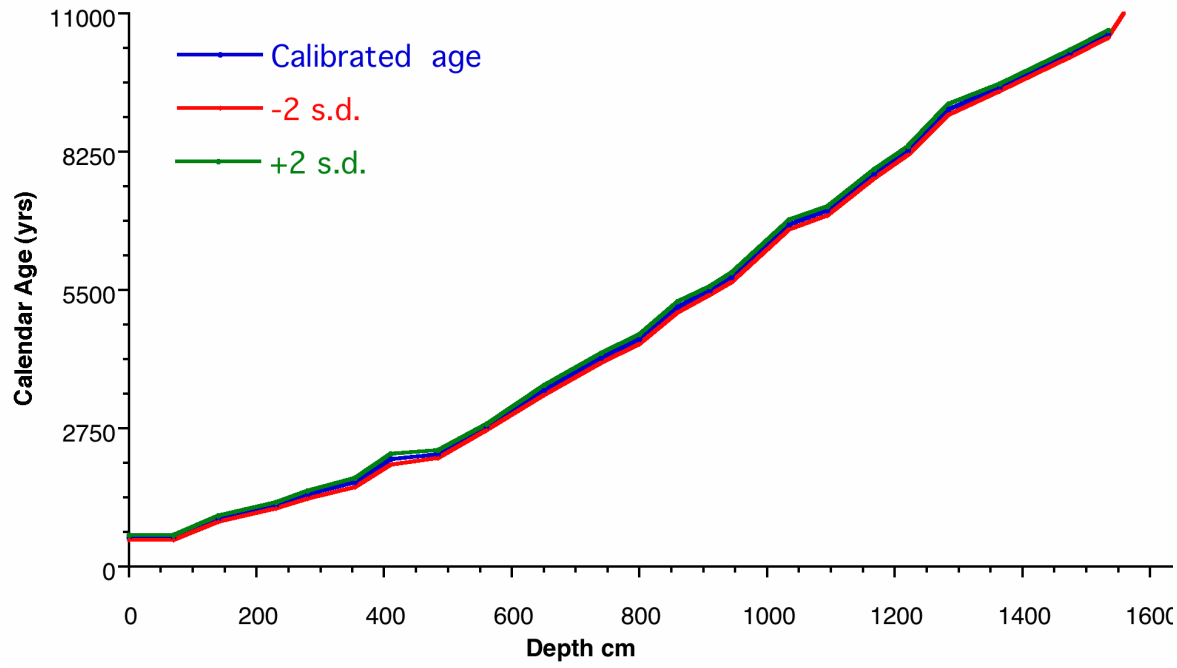

Figure 5.8 Calibrated calendar ages plus or minus two standard deviations for marine carbonate derived AMS ages for MD99-2251 Ellison *et al.*, 2006).

Laboratory Code	Depth (cm)	^{14}C date yr	Standard deviation	Calib5 midpoint age	-2sigma	+2sigma
SUERC-3063	0	991	21	578	526	630
SUERC-3067	70	1006	18	587	537	637
SUERC-3068	40	1403	21	959	896	1022
SUERC-3069	230	1666	24	1224	1166	1282
SUERC-5178	280	1888	25	1433	1354	1512
SUERC-5179	354	2094	23	1675	1581	1768
SUERC-3070	410	2469	24	2138	2024	2251
SUERC-5182	484	2576	25	2240	2156	2323
SUERC-3071	560	2995	24	2774	2714	2833
SUERC-5183	650	3615	30	3514	3419	3609
SUERC-3072	740	4100	22	4151	4061	4241
SUERC-5184	800	4386	22	4525	4428	4621
SUERC-3076	860	4864	22	5166	5058	5273
SUERC-5185	910	5109	24	5485	5399	5570
SUERC-5186	944	5385	28	5759	5659	5859
SUERC-3079	1034	6341	31	6807	6709	6905
SUERC-5188	1094	6567	27	7078	6984	7171
SUERC-5189	1168	7340	26	7810	7720	7900
SUERC-5192	1220	7815	35	8275	8187	8362
SUERC-3082	1284	8474	27	9102	8995	9209
SUERC-3086	1364	8868	30	9526	9455	9596
SUERC-3087	1474	9365	34	10212	10139	10285
SUERC-5193	1534	9737	31	10596	10520	10671
	1590				11600*	
	1604				12500*	

Table 5.1 Calibrated calendar ages plus or minus two standard deviations for marine carbonate derived AMS ages for MD99-2251 (Ellison *et al.*, 2006). * The transition into the Younger Dryas stadial event was assigned ages derived from longer counts of Greenland ice cores (Alley *et al.* 1997)

5.3 Core sampling strategies

Based on these reconstructions samples were selected to provide decadal records around the 8.2kyr event and at approximately every 250 years through the remainder of the Holocene in order to detect long term trends. Marine core MD99-2251 was specifically sampled at 2cm intervals between depths 1200-1336cm corresponding to ages of approximately 7600-8750yrs and at 1cm intervals between depths 1274-1318cms corresponding to ages of approximately 8100-8550yrs. The core was further sampled at 2cm intervals between1645-1675cm corresponding to ages of approximately 11300-12500 yrs to study the transition into the Younger Dryas. For the reminder of the Holocene samples were taken at depth corresponding to approximately 250 year intervals (Table 5.3).

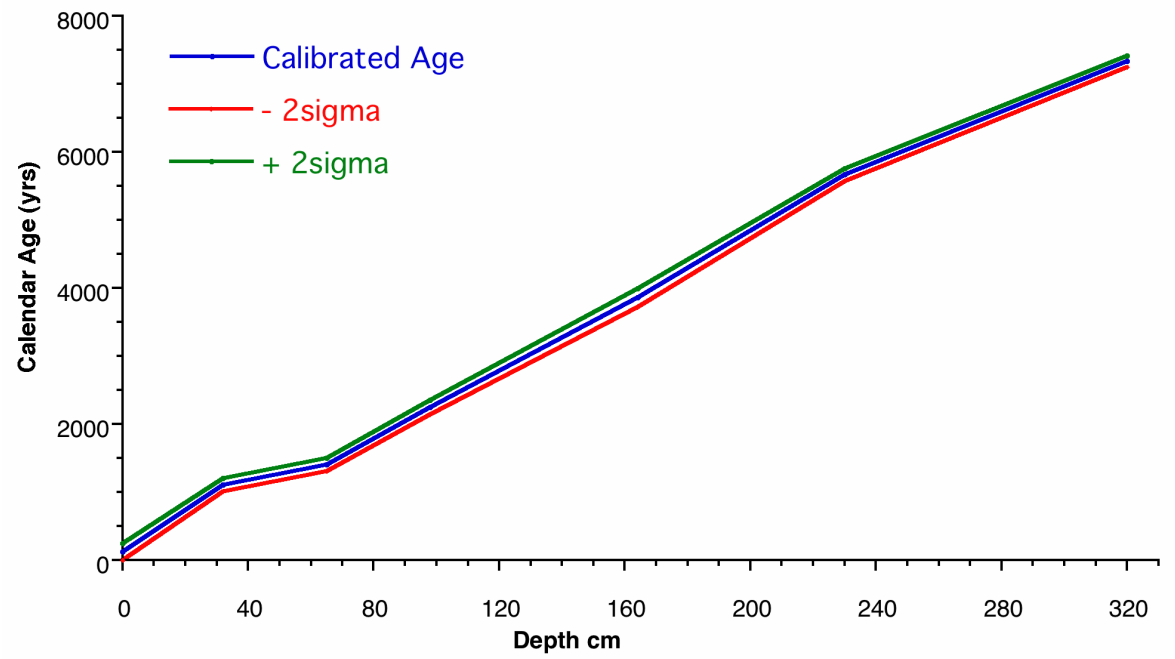

Figure 5.9 Calibrated calendar ages plus or minus two standard deviations for marine carbonate derived AMS ages for MD99-2252 (Dr M.Chapman personal communication).

Lab Code	Depth (cm)	^{14}C date yr	Standard deviation	Calib5 midpoint age	-2sigma	+2sigma
KIA9189	0	510	30	123	0	246
KIA9805	32	1550	30	1107.5	1010	1205
KIA9806	65	1855	35	1403	1308	1498
KIA9807	98	2595	40	2245.5	2141	2350
KIA9808	164	3900	40	3860	3725	3995
KIA9809	230	5305	40	5666.5	5573	5760
KIA9190	320	6815	45	7334	7249	7419

Table 5.2 Calibrated calendar ages plus or minus two standard deviations for marine carbonate derived AMS ages for MD99-2252 (Dr M.Chapman personal communication).

For marine core MD99-22521, diatom abundance counts were made at each of these depths, a total of 132 samples. In addition counts of Ice Rafted Debris abundance and lithology were taken at 2cm intervals between depths1200-1284cm corresponding to ages of approximately 7600-8200yrs and at 1cm intervals between depths 1984-1336cm, corresponding to ages of approximately 8200-8850yrs; total of 76 samples.

Marine core MD99-2252 was sampled at 8cm intervals for the entire core length of 0-336cm, corresponding to ages of 0-7200yrs, thus giving a mean resolution of around 180 years per sample. Diatom abundance counts were made for each sample, a total of 40 samples. MD99-2252 was further sampled at 2cm intervals,a total of 164 samples, for the planktonic foraminiferas *Globigerina bulloides* and *Neogloboquadrina pachyderma* dextral which were analysed for oxygen and carbon isotope analysis.

Age (yrs)	Composite Depth (cm)	Original depth(cm)
558	0	0.0
600	71.6184971	71.6
850	122.196532	122.2
1100	189.256757	189.3
1350	261.868132	261.9
1600	330.996255	331.0
1850	375.748837	375.7
2100	408.306977	408.3
2350	494.482759	494.5
2600	535.431035	535.4
2850	572.211669	572.2
3100	602.740841	602.7
3350	633.270014	633.3
3600	665.59816	665.6
3850	700.107362	700.1
4100	734.616565	734.6
4350	773.492064	773.5
4600	807.104137	807.1
4850	828.50214	828.5
5100	849.900143	849.9
5350	886.612903	886.6
5600	927	927.0
5850	953.923954	999.9
6100	975.311787	1021.3
6350	996.69962	1042.7
6600	1018.08745	1064.1
6850	1046.75748	1092.8
7100	1095.37822	1141.4
7350	1121.88252	1167.9
7600	1148.38682	1194.4
7850	1174.65354	1220.7
8100	1200.24409	1266.2
8350	1225.57798	1291.6
8600	1250.04281	1316.0
8850	1274.50765	1340.5
9100	1308.82759	1374.8
9350	1349.39554	1415.4
9600	1393.33333	1459.3
9850	1439.16667	1505.2
10100	1486.28669	1552.3
10350	1534.75138	1600.8
10600	1545.80111	1611.8
10850	1556.85083	1622.9
11100	1567.90055	1633.9
11350	1578.95028	1645.0
11600	1590	1656.0

Table 5.3 Sampling strategy for marine core MD99-2251 in order to produce a Holocene overview at least 250 year resolution

Chapter Six

Diatom Assemblage Data

"The scientific members of the expedition were busy all the time. The geologist was making the best of what to him was an unhappy situation, but not altogether without material. The pebbles found in the penguins were often of considerable interest... Clark was using the drag net frequently and secured good hauls of plankton, with occasion specimens of greater scientific interest..."

Earnest Shackleton 'South'

Chapter Six: Diatom Assemblage Data

6.1 Introduction

When considering the sampled data it is important to examine certain issues; the methods of sample preparation and whether they add any bias to the sample, the data sampling strategies adopted and their statistical reliability and repeatability. In the case of a fossil assemblage data it is also important to address issues of taphonomy. Having obtained the raw sampled data it is then necessary to assess the nature of the statistical analyses and palaeoproxies used, their inherent presuppositions and any biases.

A number of different approaches to diatom sample preparation and their limitations are considered in this chapter (section 6.2.1), the sample preparation methodology adopted in this study is outlined (section 6.2.2). The nature of the data sampling is examined, both counting strategies (section 6.3.1) and their statistical reliability (section 6.3.2). Issues of fossil assemblage preservation are addressed (section 6.4) and the nature of the transfer functions adopted (section 6.5). Results are presented of a Holocene overview (section 6.6.1) and a high resolution study of the 8.2kyr event (section 6.6.2) from marine core MD99-2251. Results are then presented for the adjacent marine core MD99-2252 which extends through the middle and late Holocene (section 6.6.3). Finally there is a consideration of analyses relating diatom floral assemblages to water mass distribution (section 6.7.1) and their application to the data from this study (section 6.7.2).

6.2 Sample Preparation

6.2.1 Methods of sample preparation

A number of different methods have been developed for the preparation of core samples for the examination of diatom populations. Although these methods vary in their specifics, they all require that carbonates, organic material and clay be removed from the mud sample while the silt size silica frustules of the diatoms are retained. Having removed these

other materials, samples are then mounted on glass slides so that the diatoms may be examined under an optical microscope.

The first methodology for cleaning diatoms was published by Kanaya & Koizumi (1966). This involved the use of HCL to remove carbonates and H_2O_2 to remove organic material from a dried sample of known weight. Clay particles are removed by washing and fractionation. This methodology was widely adopted (Schrader & Schuette, 1968; Schrader, 1973a, Schrader & Gersonde, 1978; Zhute-Mukhina 1978). While the methodology for the removal of carbonates and organic material remains largely unchanged in more recent publications, the approach to removing clays varies considerably. This is a function of the labour intensive and prolonged nature of this final stage. Many attempts have been made to decrease the length of time required for clay removal while not compromising the representative integrity of the sample. Abrantes *et al.* (2005) review seven different methods of diatom cleaning, the Abrantes (1988) method and six modifications of the Baron (1985) method for rapid sample preparation at sea. The methods variously use a 0.5% sodium pyrophosphate solution, distilled water washing, centrifuging and decanting for the removal of clay minerals. They assess the different preparation methods by statistically comparing the numbers centric, pennate, centric fragments, pennate fragments and *Chaetoceros* resting spores found in each sample and conclude that there is no significant difference in the methods except with respect to the concentration *Chaetoceros* resting spores, which increases where centrifuging was employed for the removal of clays. This is assumed to be the result of the destruction of more fragile pennate forms from the centrifuging increasing the relative abundance of the more robust *Chaetoceros* resting spores. The authors conclude therefore that a methodology avoiding centrifuging is the most effective. They further note that dispersal of the sample prior to the removal of carbonate and organic material results in a cleaner sample. The samples in this study are dispersed with heptane, prior to the removal of carbonate or organic material.

A study of the effect of four different stages of the diatom cleaning process; the amount of hydrogen peroxide used, the time allowed for digestion reaction, centrifuging and the method of settling frustules onto the cover slide, on the density, randomness and evenness of frustule distribution, the amounts of organic and inorganic material and the

quantity of broken frustules and girdle viewed forms on the microscope slide, was undertaken by Blanco *et al.* (2008). They concluded that increasing the quantity of hydrogen peroxide made no difference to the measured parameters beyond a ratio of 1:1 and an oxidizing reaction time of six hours. The authors also found that none of the variables, including centrifuging, made a significant difference to the proportion of broken frustules.

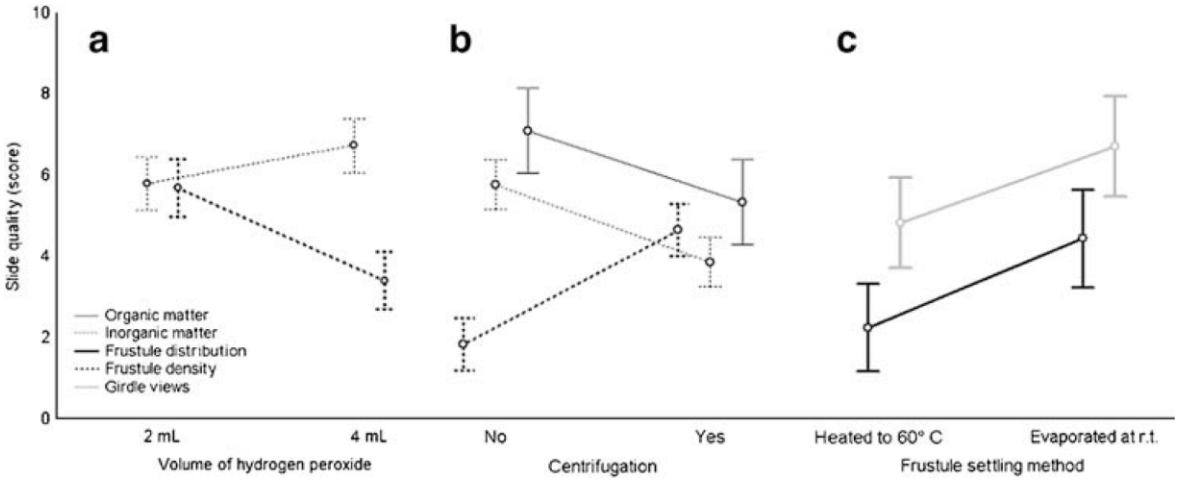

Figure 6.1 The effect of a) Volume of hydrogen peroxide b) centrifuging and c) the frustules settling method on slide quality. Blanco *et al.* (2008)

This result contradicts Battarbee *et al.* (2001) and Abrantes *et al.* (2005) but supports earlier research (Owen *et al.*, 1978), that centrifuging does not increase the proportion of frustule fragments. Blanco *et al.* (2008) do note however that the quality of the slide increased when decanting rather than centrifuging was used to remove clays, as there was an overall decrease in the concentrations of organic and inorganic material on slides where samples had been decanted (Figure 6.1). In a study of frustule breakage, Flowers (1993) attributes the presence of carbonate particles in a sample as a key cause of frustule fragmentation. Blanco *et al.* (2008) agree with Abrantes *et al.* (2005) that centrifuging increases frustule density on the slide. In the methodology outlined below and employed in this study, samples are both centrifuged and decanted for the removal of clays.

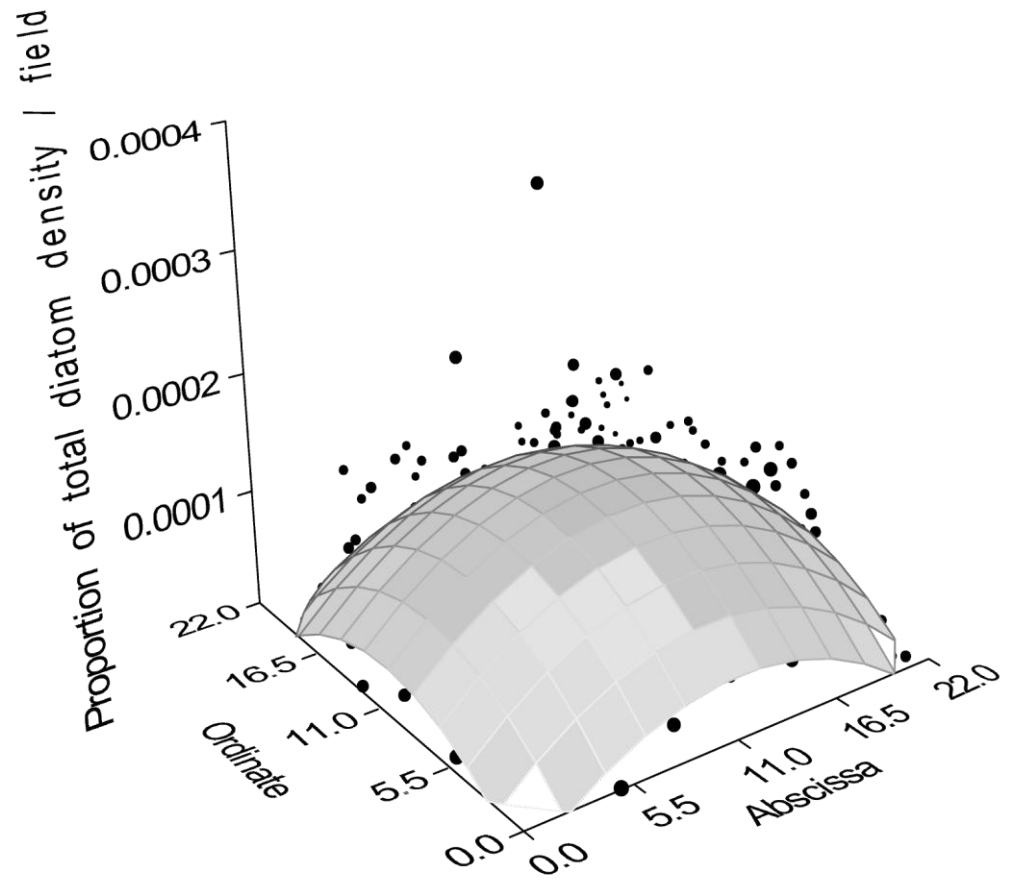

Figure 6.2 The modelled distribution of diatom frustules on a 22mm x 22mm cover slide. (The density was calculated by dividing the number of cells in a given field by the estimated total number of cells on the slide.) Alverson *et al.* (2003)

A number of different methods are employed to settle samples onto cover slides. A known volume of frustule suspension placed on a cover slide may be evaporated at room temperature, or by heating at a low temperature (Blanco *et al.*, 2008). Studies have shown that when diatoms are dried on a cover slide that the distribution of frustules is non random due to the surface tension (Battarbee, 1973). Alverson *et al.* (2003) demonstrate that frustule density is greatest at the margins of the slide (Figure 6.2). Evaporation over a low heat has been demonstrated to result in size sorting and clumping as a result of convection currents created in the suspension (Schraeder, 1974; McBride, 1988). Air-dried cover slides exhibited the least disturbance in the study undertaken by Bianco *et al.* (2008). In this study frustule were settled on to three cover slides placed in a Petri dish and Kodak photoflo added to the suspension to minimise the effects of surface tension on frustule distribution.

6.2.2 Methodology for preparation of core samples in this study

Mud samples were placed in labelled foil trays and then into an oven at 50-60˚C overnight to dry. They were then removed from the oven and placed in a desiccator for 15 minutes in order for them to fully dry. The tray and samples were then weighed before the samples were transferred into dry clean labelled 100ml beakers. The foil trays were then reweighed in order to calculate the dry weight of the sample, which was then noted. In order to disaggregate the samples, approximately 10ml of heptane was added to each sample in a fume chamber and left to stand for 10-15 minutes. Warmed distilled water was then added to the beakers to a total volume of 25ml and the beakers returned to the hotplate and heated until all the heptane had evaporated. The samples are then left to stand and cool.

Carbonates were removed from the samples by adding 10 drops of 36-38‰ HCl to each beaker in the fume chamber, stirring and leaving to stand for 15-20 minutes. If after 15-20 minutes the sample was still showing signs of reaction, two more drops of HCl were added and the sample was left until no further reaction was noted. In a similar manner the organic matter is then removed from the samples by adding 10 drops of H_2O_2 to each beakers and returning the samples to hotplate at approx for approximately 15-20 minutes until sample turns yellow or yellow/green. The samples were then removed from hotplate and allowed to stand to cool.

The samples were then transferred to 15ml centrifuge tubes, using a separate pipette tip for each sample to avoid contamination, and placed in the centrifuge for three minutes at 2000rpm. After centrifuging the suspension was decanted off each sample and the centrifuge tube refilled from the original 100ml beaker. This process was repeated until the whole sample from the 100ml beaker had been centrifuged. The samples were then centrifuged a number of additional times using distilled water to top up the centrifuge tube and in order to ensure the removal of further clays.

At this point in the process, samples may be transferred to small labelled glass bottles for storage. For additional removal of clays the samples were then poured into 1000ml glass beakers which were filled to 400-500ml of distilled water, covered and left to settle

either all day or overnight. The clay suspension was decanted off and the process repeated four to five times until the samples were clean of clays. The sample is then centrifuged and decanted again and returned to the small glass bottles.

In order to make slides, rectangular slide covers are first coated in a mixture of gelatine distilled water and Kodak Photoflo to ensure the diatoms stick to and are evenly distributed across the cover slide. This coating is allowed to dry on the cover slips on the hotplate. For each sample a 100ml beaker was labelled and filled with approx 25ml of distilled water. Using a precision pipette 100µm of the bottled sample were added at a time to the beaker containing 25ml of distilled water for each sample: 100µm, 200µm or 300µm until the mixture appeared cloudy. Then using one labelled petri dish for each sample, three cover slides were stuck to the base of the dish by one drop of distilled water. The whole cloudy mixture was then pored over the Petri dish with cover slides and left to stand for 2 hours. This allows three slides to be prepared for each sample. After two hours the excess liquid was removed using a paper towel wick which was allowed to drain over the edge of the bench.

Once fully dry the coated cover slides were transferred to hotplate in the fume chamber with the coated side facing upwards. At the same time the glass slides were also placed on the hotplate to warm. A small quantity of naphrax optical fixative was added to the top of each cover slide and allowed to warm but not bubble. The glass slides were then placed on the cover slide and naphrax and using protective gloves the slides and cover slide picked up and using tweezers pressed until the naphrax had spread evenly over the whole cover slide area. The slides were then returned to the hotplate for around 30 minutes to allow the naphrax to cook and harden. The slides were then removed from the heat and allowed to harden for couple of hours across two glass rods.

6.3 Data Sampling

6.3.1 Counting strategies

Using oil emersion phase contrast lenses, transects of each slide were counted to a total of 300 whole valves per sample, excluding *Chaetoceros* frustules. The number of transects or part transects required to reach 300 valves was noted. The protocol for the counting of valves and half valves is outlined in Figure 3

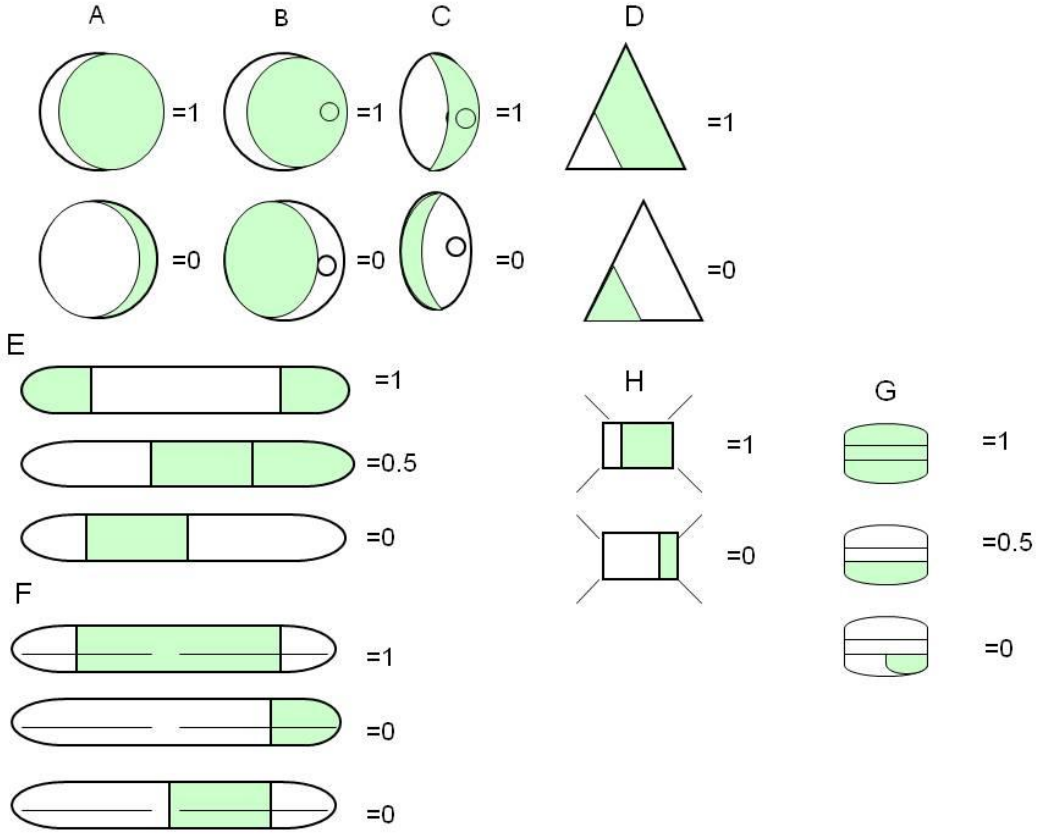

Figure 6.3 Counting conventions for whole and partial valves. Shaded areas indicate the portion of the frustule found in the slide. A. circular centric diatoms (eg *Thalassiosira*) B. circular centric diatoms with a pseudonodulus (eg *Actinocyclus*) C. non circular centric diatoms with a pseudonodulus (eg *Hemidiscus*) D. angular centric diatoms (eg *Triceratium*) E. araphid pennate diatoms (eg *Thalassionema*) F. pennate diatoms with raphes (eg *Diploneis*) G. resting spores of centrics diatoms (eg *Chaetoceros*) H. centric diatoms with filaments (eg *Chaetoceros*). After Shraeder & Gersonde (1978).

Alverson *et al.* (2003) assessed the variance of cell density, species composition and diversity for diatom samples counted from slide transects and nannoplankton chambers. They further compared slides counted of half transects, partial transects and random fields. They found very low variability between the counting methods for all three measured parameters.

6.3.2 Reproducibility studies

In order to test the reliability of counting three hundred valves to produce a representatively diverse sample of the diatom flora, 50, then 100, then 150, 200, 250, 300 and 350 valves were counted for the sample 2289-2290cm depth from MD99-2251 and the percentage of key species calculated for each count size. The total number of different species for each of these sample count sizes was also recorded in order to identify whether a count of three hundred valves is sufficient to include more rare species (Table 6.1).

	50	100	150	200	250	300	350
T.longissima	3.5	3.1	3.2	3.2	2.5	2.8	2.6
R.h.hebetata	1.8	4.5	3.2	2.9	2.3	2.0	4.4
R.h.semispina	10.6	11.6	12.7	11.7	10.9	11.8	12.2
R.styliformis	12.3	12.5	14.6	13.7	15.2	16.0	12.3
R.bergonii	0	3.6	3.2	3.4	2.3	1.9	1.7
P.alata	0	3.6	2.5	2.4	2.3	2.0	1.7
T.gravida veg	7.1	3.6	6.3	8.3	7.0	6.9	6.3
T.gravida spore	5.3	3.6	3.2	3.4	3.1	2.9	3.4
T.eccentrica	3.5	1.7	1.3	0.9	1.5	1.6	1.7
T.oestrupii	42.5	42.9	39.3	40	39.8	39.9	39.1
A.curvatulus	1.7	0.9	1.9	2.4	2.7	2.9	3.1
C.marginatus	0	0.9	1.2	1.5	1.6	1.6	1.4
Total no species	15	18	21	22	22	23	24

Table 6.1 Indicating the percentage abundance of twelve key species at sample count sizes of 50, 100, 150, 200, 250, 300 and 350 valves for sample MD99-2251 2289-2290cm.

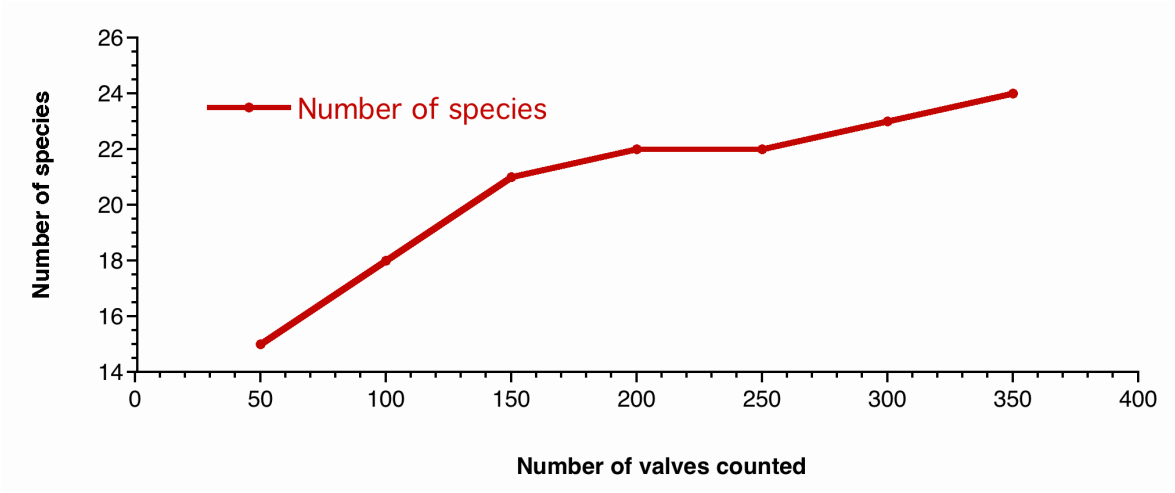

Figure 6.4 The number of species found in progressive counts of 50, 100, 150, 200, 250, 300 and 350 frustules.

MD99-2251 2289-2290	Slide One	Slide Two	Slide Three
T.longissima	2.78	3.0	4.0
R.h.hebetata	1.96	2.33	1.67
R.h.semispina	11.76	12.0	15.0
R.styliformis	16.01	11.67	11.67
R.bergonii	1.96	1.33	1.67
P.alata	4.58	1.33	1.67
T.gravida veg	6.86	5.33	6.33
T.gravida spore	2.94	4.0	6.33
T.eccentrica	1.63	3.67	2.67
T.oestrupii	39.87	45	39.67
A.curvatulus	2.94	3.33	5.67
C.marginatus	1.63	1.33	1.67

Table 6.2 Relative percentage abundance of twelve key species from counts of three separate slides from sample MD99-2251 2289-2290

As three slides are produced for each sample depth, all three samples were counted for sample 2289-2290cm depth from MD99-2251 to see if there were any significant differences between the three slides with regards to the percentage of thirteen key species (Table 7.2). Paired t-tests were used to analyse the similarity of the three counts and indicateded that there was no significant difference between the three counts (Table 6.3).

	t value	Degrees of freedom	Significance
Slide 1 and Slide 2	0.082	9	0.966
Slide 1 and Slide 3	0.043	9	0.89
Slide 2 and Slide 3	-0.142	9	0.937

Table 6.3 Paired t-test results for comparison of the three counted samples of 2289-2290cm. A significance value >0.05 indicates that there is no significant difference between the samples. The three slides therefore show a strong statistically significant similarity.

6.4 Taphonomy

Transfer functions make the basic assumption that the down core fossil assemblage represents the core top assemblage at the time of deposition of the fossil assemblage. There is some evidence however from lake studies that dissolution of the silica frustules of diatoms occurs within the sediment. This may result in a bias in favour of certain, usually more robust, species over time. Most of the quantitative work concerning diatom dissolution has been done with respect to lake sediments (Barker *et al.*, 1994; Battarbee *et al.*, 2005 Ryves *et al.*, 2006). Ryves *et al.* (2009) developed a methodology for assessing the extent of diatom dissolution under light microscope conditions that can be applied to transfer functions to improve interpretation. Taphonomic studies on marine diatoms assemblages (Johnson, 1974; Pichon *et al.*, 1992; Dixit *et al.*, 2001) indicate that a number of factors influence the extent of dissolution; temperature, pressure and the surface area and aluminium content of the diatom frustule. The inclusion of aluminate ions in the silica matrix decreases the solubility of biogenic silica (Dixit *et al.*, 2001). Pichon *et al.* (1992) developed a transfer function to quantify the extent of dissolution of biogenic in diatoms for Southern Ocean sediments.

6.5 Transfer Functions

6.5.1 Introduction to Transfer Functions

The first study to quantify the relationship between sea surface temperatures and palaeoassemblages was made by Imbrie and Kipp (1971) who studied foraminiferal assemblages in seventy-one core top samples from the Atlantic and Indian Ocean. The underlying presupposition of the transfer function method as applied in palaeoceanography is that a given species assemblage responded to the physical and chemical properties of the ocean in the same way in the past as it does in the present. Fossil assemblages may therefore be compared with modern core top assemblages in order to extrapolate past physical and chemical properties of the ocean at the time of the assemblage deposition. The Imbrie and Kipp (I&K) method employs a five step process; the counting of core top assemblages, the factor analysis of the core top data into recognised assemblages, a least squares analysis to produce palaeoecological equations which relate each of the recognised assemblages to observed oceanographic parameters, the description of down core fossil assemblages with respect to the core top assemblages and the use of the palaeoceological equations to extrapolate palaeoceanographic parameters. The five assemblages recognised were; tropical, subtropical, subpolar, polar and gyre margin, which relate to the large scale features of the ocean circulation.

Alternative methods for deriving oceanographic data from faunal assemblages include the Modern Analogue Technique (MAT) developed by Hutson (1980). This method compares the fossil assemblage with core top assemblages by using an index of faunal similarity. The fossil sample is compared to modern core tops and a subset of modern analogues identified which best represent the fossil assemblage. This subset is then used as an analogue for oceanographic parameters for the fossils sample. An average of different measured properties, such as temperature and salinity, is calculated for the subset, with a weighting factor giving more emphasis to those modern samples which are most similar to the fossil sample. This method is also therefore capable of generating confidence limits for the oceanographic data, based on the width of the range of the oceanographic variables within the subset. The MAT was further refined by Prell (1985) who used the method to evaluate the Climate: Long-range Investigation, Mapping, and Prediction (CLIMAP) sea

surface temperature reconstructions. He looked at different indices of similarity and concluded that the squared chord distance measure gave the most accurate results.

Waelbroeck *et al.* (1998) identified problems with both the I&K and the MAT approaches. They note a number of assumptions in both methods that may not reflect conditions in the real ocean. The I&K method assumes the different oceanographic parameters may be defined with respect to their relationship to the end member assemblages produced by factor analysis and that these parameters respond independently of each other. The MAT method imposes thresholds of dissimilarity and on the selection of the modern analogues and limits the number of analogues selected. In addition the method is not always able to find an analogue for the fossil sample, due to the incomplete nature of the original core top data set. The authors therefore propose the Revised Analogue Method (RAM) which differs from the MAT in the method of selection of analogues. RAM assumes that 'jumps' in the dissimilarity co-efficient may be interpreted as shifts between one ecological regime and another. Best analogues are chosen from those encountered before a 'jump'. This method showed improved reconstruction of modern SSTs but was less effective in reconstructing sea surface temperatures from cold palaeoenvironments.

The SIMMAX transfer function developed by Pflaumann *et al.* (1996) is based on 738 core top foraminiferal assemblage counts from the North and South Atlantic and the Levitus (1982) modern ocean temperature data, where temperatures were taken at 0m, 30m, 50m and 75m. The SIMMAX transfer function is a modern analogue technique with a similarity index. Sea surface temperatures are derived by taking an average of the ten best analogues and weighting these analogues with respect to their inverse geographic distance from the site of the sample. Unlike the RAM, the SIMMAX technique provides optimum performance when reconstructing SST estimates for high latitudes during glacial periods. SIMMAX-28 (Pflaumann *et al.*, 2003) further developed the transfer function by extending the number of modern analogues to 947, notably by the addition of cold samples from the Northern Hemisphere.

A comparison of the I&K, MAT, RAM and SIMMAX transfer functions with two Artificial Neural Network (ANN) techniques for estimating sea surface temperatures; ANN (Malmgren & Norlund, 1997) and ANND a modification of the ANN method using

additional geographical data, was undertaken by Malmgren *et al.* (2001). Artificial Neural Network techniques are computer systems with the ability to 'learn' target outcomes from a set of inputs, by a series of small adjustments of a set of internal parameters. A mathematical analysis of the different methods indicated that the I&K transfer function performed the most poorly, ANN and RAM performed better than MAT, but the most accurate estimates were from the SIMMAX and ANND methods which incorporated geographic data. However when the estimated SSTs were compared with a fossil data set and an independent validation data set, it was found that the SST estimates based on Artificial Neural Network techniques gave significantly different results to those produced by RAM, MAT and SIMMAX.

Evaluations of these different transfer functions have also been made by considering their statistical performance. This is usually measured as root mean square error of prediction (RMSEP). The RMSEP is the square root of the mean of the squared differences between the predicted and observed SSTs. A low RMSEP indicates that the transfer function is performing well as it indicates little difference between predicted and observed values. Telford *et al.* (2004) assess the RMSEP for the MAT, RAM , SIMMAX and ANN transfer functions. They argue that RMSEP values are under-estimated when they are calculated using a non independent test set. They conclude that RMSEP values calculated for SIMMAX and RAM are often artificially low as a result of this use of non independent test sets and that ANN does not given better SST estimates than MAT when independent test sets are employed. Telford & Birks (2005) further explore the issue of autocorrelation error in these transfer functions, that is, the tendency of adjacent sites to resemble one another more closely than those which are randomly selected. They argue that the true RMSEP for these transfer functions may be double previous estimates.

6.5.2 Diatom transfer functions

Diatom transfer functions have been used to reconstruct a wide range of ecological parameters other than sea surface temperatures: acidification in lakes (Holden *et al.*, 2008; Battarbee *et al.*, 2005; Battarbee, 2008) phosphorus content of lakes (Bennion *et al.*, 2005), salinity (Tibby *et al.*, 2007), sea level (Hill, 2007; Zong & Horton, 1999) and paleodepth (Campeau *et al.*, 1999). In the North Atlantic diatom transfer functions have been used to reconstruct sea ice concentration (Justwan & Koç, 2008) as well as sea surface temperatures (De Seve, 1999; Jiang *et al.*, 2001; Birks & Koç, 2002; Andersen *et al.*, 2004, Abrantes *et al.*, 2007; Berner *et al.*, 2008). The use of diatom assemblages to reconstruct sea surface temperatures can be considered preferable at high latitudes due to the tendency of foraminiferal assemblages to become monospecific as previously discussed. At high latitudes diatom floral assemblages remain diverse. Diatoms are present throughout the worlds oceans and dominate sediments in the Southern Oceans (Figure 6.5).

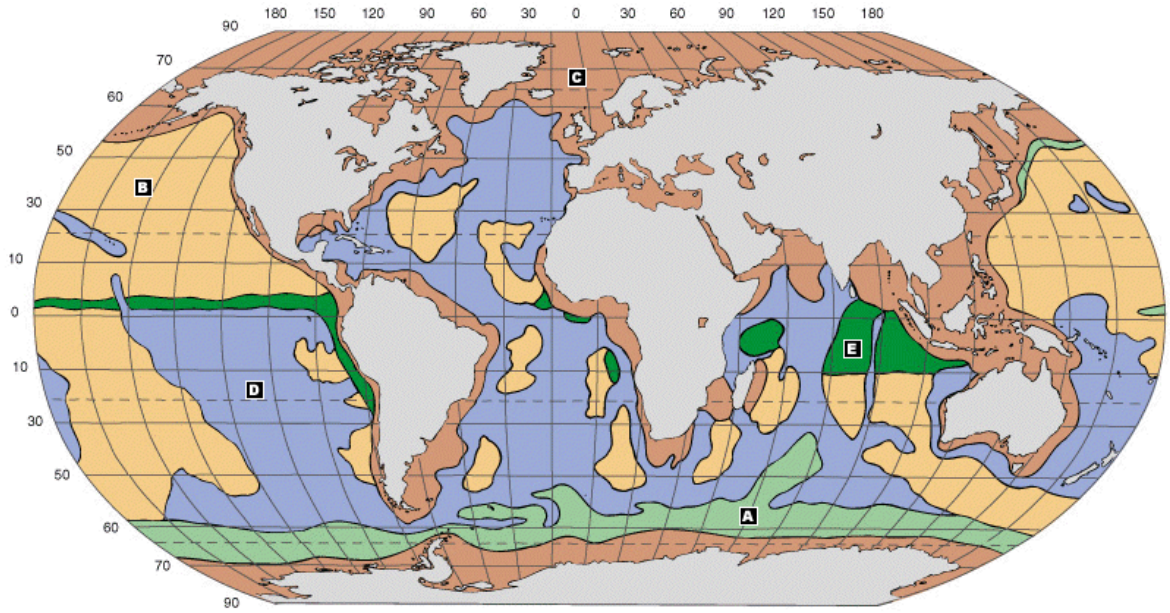

Figure 6.5 Distribution of dominant sediment types in the global oceans

A/E.Siliceous oozes (diatom and radiolarian) C. Red Clay
B.Terrigeneous sediments D..Calcareous oozes

A number of different types of transfer function have been used to derive sea surface temperatures from diatom assemblage data. Koç & Schrader (1990) derived the GINT2 transfer function, an Imbrie & Kipp Q-mode factor analysis, based on 104 core top samples from the Greenland Iceland Norwegian (GIN) Seas. The location, depth, diatom abundances and average February and August sea surface temperatures were recorded for each site. Six different assemblages were identified, each strongly reflecting surface water conditions; a Norwegian-Atlantic current assemblage, an Arctic water assemblage, a sea ice assemblage, an Arctic-Norwegian waters assemblage, an Atlantic assemblage and a Norwegian-Arctic water assemblage. These six assemblages together accounted for 91.7% of the recorded variance. This transfer function was applied in subsequent studies (Koç & Jansen, 1992; Koç & Jansen, 1993; Koç & Jansen 1994; Koç *et al.,* 1996; Birks & Koç, 2002) to reconstruct late glacial and Holocene temperature changes.

Q-mode analyses of diatom species abundance counts to identify ecological assemblages has been used by a number of other authors. Williams (1986) analysed seventy-four sea floor surface samples from Baffin Bay and the Davis Straits and identified five assemblages accounting for 87% of the observed variance. These assemblages also strongly represented surface water conditions. Factors included a Baffin Current Assemblage, a Summer Ice Pack Assemblage and a West Greenland Current Assemblage. De Sève (1999) analysed sixty-six surface sediment samples from the Labrador Sea and identified six assemblages accounting for 95.69% of the observed variance. Abrantes *et al.,* (2007) identified five floral assemblages from analysis of forty-seven surface sediment samples from the Southeast Pacific.

Other statistical analyses have been used to identify different groupings of diatom flora. Witon *et al.* (2006) use maximum-likelihood factor analysis (MLFA) to identify diatom assemblages for four cores from the Faroe Island fjords. They recognise two factor assemblages; a warmer assemblage dominated by the plantktonic species *Thalassionema nitzschioides* and *Thalassiosira angulata,* which the authors equate to the Norwegian-Atlantic Current assemblage of Koç Karpuz and Shrader (1990) and a cooler water assemblage dominated by the planktonic form *Rhizosolenia hebetata* which is equated with the Arctic-Norwegian Water mixing assemblage of Koç Karpuz and Shrader (1990). Ran *et al.* (2006) use cluster analysis (CA) and principal component analysis (PCA) to indentify

three diatom assemblages for a Holocene core from the North Atlantic Shelf. Some difficulty is encountered in equating their finding to adjacent records as a key species in their analysis is defined as *Thalassiosira spp.* The authors equate the three diatom assemblages to the relative influences of the warm Irminger Curent (IC), the cold East Icelandic Current (EIC) and East Greenland Current (EGC).

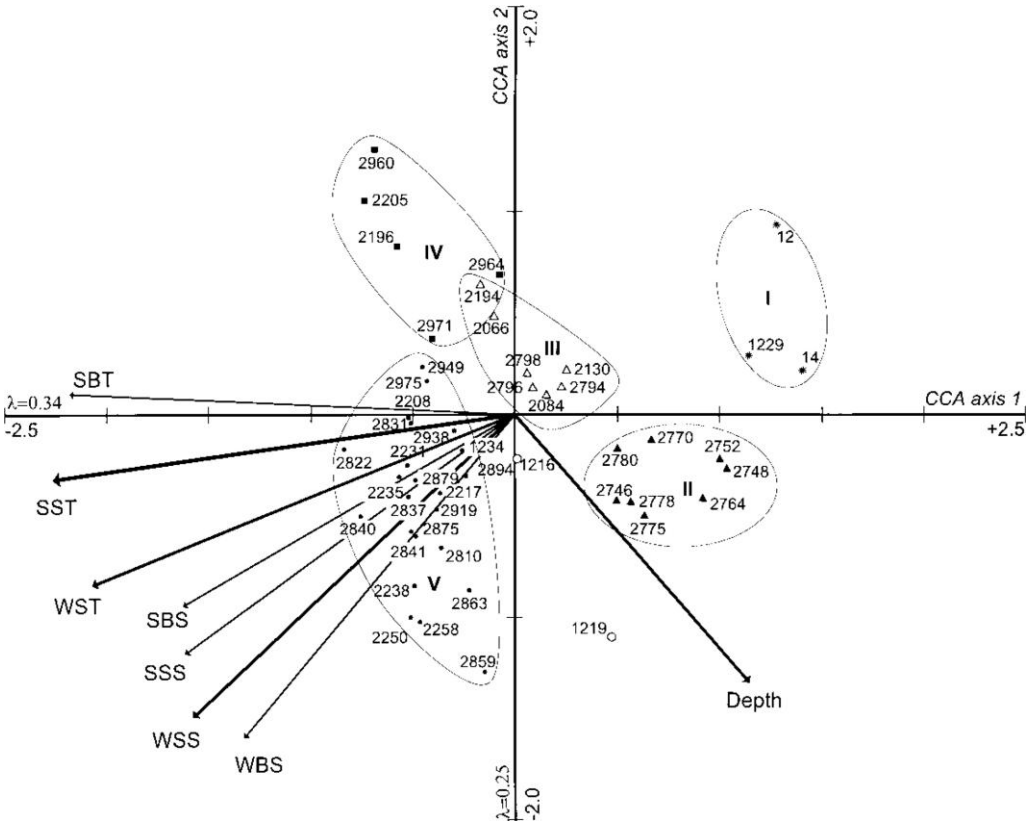

Figure 6.6 CCA biplot of environmental variables and sites around Iceland. Summer sea-surface temperature (SST) Summer sea-Bottom Temperature (SBT)Winter Sea-Surface Temperature (WST) Summer Sea-Bottom salinity (SBS) Summer Sea-Surface salinity (SSS) Winter Sea-Bottom salinity (WBS) Winter Sea-Surface Salinity (WSS) I. Sea-ice diatom assemblage II. Cold-water diatom assemblage III. Mixing diatom assemblage IV. Coastal diatom assemblage V. Warm-water diatom assemblage. From Jiang *et al*. (2001).

Jiang *et al.* (2001) analysed diatom species abundance counts from surface sediments at fifty-three sites around Iceland to identify different floral assemblages with respect to nine environmental variables, using Canonical Correspondence Analysis (CCA) (ter Braak,

1990). The results are represented by different axes on a CCA biplot (Figure 6.6). CCA is a direct gradient analysis which allows variation within the composition of a biological assemblage to be related to changes set of known environmental variables. Indirect gradient analyses, such as Principal Component Analysis (PCA) or Correspondence Analysis (CA), only allow the analysis of variation within the biological population. The assemblages identified by Jiang *et al.* (2001) do not correspond to specific water masses, such as the Arctic water assemblage, or the West Greenland Current assemblage etc, but rather to broader environmental conditions. The sea-ice diatom assemblage, for example, shows extreme negative values on temperature and salinity axes suggesting it represents the coldest and least saline water masses. The five assemblages recognised are; the sea-ice diatom assemblage, the cold-water diatom assemblage, the mixing diatom assemblage, the coastal diatom assemblage and the warm-water diatom assemblage. Justwan & Koç (2008) also employ a CCA analysis to produce a diatom-based sea ice transfer function from 99 North Atlantic surface sediment samples.

6.5.3 WA-PLS The Transfer Function adopted in this study

The method used to reconstruct sea-surface temperatures from diatom assemblage counts in this study, is weighted averaging partial least squares regressions (WA-PLS). The method combines weighted averaging regression and calibration and partial least squares regression. The weighted averaging method (WA) assumes that species occupy different environmental niches and that these niches may be described by their centres (u_k) and breadths (t_k) The weighted averaging method has three components; a WA regression, a WA calibration and a deshrinking regression.

The WA regression assumes that a species with a particular optimum will show highest abundances at sites with x-values close to this optimum. The WA regression estimates the optima for species (u_k) by weighted averaging the x-values of the sites. The WA calibration estimates the x-values for the sites by weighted averaging the species optima (ter Braak & Juggins, 1993). As averages are taken twice the range of estimated x-values (x_i*) is reduced. The quantity of this shrinking may be estimated by one of two methods; regressing (x_i*) on (x_i) or regressing (x_i) on (x_i*) (ter Braak, 1988; ter Braak &

Van Dam, 1989; Birks *et al.* 1990a). For the WAPLS method the (x_i) on (x_i*) deshrinking method is adopted as this establishes a link with the partial least squares method. Partial least squares (PLS) is a linear regression method for multivariate calibration (Wold *et al.*, 1984).

WA-PLS is a non-linear form of multivariant analysis proposed by ter Braak & Juggins (1993). It has been favoured in palaeoenvironmental reconstructions using diatoms as it is effective in the analysis of populations with a large number of species, some of which may be absent in some samples. The method does not assume linearity and is therefore less sensitive to outliers The authors define an eight step calculation process for the WA-PLS method.

Step 0	The environmental variable is centred by subtracting the weighted mean
Step 1	The centred environmental variable (x_i) as the initial site scores (r_i)
Step 2	(Steps 2-7 should be performed for each component) Calculate the new species score (u_k) by weighed averaging of the site scores
Step 3	Calculate the new site scores (r_i) by weighed averaging of the species scores
Step 4	For the first axis go to Step 5 For subsequent components make the new site scores (r_i) uncorrelated with the previous components by orthogonalization
Step 5	Standardise the new site scores (ter Braak 1987 Table 5.2b)
Step 6	Take the standardised scores as the new components
Step 7	Regress (x_i) the environmental variable on the components obtained so far in the regression and give the fitted values as current estimates (x_i). Go to Step 2 with the residuals of the regression as the new site scores (r_i). Thus the first component is a two way weighed average for the original environmental variable and subsequent components are weighted averages for the residual of this variable.

Table 6.4 Weighted average partial Squares (WA-PLS) method.
(ter Braak & Juggins, 1993).

The following species were included in the WA-PLS transfer function for this study (Table 6.5). *Rhizosolenia borealis* and *Rhizosolenia styliformis* were grouped as a single component. *Thalassiosira gravida* however was counted separately in vegetative and resting spore forms. Equally a distinction was made between *Thalassionema nitzschoides* and the smaller for *Thalassionema nitzschoides* var. *parva* for the purposes of the transfer function. In all cases the taxonomic groupings are identical to those employed for the

GINT2 transfer function (Koç Karpuz & Schrader,1990), an Imbrie-Kipp Q-mode factor analysis, based on diatom assemblage data from 104 core top samples.

In addition to the above taxa, the transfer function includes a *Thalassiosira* sp. identified as 'Sp Y'. This species is identified in only one species counts for core MD99-2251(indentified by personal communication Dr Nalan Koç) and in no samples of species counts for core MD99-2252. Two forms of *Nitzschia* sp. also occur in the WA-PLS transfer functions. Only one of these two species is identified in this study. Similarly, this species is only one count for core MD99-2251(indentified by personal communication Dr Nalan Koç) and in no samples from core MD99-2252.

Coscinodiscus asteromphalus
Coscinodiscus linearis
Coscinodiscus marginatus
Coscinodiscus radiatuss
Coscinodiscus occulus-iridis
Stellarmina stellaris
Actinocyclus curvatulus
Actinocyclus kutzingii
Actinocyclus octinarius
Azpeitia africana
Azpeitia neocrenulata
Azpeitia nodulifera
Hemidiscus cuneiformis
Roperia tesselata
Proboscia alata
Rhizosolenia bergonii
Rhizosolenia borealis
Rhizosolenia styliformis
Rhizosolenia hebetata hebetata
Rhizosolenia hebetata semispina
Asteromphalus robustus
Bacteriastrum hyalinum
Bacteriosira fragilis
Porosira glacialis
Thalassiosira angulata

Thalassiosira auguste-lineata
Thalassiosira eccentrica
Thalassiosira ferelineata
Thalassiosira gravida
Thalassiosira hyalina
Thalassiosira lineata
Thalassiosira nodulineata
Thalassiosira nordenskioeldii
Thalassiosira oestrupii
Thalassiosira pacifica
Thalassiosira trifulta
Alveus marina
Fragilariopsis atlantica
Fragilariopsis cylindrus
Fragilariopsis doliolus
Fragilariopsis rhombica
Fragilariopsis oceanica
Nitzschia braarudii
Nitzschia bicapitata
Nitzschia kolazczekii
Synedra spp
Thalassionema nitzschoides
Thalassiothrix longissima

Table 6.5. Species used in the WA-PLS transfer function SST estimates for MD99-2251 and MD99-2252 in this study

In addition to the taxa listed in Table 6.5 an ‘others’ category was recorded for each of the down core diatom flora counts of three hundred individuals. This category included all planktonic diatom taxa not listed or discussed above. This category is not included in the WA-PLS transfer function. However as percentage abundance of each recorded species is used for the transfer function, rather than raw counts, the presence of the ‘others’ category is reflected in the data. The total number of the diatom *Paralia sulcata* in each sample was recorded but not included in the WA-PLS transfer function. Other benthic taxa were recorded on count sheets with hand drawn diagrams and species counts. Separate

counts were also made in this study of resting spores of *Chaetoceros* but not used as part of the WA-PLS transfer function. The total number of *Chaetoceros* resting spores within one quarter transect for each slide was recorded.

Jiang *et al.* (2002) tested weighted average (WA), weighted average with tolerance down weighting ($WA_{(tol)}$), partial least squares (PLS) and weighted average partial least squares (WA-PLS) methods of SST reconstructions for a North Atlantic Shelf Holocene core using both root mean squared error (RMSE) and a leave-out-one jack-knifed root mean squared error of prediction ($RMSEP_{(Jack)}$) tests. The authors found that the PLS reconstructions performed best under the RMSE test but the WA-PLS performed best with the more accurate $RMSEP_{(Jack)}$ test. Similarly Knudsen *et al.* (2004) in a study of two Holocene gravity cores from the North Atlantic Shelf, tested six numerical reconstruction methods against a modern diatom-SST data set and found that the WA-PLS gave the best performance based on both the RMSE and $RMSEP_{(Jack)}$ tests.

Andersen *et al.* (2004b) applied three different transfer functions to estimate SSTs for sediment cores from the Vöring Plateau, the North Iceland Shelf and The East Greenland Shelf; the Imbrie & Kipp (I&K) Q-mode analysis, the Modern Analogue Technique (MAT) and the Weighted Averaging Partial Least Squares (WA-PLS) method (ter Braak & Juggins, 1993). The WA-PLS and I&K methods produced similar SST estimates. The MAT method failed to reproduce low amplitude variability. Using I&K analysis, the authors identified eight specific diatom assemblages; an Arctic Greenland Assemblage, a North Atlantic Assemblage, a sub-Arctic assemblage, a Norwegian Atlantic Current assemblage, a Sea ice Assemblage, an Arctic Assemblage, and East and West Greenland Current Assemblage and a Mixed Water Mass Assemblage. These factors were also identified for a study of subpolar North Atlantic cores by the same authors (Andersen *et al.*, 2004b). It is these assemblage groupings that are used this study (Figures 6.19-6.21).

Berner *et al.* (2008) compared the SST estimates from Q-mode factor analysis, a Maximum Likelihood (ML) transfer function (Upton & Cook, 2002) and the WA-PLS method for a Holocene sediment core from the Rekyjanes Ridge. The three methods showed broad agreement in SST reconstructions through the Holocene with variances of only ±1ºC for most intervals and ±2ºC in others. The authors conclude that the WA-PLS

method performs most accurately as the Q-mode analysis exhibited problems predicting SSTs above 14ºC and the ML transfer function had difficulties predicting temperatures below 5ºC. Justwan *et al.* (2008) also compare I&K, ML and WA-PLS reconstructions of SSTs for a Holocene sediment core from the North Iceland Shelf. They concluded that while the results were broadly similar, the I&K method had difficulties reconstructing temperatures 16º - 20ºC and the ML method below 4ºC for August SSTs.

6.6 Results

6.6.1 MD99-2251 Data

Species percentage abundance counts for MD99-2251 are presented plotted against core depth (Figure 6.8 and Figure 6.10) and age (Figure 6.9 and Figure 6.11). Key species were selected for plots on the basis of having represented over 10% of the total flora in at least one sample and reaching a mean representation of over 5% for the whole core. The species selected according to these criteria were *Rhizosolenia hebetata semispina, Actinocyclus curvatulus, Thalassiosira gravida* vegetative, *Rhizosolenia styliformis/borealis* and *Thalassiosira oestrupii* (Table 6.6)

Species	Average % in MD99-2251	No samples exceeding 10% of the total flora
Rhizosolenia hebetata semispina	6.4	12
Actinocyclus curvatulus	5.9	9
Thalassiosira gravida vegetative	11.4	61
Rhizosolenia styliformis/borealis	16.3	117
Thalassiosira oestrupii	28.4	133

Table 6.6 Species selected as 'key species' MD99-2251 with respect to their mean representation in the core and the number of sample in which they exceed 10% of the total flora.

As previously discussed, for the purposes of the transfer function analysis *Rhizosolenia styliformis* and *Rhizosolenia borealis* were counted jointly although factor analysis of Andersen *et al.* (2004b) indicate that *Rhizosolenia styliformis* is associated with a mixed water assemblage and *Rhizosolenia borealis* with a sub Arctic assemblage.Ten

additional species were plotted. These additional species were selected on the basis of being significant floral assemblage indicators according to the factor analysis of Andersen *et al.* (2004b) further discussed in section 7.7of this study. The key species and additional species were also plotted with the WAPLS generated SSTs.

The WAPLS generated SSTs and distribution of key species abundances indicate an initial warming in the early Holocene with relatively high variability until around 9kyr. A feature of this early Holocene variability is an increase in the number of single sample peaks of *Rhizosolenia hebetata semispina, Rhizosolenia styliformis/borealis* and *Proboscia alata* (Figure 6.7). Berner *et al.* (2008) observe in their study of an adjacent core from the Reykanes Ridge, several intervals where *Rhizosolenia borealis* reaches between 50% and 90% of the total flora; between 11 and 9kyr, 3.3 and 2,3 kyr, and 1.3 and 0.5kyr. Andersen *et al.*(2004a) record peaks of *Rhizosolenia borealis* and *Thalassiosthrix longissima* between 11 and 9.5kyr, 2.3 and 2.4 kyr and 1-3 and 0.5kyr. In this study peaks of around 40% or over are reached in *Rhizosolenia styliformis/borealis* and *Rhizosolenia hebetata semispina* between 8.3-11.4kyr. Peaks of between 20% and 30% occur between 8.2-8.1kyr and 3.6-4.6kyr.

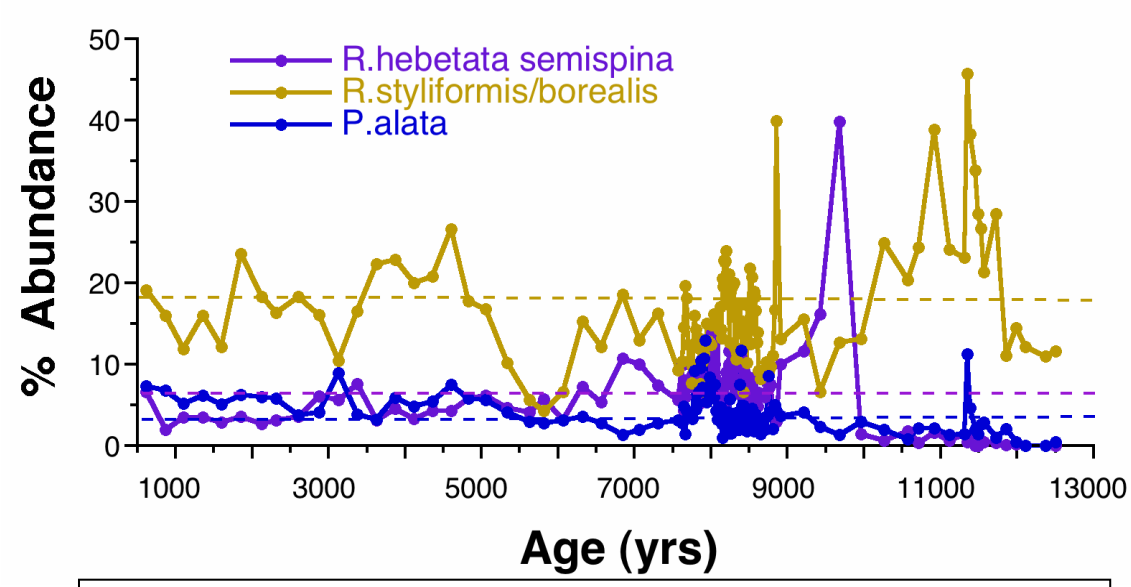

Figure 6.7 Single sample high abundance peaks of the forms *Rhizosolenia hebetata semispina, Rhizosolenia styliformis/borealis* and *Proboscia alata.* The dashed lines indicate the mean value for each species within marine core MD99-2251

A broad cooling occurs between 9.5-7kyr. This cooling is reflected in an increase in *Thalssiosira gravida* vegetative and *Actinocyclus curvatulus* and by lower SSTs (Figure 7.9). *Thalssiosira gravida* vegetative is strongly associated with the cool East and West Greenland current. *Actinocyclus curvatulus* is associated with Arctic floral assemblages.There is also slight increase in colder forms, *Thalssiosira gravid*a spore, *Fragilariopsis oceanica, Thalssiosira trifulta and Thalassiosira nordenskioeldii* associated with this cooling period and an increase in the percentage abundance of *Synedra spp* and *Probosica alata* a species associated with the Norwegian Atlantic current (Figure 6.11).

At around 7kyr there is a strong increase in the warmer flora *Thalassiosira oestrupii,* a species strongly associated with the North Atlantic Current, and the WAPLS generated SSTs increase significantly. The cooler *Thalssiosira gravida* vegetative decreases significantly at 7kyr and remains at low percentage abundances for the remainder of the Holocene (Figure 6.9). After this warming period from around 5-7kyr temperatures remain relatively stable. The overall temperature trend of the WAPLS SSTs for the Holocene is a slight increase of around 2-3 ^{o}C.

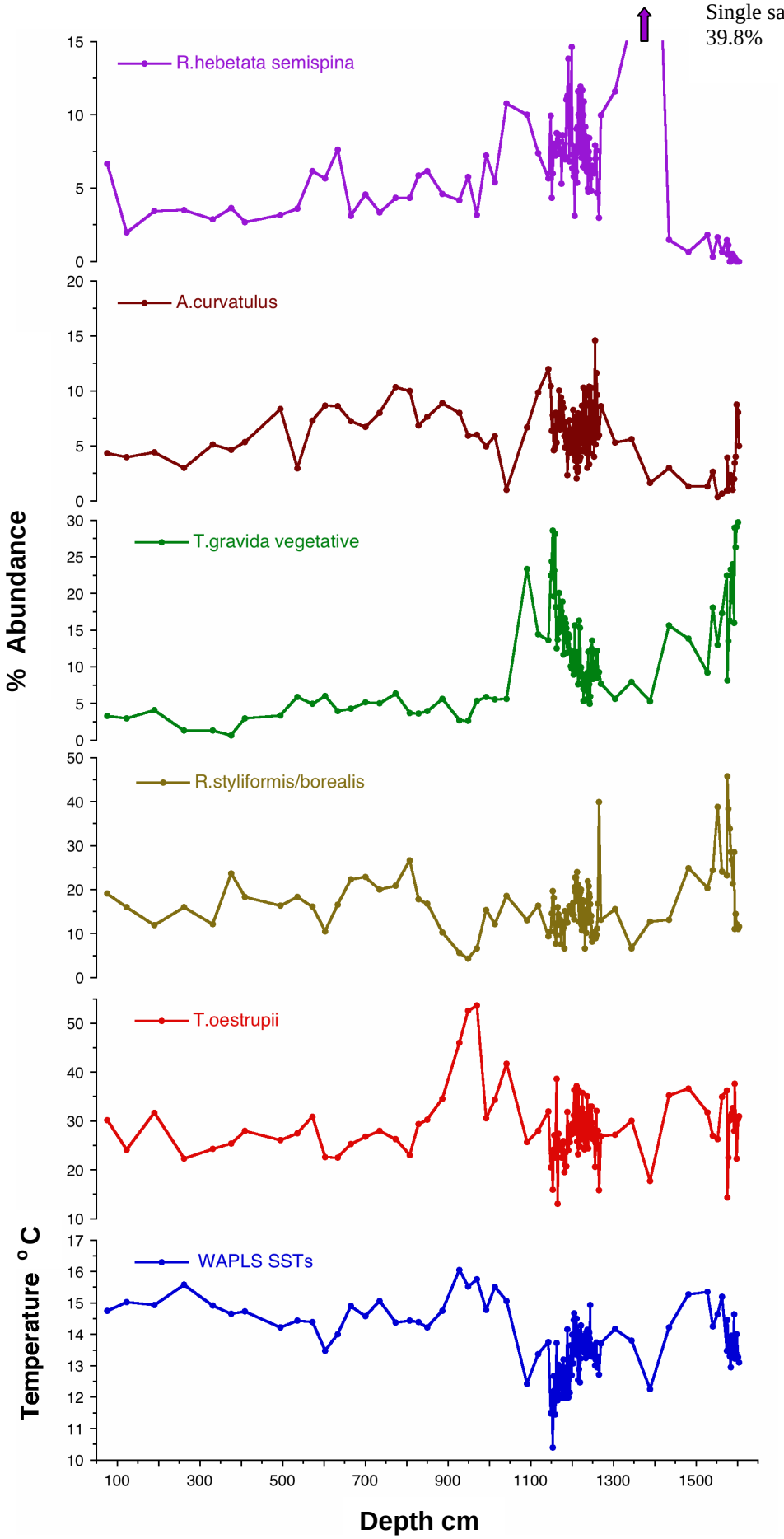

Figure 6.8 MD99-2251 key diatom species against depth

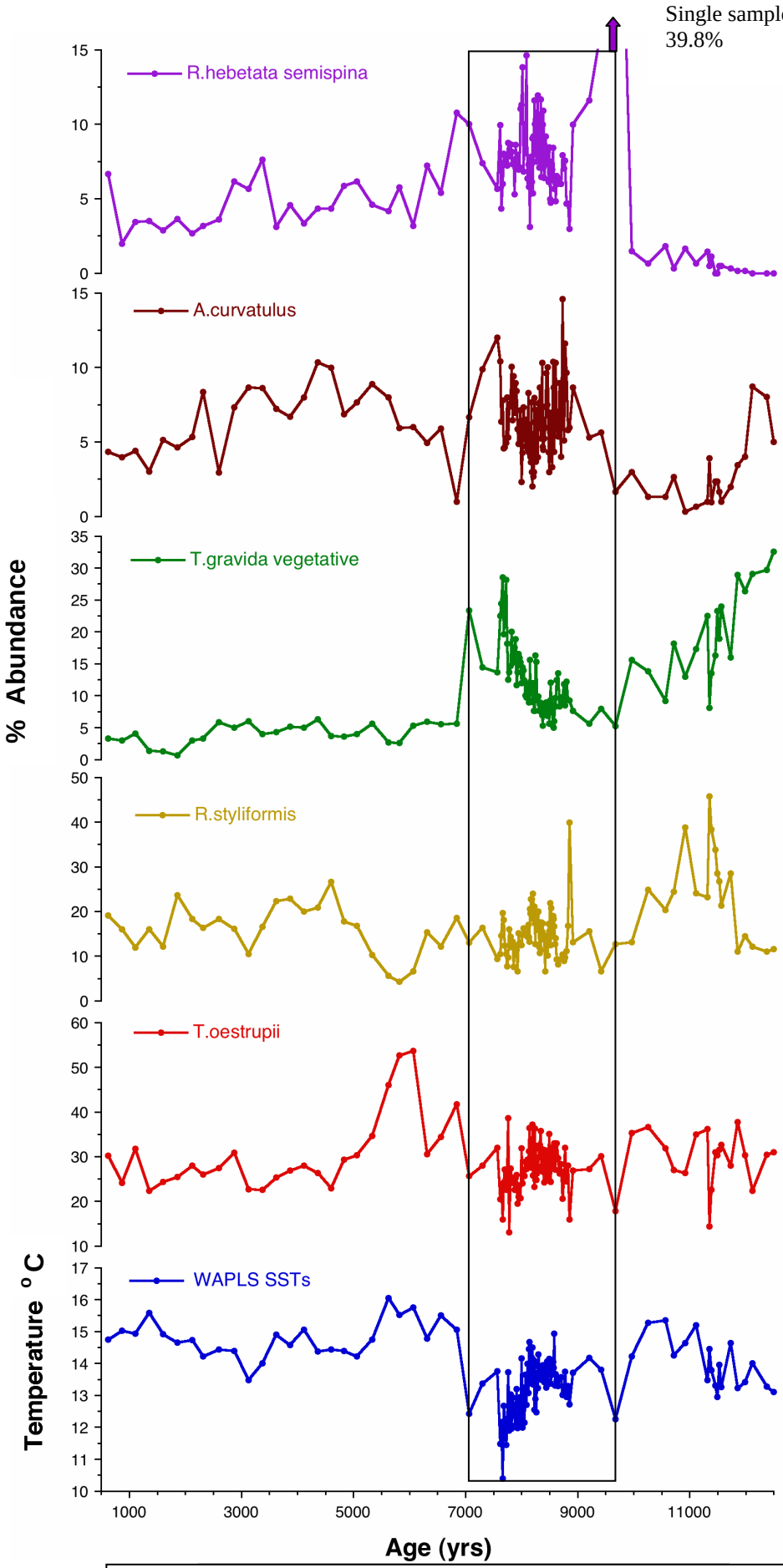

Figure 6.9 MD99-2251 key diatom species against age.
The highlighted area indicates a broad cooling between 9.5-7kyr

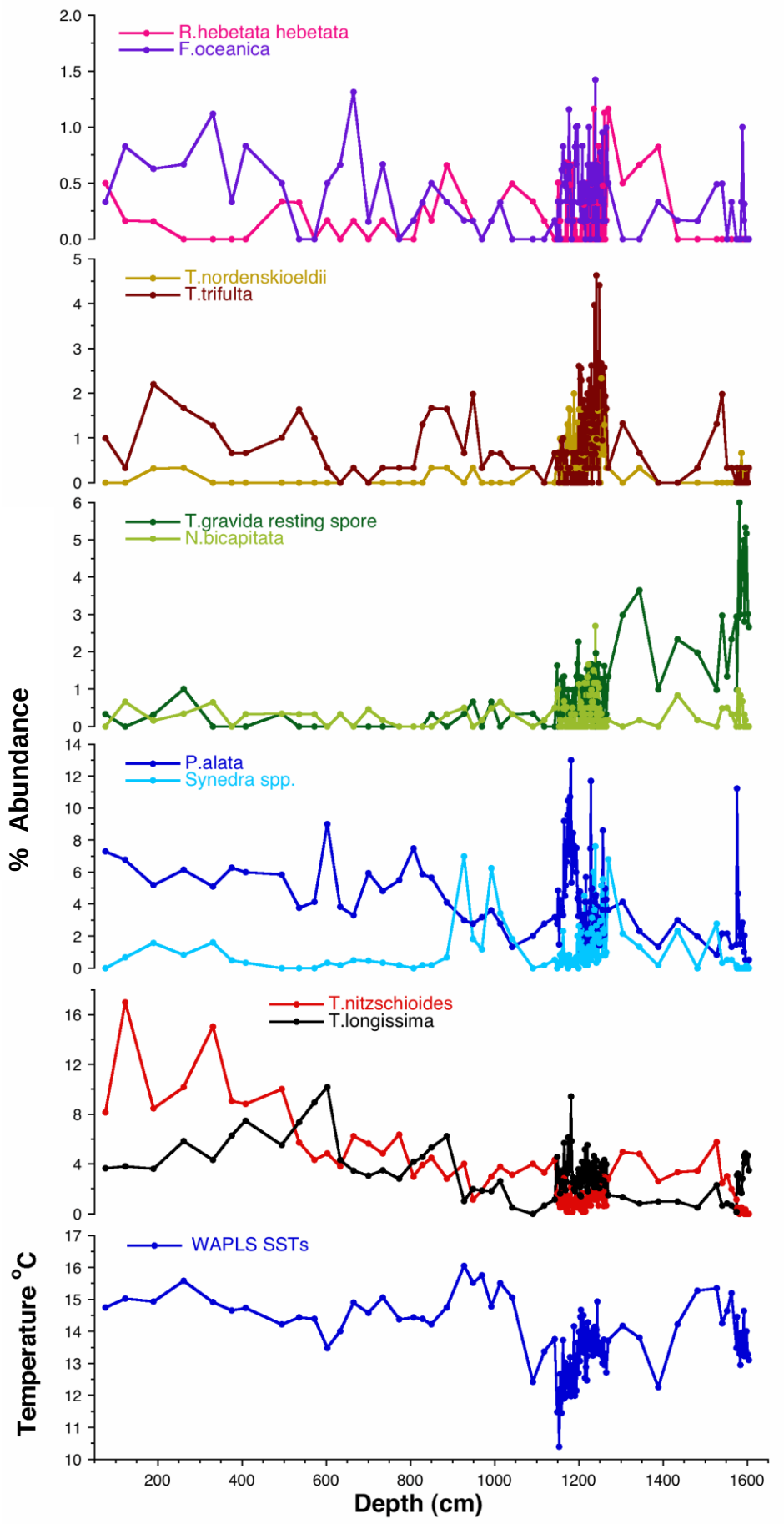

Figure 6.10 MD99-2251 additional diatom species against depth

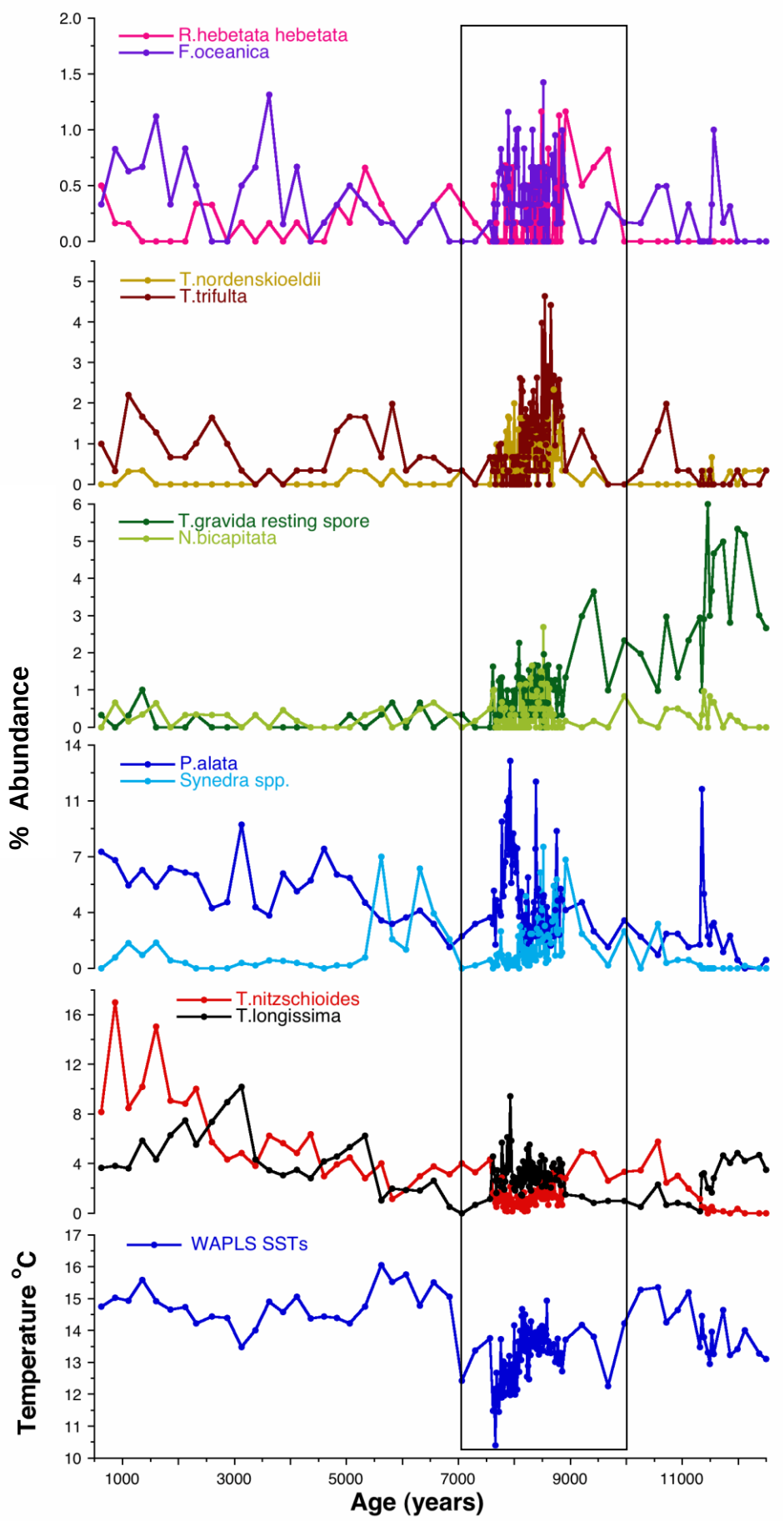

Figure 6.11 MD99-2251 additional diatom species against age. The highlighted area indicates a broad cooling between 9.5-7kyr

6.6.2 8.2kyr data from core MD99-2251

Data was plotted for the high resolution study of the 8.2kyr event as recorded in marine core MD99-2251for the same key species (Figure 6.12 and 6.13) and additional species (Figure 6.14 and Figure 6.15) as for the whole core. The data is plotted over an age range of 7.8-8.8yrs. The floral abundance and SSTs indicates a low level multidecadal to centennial variability through this time period, but no specific response at or around 8.2kyr. The period 8100-8300yrs is highlighted in Figure 6.12 and Figure 6.14. There is some increase in *Rhizosolenis styliformis/borealis* during this interval and decrease in *Proboscia alata* but these variations are not outside of the range of the overall variation for the period7.8-8.8kyr.

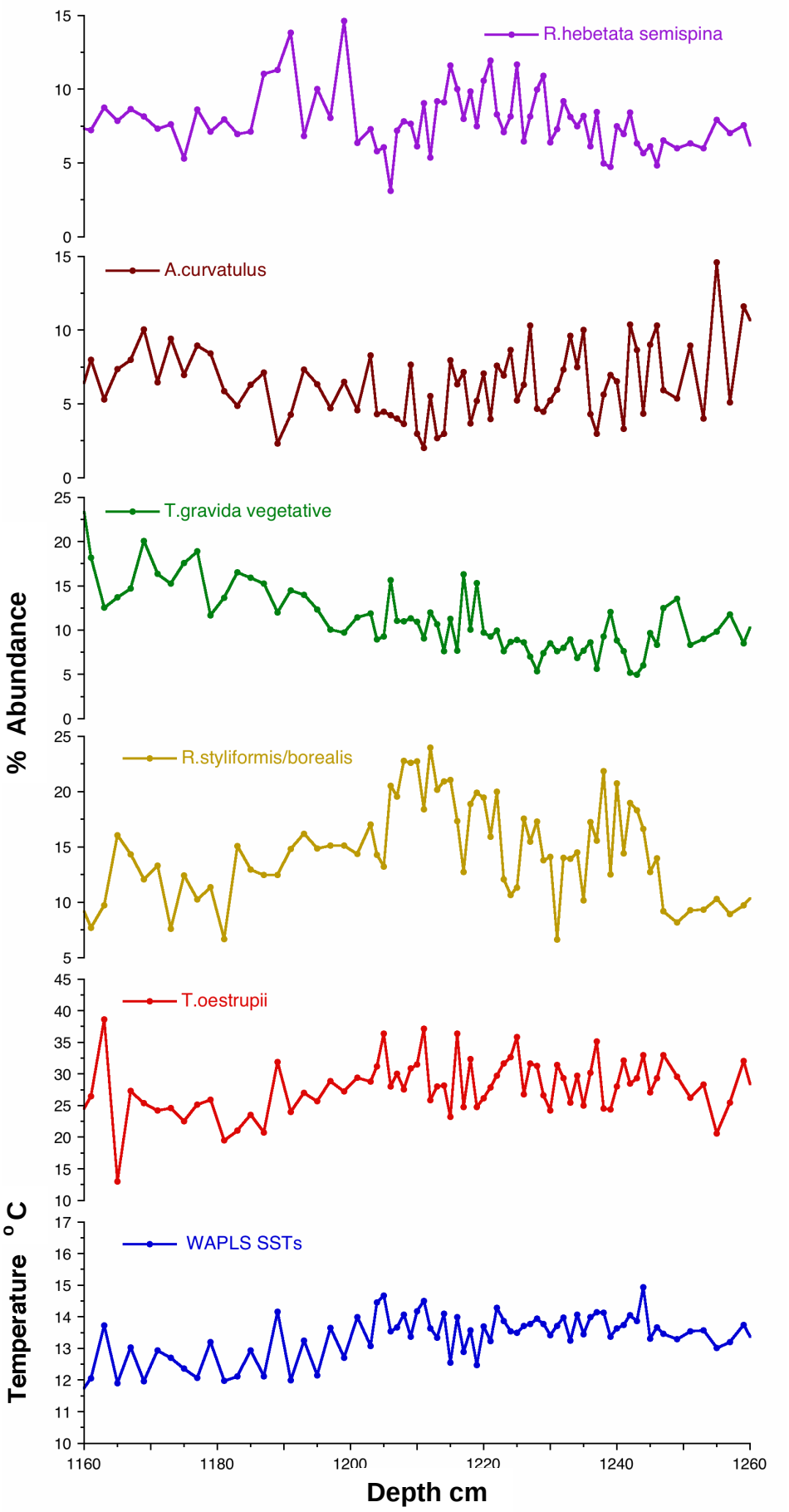

Figure 6.12 MD99-2251 8.2kyr event key diatom species against depth

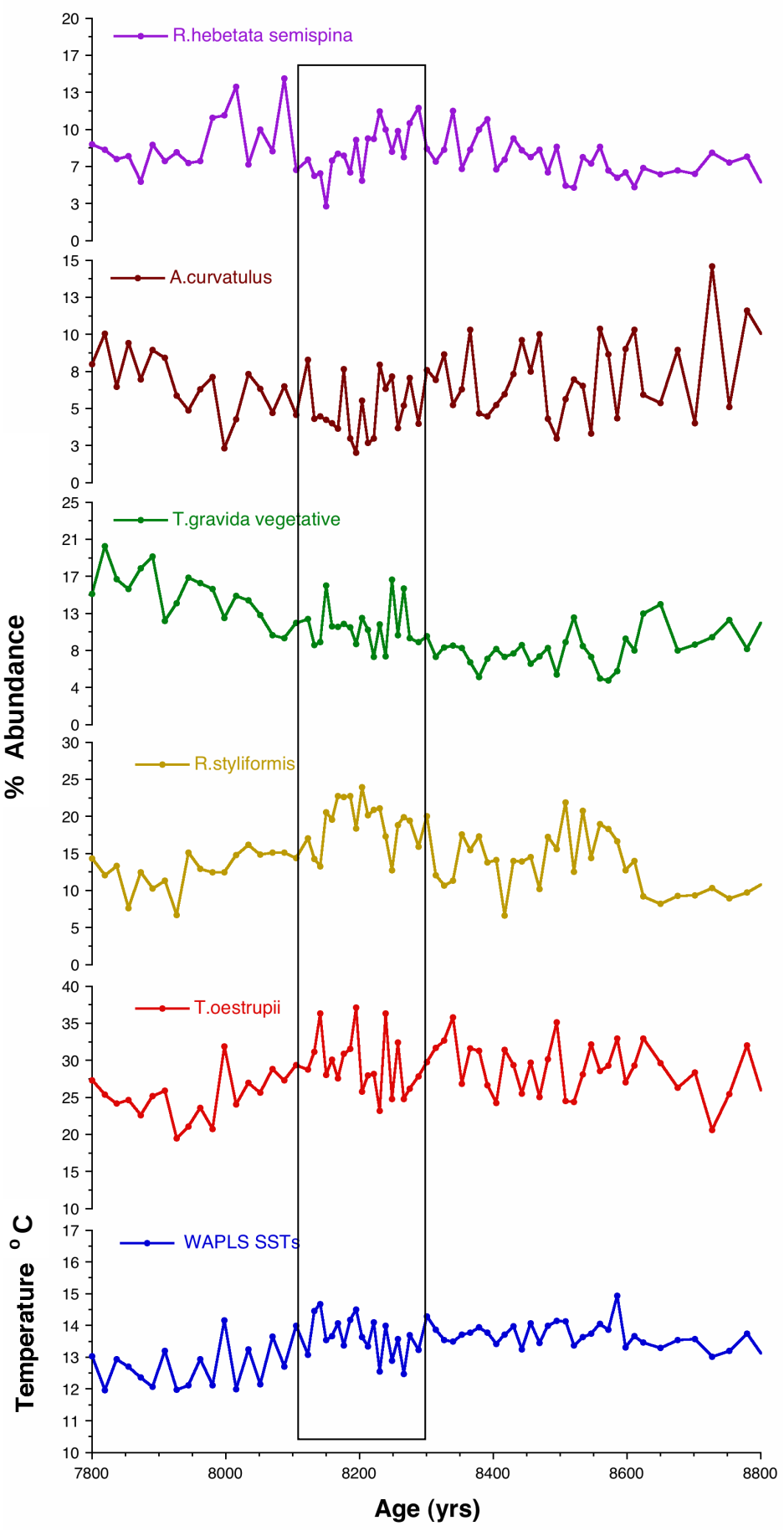

Figure 6.13 MD99-2251 8.2kyr event key diatom species against age. 8.1-8.3kyr is highlighted

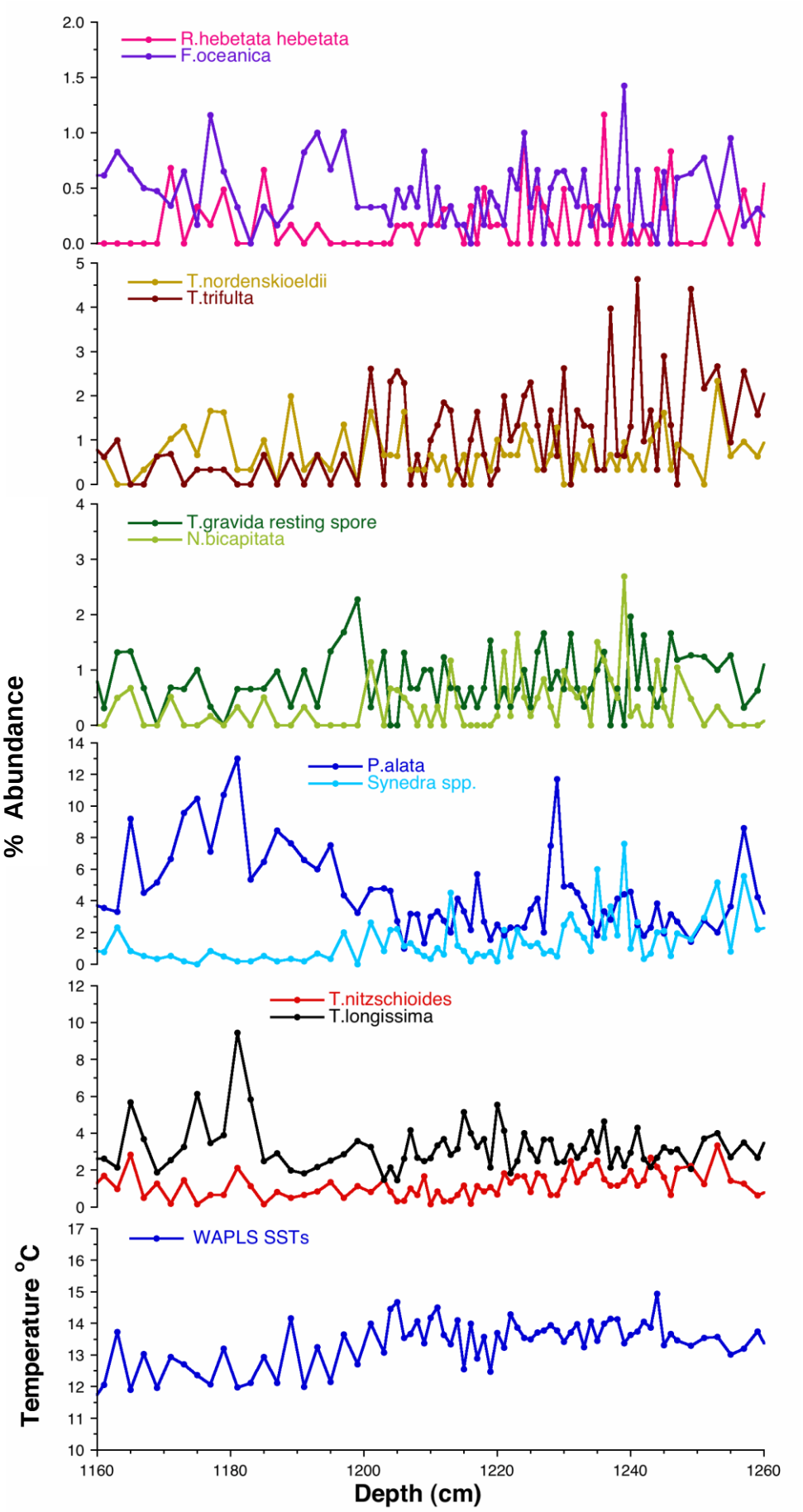

Figure 6.14 MD99-2251 8.2kyr event additional diatom species and WAPLS generated SSTs against depth

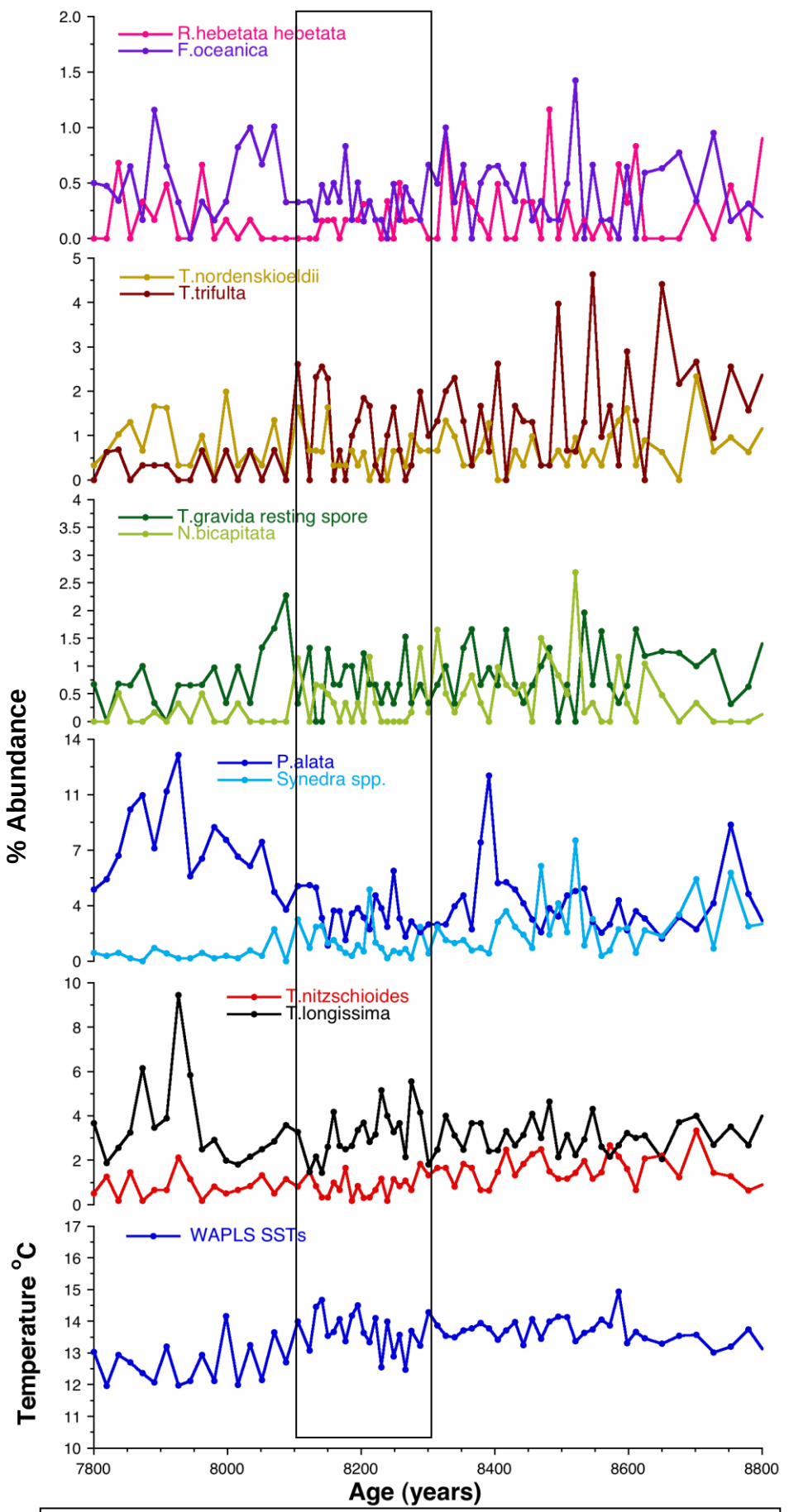

Figure 6.15 MD99-2251 8.2kyr event additional diatom species and WAPLS generated SSTs against age. 8100-8300 is highlighted

6.6.3 MD 99-2252 diatom data

The same key species and additional species plotted for MD99-2251 were also plotted for MD99-2252 (Figures 6.17, 6.18, 6.19 and 6.20). The species abundance distribution and the WAPLS generated SSTs indicate similar trends in core MD99-2252 as in MD99-2251. While MD99-2252 only extends for the last 7.2kyr, the warming trend 5-7kyr is identifiable, highlighted in Figures 6.18 and 6.20. It is characterised by an increase in the SSTs and the relative abundance of *Thalssiosira oestrupii* and a corresponding decrease in *Thalssiosira gravida* vegetative and *Rhizosolenia styliformis/borealis.* Following this warmer period, temperatures remain higher and relatively stable for the remainder of the Holocene as also indicated in core MD99-2251.

A comparison of the percentage abundance distribution of the key species and the SSTs for MD99-2251 and MD99-2252 is shown in Figure 6.21. It can be seen that the two records generate highly consistent absolute percentage and temperature values and trends. The least consistent section of the record occurs at the onset of the warming period (highlighted in Figure 6.21). For the late Holocene *Rhizosolenia hebetata semispina* and *Thalassiosira gravida* vegetative show the most consistent similarity between the two cores.

6.6.4 MD99-2252 stable isotope data

In addition to the diatom abundance counts and SSTs estimates, stable isotope measurements were generated for marine core MD99-2252. Samples were taken every 2cm, washed and sieved at 250-300 μm and 300-355μm. Each $\delta^{18}O$ anlaysis was made using 30 specimens of the planktonic foraminifers *Globigerina bulloides* picked from the 300-355μm size fraction and 30 specimens of *Neogloboquadrina pachyderma* dextral (dextral coiling). Stable isotope measurements were made using a SIRA mass spectrometer fitted with the VG isocarb common acid bath system at the Godwin Laboratory, University of Cambridge. The analytical precision of laboratory standards is better than ±0.08‰ for $\delta^{18}O$. Calibration to VPDB is via the NBS19 standard.

The stable isotope measurements are consistent with the WAPLS-generated SST estimates (Figure 6.16) reflecting a relatively stable mid and late Holocene climate. The range of temperature variation reflected in the stable isotope record is consistent with the temperature range of the SST estimates. Assuming the stable isotope variation is a temperature only signal, a decrease in stable isotope values of 0.25‰ equates approximately to a 1°C difference in temperature. Temperatures in this record vary in the range of 12-16 °C, a range of 4 °C. The isotope values vary from around 0.8-1.8‰, a range of 1.0‰ equating to approximately 4 °C. The warmer period from 5-7kyr is shown in higher SSTs and a corresponding lower stable isotope values especially for *Neogloboquadrina pachyderma* dextral.

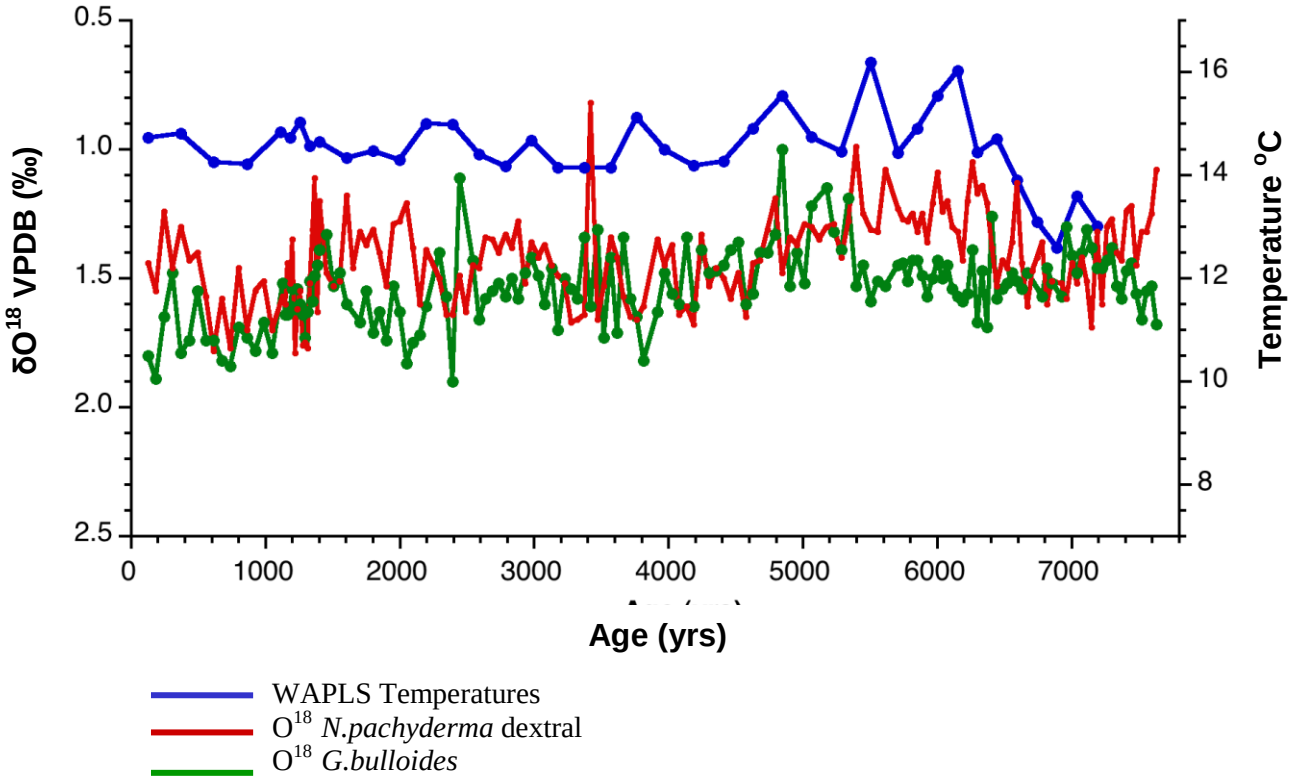

Figure 6.16 Oxygen isotope and WAPLS generated SST values for MD99-2252. Oxygen isotopes are generated from the foraminfera *Globigerina bulloides* and *Neogloboquadrina pachyderma* dextral.

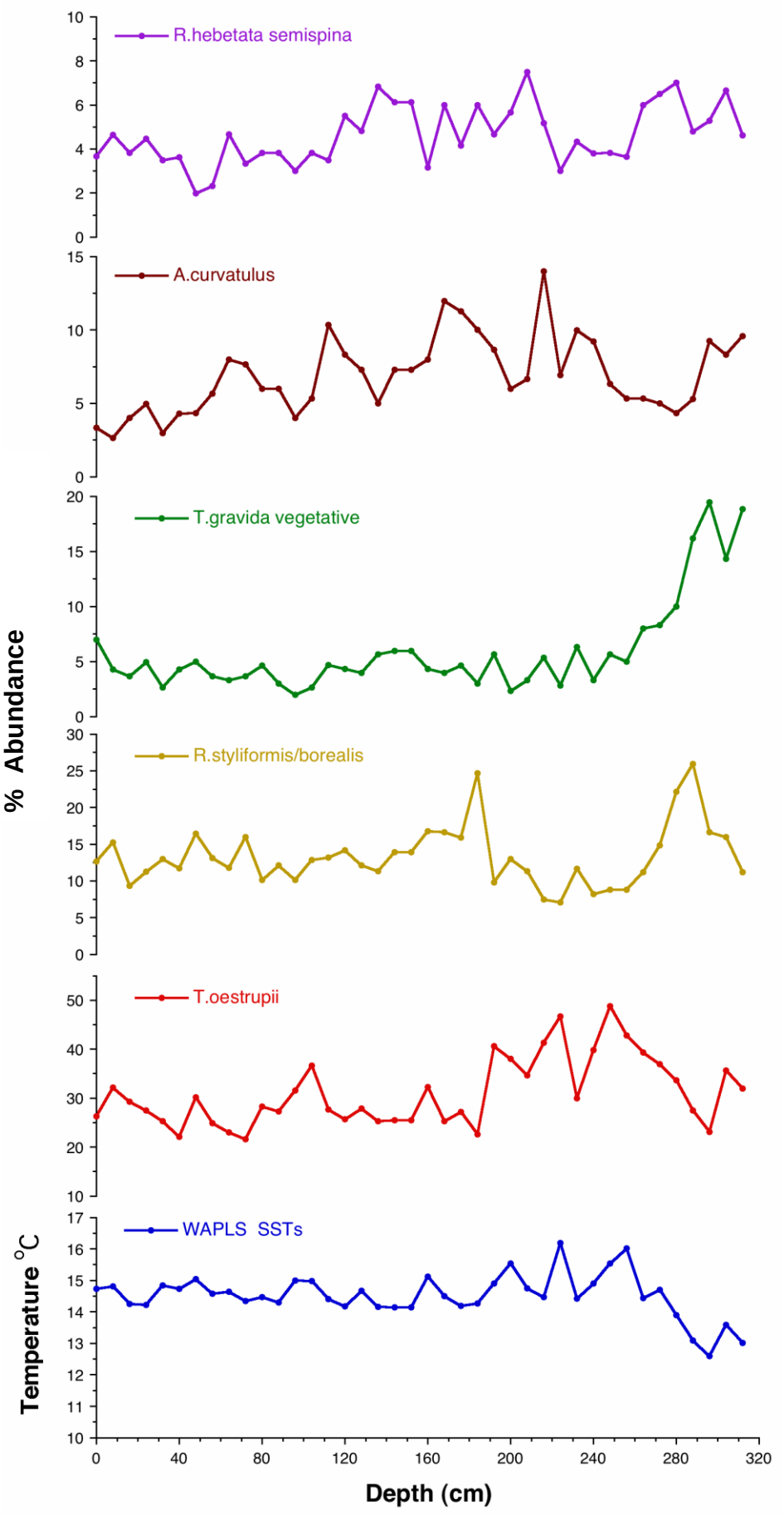

Figure 6.17 MD99-2252 key diatom species against depth

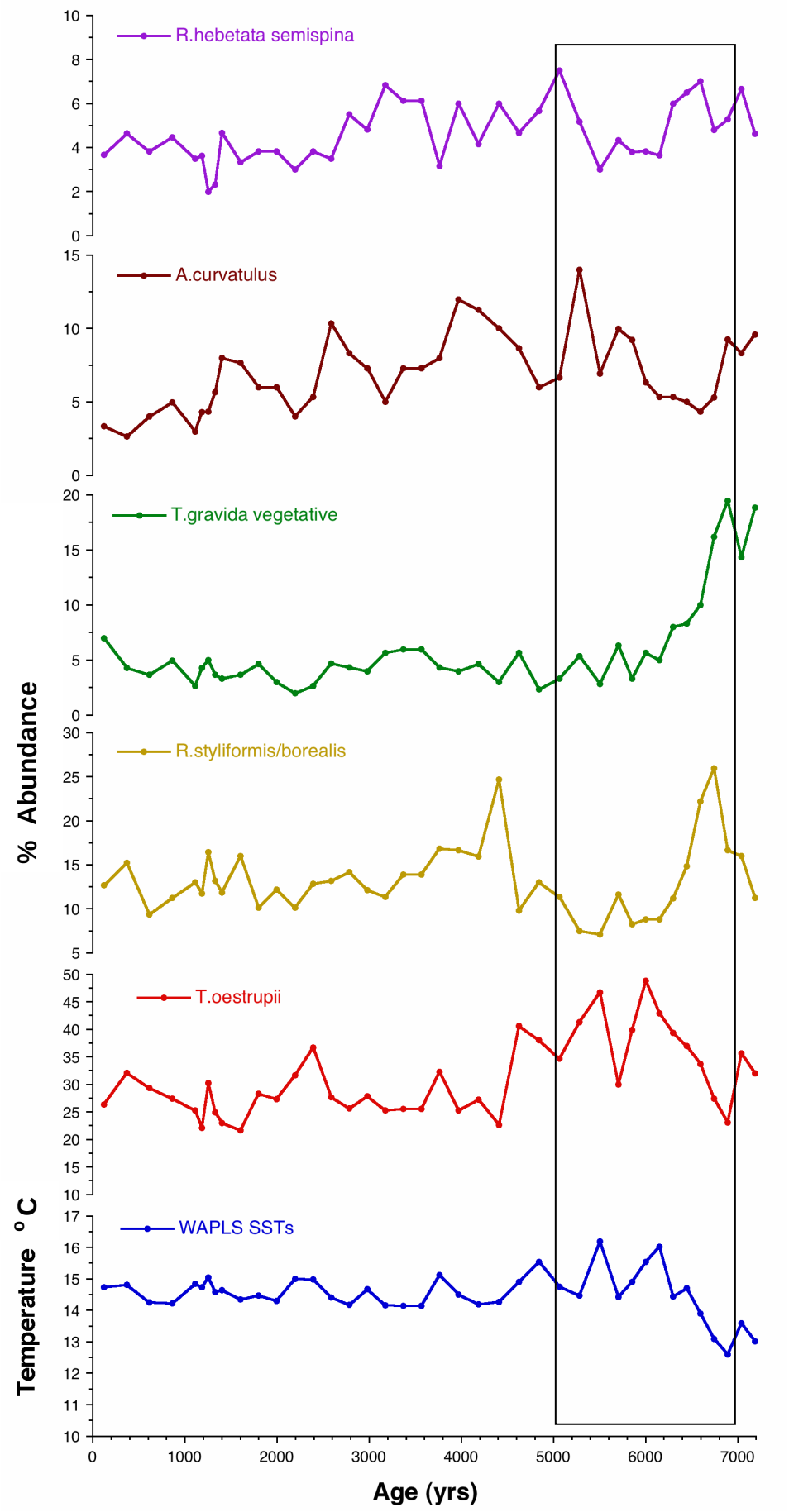

Figure 6.18 MD99-2252 key diatom species against age.
Highlighted area indicates 7-5kyr warming

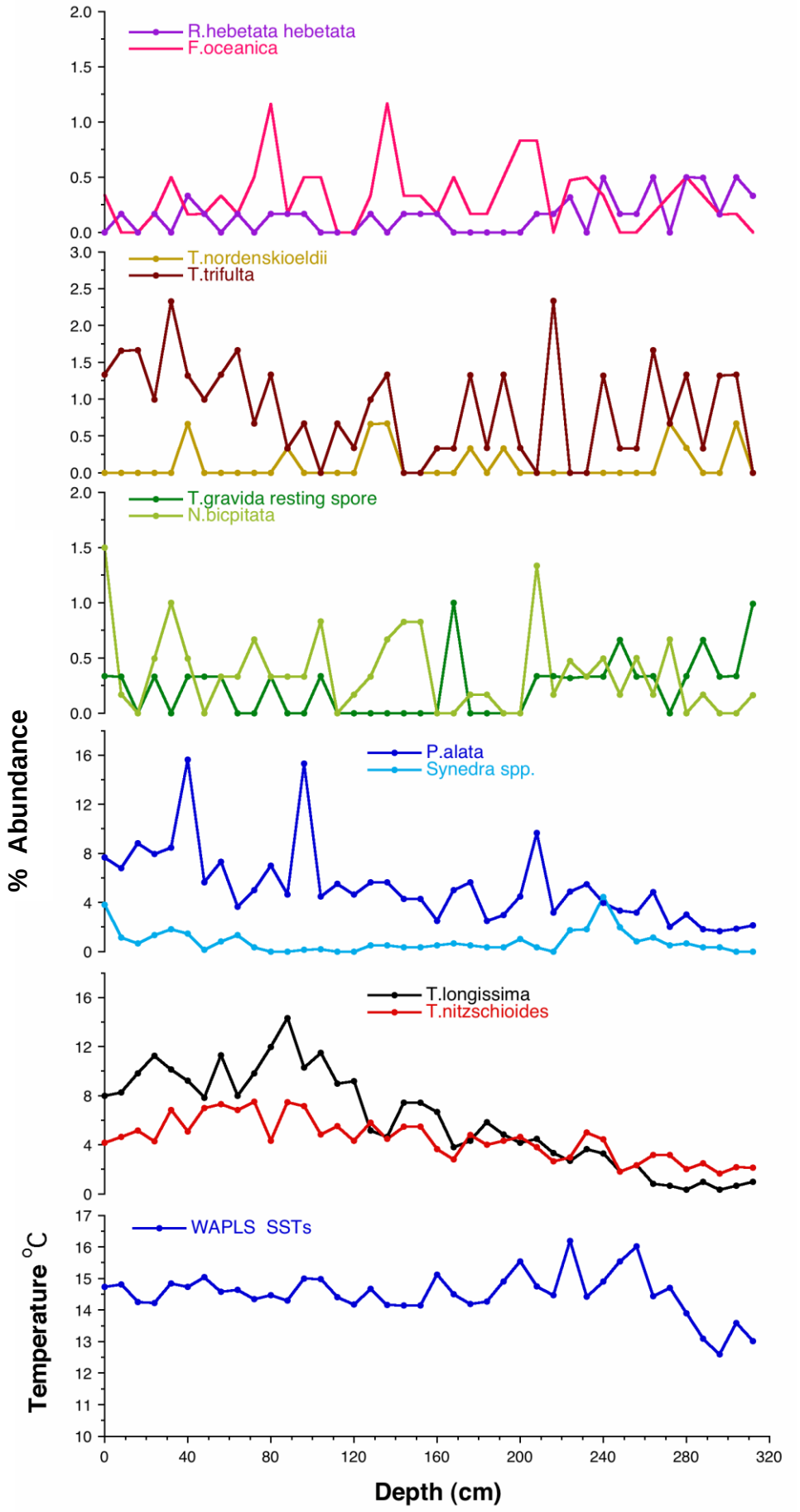

Figure 6.19 MD99-2252 additional diatom species against depth

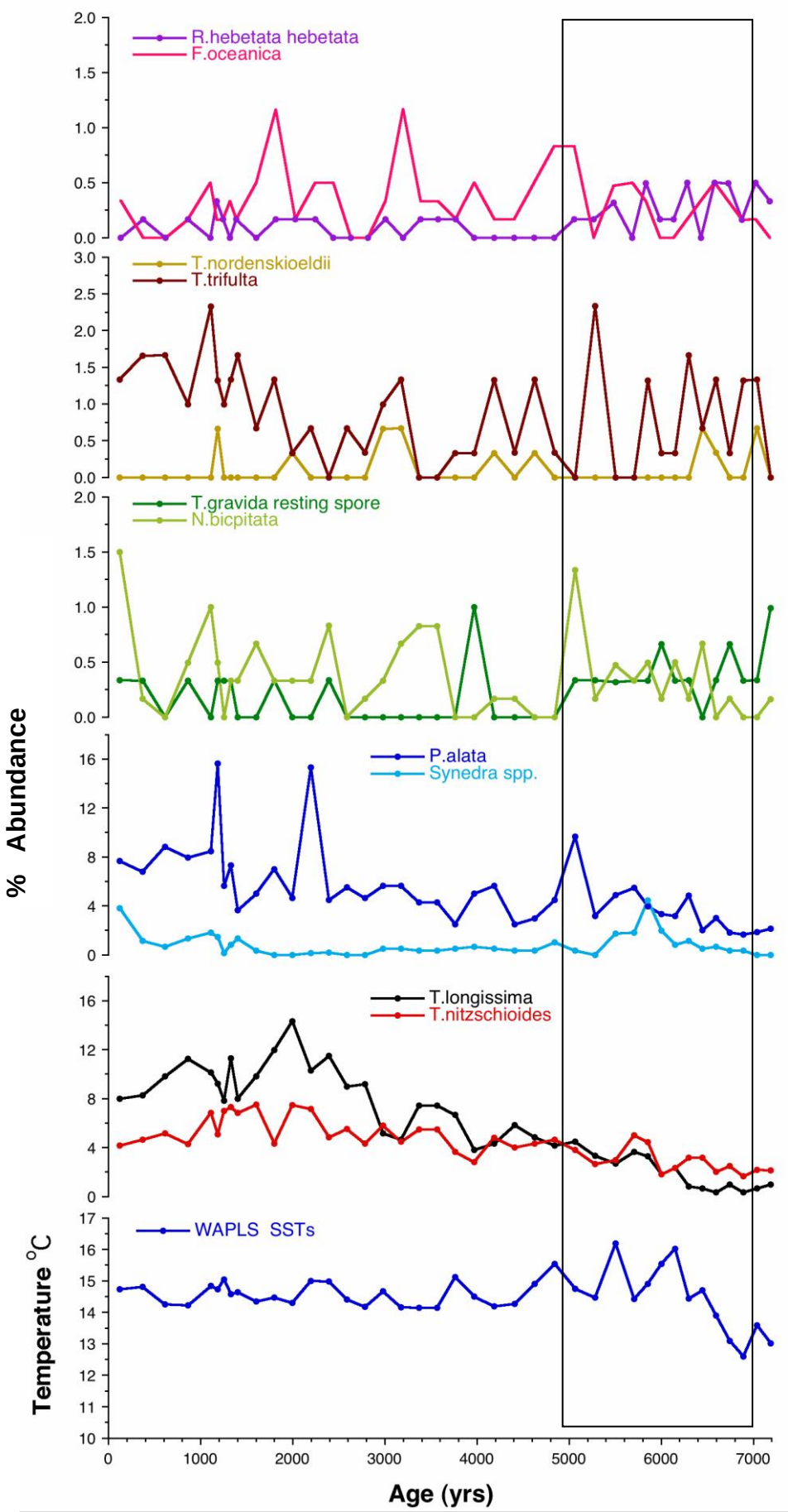

Figure 6.20 MD99-2252 additional species against age. Highlighted area indicates 7-5kyr warming

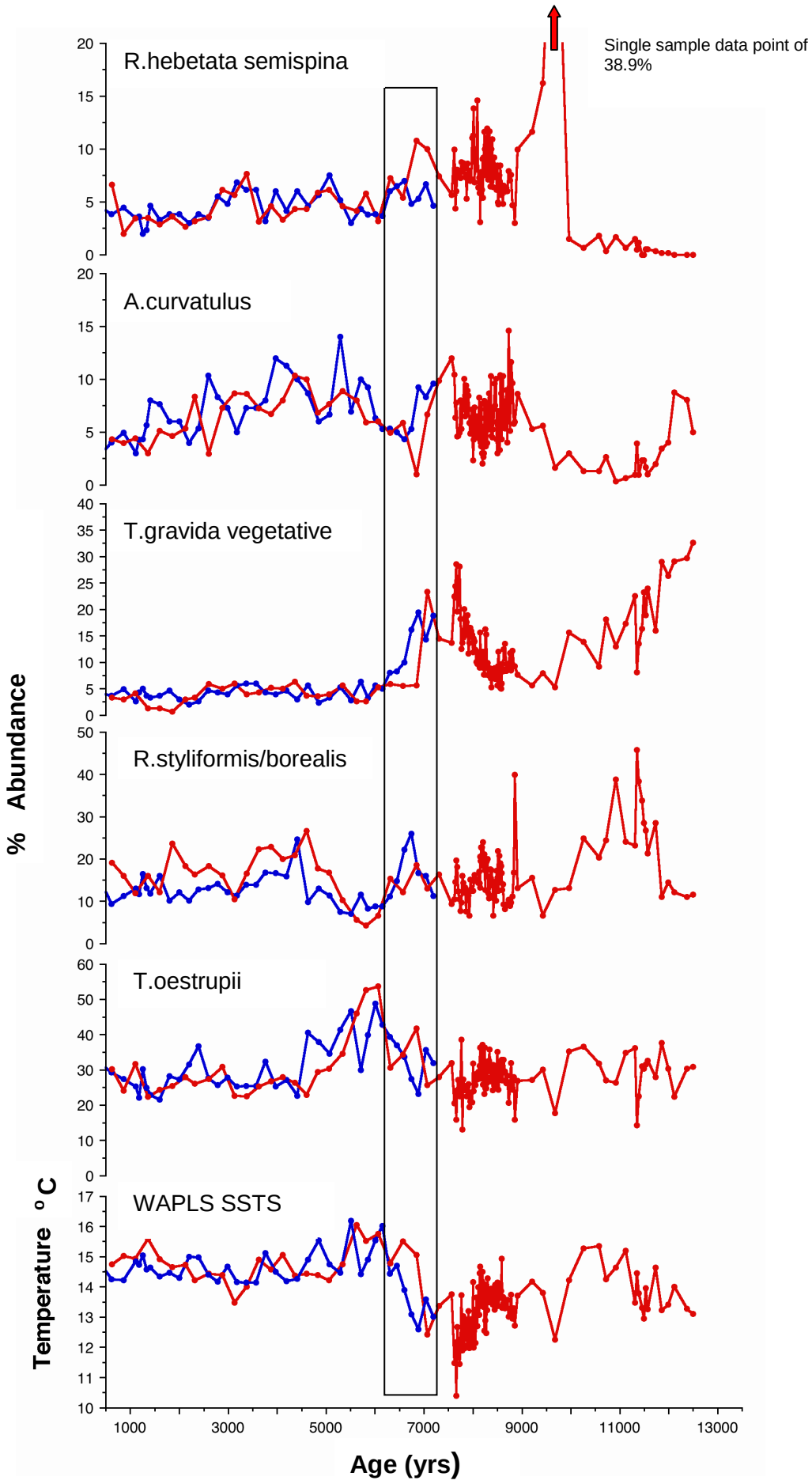

Figure 6.21 Comparison of key diatom species percentage abundance and SSTs between MD99-2251 (in red) and MD99-2252 (in blue). Highlighted area indicates 7-5kyr warming

6.7 Floral Assemblages and water masses

In addition to the plots of key and additional species, plots were made of floral assemblages (Figures 6.23, 6.24 and 6.25). These floral assemblages are based on Andersen *et al.* (2004a). As previously discussed (section 4.7) , using I&K analysis, the authors identified eight specific diatom assemblages; an Arctic Greenland Assemblage, a North Atlantic Assemblage, a Sub-Arctic assemblage, a Norwegian Atlantic Current assemblage, a Sea ice Assemblage, an Arctic Assemblage, and East and West Greenland Current Assemblage and a Mixed Water Mass Assemblage. Figure 6.22 indicates the distribution of these floral assemblages. The key species identified as characteristic of each assemblage are indicated in Table 6.5. The authors indentify both species which strongly reflect the assemblage (recorded here at Primary assemblage species) and species which also contribute to the assemblage (recorded here as Additional assemblage species).

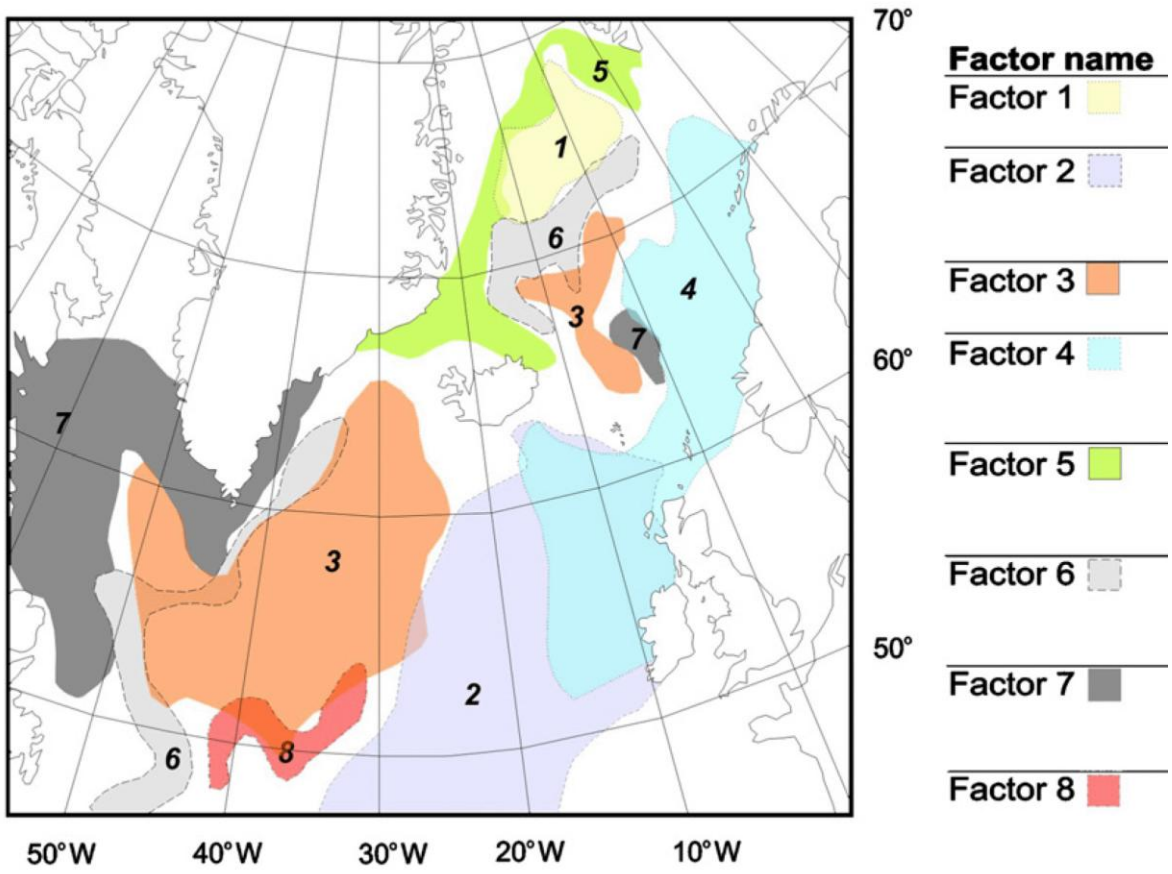

Figure 6.22 The modern distribution of the floral assemblage factors of Andersen *et al.* (2004a) (redrawn Justwan *et al.*,2008). Factor 1 Arctic Greenland Assemblage, Factor 2 North Atlantic Assemblage, Factor 3 Sub Arctic Assemblage, Factor 4 Norwegian Atlantic Current Assemblage, Factor 5 Sea-Ice Assemblage, Factor 6 Arctic Assemblage ,Factor 7 East and West Greenland Current Assemblage, Factor 8 Mixed Water Mass Assemblage.

Factor Number	Factor Name	Primary assemblage species	Additional assemblage species
1	Arctic Greenland Assemblage	*Thalassiosira auguste-lineata, Thalassiosira trifulta*	
2	North Atlantic Assemblage	*Thalassiosira oestrupii*	*Thalassiosira nitzschioides, Nitzschia bicapitata, Rhizosolenia bergonii, Roperia tesselata, Alveus marina*[*]
3	Sub-Arctic Assemblage	*Rhizosolenia hebetata* f. *semispina*	*Rhizosolenia borealis Thalssiosthrix longissima*
4	Norwegian Atlantic Current Assemblage	*Thalassionema nitzschioides*	*Proboscia alata Thalassiosira angulata*
5	Sea Ice Assemblage	*Fragilariopsis oceanica**	*Thalassiosira hyalina Thalassiosira gravida* resting spores *Thalassiosira nordenskioeldii Bacterosira fragilis Fragilariopsis cylindrus**
6	Arctic Assemblage	*Thalassiosira gravida* resting spores	*Thalassiosira gravida* vegetative cells *Actinocyclus curvatulus Rhizosolenia hebetata* f. *semispina Rhizosolenia hebetata* f. *hebetata*
7	East and West Greenland Current Assemblage	*Thalassiosira gravida* vegetative cells	
8	Mixed Water Mass Assemblage	*Rhizosolenia borealis*	

Table 6.7 Primary and additional species for the flora assemblages of Andersen *et al.* (2004a). (* taxonomic nomenclature employed in this study has been adopted. Andersen *et al.* (2004a) refers to *Alveus marina* as *Nitzschia marina, Fragilariopsis oceanica* as *Nitzschia grunowii* and *Fragilariopsis cylindrus and Nitzschia cylindra*)

For the purposes of this study the percentage abundance of each of the primary and additional species for the particular floral assemblage found in MD99-2251, for the 8.2 kyr event high resolution study and for MD99-2252 were summed and plotted. (As the East West Greenland Current assemblage is clearly synonymous with the abundance of *Thalassiosira gravida* vegetative cells, it was not included). The North Atlantic Current Assemblage strongly reflects the distribution of *Thalassiosira oestrupii.* It was not possible to plot the Factor 8, the Mixed Water Mass Assemblage as *Rhizosolenia borealis* was not distinguished from *Rhizosolenia styliformis* for the purposes of the transfer function

species abundance counts. Where the Sub Arctic assemblage identifies *Rhizosolenia borealis,* the joint counts of *Rhizosolenia borealis* and *Rhizosolenia styliformis* were used.

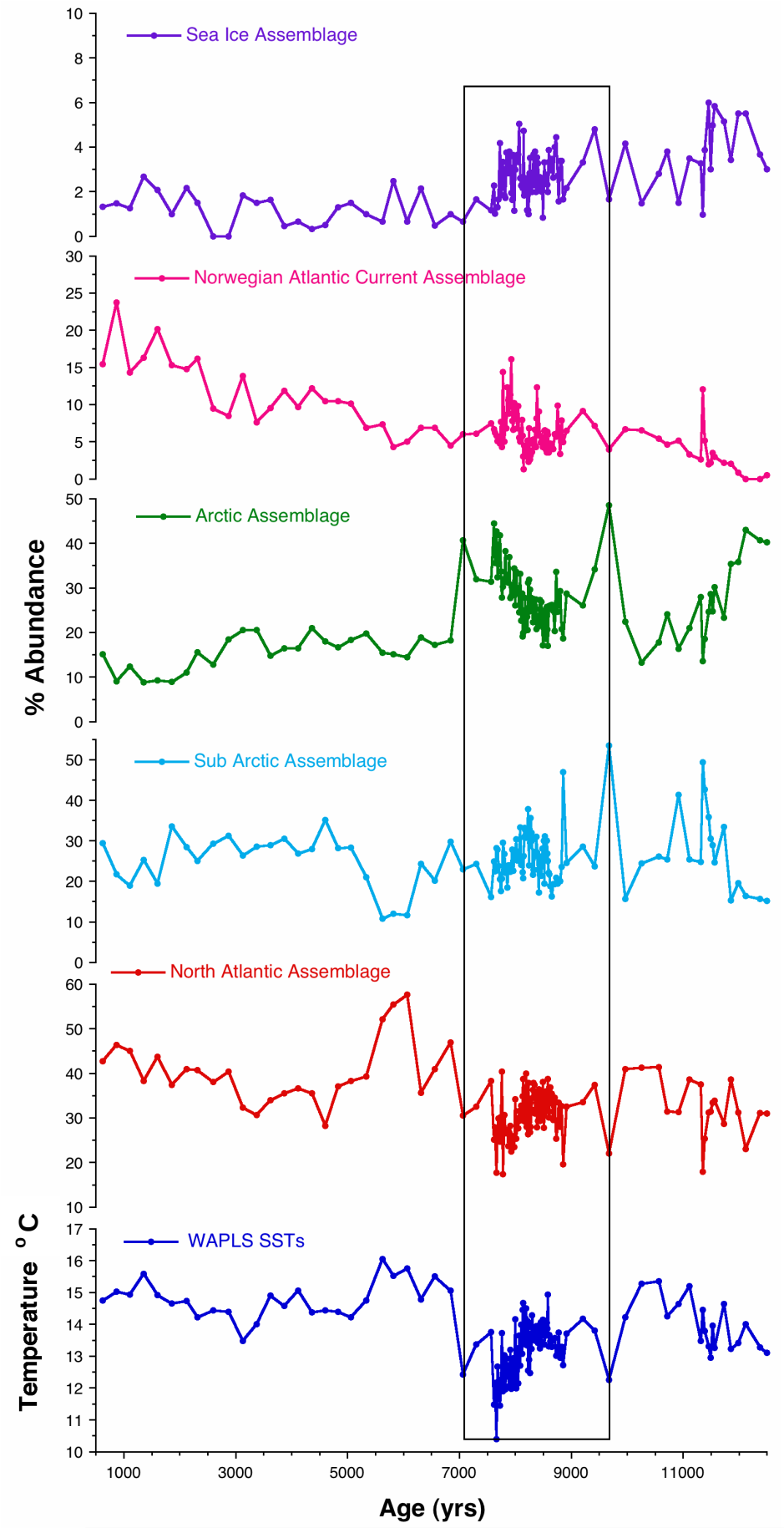

Figure 6.23 MD99-2251 floral assemblages. Highlighted area indicates the broad cooling 9.5-7kyr

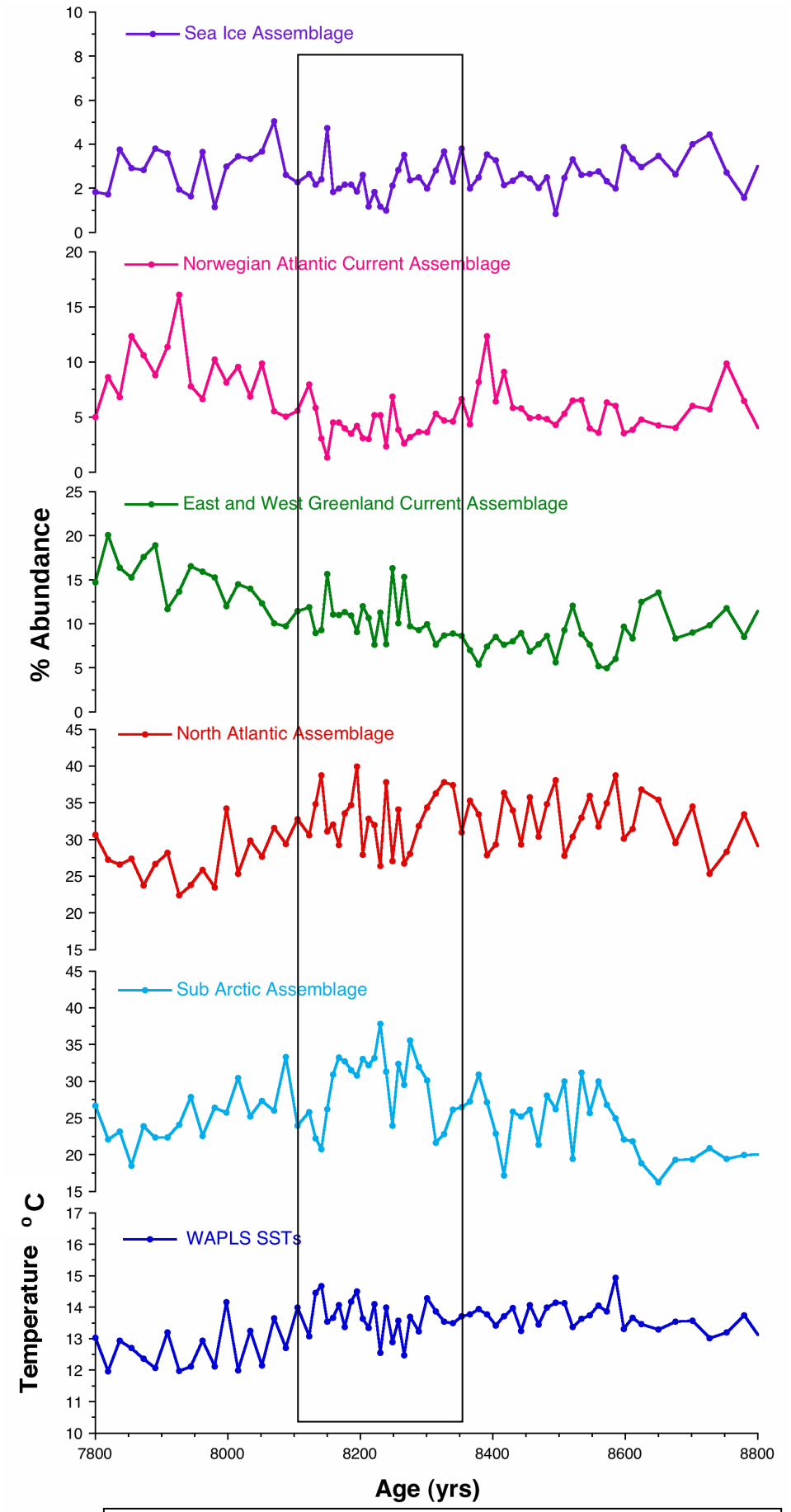

Figure 6.24 MD99-2251 8.2kyr event floral assemblages
8.1-8.3 kyrs is highlighted

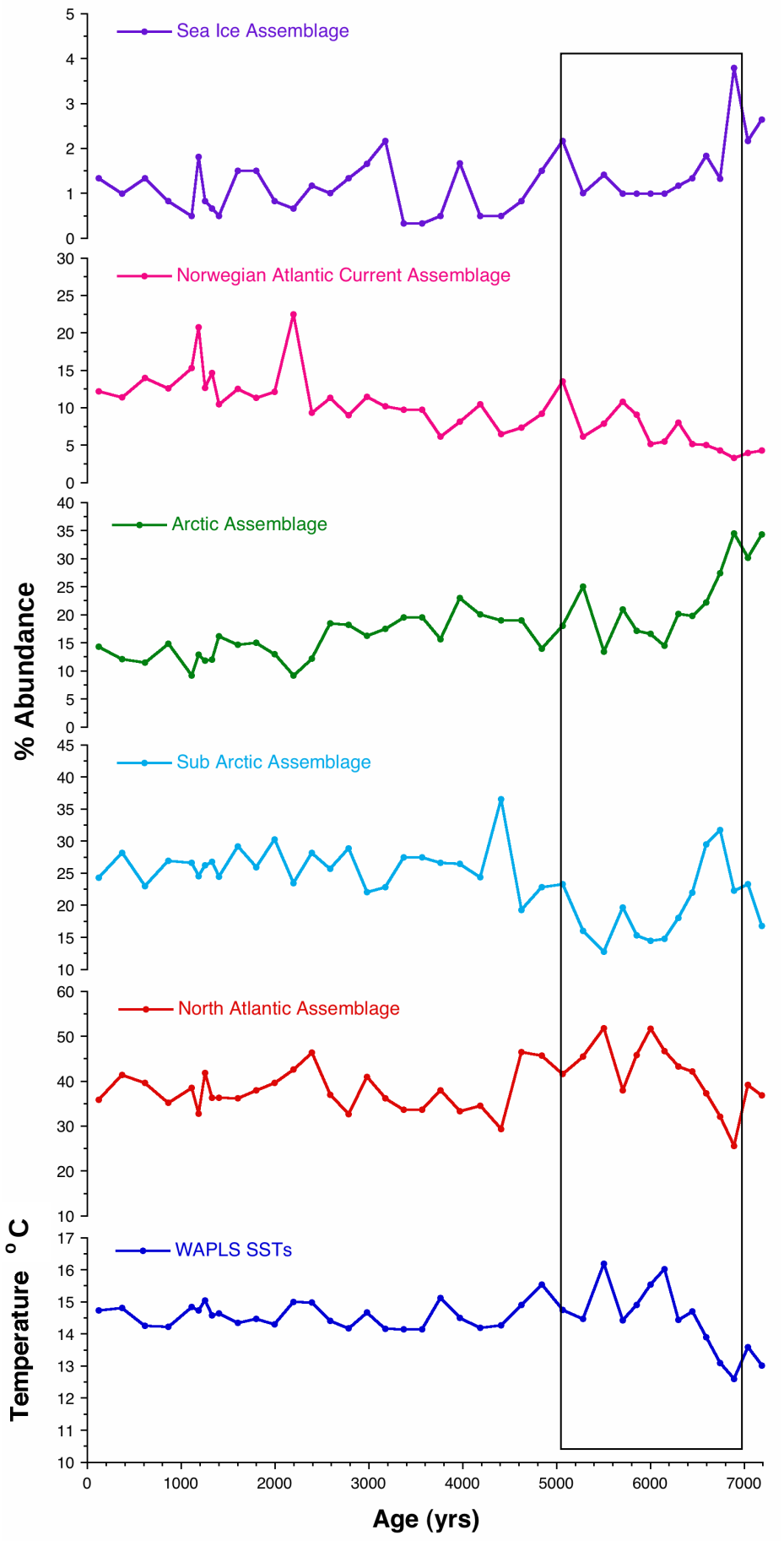

Figure 6.25 MD99-2252 floral assemblages Highlighted area indicates 7-5kyr warming

The floral assemblage data reflects the Holocene trends defined by analysis of the individual species abundance data and SST estimates. The initial warming at the beginning of the Holocene is reflected in the floral assemblage data as a decrease in the Arctic assemblage and an increase in the Norwegian Atlantic Current assemblage (Figure 6.23). The broad cooling at around 9.5-7kyr, highlighted in Figure 6.23, is marked by an increase in the Arctic assemblage and an increase in Norwegian Atlantic Current flora. Notably however within this broad cooling, the 8.2kyr event high resolution study from 7.8-8.8kyr (Figure 6.24) shows a broad increase in the Sub Arctic flora for the interval 8.15-8.42kyrs, highlighted in Figure 6.24. The pronounced warming 5-7kyr is marked by a significant increase in the North Atlantic Assemblage and a corresponding significant decrease in the Sub Arctic Assemblage (Figure 6.23). A trend also reflected in the assemblage data for MD99-2252 (Figure 6.25). Both cores indicate a relatively stable late Holocene although the record for MD99-2251 indicates a more pronounced gradual increase in the abundance of the Norwegian Atlantic Current flora for the late Holocene than does the record for MD99-2252.

One problem that may be highlighted with this floral assemblage data employed so far in this study is that certain species are included in more than one assemblage. For example, *Thalassionema nitzschioides* is both a primary species for the Norwegian Current assemblage and an additonal species for the North Atlantic current assemblage; *Thalassiosira gravida* vegetative is the only species reflecting the East West Greenland Current assemblage but also a factor in the Arctic floral assemblage. In the case of this study, where the percentages of *Thalassiosira gravida* resting spore are very low, the vegetative form of *Thalassiosira gravida* becomes the dominant species for both the East and West Greenland and Arctic assemblages. In order to overcome this issue of repeat counting of species across the assemblages, the factor weightings from Berner *et al.* (2008) were examined (Table 6.6) and cold, intermediate and warm water floral grouping devised which included no repetition of species (Table 6.7) Species were selected that scored over 0.1 on the factor weighting. Where a species scored more than 0.1 in two categories the highest score was used to assign it to an assemblage. The new assemblage data is plotted in Figures 6.26 and 6.28.

	Factor 1 Arctic Greenland	Factor 2 North Atlantic Current	Factor 3 Sub Arctic	Factor 4 Norwegian Atlantic Current	Factor 5 Sea Ice	Factor 6 Arctic	Factor 7 E & W Greenland Current
T.longissima	0.0542	0.0544	0.1632	0.0272	-0.0068	-0.0011	-0.0020
T.nitzschioides	-0.0424	0.1752	-0.1045	0.8029	0.0173	-0.0083	-0.1515
R.h.hebetata	0.0489	-0.0080	0.0401	0.0158	-0.0203	0.0679	-0.0224
R.h.semispina	-0.0112	-0.290	0.8861	-0.0016	0.0278	0.0764	-0.1574
R.borealis	-0.0375	0.0118	0.3720	0.1865	0.0263	-0.858	-0.0908
P.alata	0.0392	-0.0370	-0.0066	0.3943	0.0008	-0.0463	-0.0738
B.fragilis	0.0172	0.0014	-0.0040	-0.0041	0.0718	0.0113	0.0006
R.tesselata	0.0002	0.0822	-0.0153	0.0495	0.0019	-0.0007	-0.0070
A.curvatulus	0.1236	0.0102	-0.0107	0.0476	-0.0144	0.1322	-0.1135
T.gravida resting spore	0.0118	0.0308	-0.0836	-0.0267	0.1018	0.9384	-0.2259
T.gravida veg	0.1752	-0.0580	0.1464	0.2055	-0.0217	0.2475	0.9118
T.auguste-lineata	0.8742	0.0031	-0.0131	-0.0163	-0.0575	-0.0541	-0.1457
T.trifulta	0.3740	0.0041	-0.0056	0.0155	-0.0575	-0.0233	-0.0656
T.nordenskioeldii	0.0028	-0.0233	0.0362	0.0943	0.1006	0.0369	-0.0415
T.oestrupii	0.0086	0.9550	0.0447	-0.1045	-0.0074	-0.0111	0.0815
T.hyalina	0.1103	-0.0005	-0.0080	-0.0034	0.2090	-0.0402	-0.0032
T.angulata	-0.0225	-0.631	-0.0435	0.2154	0.0288	0.0038	-0.0164
A.marina	0.0023	0.0592	0.0120	-0.0136	-0.0001	-0.0055	0.0045
N.bicapitata	0.0035	0.1159	-0.0087	0.0055	-0.0003	0.0030	-0.0083
F.cylindrus	0.1141	0.0011	-0.0130	-0.0114	0.2647	-0.0730	-0.0038

Table 6.8 The factor score matrix for key species from factor analysis of surface sediments. After Berner *et al.* (2008). All positive scores over 0.1 are highlighted.

Colder Species: those with highest factor scores for Arctic, Sea Ice, E&W Greenland Current and Arctic Greenland Assemblages	Intermediate Species: those with highest factor scores for Sub Arctic and Norwegian Atlantic Assemblages	Warmer Species: those with highest factor scores for North Atlantic Assemblage
Actinocyclus curvatulus	*Thalassiothrix longissima*	*Thalassiosira oestrupii*
Thalassiosira gravida resting spore	*Thalassionema nitzschioides*	*Nitzschia bicapitata*
Thalassiosira gravida veg	*Rhizosolenia h.semispina*	
Thalassiosira auguste-lineata	*Rhizosolenia borealis*	
Thalassiosira trifulta	*Proboscia alata*	
Thalassiosira nordenskioeldii	*Thalassiosira angulata*	
Thalassiosira hyalina		
Fragilariopsis cylindrus		

Table 6.9 Species selected from varimax factor analysis (Berner *et al.*,2008) to reflect warm and cold water assemblages. Species are assigned according to the highest factor score they obtain in the matrix (Table 6.6)

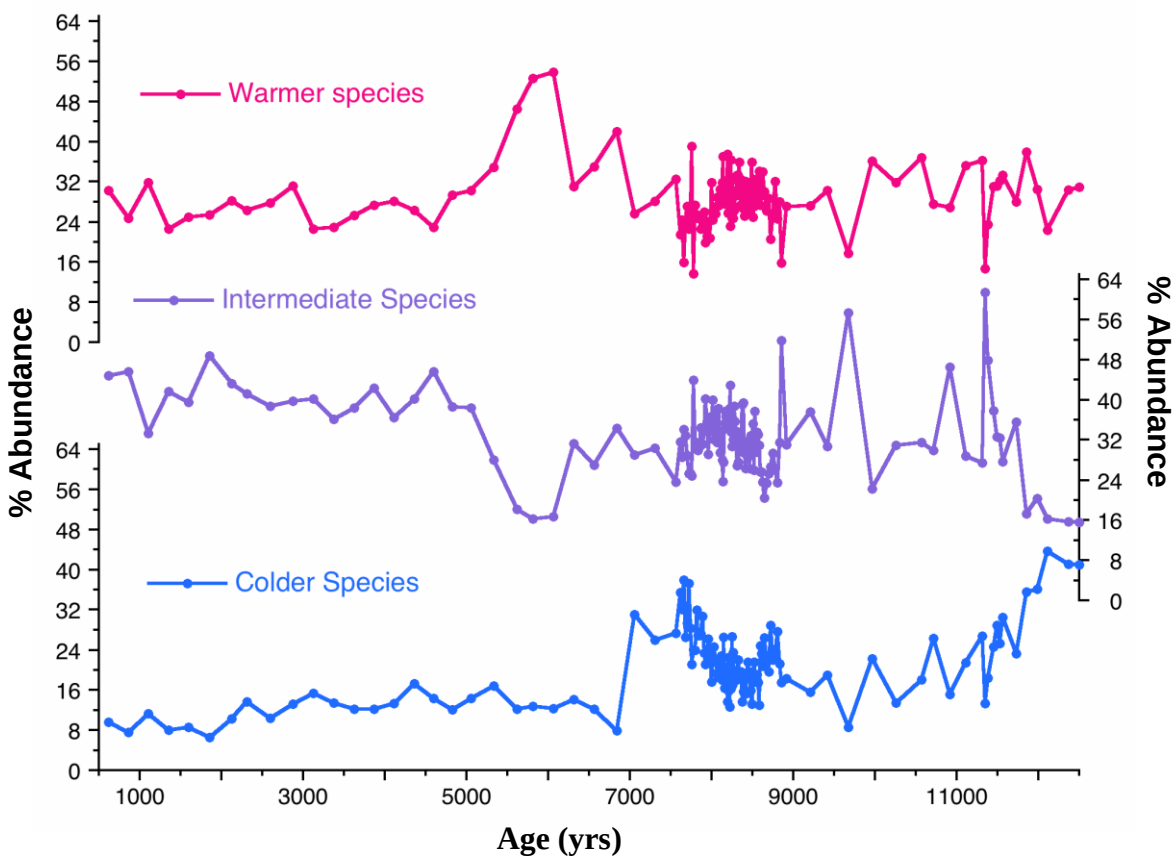

Figure 6.26 The distribution of colder, intermediate and warmer water diatom species groupings in marine core MD99-2251 as derived from varimax factor analysis scores Berner *et al.*(2008)

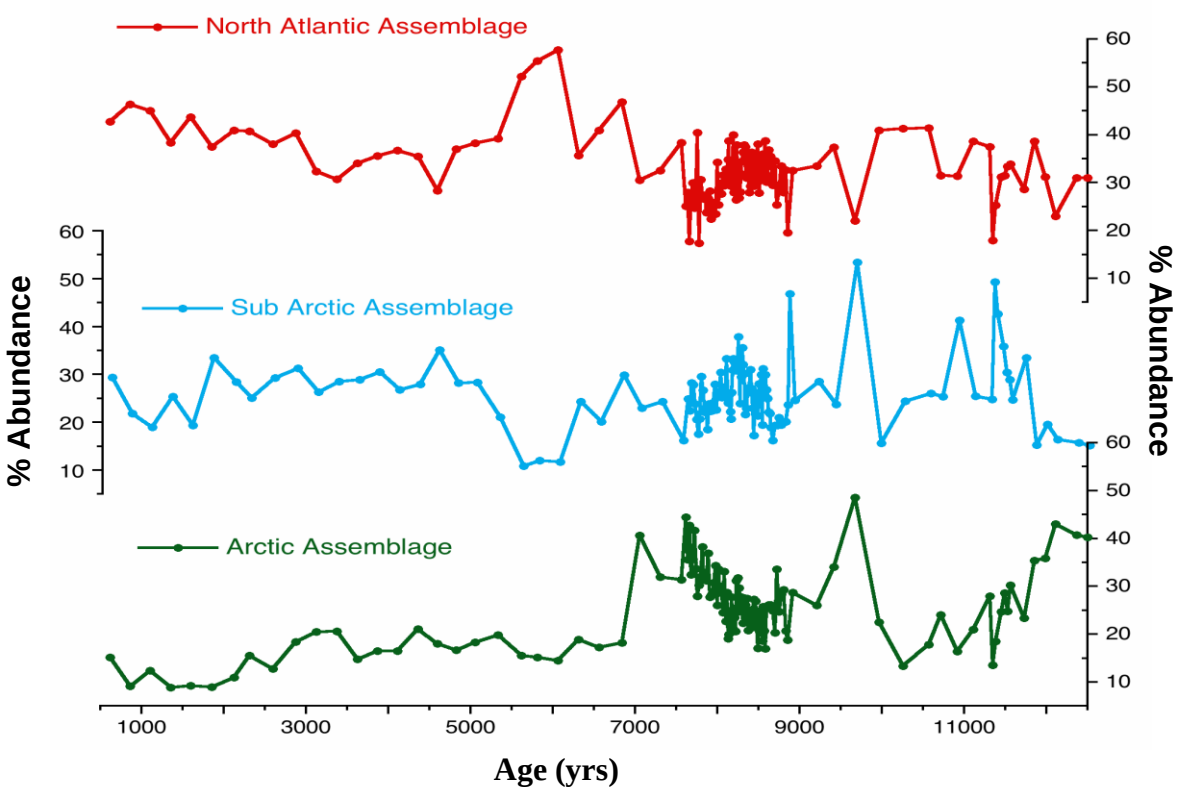

Figure 6.27 The distribution of Arctic SubArctic and North Atlantic Current Assemblages (Andersen *et al.*, 2004a) in marine core MD99-2251

Similar trends are observed with the new species groupings as with the raw species abundance data and the previous assemblage groupings, an initial warming at the beginning of the Holocene, a more variable early Holocene, a broad cooling around 7-9.5kyr, a warming around 5-7kyr and a relatively stable late Holocene. The most noticeably difference between the two assemblage groupings (Figure 6.26 and Figure 6.27) is that in the new assemblage groupings the late Holocene is dominated by an intermediate rather than warmer flora.

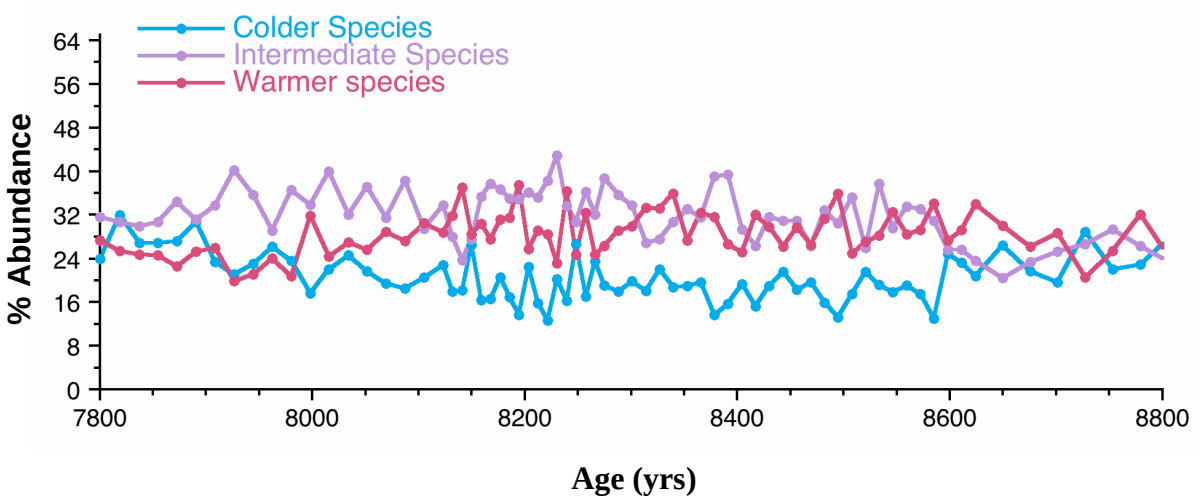

Figure 6.28 The distribution of colder, intermediate and warmer water diatom species for 8.2 kyr event in marine core MD99-2251 as derived from varimax factor analysis scores Berner *et al.*(2008)

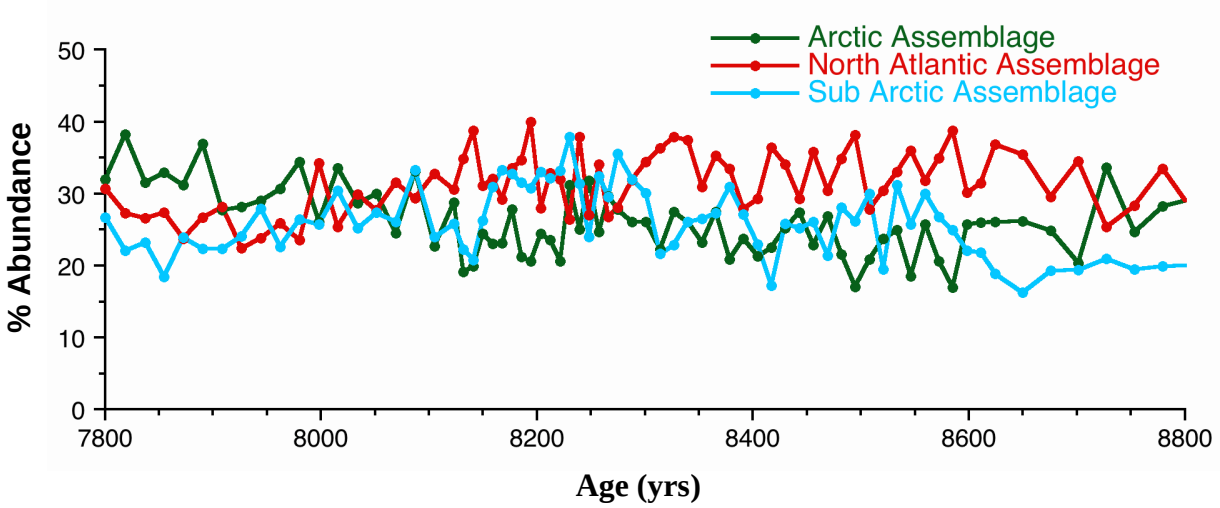

Figure 6.29 The distribution of Arctic Subarctic and North Atlantic Current Assemblages (Andersen *et al.*, 2004a) in marine core MD99-2251 for the 8.2kyr event

There is little difference between the distribution of the two assemblage groupings for the high resolution study, although again in the new groupings, as with the late Holocene, an intermediate flora is more dominant than a North Atlantic flora. There is no distinct event at 8.2kyr indentified in either assemblage grouping but rather a general decadal and centennial scale variability.

6.8 Multivariate analysis of down core diatom data

In order to examine down core zonations and species groupings within the diatom flora; for MD99-2251, two multivariate analyses were undertaken; a principal components analysis (PCA) and a K-means cluster analysis. The groupings identified from these analyses were then compared with the down core distribution of individual abundance diatom taxa in and diatom assemblages identified by Andersen *et al.* (2004a).

6.8.1 Principal component analysis

Principal component analysis is a multivariant statistical technique for indentifying linear components within large data sets. With PCA, the large data matrix is reduced to two smaller ones that consist of principal component scores and loadings. PCA is based solely upon eigenanalysis of a correlation or covariance matrix. Principal component loadings are the eigenvectors of the correlation or covariance matrix (depending on which is used for the analysis). Eigenvalues define the amount of variance. They may be envisaged as describing the dimensions formed by a scatterplot of the variables (Field, 1999). Principal component scores contain information on all variables (in the case of this study, diatom taxa) and indicate the relative contribution each variable makes to that score (Farnham *et al.* 2003). Principal component analysis is used where it may be reasonably assumed that all variance is common variance. In factor analysis it is necessary to first estimate the amount of common variance within the data set by estimating communality values for each variable (Field, 1999). Studies have indicated however that with datasets of more than thirty variables and communalites of greater than 0.7 for all variables, there is little difference between the solutions for PCA and factor analysis (Stephens, 2002).

For these analyses the diatom count data for MD99-2251 was arranged into a data matrix with forty-eight columns representing diatom taxa. These forty-eight taxa are the same as those i+dentified in Table 6.4 with the exception of *Actinocyclus kutzingii* which was removed from the analysis as none were present in the floral counts. As for the transfer function, *Thalassiosira gravida* vegetative and *Thalassiosira gravida* resting spore were recorded separately as were *Thalassionema nitzschioides* and *Thalassionema nitzschioides* var. parva. *Rhizosolenia styliformis* and *Rhizosolenia borealis* were also

considered together as for the WA-PLS transfer function and Sp Y and *Nitzschia* sp 1 were similarly included. The data matrix consisted of one hundred and thirty-three rows, each representing individual depth percentage counts of the diatom taxa.

The analysis in this study was undertaken using a co-variance matrix, components were extracted on the basis of eigenvalues with twenty-five maximum iterations for convergence and a varimax rotation. Six components were extracted. A simplified version of the component score co-efficient matrix is displayed below. All species that received a component score of at least 0.01 for at least one of the components are shown (Table 6.10). These six components account for 91.5% of the variance. The first four factors account for 85% of the variance (Table 6.11)

Component Score Coefficient Matrix[a]

	Component					
	1	2	3	4	5	6
Thalassiothrix_longissima	.044	-.030	-.005	.015	.052	.139
Thalassionema_nitzschoides	.615	-.149	.033	-.051	-.356	-.252
Rhizosolenia_hebetata_semispina	-.240	.675	-.009	-.223	-.635	-.052
Rhizosolenia_styliformisborealis	-.480	-.025	-.671	-.519	.200	-.227
Proboscia_alata	-.042	-.022	-.161	.081	.130	.898
Rhizosolenia_bergonii	.010	-.001	-.002	-.001	-.005	-.004
Roperia_tesselata	.025	-.006	.005	-.001	.000	-.013
Actinocyclus_curvatulus	-.317	.108	.261	.030	.651	-.401
*Thalassiosira_gravida*_resting_spore	.011	-.014	.006	-.009	-.031	-.045
*Thalassiosira_gravida*_vegetative	-.308	-.516	.450	-.188	-.482	.143
Thalassiosira_trifulta	-.001	.003	.002	.004	.009	-.014
Thalassiosira_lineata	.004	.009	.014	.005	.022	-.021
Thalassiosira_oestrupii	-.476	-.130	-.446	.683	-.142	.075
Thalassiosira_ferelineata	.035	-.012	-.003	.001	-.014	.000
Coscinodiscus_marginatus	.089	-.042	.019	-.015	-.063	-.080
Azpeitia_nodulifera	.011	-.003	-.004	-.005	-.030	-.013
Bacteriastrum_hyalinum	-.021	.018	.021	.001	.063	-.043
Synedra_sp#	.001	.011	.015	.010	.013	-.061
*Thalassionema_nitzschoides*_parva	-.002	.000	-.006	.015	.014	.008

Table 6.10 Component score coefficient matrix for principal component analysis of down core diatom species counts for MD99-2251. Species selected as representative of each component are highlighted in yellow.

	Percentage of variance	Cumulative percentage of variance
Component 1	30.761	30.761
Component 2	26.261	57.021
Component 3	19.524	76.545
Component 4	8.736	85.281
Component 5	3.391	88.672
Component 6	2.816	91.488

Table 6.11 The percentage of variance and cumulative variance of each component for the down core principal component analysis of MD99-2251

Key species for each component were identified on the basis of those receiving a positive component score greater than 0.1 in the component score coefficient matrix (Table 6.10). The species selected are highlighted on the Table 6.10 and listed in Table 6.12.

Component	Species
Component 1	*Thalassionema nitzschioides*
Component 2	*Rhizosolenia hebetata semispina* *Actinocyclus.curvatulus*
Component 3	*Thalassiosira gravida* vegetative *Actinocyclus curvatulus*
Component 4	*Thalassiosira oestrupii*
Component 5	*Actinocyclus curvatulus* *Rhizosolenia styliformis/borealis* *Proboscia alata*
Component 6	*Proboscia alata* *Thalassiosira gravida* vegetative *Thalassiothrix longissima*

Table 6.12 Key species associated with down core principal component analysis. Species were selected on the basis of positive component scores greater than 0.1

Components were plotted against age and key species as well as assemblages identified by Andersen *et al.* (2004a) which most closely corresponded to the species composition of the new components (Figures 6.30-6.37). Three of the components showed strong correlation to an individual species. Component one exhibits a strong correlation

with the distribution of *T.nitzschioides* through the core (Figure 6.30). This is unsurprising as the Component score coefficient matrix (Table 6.10) indicates the strongest weighting for this species in component one. Component one also shows a good correlation with the Norwegian Atlantic assemblage of Andersen *et al.* (2004a) (Figure 6.30). *Thalassionema nitzschioides* is recognised by the authors as the primary assemblage species and *Proboscia alata* and *Thalassiosira angulata* as secondary assemblage species (Table 6.7).

Component two exhibits a strong correlation with the down core distribution of *Rhizosolenia hebetata semispina* (Figure 30.1). Again the Component score coefficient matrix (Table 6.10) indicates this species as having the strongest weighting for the

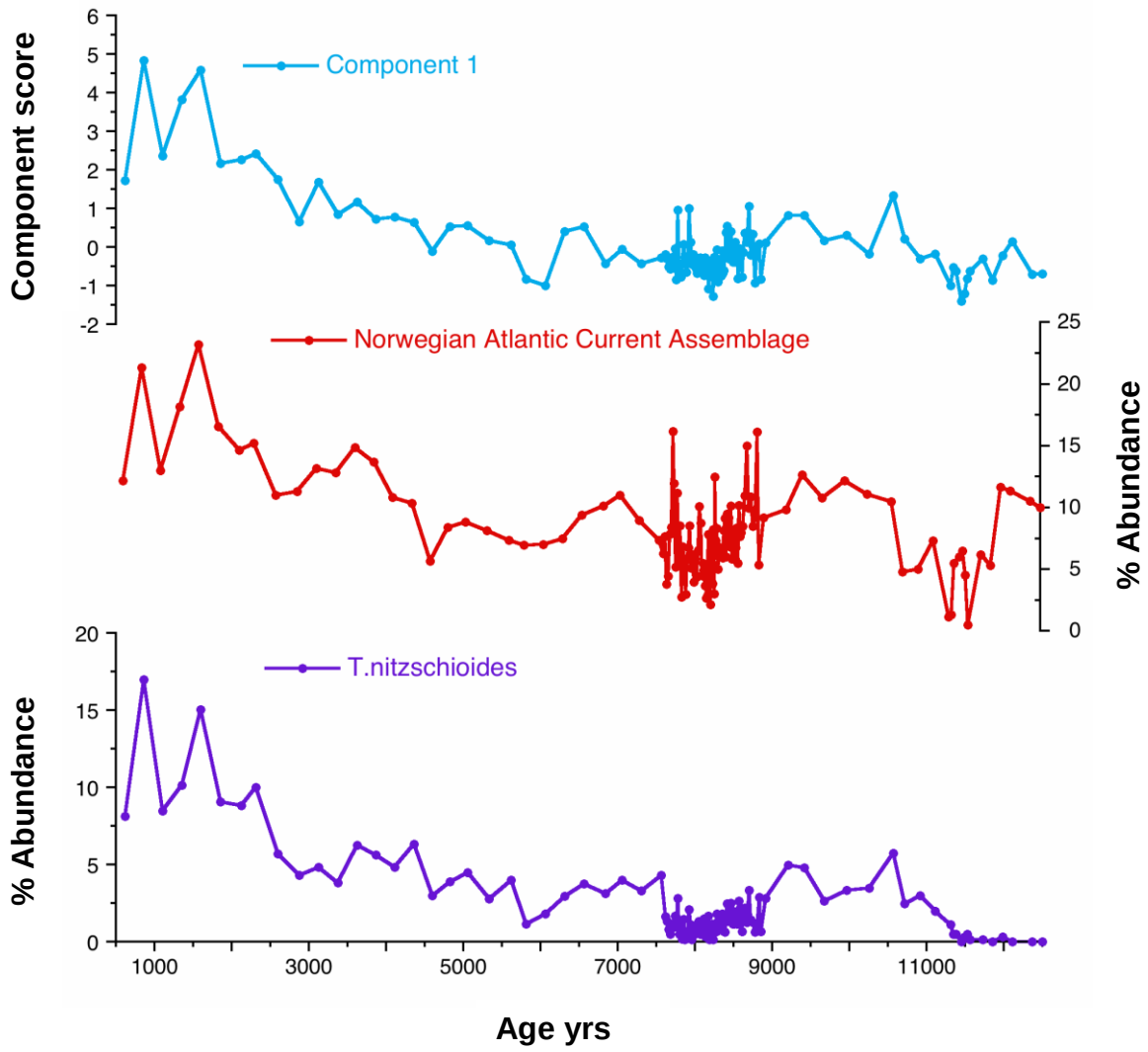

Figure 6.30 Component one of the down core principal component analysis plotted against age and compared with *T.nizschioides* and Norwegian Atlantic flora Andersen *et al.* (2004a)

component. Component two does not show a strong correlation with any of the assemblages of Andersen *et al.* (2004a). Both the Arctic and Sub Arctic assemblages show a peak in percentage abundance co-incident with the large *Rhizosolenia hebetata semispina* peak at around 9.5kyr, but otherwise the distribution patterns of the assemblages and component two are dissimilar (Figure 30.1). *Rhizosolenia hebetata semispina* is a primary assemblage species for Sub Arctic flora and a secondary assemblage species for Arctic flora (Table 6.7). Component four shows a strong correlation with both the down core distribution of *T.oestrupii* and the North Atlantic Assemblage of Andersen *et al.* (2004a). (Figure 6.32). *T.oestrupii* is the primary assemblage species for the North Atlantic assemblage (Table 6.7) and the most weighted species in component score coefficient matrix (Table 6.10) for component four.

Components three, five and six show slightly more complex relationships to downcore species distribution and to the floral assemblages of Andersen *et al.* (2004a). The most weighed species in the component score coefficient matrix for component three are *Actinocyclus curvatulus* and *Thalassiosira gravida* vegetative (Table 6.10). The combined species abundance of these two taxa closely resembles the down core distribution of component three (Figure 6.33). The regional assemblage most similar to component three is the East and West Greenland current assemblage Andersen *et al.* (2004a). He only species identified as significant in this assemblage is *Thalassiosira gravida* vegetative (Table 6.7).and so the distribution of the East and West Greenland current assemblage mirrors that of *Thalassiosira gravida* vegetative. However in the analysis of MD99-2251 groupings alone, it can be seen that the East and West Greenland current assemblage best reflects a combined species abundance of *Actinocyclus curvatulus* and *Thalassiosira gravida* vegetative (Figure 6.33).

The most weighed species in the component score coefficient matrix for component three are *Actinocyclus curvatulus Actinocyclus, Rhizosolenia styliformis/borealis* and *Proboscia alata* (Table 6.10). The down core distribution of component five does not strongly represent the down core distribution of any of these individual species or of the combined percentage abundances of the three taxa. However component five does show a strong correlation to the Arctic assemblage of Andersen *et al.* (2004a). (Figure 6.34).

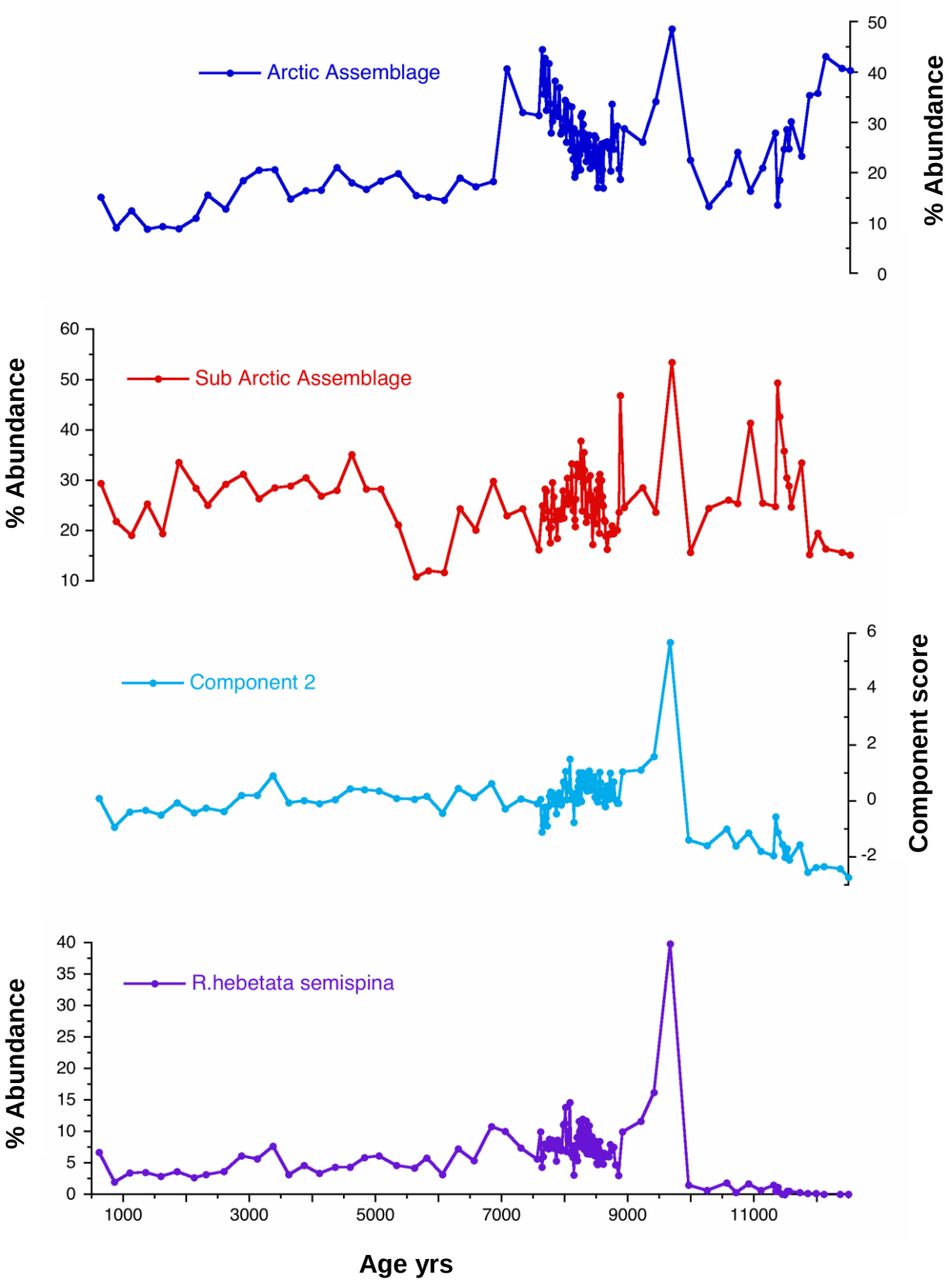

Figure 6.31 Component two of the down core principal component analysis plotted against age and compared with *R.semispina* Sub Arctic and Arctic flora Andersen *et al.* (2004a)

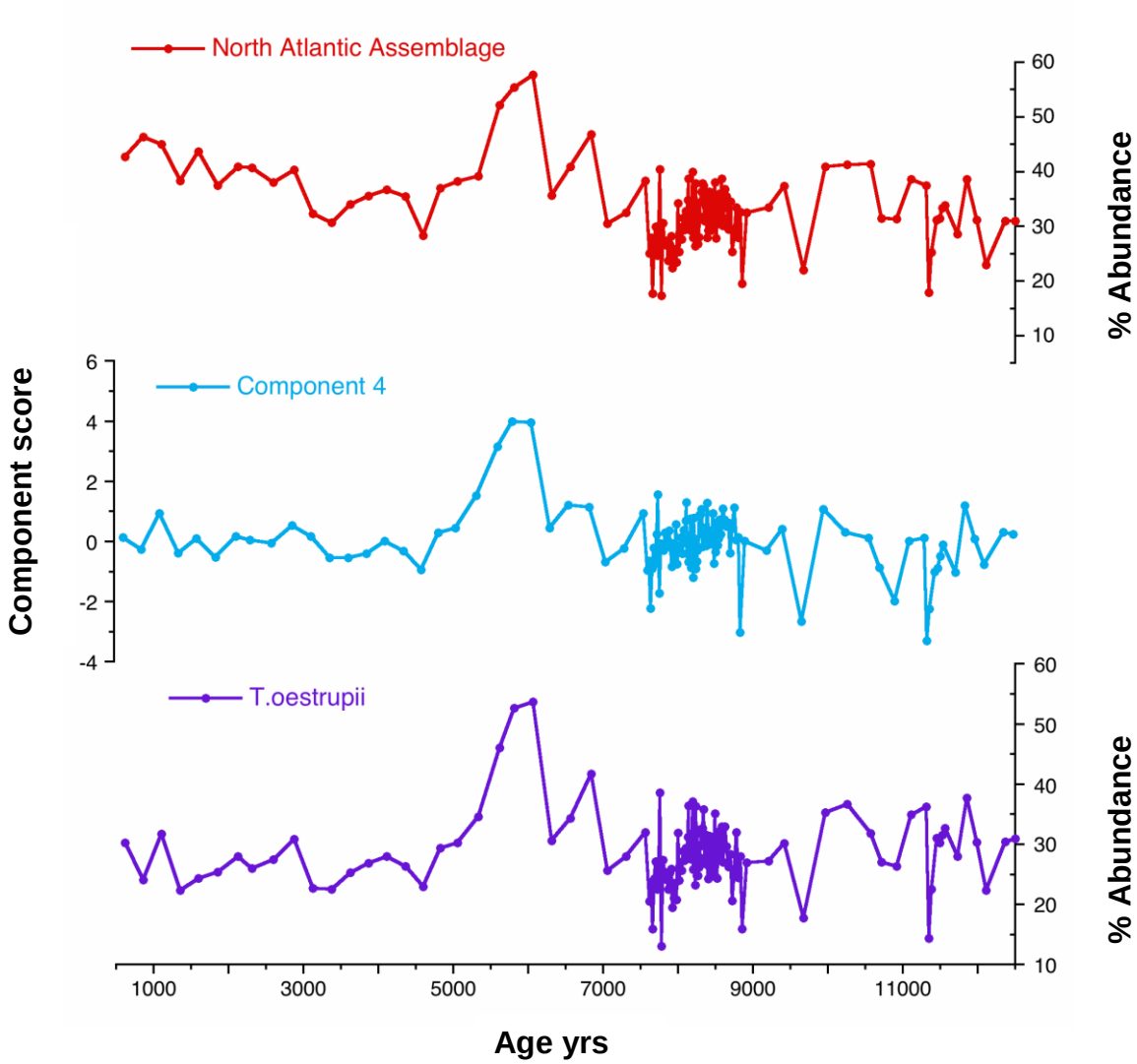

Figure 6.32 Component four of the down core principal component analysis plotted against age and compared with *R.semispina* and North Atlantic Assemblage Andersen *et al.* (2004a)

Component six of the down core principal component analysis is plotted against age and compared with the down core species abundance for *P.alata*, *T.gravida* vegetative and *T.longissima*, a combined species abundance for the three species and the Arctic and Sub Arctic, and sea-ice assemblages of Andersen *et al.* (2004a). (Figure 6.35). The component shows the most correlation with the down core distribution of *P.alata* which is strongly weighed in the component score coefficient matrix (Table 6.10). It is important to note that both components five and six only represent a small amount of the variance in core MD99-2251; 3.391% and 2.816% respectively (Table 6.11) so it may be unreasonable to draw any strong conclusions for the correlations of these components.

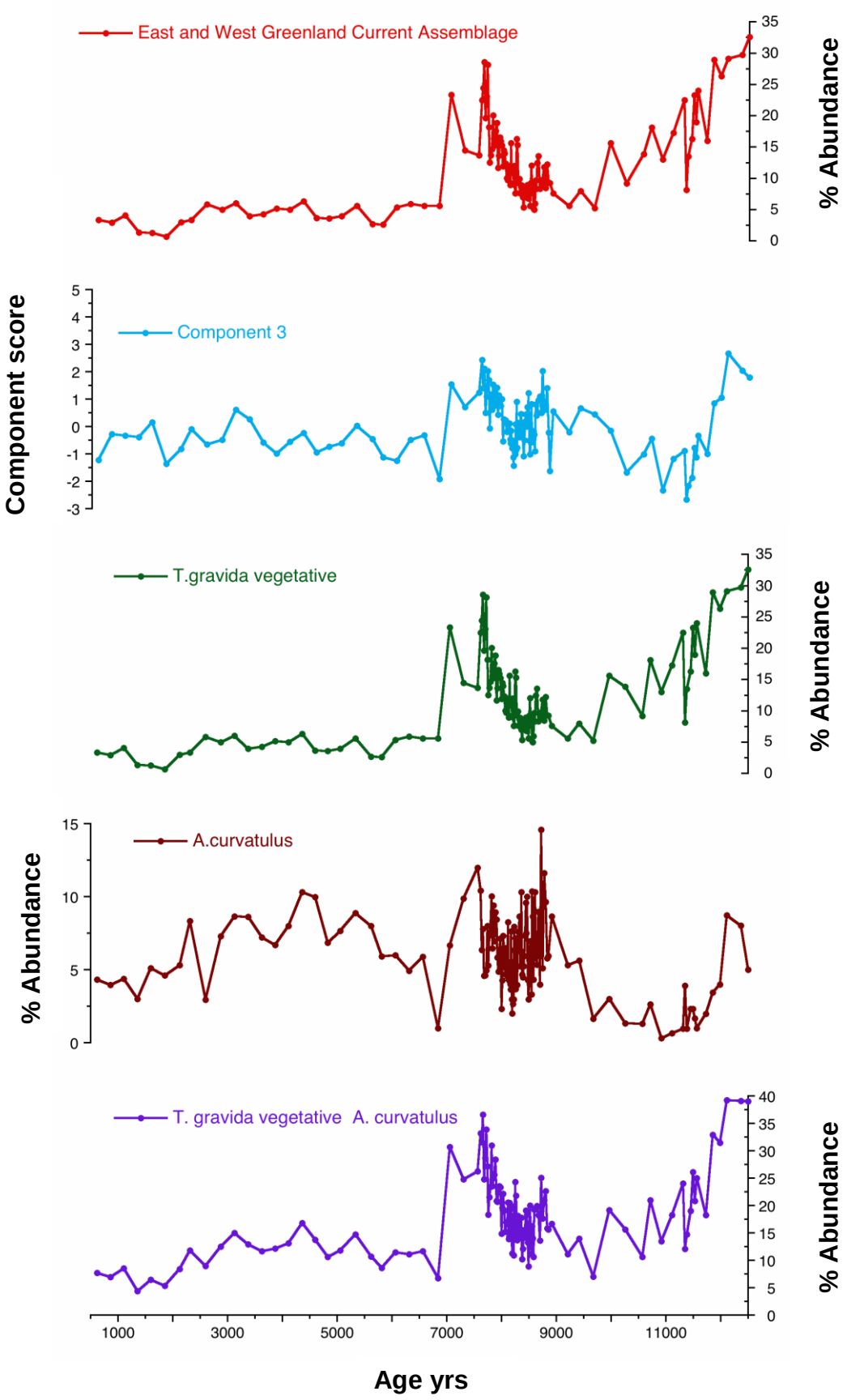

Figure 6.33 Component three of the down core principal component analysis plotted against age and compared with percentage abundance of *T.gravida* vegetative, *A.curvatulus*, a combined species abundance for *T.gravida* vegetative *A.curvatulus* and East West Greenland Current flora Andersen *et al.* (2004a)

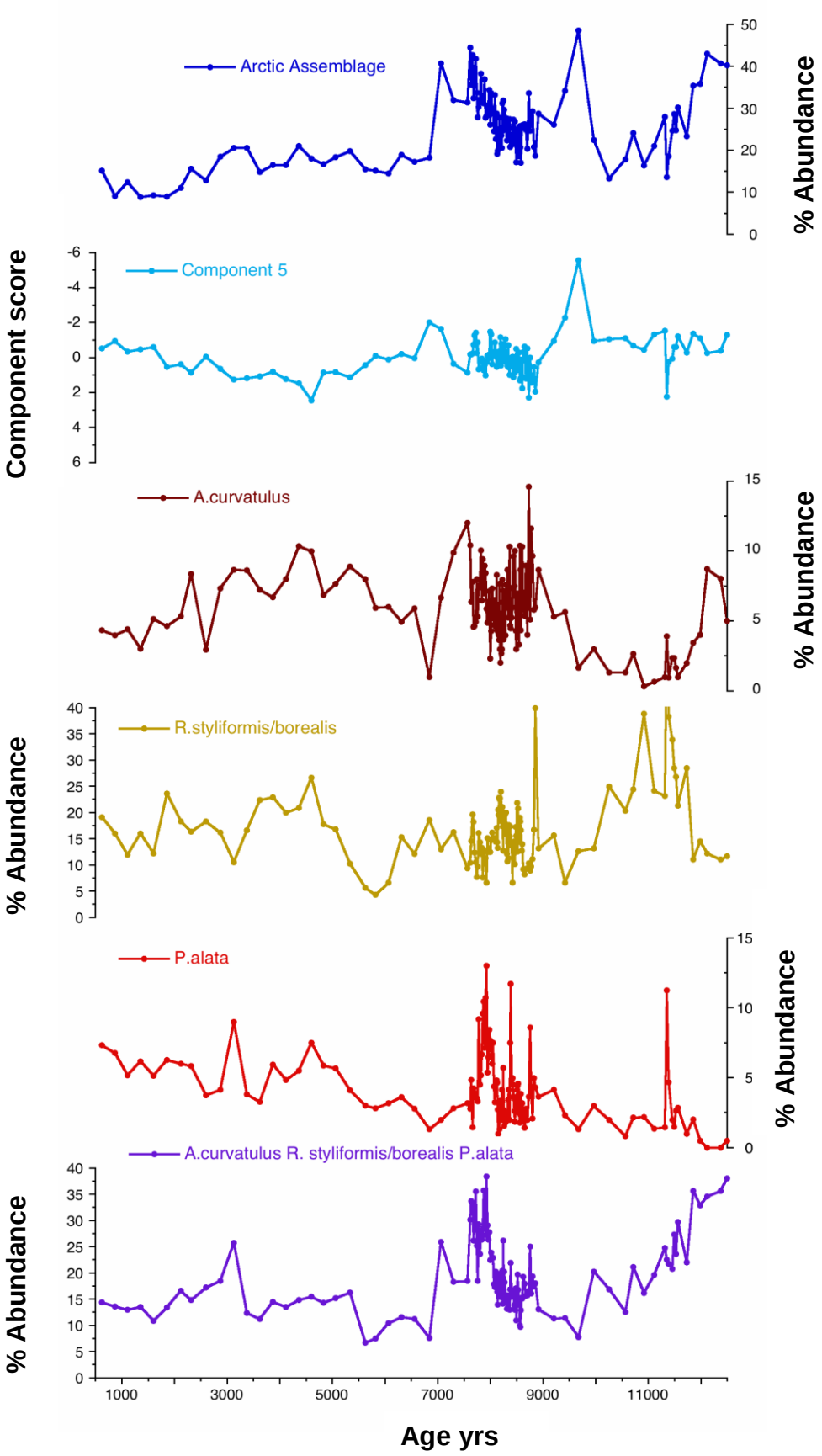

Figure 6.34 Component five of the down core principal component analysis plotted against age and compared with the down core distribution of *Actinocyclus curvatulus*, *Rhizosolenia stlyliformis/borealis*, *Proboscia alata*, a combined species abundance of the above three taxa and the Artcic assemblge Andersen *et al.* (2004a).

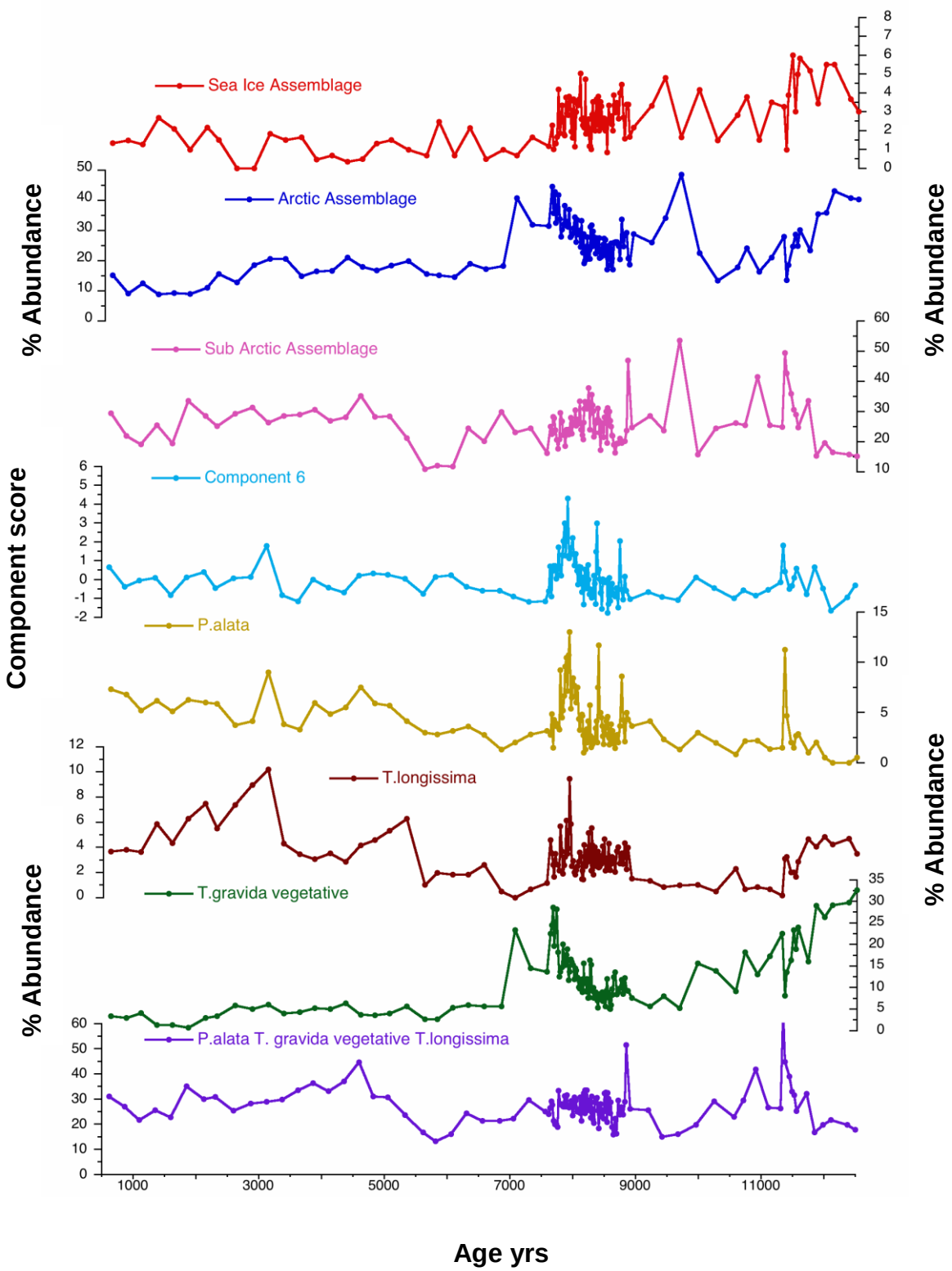

Figure 6.35 Component six of the down core principal component analysis plotted against age and compared with the down core species abundance for *P.alata*, *T.gravida* vegetative and *T.longissima*, a combined species abundance for the three species and the Arctic and Sub Arctic, and sea-ice assemblages of Andersen *et al.* (2004a).

6.8.2 K-means cluster analysis

A K-means cluster analysis was also undertaken for core MD99-2251. K-means cluster analysis divides observations (in this study each diatom species abundance count with depth) into a number of clusters 'K'. Each observation is then assigned to the cluster with the nearest mean using the K-means algorithm which seeks to minimise the squared error between of distance between the observation and the cluster centre (Johnson & Feldstein, 2010).

Six clusters were selected for analysis of the down core diatom species abundance counts for core MD99-2251. Table 6.13 indicates the final cluster centres with respect to diatom key species.

Final Cluster Centers

	Cluster					
	1	2	3	4	5	6
Thalassiothrix_longissima	3.01	2.52	3.40	1.01	3.68	1.77
Thalassionema_nitzschoides	.81	1.04	1.63	2.69	3.59	2.02
Rhizosolenia_hebetata_semispina	1.12	2.81	8.40	40.67	6.60	5.55
Rhizosolenia_styliformisborealis	38.08	17.77	12.45	12.94	18.41	6.69
Proboscia_alata	4.28	2.10	5.46	1.34	3.93	3.11
Rhizosolenia_bergonii	1.05	.44	.69	1.68	1.11	.84
Roperia_tesselata	.51	.55	.98	.00	1.32	.59
Actinocyclus_curvatulus	2.63	4.36	7.65	1.68	5.85	6.38
*Thalassiosira_gravida*_resting_spore	2.80	2.37	.90	1.01	.62	.59
*Thalassiosira_gravida*_vegetative	12.91	24.23	12.89	5.38	7.11	5.91
Thalassiosira_trifulta	.39	.46	.94	.00	1.14	1.01
Thalassiosira_lineata	.34	.72	2.19	1.68	1.95	2.86
Thalassiosira_oestrupii	23.38	29.44	27.13	18.15	30.19	48.38
Thalassiosira_ferelineata	1.61	1.51	1.73	1.34	1.97	2.18
Coscinodiscus_marginatus	2.12	2.24	.46	.67	.85	.33
Azpeitia_nodulifera	.84	1.29	.56	2.69	.79	.25
Bacteriastrum_hyalinum	1.12	.74	2.15	1.68	2.08	1.34
Synedra_sp#	.25	.38	1.61	.17	1.20	3.11
*Thalassionema_nitzschoides*_parva	.36	.82	1.06	.34	1.76	3.06

Table 6.13 Cluster centres with respect to key diatom taxa for K-mean cluster analysis of core MD99-2251

Number of Cases in each Cluster

Cluster	1	6.000
	2	19.000
	3	46.000
	4	1.000
	5	57.000
	6	4.000
Valid		133.000
Missing		.000

Table 6.14 The number of cases assigned to each of the six clusters assigned for the K-means Cluster analysis of core MD99-2251

The mean distance from the cluster centre and the assigned cluster for each diatom species abundance count were plotted against age (Figure 6.36a).An examination of species abundance for each cluster indicates that clusterone represents those samples with a high abundance of *R.styliformis/borealis* as observed in the early Holocene. Cluster two represents samples with a high abundance of *T.gravida* vegetative. Cluster three represents a group of samples from 7-2-9.2 kyr in correspondence with the broad cooling previously identified for this interval. An expanded plot for this interval is represented in Figure 6.36b). Cluster four is the single high abundance peak of *R.hebetata semipina*.having only one case to the cluster (Table 6.14). Cluster five represents dominance of *T.oestrupii* and cluster 6 extremes of the dominance of *T.oestrupii*.

The K-means cluster analysis may therefore be seen to support previous analyses in this study of down core species abundances in core MD99-2251. The early Holocene (11.5-9.5kyr) indicates an alternation between the cold *T.gravida* vegetative dominated assemblage of cluster two and the *R.styliformis/borealis* dominated events of cluster one which as previously discussed may be a response to stratification of the water column due to the proximity of the Sub Polar front. The broad cooling (9.5-7kyr) is represented by a dominance of cluster three alternating with cluster five. The warm 7-5kyr interval is represented by a dominance of cluster five. This is the cluster dominated by *T.oestrupii,* a taxa representative of input from the North Atlantic current. At the peak of this interval cluster six becomes dominant which represents the highest percentage abundances of

T.oestrupii. and the warmest SSTs (Figure 6.21) around 6kyr. The late Holocene 5kyr to present is dominated by cluster five representing the North Atlantic flora.

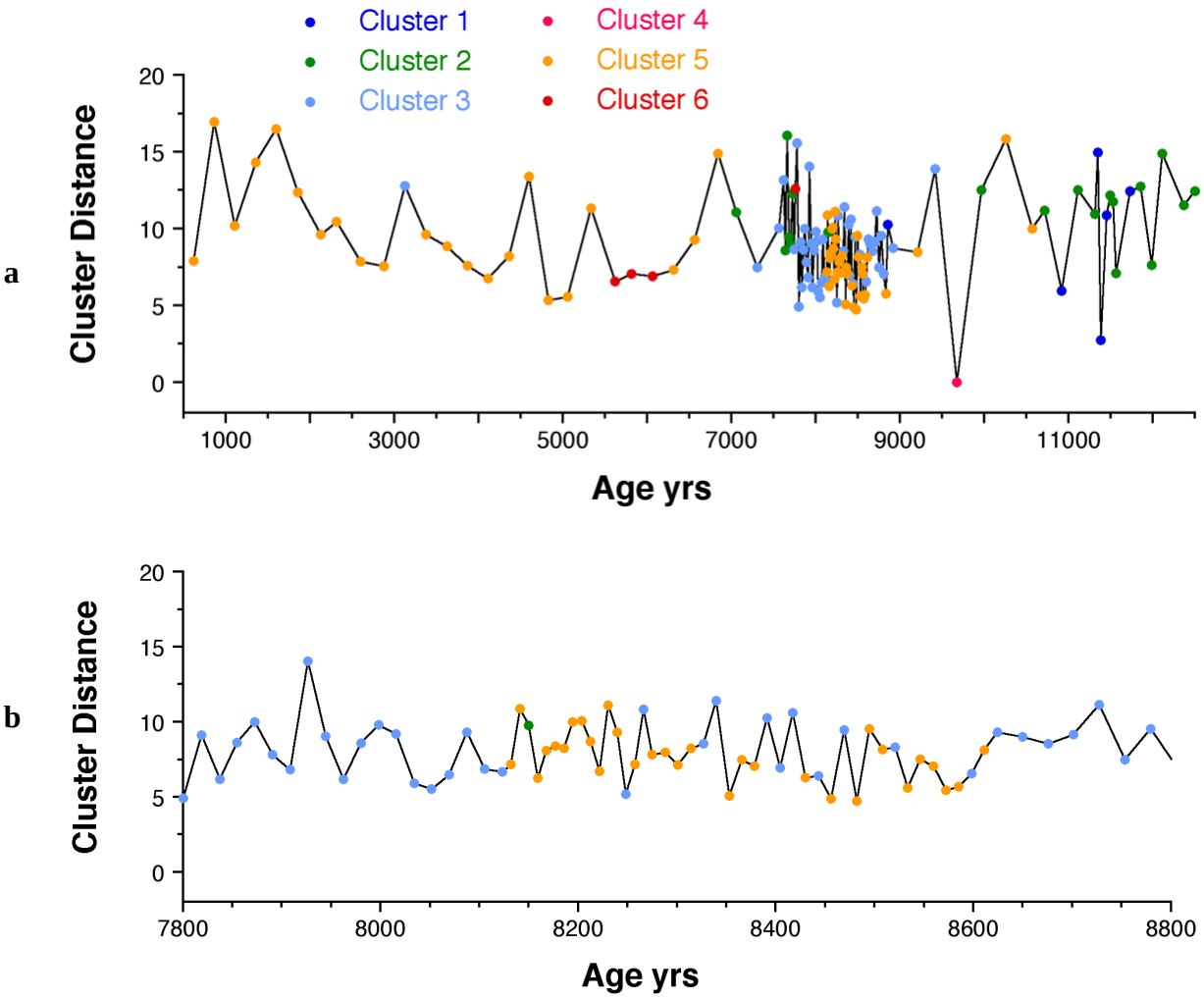

Figure 6.36 Cluster distance and cluster number against age for K-means cluster analysis of core MD99-2251 for a) the entire Holocene b) 7.8-8.8kyr high resolution study.

Chapter Seven

Regional Analysis of Diatom Core Top Floras

"The swirl of the ship's wash brought diatomaceous scum from the sides of this ice. The water became thick with diatoms at 9am , and I ordered a cast to be made. No bottom was found at 210 fathoms..."

Ernest Shackleton 'South'

Chapter Seven: Regional Analysis of Diatom Core Top Floras

7.1 NEAP Core top Study

The WAPLS transfer function employed to reconstruct SSTs for MD99-2251 and MD99-2252 (ter Braak & Juggins, 1993) is based on core top data from the northern North Atlantic and Nordic seas (this transfer function has been discussed in section 7.3.2 of this study). In order to generate a more regionally focused transfer function for MD99-2251 and MD99-2252, eight new core tops were counted for diatom species assemblage abundance. These core top are NEAP 3B, NEAP 4B NEAP 11B, NEAP 12B, NEAP 15B, NEAP 16B, NEAP 18B and NEAP 20B (Figure 8.1). These eight core tops count were then combined with other published data (Jiang *et al.,* 2001) to create a new regional transfer function.

7.1.1 The NEAP Core Sites

Core Name	Lat N deg	Long E deg	Water Depth m	Winter T ^{o}C 0m	Winter T ^{o}C 10m	Summer T ^{o}C 0m	Summer T ^{o}C 10m
NEAP 3B	61.87	-23.94	1502	7.20	7.22	10.96	10.88
NEAP 4B	61.37	-24.17	1627	7.39	7.41	11.16	11.09
NEAP 11B	59.79	-22.65	2484	8.11	8.17	11.85	11.82
NEAP 12B	58.64	-23.99	2786	8.18	8.25	12.05	12.02
NEAP 15B	57.68	-25.64	2703	8.07	8.13	12.05	12.07
NEAP 16B	56.37	-27.82	2847	7.84	7.92	12.10	12.09
NEAP 18B	54.69	-28.35	2879	8.19	8.30	12.67	12.62
NEAP 20B	42.49	-28.42	2878	14.27	14.31	20.49	20.32

Table 7.1 Location and environmental data for NEAP box cores 3B, 4B, 11B, 12B, 15B, 18B and 20B in the subpolar North Atlantic. summer and winter sea surface temperatures are from Levitus & Boyer (1994)

The eight NEAP cores were collected as part of the NEAPACC (North East Atlantic and Climate Change community research project) Cruise 88 of the RRS Charles Darwin July 25th – August 15th 1994. The study was initiated to examine changes in the flow of Iceland Scotland Overflow Water (ISOW) over the last glacial interglacial cycle. The NEAP cores are located (Figure). Both kasten and box cores were recovered as part of the NEAPACC study. All the NEAP cores in this study are box cores. Standard sampling of the box cores was employed, two 10cm diameter drainpipes, two surface scrapes (of approximately 0.5cm) for benthic foraminifera and the remainder of the top 0-5cm removed and stored in plastic bags. Eight of these NEAP box core, core top samples were analysed in this study. The location, water depth and Levitus & Boyer World Atlas 1994 winter and summer temperatures at 0m and 10m, are summarised in Table 7.1

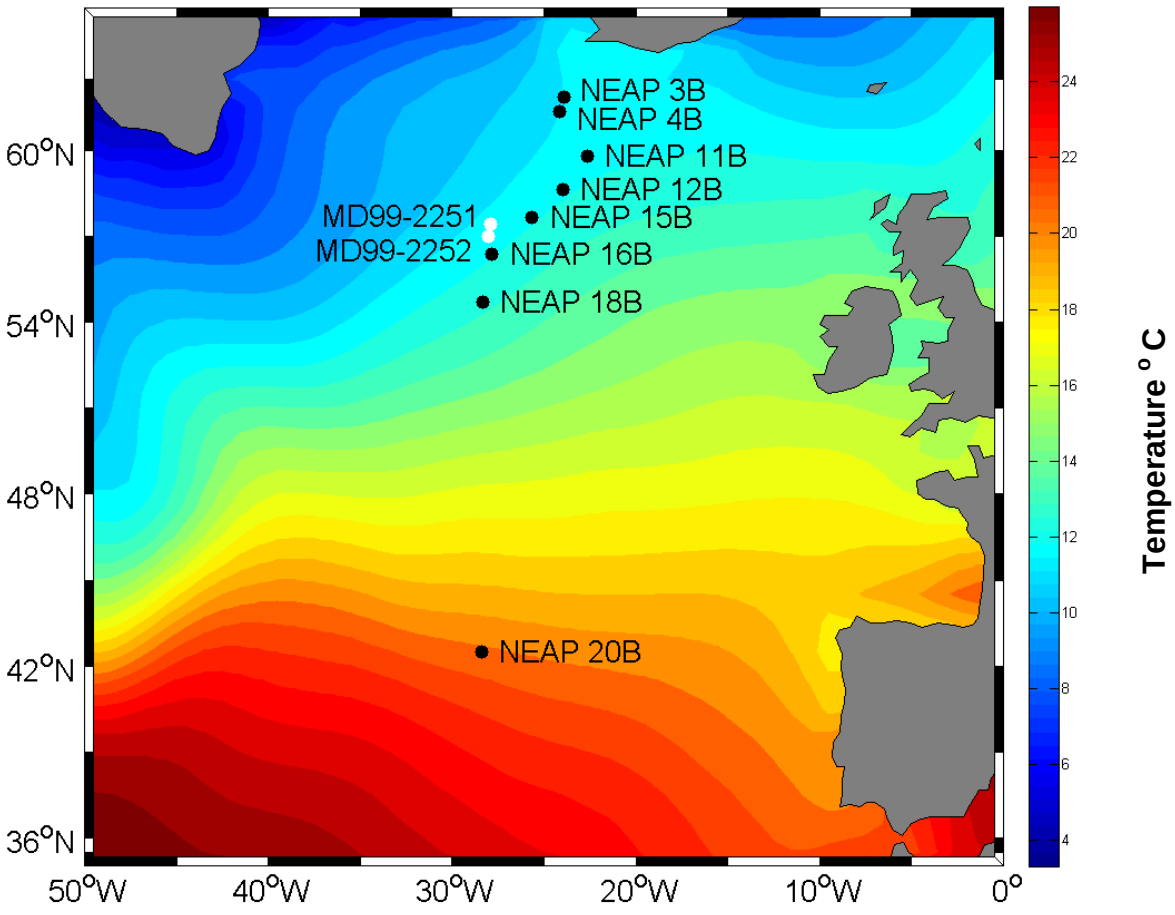

Figure 7.1 Location of MD99-2251, MD992252 (white circles) NEAP core tops (black black circles). After Farmer *et al* (2010). Sea surface temperatures based on WOA98 NODC WOA98 http://www.esrl.noaa.gov/psd/

7.1.2 Diatom abundance studies at the core top sites

Species abundance counts were undertaken for the eight NEAP core tops following the same procedure as for the down core diatom abundance studies for cores MD99-2251 and MD99-2252. A comparison of the WAPLS generated SSTS and the World Ocean Atlas (Levitus & Boyer, 1994) 0m and 10m summer and winter temperatures for each of the core sites indicates that the WAPLS SSTs most closely correspond to the WOA summer sea surface temperatures (Figure 7.1). In all but one case however the WAPLS generated SSTs are between 1-3º C higher than the WOA summer temperature.

The core top sample for NEAP 20B most closely corresponds to the WOA data. However this sample was significantly different to the other core top samples, being noticeably lighter in colour, less clay rich and drier. The diatoms counted were strongly biased towards more robust highly silicified forms and so the assemblage for this sample must be treated with some suspicion as it seem probable that there was selective preservation of taxa at this site. However it must also be noted that the WA-PLS SST estimate most closely matches the atlas SST values, most probably on account of the adjacent two core tops at the limit of the calibration (Figure 7.2).

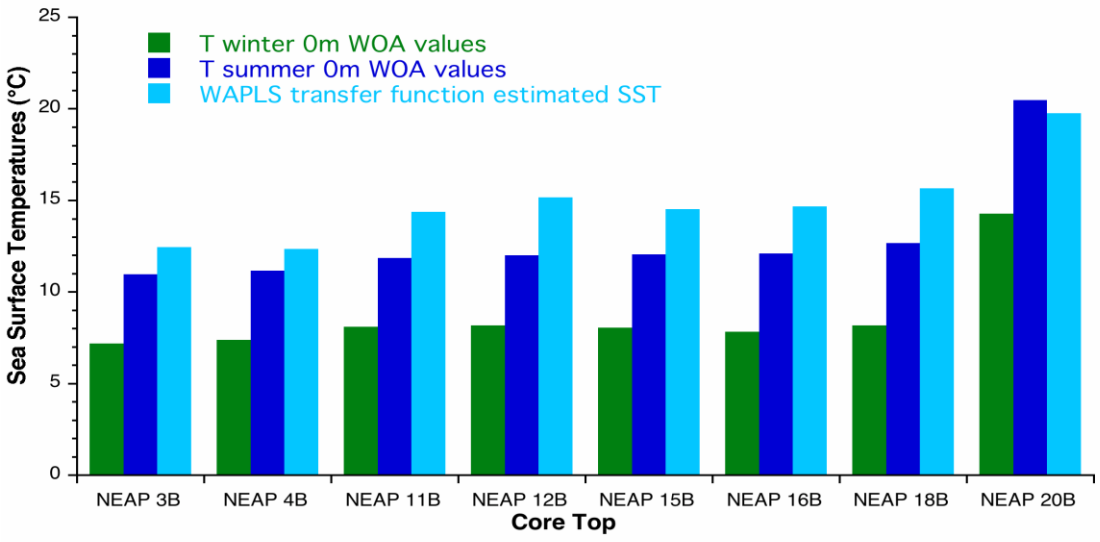

Figure 7.2 World Ocean Atlas summer and winter and WAPLS generated SSTs for the NEAP box cores 3B, 4B, 11B, 12B, 15B, 18B and 20B in the Sub Polar North Atlantic

7.1.3 Generating a regionally derived core top transfer function

The eight core tops together with other published data (Jiang *et al.*, 2001) were then used to generate a simple transfer function using the 'Parks Distance Index' (Hecht, 1973), which measures the similarity of the core top assemblage to a reference core top assemblage. The Parks Distance Index (Pd) for a given core top is derived by calculating the differences of the percentage abundance of each represented species in that core top assemblage (f_i) with the percentage abundance of the same species in a reference core top assemblage (r_i). This value is then squared and the squared values for each species in the core summed and divided by the number of species considered (n). The Parks Distance Index is the square root of the sum of the squared differences divided by the number of species. The Pd values for each core top sample are then plotted against sea surface temperature. The best fit regression line is calculated for the data set. This line is the transfer function in that sea surface temperatures may be calculated using from the equation of the line given the Parks Index.

$$P_d = \sqrt{\left[\frac{1}{n}\sum_{i=1}^{n}(r_i - f_i)^2\right]}$$

The Parks Distance Index Equation

For the purposes of constructing the regional transfer function using the combined data set. Core top 2748 (marked in red in Figure 7.3), was selected as the reference core for calculating the Parks Distance Index for both the Jiang *et al*., (2001) and the NEAP core tops. This core was chosen as the sea surface temperatures recorded at the site represented an extreme in the data set. In order to create a transfer function using both datasets this it was first necessary to create a consistent diatom taxonomy for Jiang *et al.* (2001) and the NEAP core top counts. The existing diatom species lists for the two data sets were combined in the following manner; all species that appeared in both counts were first included in the new list.

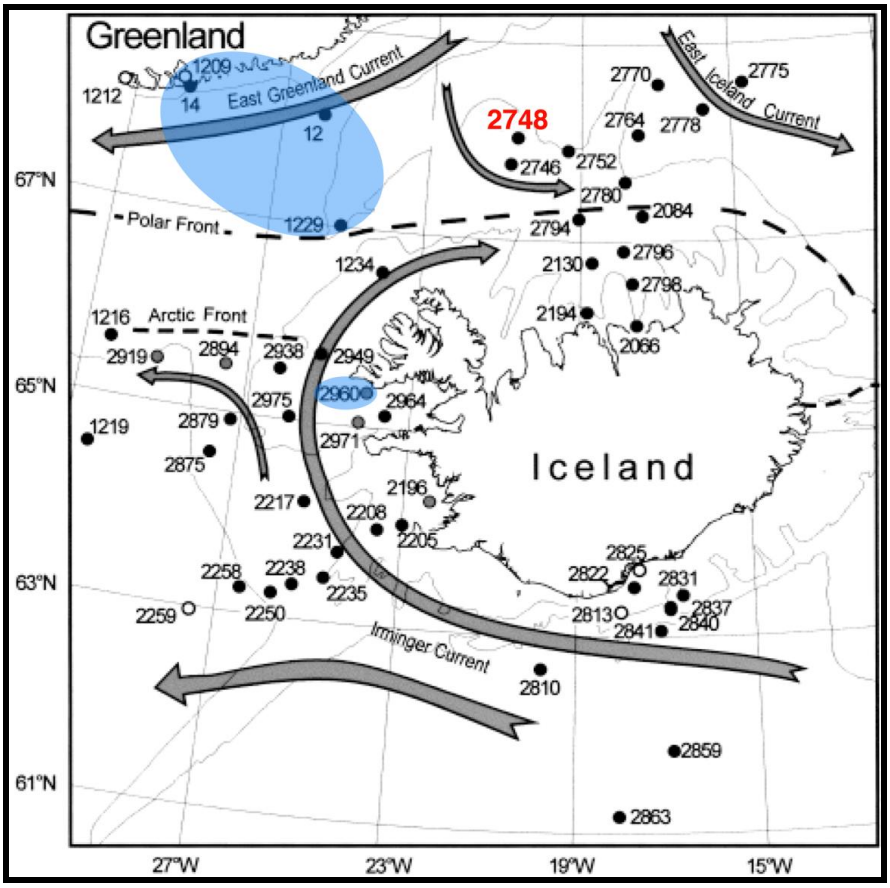

Figure 7.3 The location of the northern North Atlantic core tops used in constructing the regional transfer function with the NEAP core top data. Core top 2748 marked in red is used as the reference core for the Parks Distance Index calculations. The cores marked in blue were excluded from the data set on the grounds of not being fully open marine or sea-ice dominated assemblages. Cores marked with an open circle were excluded due to insufficient diatom data. After Jiang *et al.*, (2001)

Where the NEAP core top counts recognised a subspecies which was not distinguished in Jiang *et al.* (2001), the percentage counts for the species and the subspecies were combined. This occurred only in two cases; *Thalassionema nitzschioides* and *Thalassionema nitzschioides* var. *parva* were combined in the NEAP percentage counts and recorded as *Thalassionema nitzschioides*. Similarly percentage counts of *Rhizosolenia hebetata hebetata* and *Rhizosolenia hebetata semispina* were combined in the NEAP counts and recorded as *Rhizosolenia hebetata* in the new list. The Jiang *et al.* (2001) species list only recognises *Thalassiothrix* to genus level, distinguishing both *Thalassiothrix* sp.. and *Thalassiothrix*? sp. The NEAP core top list recognises *Thalassiothrix longissima* only. The percentages for the two forms of *Thalassiothrix* recognised in Jiang *et al.* (2001) were combined and recorded in the new list as *Thalassiothrix* sp.. The percentage counts for

Thalassiothrix longissima in the NEAP core tops were also recorded as *Thalassiothrix* sp. in the new species list. Jiang *et al.* (2001) recognises both *Thalassiosira eccentrica* and *Thalassiosira* spp. *eccentrica* group. The percentage counts for these two forms were combined and recorded as *Thalassiosira eccentrica* in the new list. Only *Thalassiosira eccentrica* was recognised in the NEAP cores and recorded as such. Further, the Jiang *et al.* (2001) counts recognise *Rhizosolenia borealis* as a separate whereas the NEAP counts combine *Rhizosolenia borealis* with *Rhizosolenia styliformis.* In the new species list therefore these species are recorded as *Rhizosolenia borealis/styliformis.* Similarly Jiang *et al.* (2001) combine *Thalassiosira gravida* with *Thalassiosira antarctica* in both resting spore and vegetative form, while the NEAP count recognise only *Thalassiosira gravida.* In the new list therefore, the species are recorded as *Thalassiosira gravida/antarctica* as in the Jiang *et al.* (2001) list.

Having rationalised the diatom species appearing in both data sets, it was then necessary to examine all species not included in both data sets. Of all the remaining species in the NEAP list, none exceeded 5% of the total abundance of the diatom flora in any core except NEAP 20B. Due to other preservational concerns regarding NEAP 20B, previously discussed, it was decided that it should be excluded from the combined data set. Of the species remaining in the Jiang *et al.* (2001) data set, only seven species exceeded 5% of the total abundance of the diatom flora in any core. Of these six species, four did not exceed 7.5% of total floral abundance; *Pseudo-nitzschia seriata* (6.2%) *Podosira* sp. (5.3%) and two unidentified species of *Thalassiosira, Thalssiosira* sp. (7.3%) and *Thalssiosira* sp. < 10 (7.4%). These four species were also excluded from the joint list. Of the remaining three species exceeding 7.5% of floral abundance, *Paralia sulcata* reached 36.5% in a single core, 2960, and otherwise remained below 6% except in one other core, 2964, where it reached 11.6% abundance. *Paralia sulcata* is a coastal species as is *Odontella aurita* which also reached > 30% abundance only in core 2960. As a result it was decided to remove core 2960 from the transfer function calculations as not representing a fully marine floral assemblage. The remaining species only represented in the Jiang *et al.,* (2001) data set was *Pseudo-nitzschia turgidula.* As a fully marine species it was decided to leave this species in the joint list and simple record it as absent in the NEAP cores. The final species list for the joint data set is recorded in Table 7.2.

Thalassiothrix
Thalassionema nitzschioides
Rhizosolenia hebetata
Proboscia alata
Bacteriosira bathyomphala
Roperia tesselata
Porosira glacialis
Actinocyclus curvatulus
Asteromphalus robustus
Thalassiosira gravida resting spore
Thalassiosira gravida vegetative
Thalassiosira auguste-lineata
Thalassiosira eccentrica
Thalassiosira trifulta
Thalassiosira nordenskioeldii
Thalassiosira oestrupii
Thalassiosira hyalina
Thalassiosira angulata
Thalassiosira pacifica
Coscinodiscus marginatus
Coscinodiscus occuls-iridis
Nitzschia bicapitata
Fragilariopsis cylindrus
Fragilairopsis oceanica
Fragilairopsis atlantica
Actinocyclus octonarius
Rhizosolenia styliformis
Pseudo-nitzschia cf.turgidula

Table 7.2 The joint diatom species list used for the regional transfer function created from Jiang *et al.* (2001) and the NEAP core top data.

The final adjustment made to the data set was the removal of cores which exhibited a strong sea ice based floral assemblage; cores 12, 14 and 1229, indicated in Figure 7.2 in blue. Cores 14 and 1229 record percentages of *Fragilariopsis oceanica* above 50% with a 29.9% abundance in core 12. As the transfer function was designed to predict open marine conditions, these cores were excluded.

The Pd values for each core top sample are then plotted against the sea surface temperature for that sample. A best fit regression line is calculated for the data set (Figure 7.4). The R value is statistically robust at 0.76632. The equation of this line, y= 1.1994 + 069327x, is the transfer function. A sea surface temperature may be calculated using the equation of the line for any given Parks Index. The R^2 value for the relationship between the Pd values and Sea Surface Temperatures generated from the eight NEAP core tops was 0.0534 and so it was not possible to generate a statistically significant regression line for the data set. This was probably a result of the low sample size.

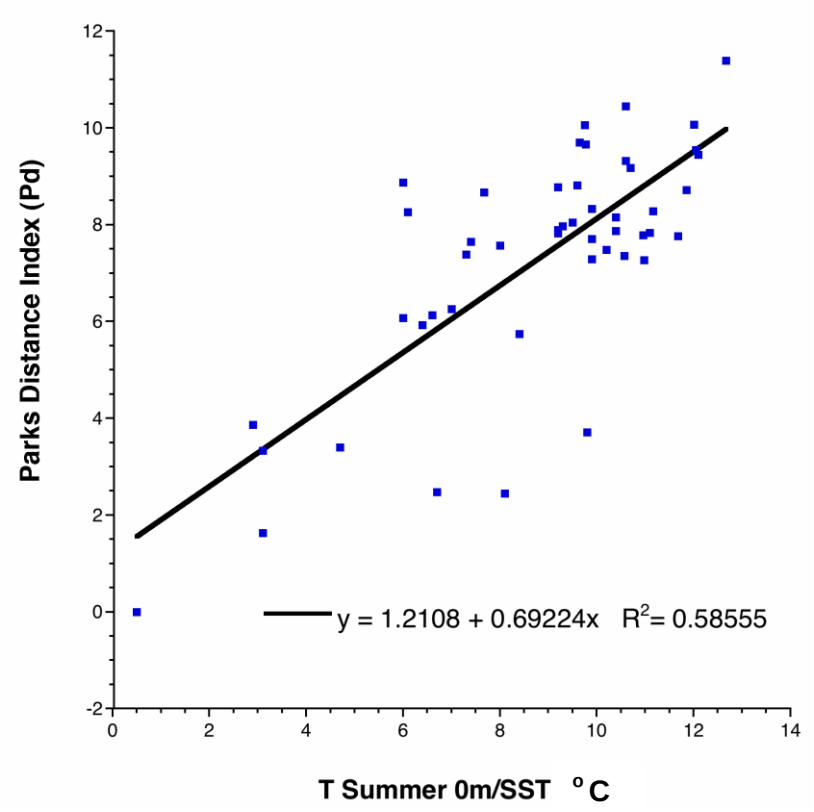

Figure 7.4 A regional derived transfer function constructed from core top data from diatom floral counts for forty-eight northern North Atlantic marine cores

7.2 Validation of the Transfer Function

This transfer function was then applied to the down core floral abundance counts for MD99-2251 (Figure 7.5) and MD99-2252 (Figure 7.6) and compared with the Sea Surface Temperature values derived using the WAPLS transfer function and a Nordic Sea based floral data set. The trends in the data are partially consistent between the two methods with high variability in the early Holocene, a broad decrease in SSTs between 9.5kyr and 7kyr, a marked increase around 7kyr resulting in optimum temperatures between 5 and 7kyr. There is lower variability in the late Holocene. One important difference between the two temperature estimates is that the WAPLS generated SSTs indicate an overall increase in temperatures throughout the Holocene, while the Pd generated SSTs show a slight overall cooling for the Holocene.

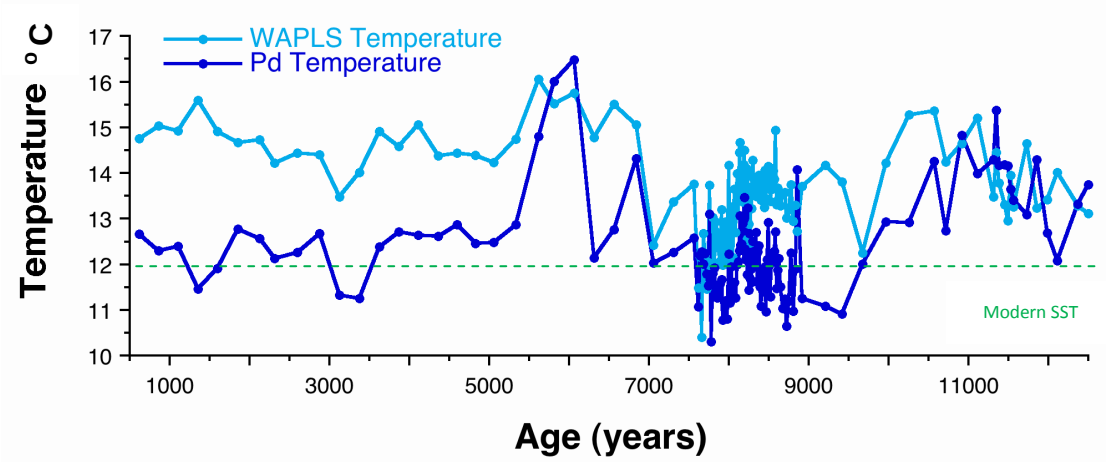

Figure 7.5 SSTs for marine core MD99-2251 derived from WA-PLS and a Nordic Sea based floral data set and from a Parks Distance Index derived transfer function using a northern North Atlantic floral data set

In both cores however, the Parks Distance Index (Pd) derived transfer function using the northern North Atlantic floral data set, gave significantly lower temperatures than the WAPLS derived transfer function using a Nordic Sea based floral data set (Figure 7.5 and Figure 7.6). The Pd derived Sea Surface Temperatures (SST) more closely resemble the modern SST values.

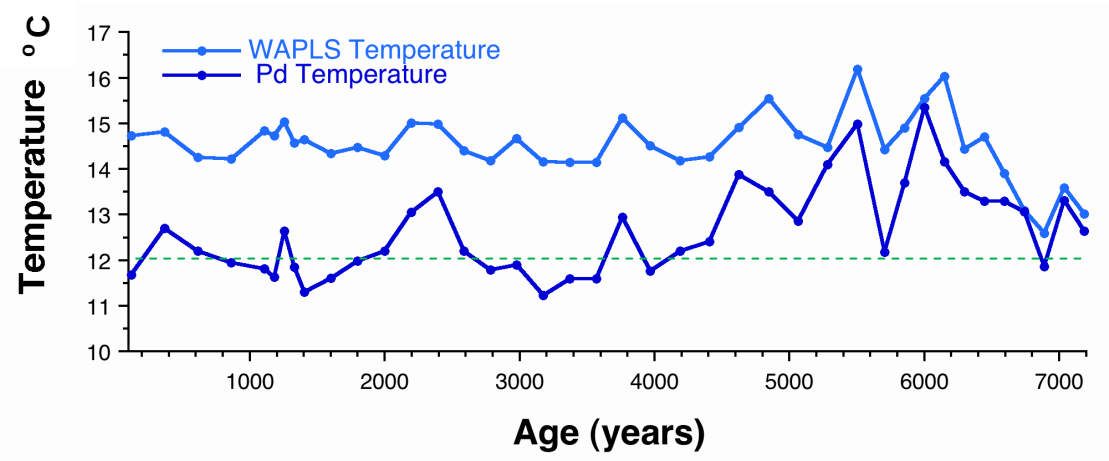

Figure 7.6 SSTs for marine core MD99-2252 derived from WA-PLS and a Nordic Sea based floral data set and from a Parks Distance Index derived transfer function using a northern North Atlantic floral data set

An important consideration in evaluating the transfer function is to examine the percentage of the total floral assemblage used to calculate the Pd generated SST estimates. For MD99-2251 the percentages used are between 75-95% of the flora. There appears to be some correlation between the trends in the percentage of the floral used and the sea surface temperature. A higher percentage of the flora appears to have been employed at times of higher SSTs (Figure 7.7). However there is no direct correlation between higher temperatures and higher proportions of flora used. The highest temperature, around 17°C relate to an average percentage of flora used.

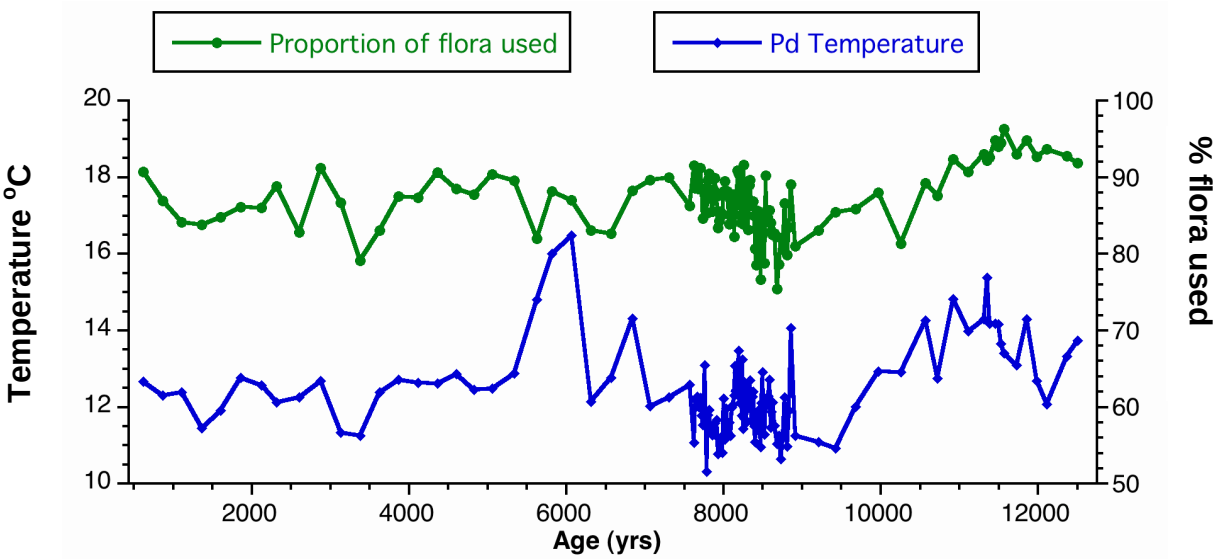

Figure 7.7 MD99-2251 Pd generate SSTs and the percentage of the total floral count used to generate the temperature.

. For MD99-2252, the floral percentages used to generate the Pd SSTs are between 80-95% and there is a less direct correlation between the trends in the SSTs and the percentage of flora employed. For both cores the Pd generated SSTs closely follow the trends of the WAPLS generated SSTs while giving lower overall temperatures, as previously stated. The Pd temperatures are most significantly lower than the WAPLS temperatures during the late Holocene. The Pd temperatures for this time period are however generated from average to high percentages of the total flora and therefore cannot be assumed to be an artefact of the percentage of data employed.

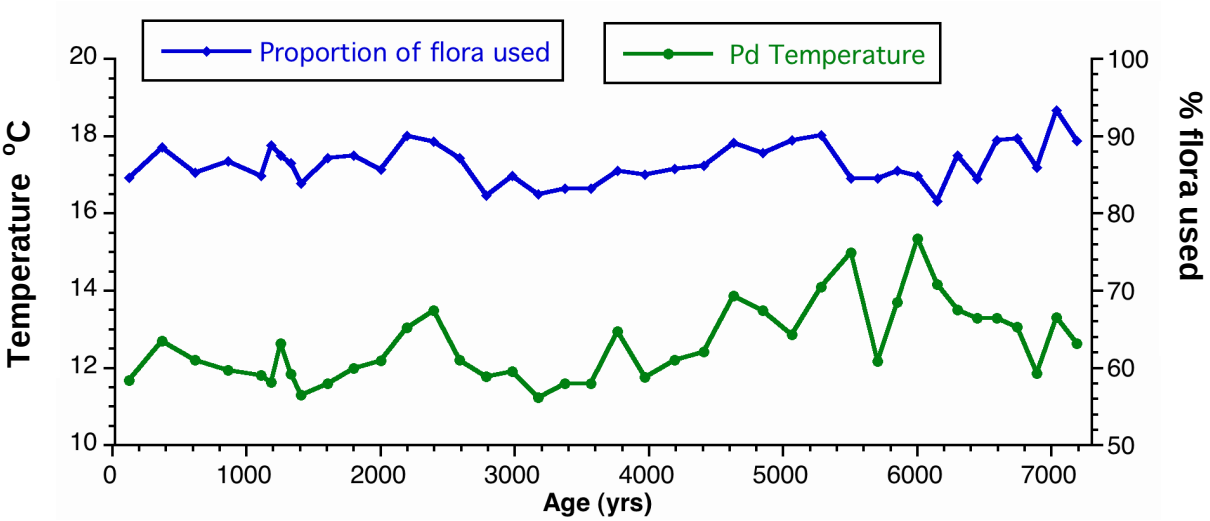

Figure 7.8 MD99-2251 Pd generate SSTs and the percentage of the total floral count used to generate the temperature.

Finally the Pd transfer function was reapplied to the NEAP cores to calculate a Pd derived temperature for those cores (Figure 7.9 and Table 7.3). The results indicate that for NEAP 3B and NEAP 4B the Pd transfer function performs as well as the WAPLS transfer function and for the remaining core tops the Pd transfer function performs better than the WAPLS transfer function at estimating summer sea surface temperatures.

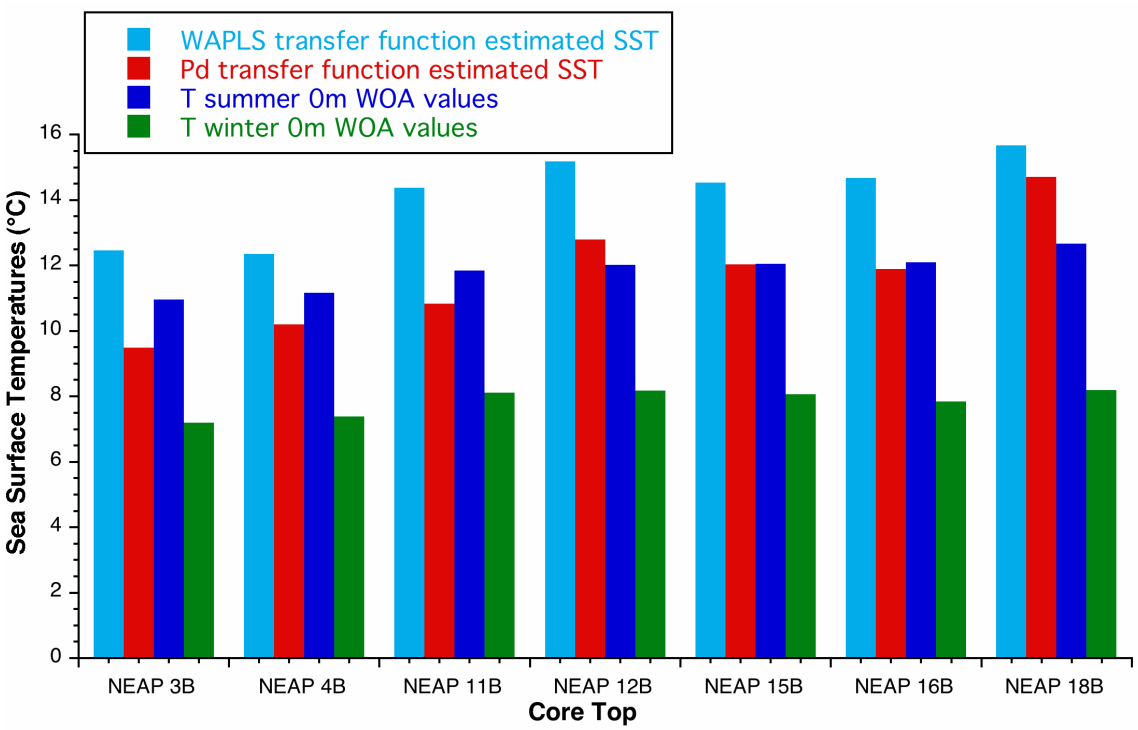

Figure 7.9 shows the World Ocean Atlas 0m summer and winter and WAPLS and Pd generated SSTs for the NEAP box cores 3B, 4B, 11B, 12B, 15B, 18B and 20B in the subpolar North Atlantic

Sample	WOA Summer 0m temperature	WOA Winter 0m temperature	WAPLS generated SST	Pd generated SSTS
NEAP 3B	10.96	7.20	12.46	9.50
NEAP 4B	11.16	7.39	12.35	10.21
NEAP 11B	11.85	8.11	14.38	10.84
NEAP 12B	12.01	8.18	15.19	12.80
NEAP 15B	12.05	8.17	14.53	12.03
NEAP 16B	12.10	7.84	14.68	11.90
NEAP 18B	12.67	8.19	15.67	14.71

Table 7.3 World Ocean Atlas 0m summer and winter and WAPLS and Pd generated SSTs for the NEAP box cores 3B, 4B, 11B, 12B, 15B, 18B and 20B in the subpolar North Atlantic

7.3 Discussion

The Parks Distance Index is clearly a far less advanced mathematical method than the WAPLS. However, these results suggests that regional constraint of the data set may be more important than the mathematical sophistication of the transfer function when deriving SSTS from diatom floral advance counts, as the Pd transfer function consistently produces SST values nearer the observed modern values. These results also highlight the need for further work on the distribution of diatom species in the mid latitudes.

Chapter Eight
Ice Rafted Debris Data

“ We climbed around ice foot and found it much broken up on the south side; the sea spray had washed far up on it...There is a curious weathering on the ice blocks on the North side; also the snow drifts show interesting dirt bands...”

Robert Falcon Scott ‘Journals’

Chapter Eight: Ice Rafted Debris

8.1 Heinrich Events

Ruddiman (1977) first noted a distinct band of ice rafted deposition across the North Atlantic during the last glacial cycle. That this deposition was in distinct layers was first recognised by Heinrich in a study of fourteen marine from the Northeastern North Atlantic (Heinrich, 1988). Heinrich identified six well-defined peaks in lithic sediment input during the last glacial period between 14kyr and 70kyr (Figure 8.1). He concluded that these peaks were the result of periodic episodes of intense ice rafting. Further studies recognised these 'Heinrich events' across the whole North Atlantic in a band from approximately 40°N to 55°N indicating that these were not localised events but regional events (Broecker *et al*. 1992; Grousset *et al*. 1993; Bond *et al*. 1993).

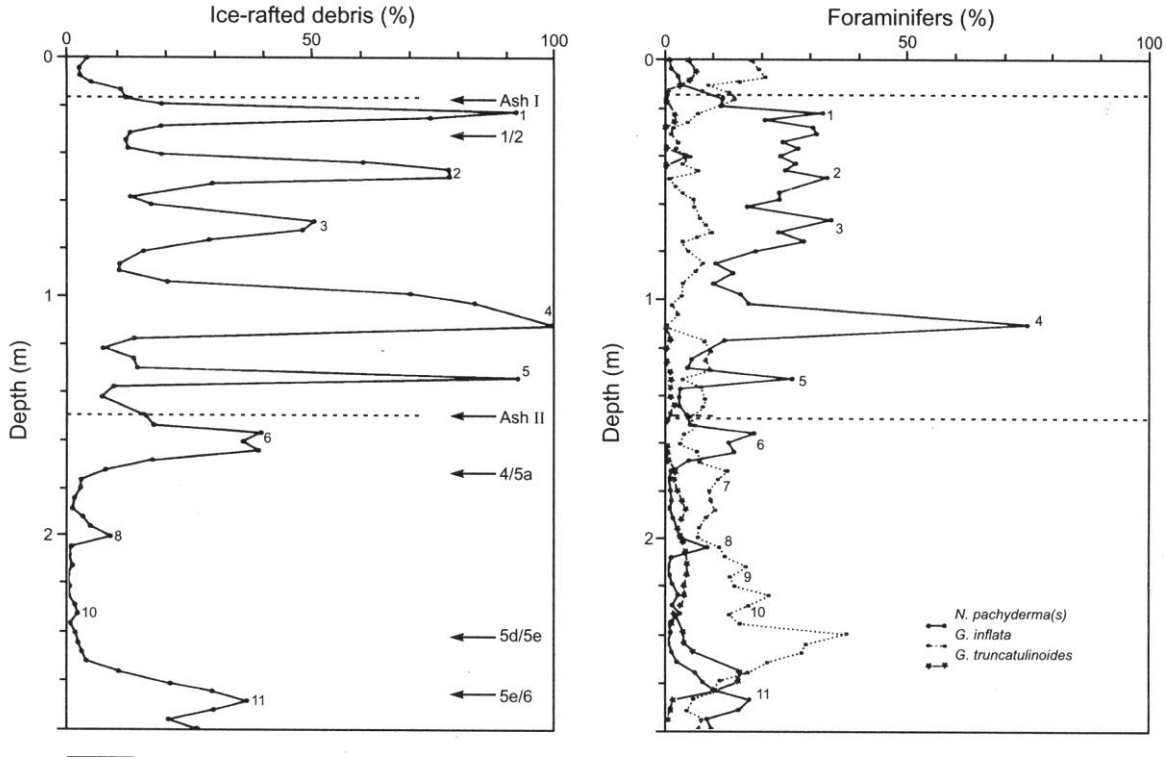

Figure 81 The relationship between peaks in ice rafted debris input and abundances of the cold water planktonic foraminifera *Neogloboquadrina pachyderma* sinistral Peaks in the percentage IRD with depth match peaks in the percentage abundance of *Neogloboquadrina pachyderma* sinistral (Heinrich, 1988).

Studies of the composition of the lithic fragments in the Heinrich layers were then undertaken to determine their origin. Various evidence indicates an eastern Canadian source for all but Heinrich layer three (H3). In the western North Atlantic Heinrich layers have been identified as containing 20-25% detrital carbonate, with the percentage of carbonate diminishing eastwards. This concentration of carbonate is uncharacteristic of the background glacial sediment which consists predominantly of quartz, feldspar and volcanic glass (Bond *et al.*,1992; Bond & Lotti 1995). These carbonate sediments have been shown to be derived from limestone and dolomite bedrock in the Hudson Bay (Andrews & Tedesco, 1992). Strontium Neodymium isotope analyses indicate a different source for the sediments in H3 than for the other Heinrich layers (Grousset *et al.,* 1993: Revel *et al.,* 1996). Potassium Argon ages from the clay minerals in the detrital carbonate rich Heinrich layers indicate a Labrador Sea source (Huon & Ruch 1992; Jantschik & Huon, 1992; Hemming *et al.,* 1998; Hemming *et al.,* 2002). Lead isotopes from the feldspar grains in the Heinrich layers indicate a Hudson Bay provenance for all Heinrich layers but H3 which shows a Scandinavian Greenland provenance (Gwiazda *et al.,* 1996).

In addition to the increased input of sediment, the Heinrich layers are also characterised by changes to the sea surface hydrology and deep water circulation. These changes include significant reductions in sea surface temperature and salinity and reduced or even a shut down of North Atlantic Deep Water (NADW) formation in the North Atlantic. Peaks in lower $\delta^{18}O$ values for the planktonic foraminifera *Neogloboquadrina pachderma* sinistral correlate with peaks in ice rafted debris input suggesting meltwater pulses occurring concurrently with the Heinrich events (Bond *et al.,* 1992; Bond *et al.,* 1993; Labeyrie *et al.,* 1995; Vidal *et al.,* 1997). Similar results were found from analysis of $\delta^{18}O$ values for the planktonic formaninfera *Globigerna bulloides* (Chapman *et al.,* 2000). Decreases in temperature of around 2°C were measured for Heinrich Event 4 (Cortijo *et al.*, 1997). Negative peaks in $\delta^{13}C$ values for the benthic foraminifera *Cibicidoides wullerstorfii* occurring simultaneously with Heinrich events indicate reductions in NADW (Vidal *et al.,* 1997; Elliot *et al.,* 2002) (Figure 8.2). A further characterictic of the Heinrich layers is a reduction in the concentration of foraminifera in the sediments. It has also been argued that the peaks in concentration of lithic fragments during Heinrich events reflect extremely low foraminifera concentrations rather than unusually increased lithic input (Broecker *at al*., 1992).

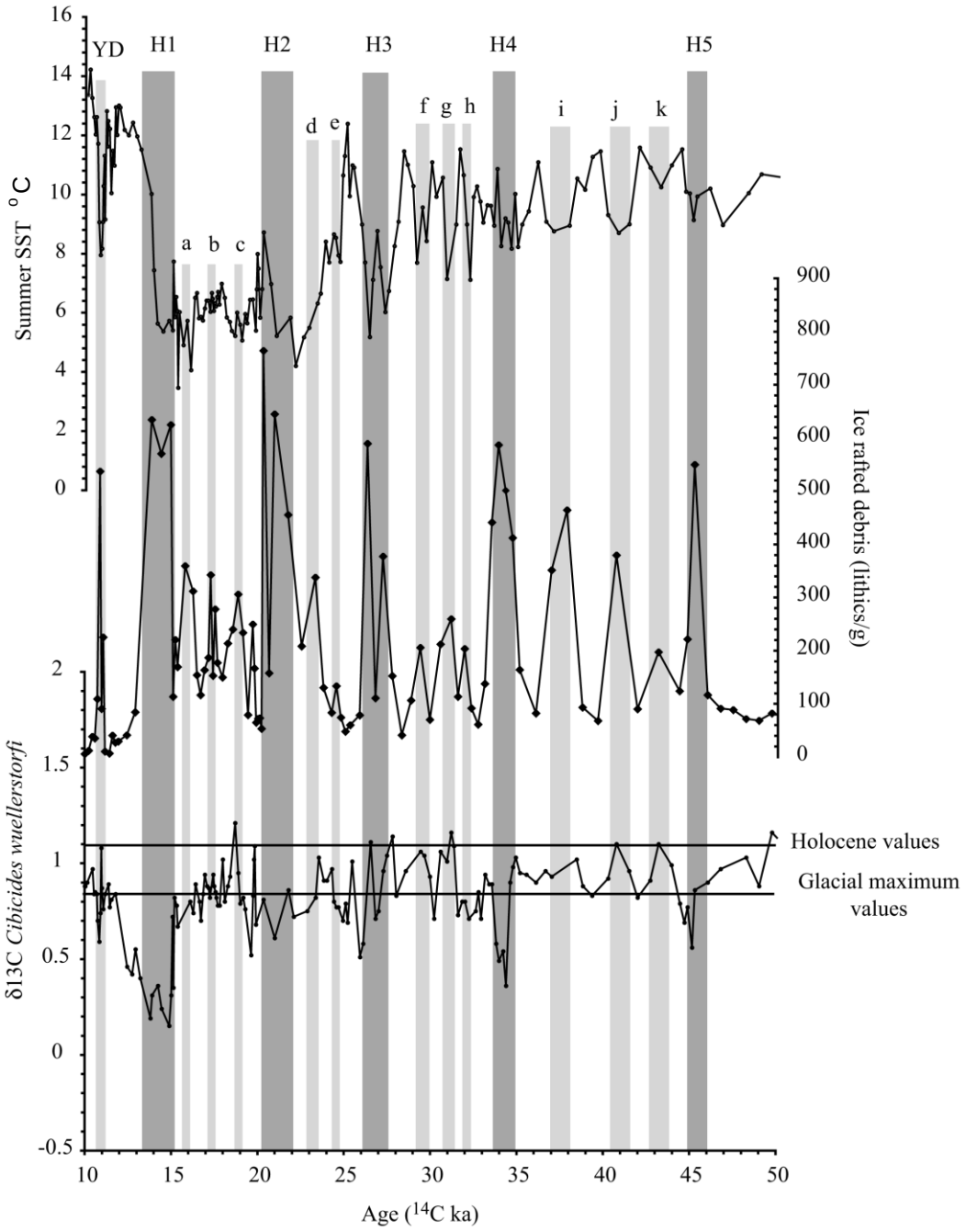

Figure 8.2 Indicating the relationship between decreases in Summer SSTs, increases in the concentration of IRD in number of lithic grains (>150 μm) per gram and decreases in NADW flow as indicated by decreases in the $\delta^{13}C$ of benthic forminifera *C. wuellerstorfi* (Elliot *et al.*, 2002).

A number of mechanisms have been proposed to explain these abrupt increases in iceberg discharge. These include variations in solar radiation due to orbital patterns, internal ice sheet dynamics, changes in ocean circulation and sea-level changes. Heinrich proposed that the increased ice rafting was a response to changes in Northern hemisphere

insolation due to orbital forcing, specifically the precessional orbital signal. He recognised a cyclicity of half the processional signal at 11,000 ± 1000yrs relating to maximum and minimum summer insolation (Heinrich 1988). Internal dynamics of the ice sheet as a forcing mechanism for Heinrich cycles were suggested by MacAyeal (1993a), MacAyeal, (1993b). Alley & MacAyeal (1994) propose a binge-purge model for ice sheets to explain Heinrich events. They argue that the Laurentide Ice Sheet experienced long periods of slow ice accumulation (binge) followed by short periods of rapid discharge (purge). Geothermal heat heats the base of the ice sheet to the point where there is a catastrophic discharge of water saturated sub glacial till. This would explain the detrital carbonates in the Heinrich layers being derived from bedrock in the Hudson Bay and Labrador Sea. Once the ice sheet has thinned sufficiently from the discharge, it refreezes to the glacial bed and a new binge cycle begins. This model is seen as having a periodicity of approximately 7700 years. It requires no external forcing mechanism such as variations in the intensity of insolation. These conclusions are supported by more recent modelling studies of ice sheet dynamics. Marshall & Clark (2002) model the basal ice temperature for the Laurentide Ice sheet and conclude that as ice sheets mature they become independent of orbital forcing and surge due to internal feedback dynamics. Alvarez-Solas *et al.* (2009) model instabilities in northern hemisphere ice sheets and conclude that ice surges are the result of feedback mechanisms between the ocean, ice shelves and ice streams. It has also been suggested that surges may occur as a result of earthquake activity triggered by ice loading (Hunt & Malin, 1998).

Another proposed mechanism to explain Heinrich events is global sea level change. Chappell (2002) recognises a correlation between sea level cycles shown in coral terraces of the Huon Peninsula, Papua New Guinea and 6000-7000 climate cycles recorded in marine sediments and ice cores during the last glacial. Each climate cycle culminates is sea level rises of 10-15m persisting for 1000-2000 years. All but one of these sea level rises correspond to a Heinrich event. Chappell proposes therefore that sea level rise may be the trigger for these ice calving events across the North Atlantic. He further notes that these sea level cycles can be correlated with cycles of oxygen isotope variations in benthic foraminifera from marine core MD99-2042 (Shackleton *et al.*, 2000). The amplitude of the Oxygen isotope variations in this core suggests not only a variation in sea level but a cooling of the deep ocean of around 1-2°C for each of these 6000-7000 year climate

cycles. Similarly Arbic *et al.* (2004) suggest unusually large ocean tides in the Labrador Sea may have triggered Heinrich events.

8.2 High Resolution Ice Rafting Events

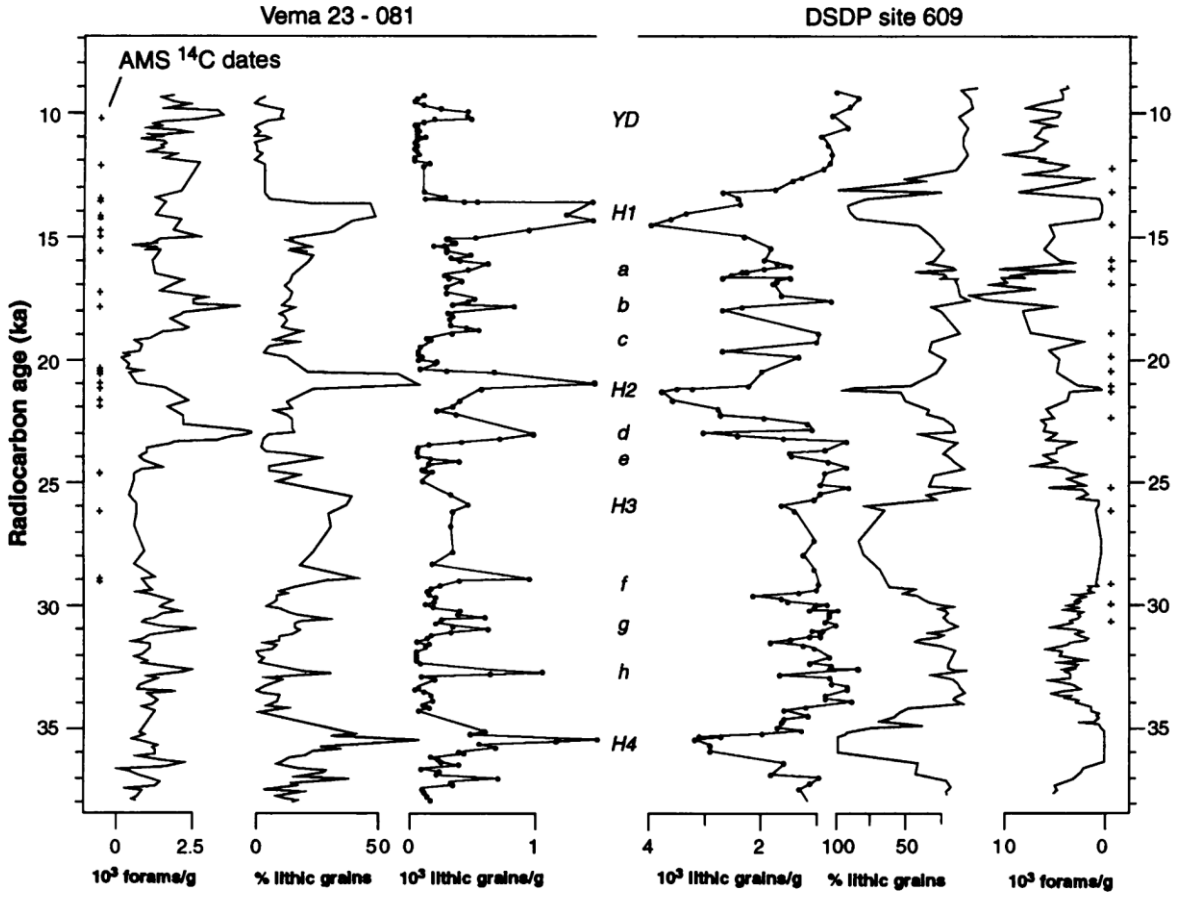

Figure 8.3 Cycles of increased IRD deposition at higher frequency than Heinrich events Bond & Lotti (1995)

Bond & Lotti (1995) in a high resolution study of North Atlantic marine cores DSDP 609 and VM23-81, identified cycles of IRD deposition at a higher frequency than Heinrich event deposition . As the two cores were located in different depositional environments and at different latitudes, they concluded that the IRD cycles were not simply a product of local conditions but represented a more widespread climate signal. Heinrich events have a periodicity of 7000-10,000 years. The IRD deposition cycles identified in this study had a

periodicity of 2000-3000 years. This matches the periodicity of the Dansgaard-Oeschger temperature cycles identified from Greenland ice cores (Dansgaard *et al.*, 1993). Bond & Lotti (1995) were able to correlate one of their IRD peaks to the Dansgaard-Oeschger events (Figure 8.3). Two IRD peaks occurred independently of Dansgaard-Oeschger events. They concluded that this is the result of the cooling signal being more strongly recorded in the ice rafting signal than in the Greenland ice core.

A study of the lithology of the IRD identified peaks in three grain types; basaltic glass (derived from Iceland), haematite stained quartz and feldspar (from various locations on either side of the North Atlantic) and detrital carbonate grains (derived from northeastern Canada). As these peaks in the different grain types were found to be synchronous, it was concluded that ice calving events occurred simultaneously from the Icelandic Ice cap and the Gulf of Lawrence every 2000-3000 years coincident with the Dansgaard-Oeschger cooling events identified in the Greenland ice cores. This simultaneous calving from more than one source suggests that the calving cycles resulted from a response to external forcing factors rather than internal physical processes within the glaciers, which is unlikely to have occurred simultaneously.

A number of other authors identified these millennial scale changes in terrigenous input into deep sea cores. Raymo *et al.* (1998) identify such a cyclicty in ice rafting during the early Pleistocene in the North Atlantic. Elliot *et al.* (1998) recognise these millennial scale ice discharge events in the Irminger Basin over the last 45kyr. McManus *et al.* (1999) identify a 0.5 million year record of millennial scale variability in ice sheet discharge into the North Atlantic.

8.3 Holocene Ice Rafting Variability

In addition to the well documented Heinrich events (Heinrich, 1988; Broecker *et al*., 1992; Grousset *et al*., 1993; Bond *et al.*, 1993) and higher resolution events of increased ice rafting (Bond & Lotti, 1995; Oppo *et al.*,1998; Elliot *et al.*,1998), certain authors have also recognised periodic increases in lithic sediment input during the Holocene.

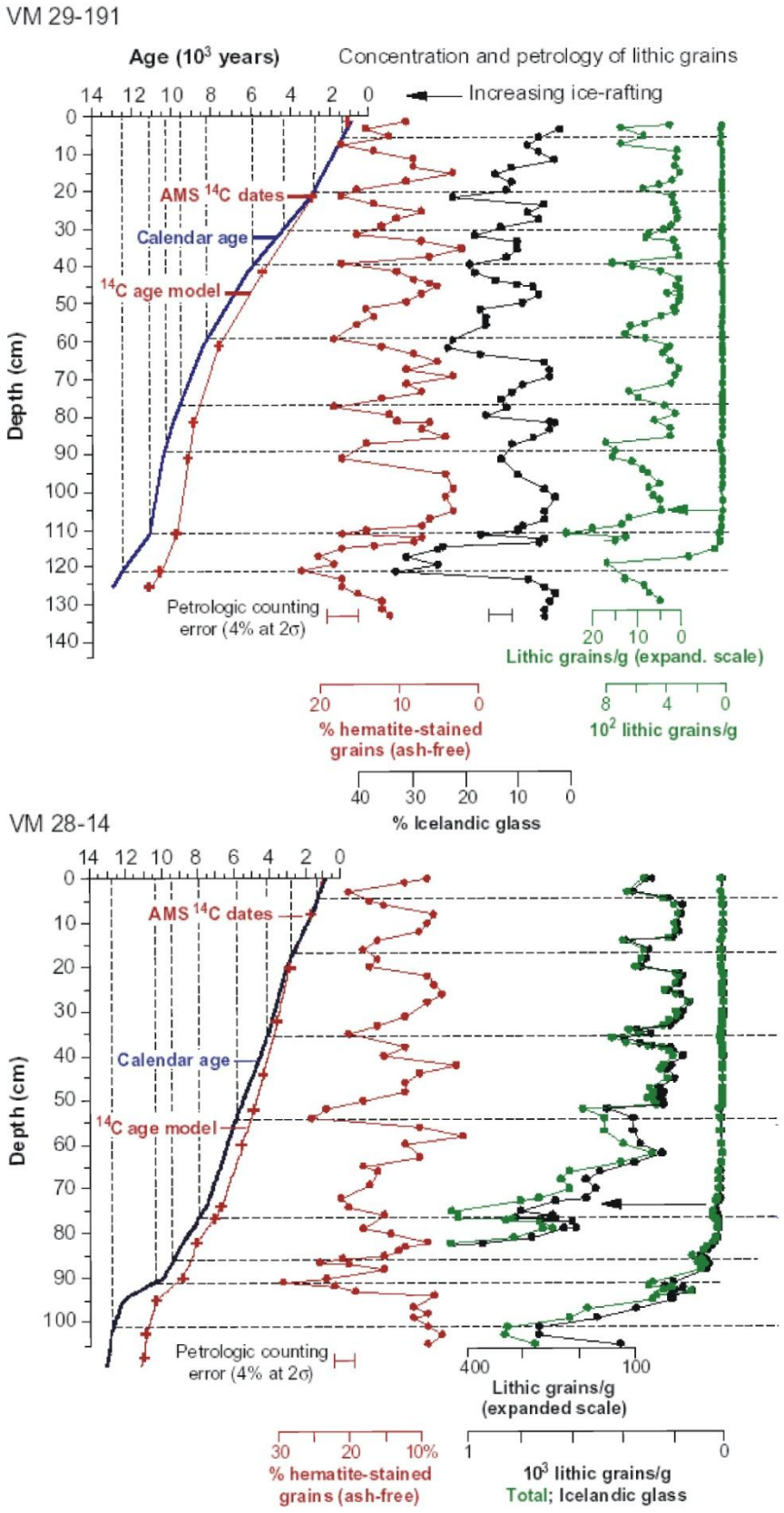

Figure 8.4 Holocene Ice rafted debris flux in two North Atlantic marine cores VM 28-14 (64° 47´ N, 29° 34´ W) and VM 29-191 (54° 16´ N 16° 47´ W) Bond *et al*. (1997)

Bond *et al*. (1997) recognise eight cycles of increased input from ice rafted material for the Holocene from cores VM 28-14 (64° 47´ N, 29° 34´ W) and VM 29-191 (54° 16´ N 16° 47´ W) in the North Atlantic. These increases in input of ice rafted material occur at 1400, 2800, 5900, 8100, 9400, 10300 and 11,100 yrs BP (Figure 8.4). The authors attribute these 1470 ± 500 year cycles to solar forcing, indicating the presence of a 1500 year climate cycle acting independently of glacial interglacial cycles. They measure IRD flux according to three proxies; concentration of grains > 150µm per gram and the percentages of glass lithics of Icelandic origin and haematite stained grains. The Icelandic glass includes both clear rhyolitic glass and dark basaltic glass. Haematite stained grains are considered to originate from the east coast of Greenland and Svalbard or from red beds around the Arctic Ocean.

Numerous studies have sought to identify these Holocene fluctuations in ice rafted debris input identified by Bond (Jennings *et al.,* 2002; Reeh, 2004; Moros *et al.,* 2004b; Moros *et al.,* 2006; Andrews *et al.,* 2009). These studies cover a variety of locations in the North Atlantic and Greenland, Iceland, Norwegian Seas and use differing proxies for measuring IRD input. An Arctic Ocean study of two marine sediment cores from the Nansen Trough and the East Greenland shelf, JM96-1206/1-GC (68º 06.0'N, 29º25.5'W) and JM96-1207/1-GC (68º 06.0'N, 29º21'W) looked at IRD flux, measured as the variations in the calcium carbonate content of the sediments (Jennings *et al.*, 2002). This Arctic Ocean IRD study shows no persistent 1500 year cyclicity in terrigenous input but rather a shift from early to mid Holocene warm conditions with low IRD input to colder fresher conditions with increased IRD input at around 5kyr. IRD appears in the East Greenland core between 6kyr and 4kyr with the first detrital carbonate peak at around 4.7kyr. The authors conclude therefore that earlier Holocene coolings, such as the 8.2kyr event were not associated increases in terrgenious input.

An investigation of IRD in two Holocene marine cores, one from the Reykjanes Ridge (L009-14 59^{o}N 31^{o}W) and one from the Norwegian Sea (MD95-2011 66^{o} 58'N 7^{o}38'W) (Moros *et al.,* 2004b) also indicates long term variability in terrigenous input through the Holocene rather than the 1500 year cyclicity recognised by Bond *et al.* (1997). The authors measure IRD by sieving and counting the > 150µm and the > 63 µm fractions and by X-ray diffraction (XRD) measurements of the bulk sediment and the < 63 µm fraction.

The authors recognise four climatic phases for the Holocene; an early warm period with a thermal maximum around 6.5kyr, a cooler period which is associated with increased ice rafting from 6.5 to 3.7kyr, a warm unstable period from 3.7 to 2kyr and then a general; decline in sea surface temperatures from 2kyr to the present. The 8.2kyr event is marked in these cores by an increase in terrigenous input (Figure 8.5).

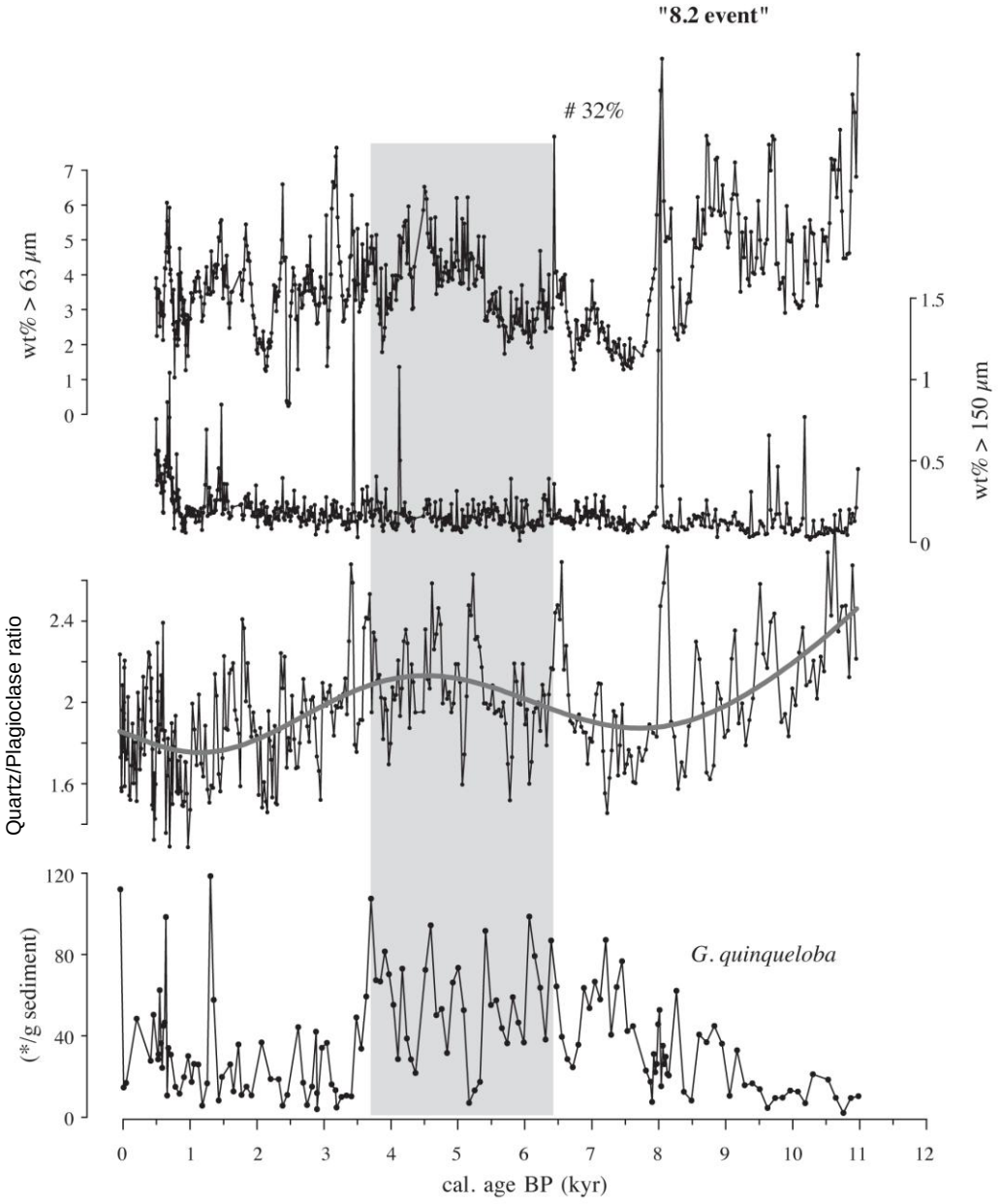

Figure 8.5 Holocene IRD variability rafting reconstructed by measuring the quartz-to-plagioclase ratio using XRD from core MD95-2011 from the Norwegian Sea indicating an increase in terrigenous input between 6.5 and 3.7 kyr and associated with the 8.2kyr event. G. quinqueloba content (*) per g of sediment (Risebrobakken et al., 2003) is also shown.(Moros *et al.*, 2004b)

Further, Moros *et al*. (2006) in their study of ice rafted debris distribution, using XRD measurements of quartz content and the quartz plagioclase ratios for four cores off Iceland, conclude that patterns of iceberg rafting and sea ice advection were not uniform across the North Atlantic throughout the Holocene. The authors recognise two modes of variability; regions influenced by cold polar outflows and regions influenced by warm inflowing currents. They record long term increases in terrigenous input into the North Atlantic from approximately 6kyr in areas underlying the cold East Greenland Current but a contrasting decrease in terrigenous input for this period where sites are influenced by the warm North Atlantic Drift (Figure 8.6)

Andrews *et al*. (2009) in a study of drift ice quartz deposits in sixteen Holocene cores off northern Iceland, using XRD analysis of the < 2mm fraction, found no 1500 year periodicity as in the Bond *et al*. (1997) study, but rather an approximately 670 year periodicity. There was also indication of periodicities between 87 and 61 years which the authors suggest bear a resemblance to the North Atlantic Oscillation. They conclude with Moros *et al*. (2006) that the prevailing oceanographic conditions will have a greater influence on drift ice distribution than a prevailing climate signal. The area of their study is on the boundary of Polar/Arctic and Atlantic water masses and so, they argue, exhibits a different IRD signal to the VM129-191 core of Bond *et al*. (1997) which lie of Ireland in water predominantly influenced by the North Atlantic Current.

In summary, certain authors have found a peak in terrigenous input (Moros *et al.*, 2004), corresponding to the 8.1kyr IRD peak identified by Bond *et al.* (1997), while others have not (Jennings *et al.*, 2002). It is important to note that both the location of these core and the method of counting IRD input varied between these studies. It is possible that both Holocene IRD peaks are only registering in certain regions and with certain methods of recording IRD.

Figure 8.6 Down-core records of four cores off Iceland. (a) quartz content and (b) Quatz/Plagioclase ratio of north Iceland core MD99-2269 (Small vertical arrows in Figure 4a indicate positions of AMS 14C dates in MD99-2269). (c) Benthic foraminifer data of Cassidulina reniforme (reverse scaled) of MD99-2269[Giraudeau et al., 2004]. (d) Ice-rafting proxy data east Greenland shelf core [Andrews et al., 1997]. (e) VM29-191 [Bond et al., 1997, 2001] (hematite-stained grains (HSG)) and (f) MD95-2011 [Moros et al., 2004a], taken at sites influenced by the warm North Atlantic Current. Planktic foraminifera abundance data of (g) N. pachyderma (sinistral) and (h) N. pachyderma (dextral,reverse scaled) of MD95-2011 [Risebrobakken et al., 2003]. After 3–4 ka. Moros *et al* . (2006)

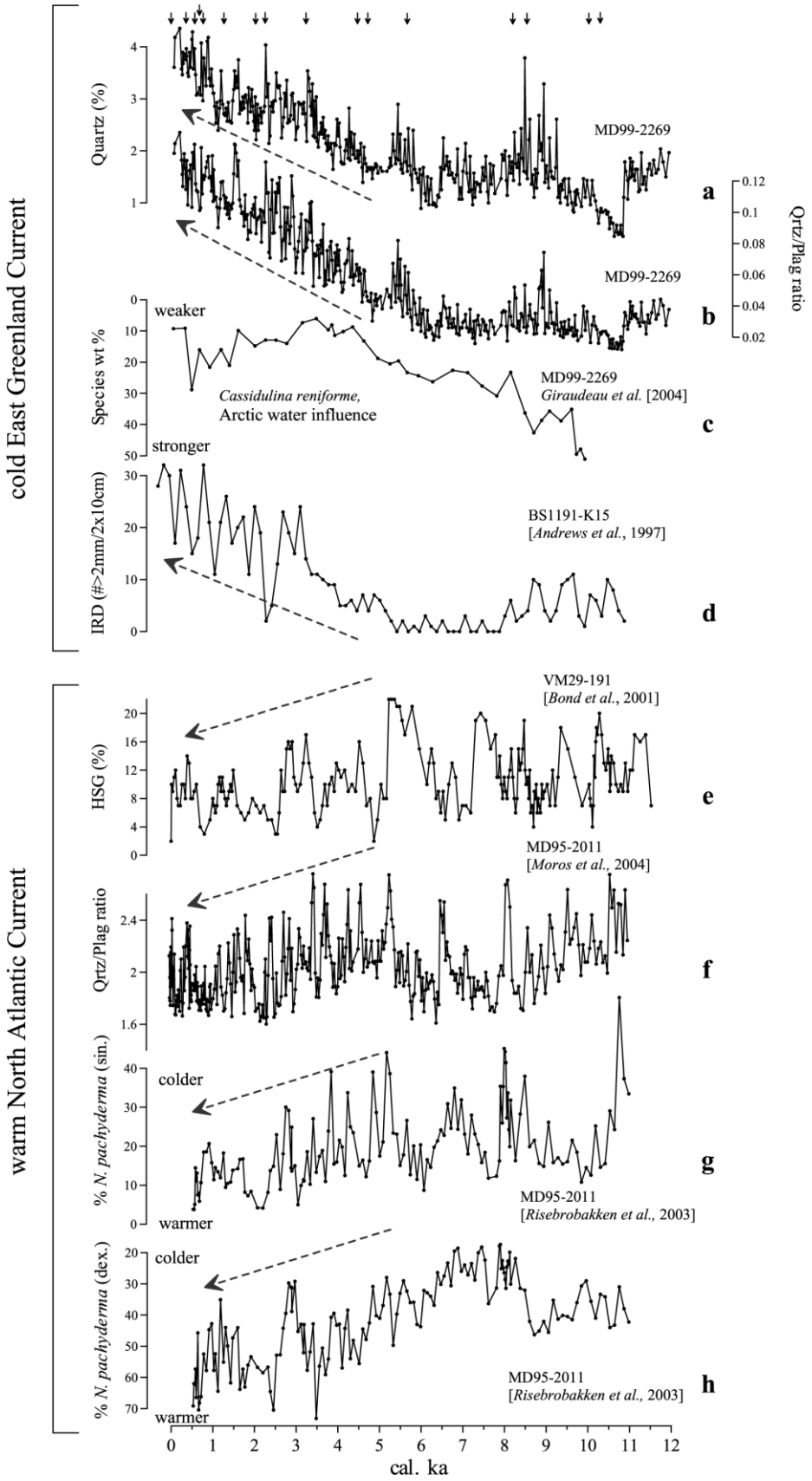
cold East Greenland Current
warm North Atlantic Current
Quartz (%)
MD99-2269
a
Qrtz/Plag ratio
MD99-2269
b
weaker
Species wt %
Cassidulina reniforme,
Arctic water influence
MD99-2269
Giraudeau et al. [2004]
c
stronger
IRD (#>2mm/2x10cm)
BS1191-K15
[Andrews et al., 1997]
d
HSG (%)
VM29-191
[Bond et al., 2001]
e
MD95-2011
[Moros et al., 2004]
Qrtz/Plag ratio
f
% N. pachyderma (sin.)
colder
warmer
MD95-2011
[Risebrobakken et al., 2003]
g
% N. pachyderma (dex.)
colder
warmer
MD95-2011
[Risebrobakken et al., 2003]
h
cal. ka

8.4 Ice Rafted Debris Study for marine core MD99-2251

8.4.1 Introduction

This study seeks to identify whether there is any increase in the input of ice rafted debris (IRD) recorded in marine core MD99-2251 (57°26.87 N 027°54.47 W) associated the 8.2 kyr event as would be expected from a period of significant cooling and inferred increased ice rafting; and corresponding to the 8.1kyr IRD event of Bond *et al.* (1997). As the Bond *et al.* (1997) study recognised peaks in specific lithologies; dark basaltic glass and haematite stained grains, not only were total IRD concentrations counted for this study, but the concentrations of specific lithologies.

8.4.2 Methodology

MD99-2251 was sampled at 1cm intervals between the depths 1200-1336cm corresponding to ages of around 7.8 to 8.8kyr. Samples were sieved at 63μm and all lithic grains counted under a light microscope. The samples had been previously processed for diatom sampling. As this process involves the removal of carbonates, the ice rafted debris signal recorded therefore excludes any possible carbonate grains that may have been present. The following lithologies were identified; clear quartz, opaque quartz, haematite stained quartz, dark basaltic glass, vesicular volcanic, dark volcanic and 'other lithologies'. The dark basaltic glass corresponds to corresponding to the 'Icelandic Glass' of Bond *et al.*(1997)

The total number of grains varied considerably. The variation in number of grains present and the concentration per gram (total number of grams divided by dry wt) are shown in Figure 8.7. The IRD concentration closely follows the number of grains counted indicating that there is no significant bias introduced by the difference in sample dry weight. The mean, maximum, minimum and standard deviation of grains per gram for each of the recognised lithologies were calculated and are presented in Table 8.1.

8.4.3 Results

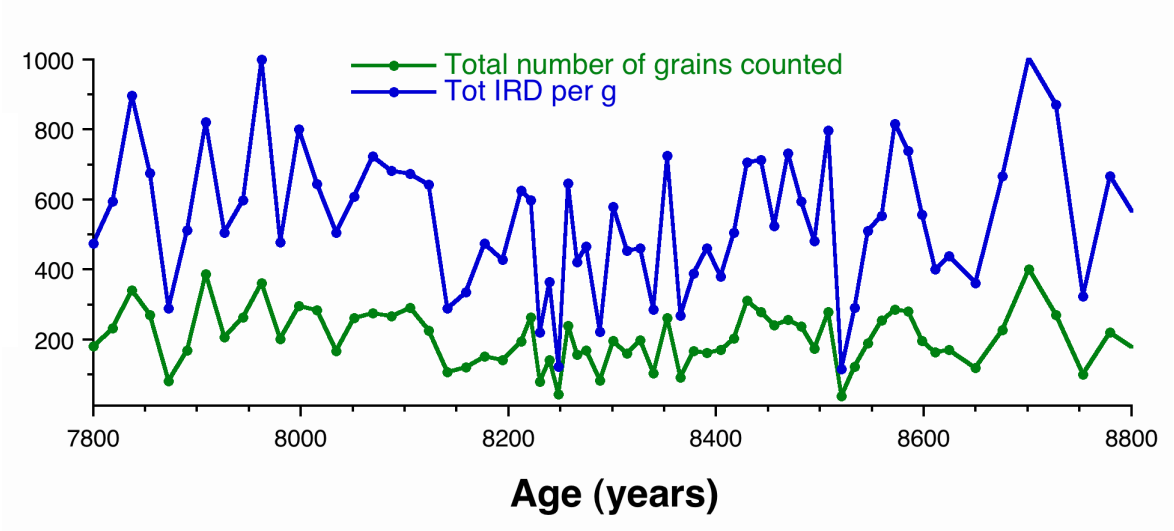

Figure 8.7 IRD per gram and total number of IRD grains counted for the interval 7.8-8.8kyr in core MD99-2251

Lithology	Mean per g abundance	Standard deviation	Minimum per g abundance	Maximum per g abundance
Quartz	330	132.5	63	687
Opaque quartz	28.5	15	6	63
Haematite stained Quartz	64	26	6	147
Dark Basaltic Glass	22.5	13	3	58
Vesicular Volcanics	8.5	7.5	0	33
Dark Volcanics	44	18	12	88
Other	40	23	2.5	131
Total IRD	537.5	192.5	114	1002.5

Table 8.1 Mean, maximum, minimum and standard deviation of different IRD lithologies for MD99-2251 7.8-8.8kyr

No significant increase was identified in IRD input with respect to quartz grains, haematite stained grains, dark basaltic glass or the total IRD content per gram, associated with the 8.2kyr event (Figure 8.8), but rather a multidecadal variability. The total IRD per gram signal is dominated by the concentration of quartz grains which make up around two thirds of the total IRD. Patterns of IRD show similar patterns for each lithology types.

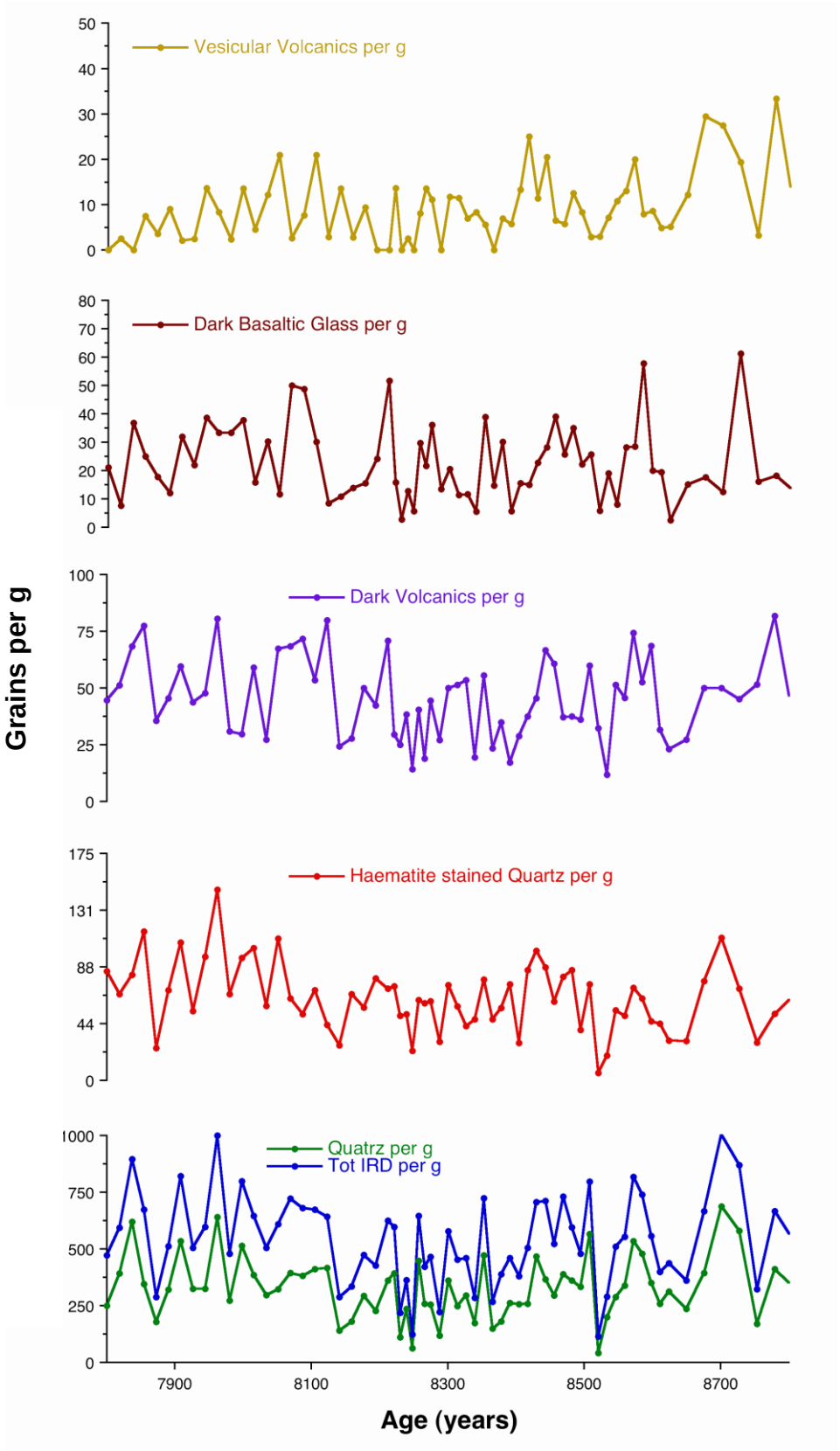

Figure 8.8 MD99-2251 7.8-8.8kyrs study. Abundance per gram of IRD lithologies and total IRD per gram.

If we accept the hypothesis of a prevalent 1500yr climate signal driving IRD flux (Bond *et al.,* 1997), then this result is unexpected. There is also evidence that other records which do not show the prevalent 1500yr signal in IRD flux, do indicate a peak in input associated with the 8.2 kyr event (Moros *et al*., 2004b). However other interpretations attribute IRD flux to prevailing oceanographic conditions (Moros *et al*., 2006; Andrews *et al*., 2009). It may be suggested therefore that a dominance of warmer currents over the core site for the time period study had a stronger influence on IRD flux than the wider climate cooling. The diatom data for this interval indicates a predominance of North Atlantic Current flora. The multidecadal variability in the IRD signal of MD99-2251 may be related to multidecadal variability in the strength of the North Atlantic Current.

Section Three

Discussion and Conclusions

Chapter nine

Discussion

“ As long as the human ear can hear the breaking of waves over deep seas, as long as the human eye can follow the track of the northern lights over silent snow-fields, as long as human thought seeks distant worlds in infinite space, so long will the fascination of the unknown carry the human mind forward and upward...”

Fridtjop Nansen ‘In Northern Mists’

Chapter Nine: Discussion

9.1 Holocene Overview

9.1.1 Variations in Sea Surface Temperatures

The palaeoproxies used in this study reveal distinct climate variability for the Holocene. Diatom abundance counts for MD99-2251 are used to reconstruct sea surface temperature (SST) using two different transfer functions (Figure 9.1). The WAPLS transfer function is based on core top data from the northern North Atlantic and Nordic seas while the Pd transfer function is based on core top data from the subpolar North Atlantic. Both the WAPLS and the Pd generated SST estimates indicate an initial warming in the early Holocene followed by a period relatively high variability until around 9.5kyr, a broad cooling between 9.5 and 7kyr, a distinct warming between 7 and 5kyr and higher but less variable temperatures for the late Holocene. The significant difference between the two SST records being that the Pd generated temperatures are 2-3^{o}C lower than the WAPLS generated temperatures. Also, the WAPLS generated temperatures indicate an overall warming of sea surface temperatures for the Holocene while the Pd temperatures indicate an overall cooling. This difference is especially pronounced in the late Holocene. These sea surface temperature trends are reproduced in nearby marine core MD99-2252 indicating that the observed changes are at least of regional significance. Core MD99-2252 only extends for the last 7.2kyr, however the warming at around 7kyr is clearly reflected in both the WAPLS and Pd generated SSTs for this core.

A number of similar investigations have been undertaken to generate sea surface temperatures using diatom assemblage data from the subpolar North Atlantic. Berner *et al.* (2008) uses three separate transfer functions to analyse marine core L009-14 (58^{o} 56.3' N 20^{o}24.5' W) from the western side of the Rekyjanes Ridge (Figure 9.2). The different approaches used are: (i) I&K - Q-mode factor analysis (Imbrie & Kipp, 1971), (ii) ML - maximum likelihood (Upton & Cook, 2002), and (iii) WAPLS (ter Braak & Juggins, 1993). The authors summarise the SST history from this core as indicating a relatively cool and highly variable early Holocene (11-7kyr), a relatively warm mid Holocene Climate

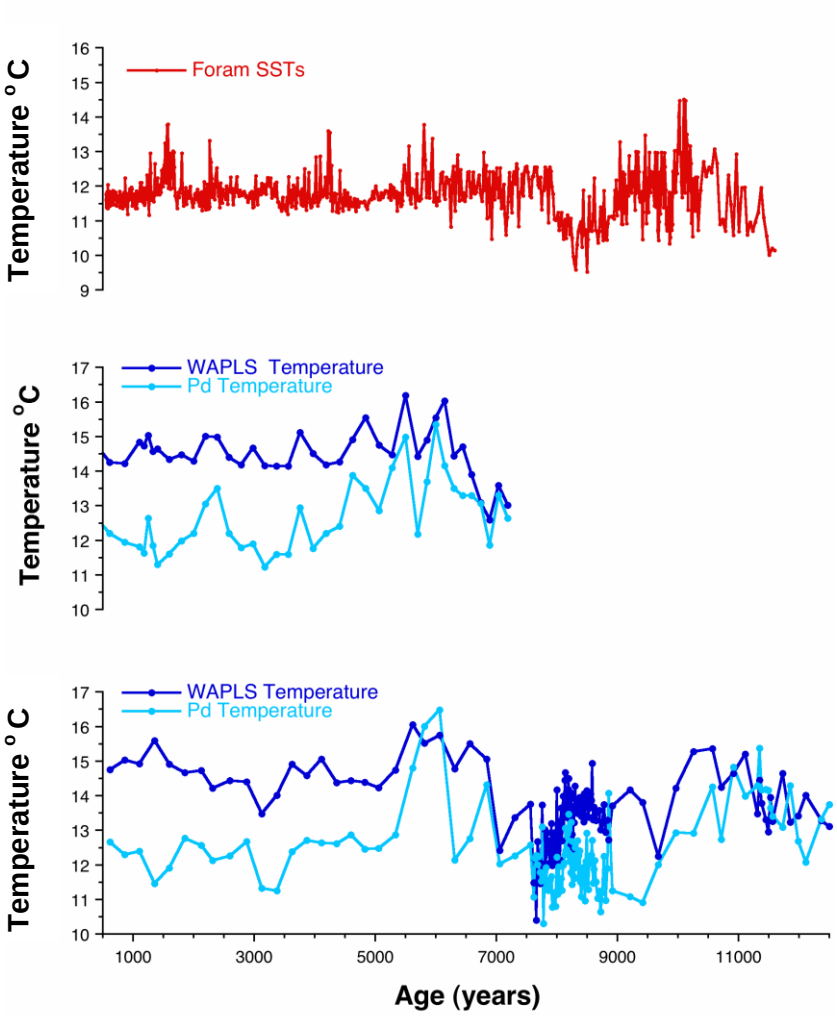

Figure 9.1 Sea surface temperature reconstruction for core MD99-2251 (57°26.87' N 27°54.47' W) generated from foraminiferal analysis (Ellison *et al.* 2006) plotted against SST estimates (WAPLS and Pd) from diatom analyses of cores MD99-2251 and MD99-2252 (57°26.84' N 27°55.83'W).

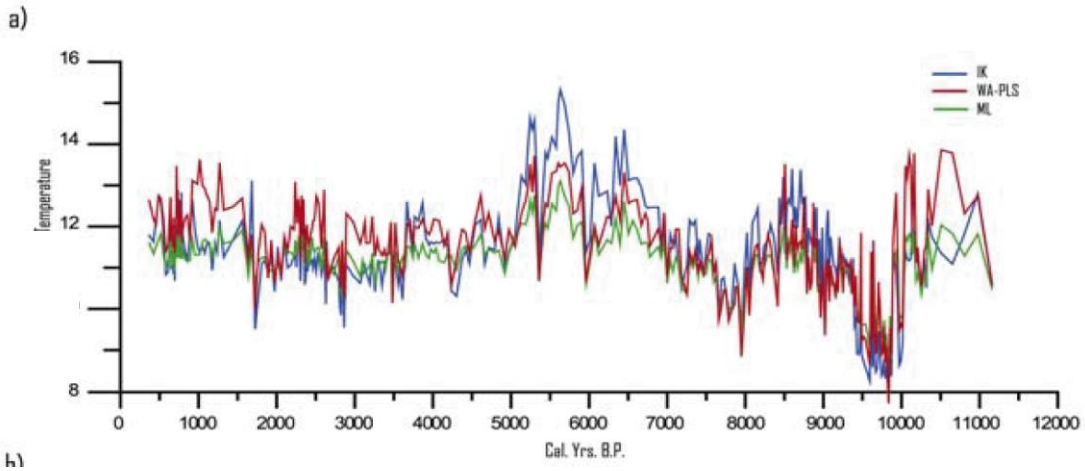

Figure 9.2 Imbrie & Kipp, WAPLS and ML generated SSTs for core L009-14 (58° 56.3' N 20°24.5'W). From Berner *et al.* (2008).

(Chardhuri & Marron, 1999) is applied to the Berner *et al.* (2008) sea surface temperature trends to identify significant trends. The analysis indicates a general temperature increase for the Holocene and two significant cooling periods from 10-9.4kyr and 8-7kyr, with significant warmings at 11-10kyr, 9.4-8kyr, and 7-5kyr.

This overall warming trend for the Holocene identified by Berner *et al.* (2008) agrees with the WAPLS transfer function results from core MD99-2251 but not the Pd results, as previously discussed. The sea surface temperatures generated from foraminifera for MD99-2251 (Ellison *et al.* 2006) suggest a more stable overall trend in SSTs for the Holocene (Figure 9.1). In addition the warming identified in the Berner *et al.* (2008) for the mid Holocene Climate Optimum (5-7kyr) is also clearly indicated in this study, though in a more pronounced manner with the WAPLS than the Pd transfer function (Figure 10.1). This warming event is observed in both MD99-2251 and MD99-2252. The warm, more stable late Holocene (5kyr to present) identified by Berner *et al.* (2008) is also a feature of the SST reconstructions of both cores examined in this study.

A detailed analysis of cooling events identified in this study with those recognised by Berner *et al.* (2008) reveals clear differences despite the proximity of cores L009-14 and MD99-2251; although, as for the warming events, the WAPLS generated temperatures show the greatest correlation between the two cores. The two significant cooling events identified by Berner *et al.* (2008) at 10-9.4kyr and 8-7kyr, are not replicated in MD99-2251. The WAPLS generate SSTs for MD99-2251 do indicate significant decreases in SSTs around 9.7 and 7.7kyr, which may be the same events found in core L009-14 given uncertainties in chronology and sampling density of the cores. The 7.7kyr cooling episode records the lowest registered SSTs for MD99-2251, whereas the lowest temperatures are recorded for the 10-9.4kyr cooling event in core L009-14. It is also significant to note that the WAPLS generated temperature history from Berner *et al.* (2008) more closely resembles the Pd generated SST record of this study, being 2-3^{o}C lower than the WAPLS generated temperatures from MD99-2251. The lowest WAPLS generated SSTs for L009-14 are recorded at around 8-9 ^{o}C and at 10-11 ^{o}C for MD99-2251. Correspondingly the highest WAPLS generated Holocene SSTs for L009-14 are in the region of 14 ^{o}C and around 16 ^{o}C for MD99-2251.

Andersen *et al.* (2004a), also in a study of core L009-14 from the Reykjanes Ridge, recognise relatively low highly variable SSTs for the early Holocene, a mid Holocene thermal optimum between 7.5-5kyr and a more stable late Holocene. This, unsurprisingly, concurs with the findings of Berner *et al.* (2008). However Andersen *et al.* (2004b) in a comparison three cores, from the Vøring Plateau, North Iceland Shelf and East Greenland Shelf, identify significantly different trends in diatom generated sea surface temperature for the Holocene. They identify a Holocene Climate Optimum at around 9.5-6.5kyr, a Holocene Transition Period 6.5-3kyr and a Cool Late Holocene period 3kyr to present, indicating distinct regional variation in diatom generated SSTs.

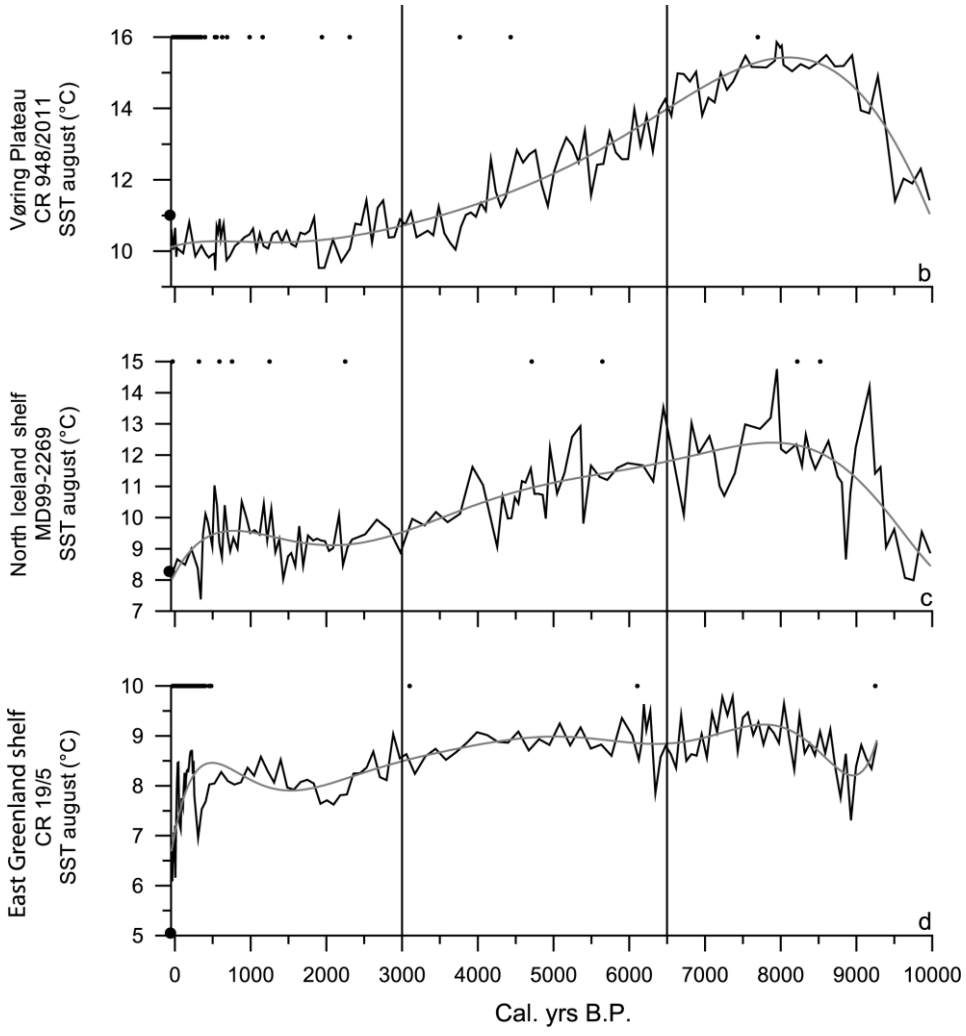

Figure 9.3 Diatom abundance generated SSTs for three Nordic sea cores.
MD99-2269 from the North Iceland Shelf. CR19/5 from the East Greenland Shelf.
CR948/2011 from the Vøring Plateau.
Black dots indicate AMS-dates. After Andersen *et al.* (2004a).

Justwan *et al.* (2008) in a more detailed study of core MD99-2269 from the North Icelandic shelf, use three methods to estimate SSTs from diatom assemblages (Figure 9.4). These authors recognise the Holocene climate optimum between 10.4-4.7kyr and August SSTs around 2^{o}C cooler for the late Holocene than the early and middle Holocene. This SST pattern is very different from those observed to the south in the Iceland Basin (cores L009-14 and MD99-2251). These differences reflect the usefulness and sensitivity of diatom assemblage counts as a climate proxy but these studies also reveal the potential for inconsistencies in the usage of terms such as the "Holocene climate optimum".

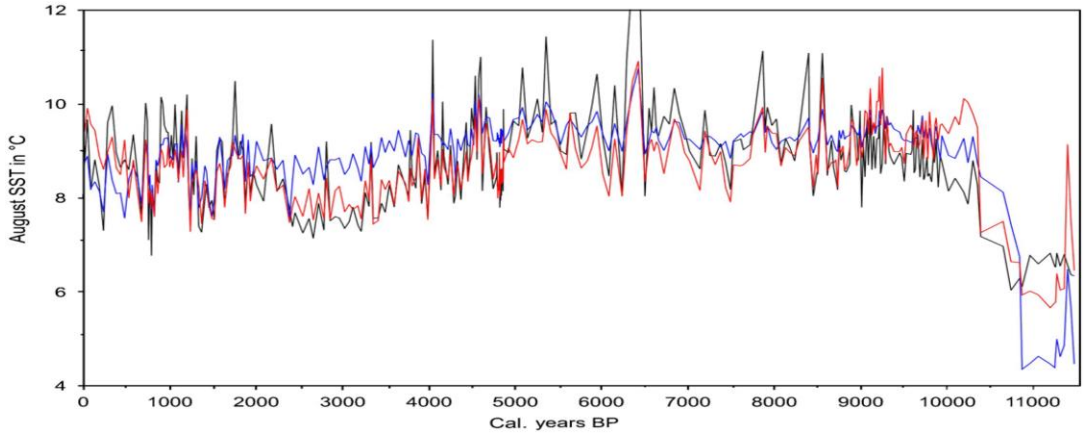

Figure 9.4 MD99-2269 August SST reconstructions using WAPLS (red), ML (Blue) and I&K (black) transfer functions. After Justwan *et al.* (2008)

9.1.2 Variations in Floral Assemblages and individual species distribution

Sea surface temperature reconstructions are important but not the only means of investigating the significance of variations in the Holocene diatom flora. Factor analysis identifying particular diatom floral grouping with surface water masses and currents can be informative, and has been applied here and in other studies (Jiang *et al.*,2001; Andersen *etal.*,2004a). The distribution of individual species also can provide important information about ecology and/or surface conditions. A summary of the distribution of three of the most abundant species found in MD99-2251, floral assemblage distributions after Andersen *et al.* (2004a), and floral assemblages as defined in section 7.7 of this study are

summarised in Figure 9.5. The trends evident in these records are reflected in the SST estimates.

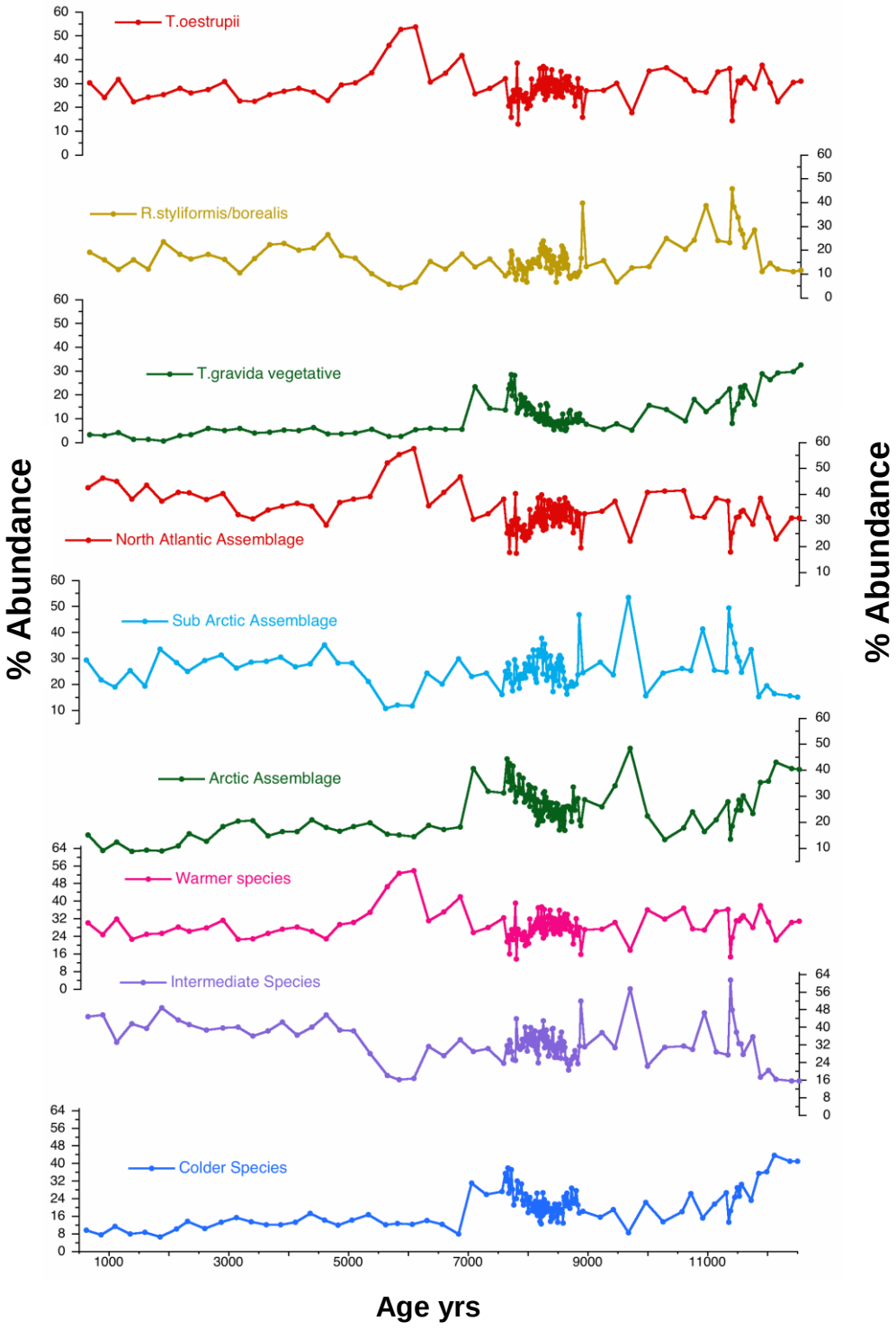

Figure 9.5 Significant species and floral assemblage data from MD99-2251. a) key abundant species. b) Floral assemblages after Andersen *et al.* (2004b). c) Floral assemblages based on temperature preference.

The early Holocene interval shows the greatest variability, reflected in a fluctuation of dominance between North Atlantic, Arctic, Sub Arctic and Warm, Cool and Intermediate assemblages. The broad cooling indentified in the SST data from 9.5-7kyr is reflected in an increase in the percentage abundance of Arctic assemblage flora and colder species. The only other times when the Arctic flora was as abundant occurred during the post Younger Dryas climatic amelioration and during the cooling episode at 9.7 kyr. The warming from 7-5kyr is recognised by a decrease in Arctic assemblage flora and colder species and a corresponding increase in the North Atlantic Assemblage flora and warmer species, especially *Thalassiosira oestrupii.* The most recent 5kyr is identified by a mix of North Atlantic and Sub Arctic floral assemblages and warmer and intermediate species (Figure 9.5).

Other similar approaches to diatom floral analysis have been undertaken by Jiang *et al.* (2001), Andersen *et al.* (2004a,b), Witak *et al.* (2005), Ran *et al.* (2006), Witon *et al.* (2006), Berner *et al.* (2008), Justwan *et al.* (2008). Figure 10.6 summarises the floral assemblage data for L009-14 from the Reykjanes Ridge. These data agree with the findings of this study. The early Holocene shows the highest variability and a fluctuation of dominance between the Sub Arctic and North Atlantic assemblages and colder East and West Greenland current assemblage (an assemblage dominated by *Thalassiosira gravida* vegetative which is included in the 'colder species' assemblage for this study and the Arctic assemblage of Andersen *et al.* 2004a). In both L009-14 and MD99-2251 the warmer mid Holocene 7-5kyr interval is dominated by the North Atlantic assemblage and exhibits a decrease in the colder assemblages; though the Sub Arctic assemblage also remains high during this interval. Both L009-14 data sets indicate that the Sub Arctic assemblage remains dominant for the last 5kyr, with a secondary influence of the Norwegian Atlantic current floral and the North Atlantic flora. This reflects the dominance of the intermediate species shown for the last 5yr, using the assemblage groupings developed in this study, and North Atlantic and Sub Arctic assemblages derived from the application of the Andersen *et al.* (2004a) assemblage groupings to the MD99-2251 data (Figure 9.5).

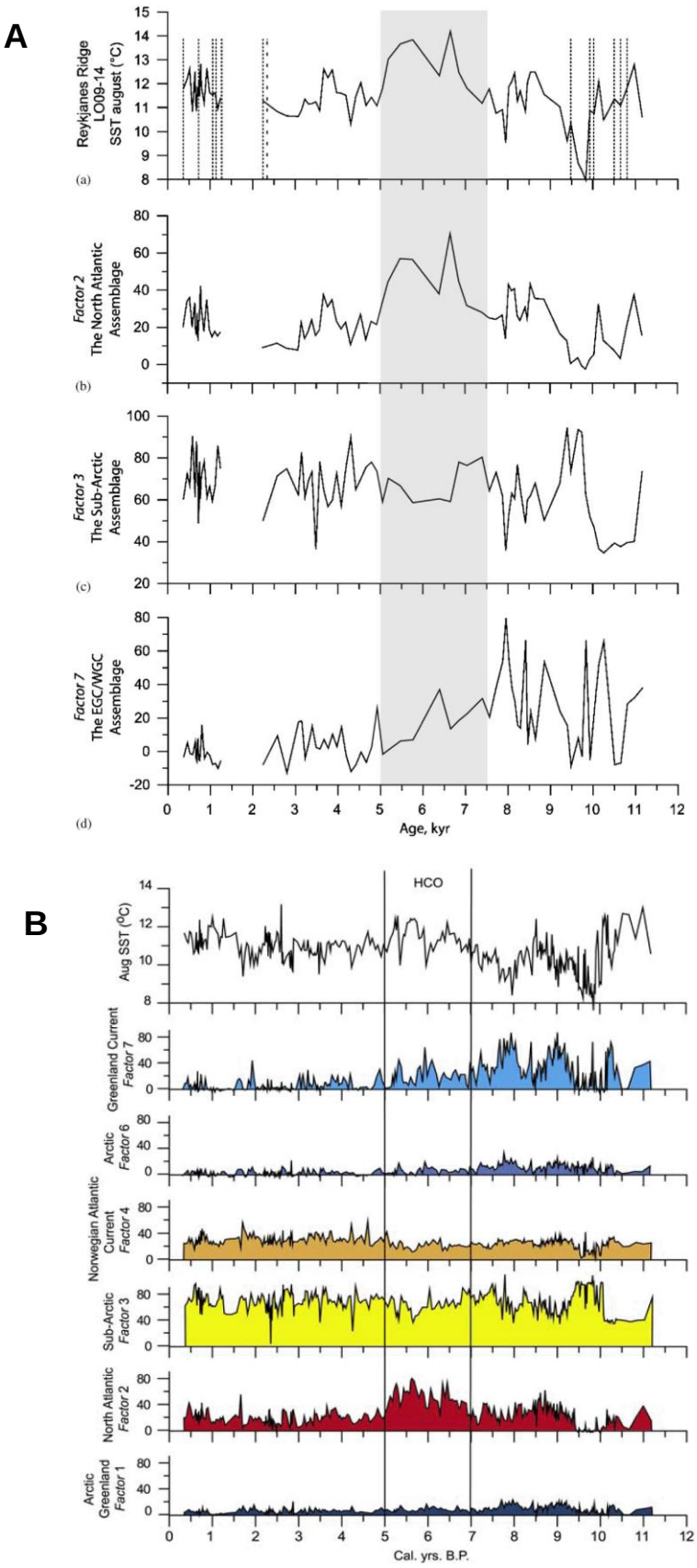

Figure 9.6 Floral assemblage abundances for core L009-14. A) from Andersen *et al.* (2004a). B) from Berner *et al.* (2008)

Witak *et al.* (2005) analyse the relative diatom species abundance of a Holocene sediment core also from the Reykjanes Ridge, core DS97-2P (58°56'33''N, 30°24'59''). The authors identify a predominance of cold flora for the entire Holocene, usually in abundances over 70%, with warm water flora fluctuating between 2% and 35% (Figure 9.7). The principal warm water species identified, as with the previous studies discussed is *Thalassiosira oestrupii* but Witak *et al.* (2005) also include *Thalassiosira tetraoesturpii*, which is not distinguished as a separate species in other studies, and *Thalassiosira lineata* in their warm grouping. Taxonomic issues concerning *Thalassiosira oestrupii* are discussed in section 5.2.13 of this study. *Thalassiosira lineata* is of minor importance in MD99-2251 and not included in any of the floral assemblage groupings, but this is unlikely to influence any comparison as the species constitutes only 1-3% of the total flora.

The key cold water flora identified by Witak *et al.* (2005) are consistent with Cold and Intermediate, Arctic, Sub Arctic and Norwegian Atlantic Current assemblage floras from previously discussed studies; *Thalassiosthrix longissima, Actinocyclus curvatulus, Thalassiosira gravida* (vegetative), *Thalassiosira gravida* (resting spore) *Rhizosolenia styliformis, Rhizosolenia borealis, Rhizosolenia hebetata semispina, Proboscia alata* and *Thalassiosira trifulta.* The timing of key changes in the diatom flora expressed on the basis of a ^{14}C time scale in the original study have been converted to calendrical ages using Calib 5.1 (Reimer *et al*., 2004). Witak *et al.* (2005) identify the onset of the Holocene as being characterised by Arctic and sea-ice flora. At around 11.3kyr this flora is replaced by a more northern North Atlantic assemblage, especially, *Thalassiosira gravida* (vegetative) and *Rhizosolenia styliformis,* with an increase in warmer North Atlantic assemblage forms, especially *Thalassiosira oestrupii* at around 10.9kyr. The Arctic-boreal flora *Rhizosolenia hebetata semispina* dominates in the interval 9.8-9.1kyr and *Rhizosolenia borealis* 9.1-6.8kyr in addition to various Arctic forms. Warm water floras peak in abundance at 6.8kyr with a distinct increase in colder-water taxa at 5.5kyr. These finding broadly reflect the floral sequence found in the previously considered studies; warming out of the Younger Dryas, a cooler flora then establishing round 9-7kyr, a distinct warming peaking at 6kyr and then a Sub Arctic flora dominating during the Late Holocene.

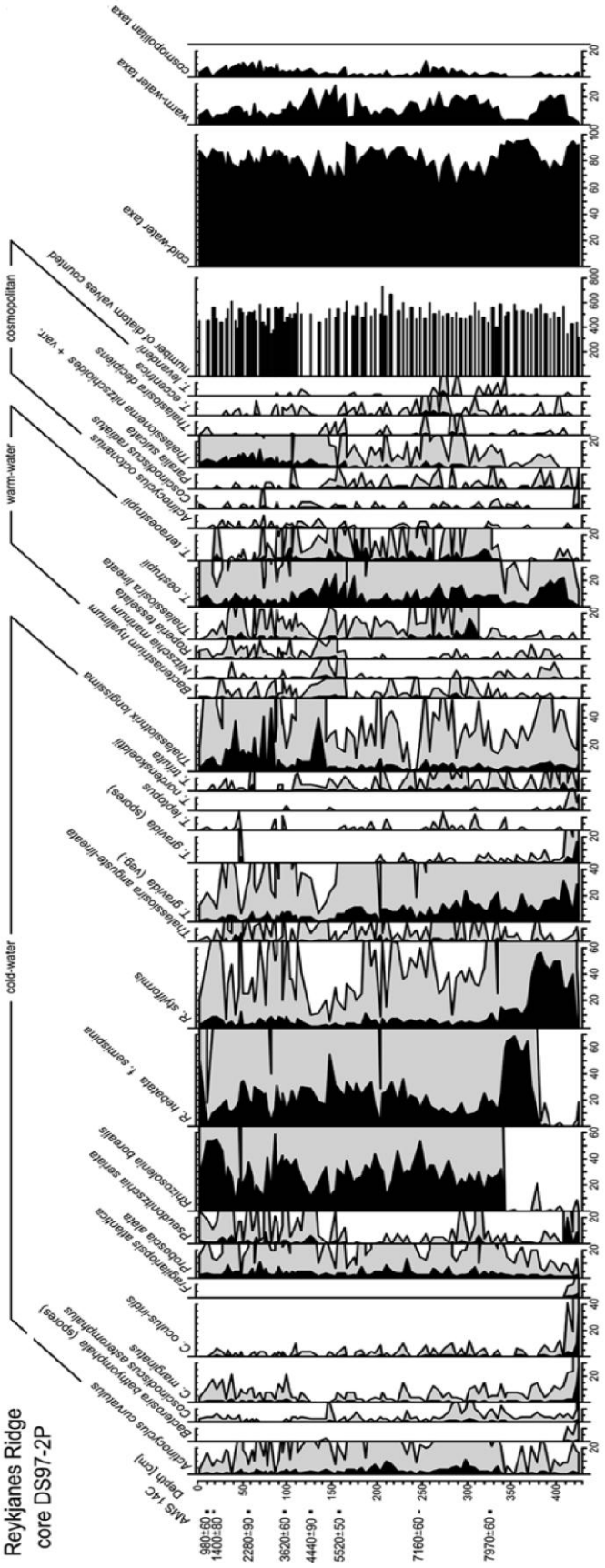

Figure 9.7 Relative abundance of individual species and temperature groupings for Reykjanes Ridge core DS97-2P. After Witak *et al.* (2005).

A number of related studies from the North Icelandic shelf (Jiang *et al.*, 2001; Jiang *et al.*, 2002; Knudsen *et al.*, 2004; Jiang *et al.*, 2005; Ran *et al.*, 2006; Knudsen *et al.*, 2009) also reflect similar SST variability for the Holocene. Jiang *et al.*, (2001) identify five diatom floral assemblages using canonical correspondence analysis (CCA) of fifty-three core top samples from around Iceland; a sea-ice diatom assemblage associated with the Polar waters of the East Greenland Current, a cold diatom assemblage associated with the East Icelandic Current, a warm diatom assemblage associated with the warm Irminger Current, a mixed diatom assemblage where these three currents interact and a coastal diatom assemblage. This modern data set is then applied to down core analyses of various Holocene marine cores. Jiang *et al.* (2002) examine core HM107-03 from the North Iceland shelf which extends for the last 4.6kyr and identify little variation in SSTs for this period 1-2^{o}C but six diatom floral assemblages which reflect the relative strengths of cold and warm water current over the core site. Similarly Ran *et al.* (2006) interpret changes in diatom assemblages for core MD99-2275 on the North Icelandic shelf with respect to the relative strengths of the Irminger Current, East Greenland Current and East Icelandic Current. The results more closely resemble the Nordic Sea diatom records than those from the Reykjanes Ridge with a warmer Early and mid Holocene. MD99-2275 registers the 8.2kyr event as an increase in colder flora and the influences of the colder East Greenland Current and East Icelandic Currents from 8.1 to 8.3kyr.

9.1.3 Palaeoceanographic Variability

Variations in the SSTs and diatom floral assemblages for marine cores MD99-2251 and MD99-2252 are interpreted as reflecting changes in surface oceanography over the core sites through the Holocene. The cores are situated on the Gardar Drift on the eastern side of the Reykjanes Ridge (section 6.1). In the present day surface hydrography, the core sites lie under the margins of the warm Irminger Current (section 2.4.2), a branch of the warm North Atlantic Current. However the site is also influenced by cooler Sub Arctic and Arctic waters brought into the Irminger Sea by the East Greenland Current (section 2.4.3) and lies close to the Sub Arctic Front (SAF) separating Sub Polar and Sub Arctic waters. The sites are therefore ideally situated to record changes in the strength of the North Atlantic Current and the position on the Sub Arctic Front through the Holocene.

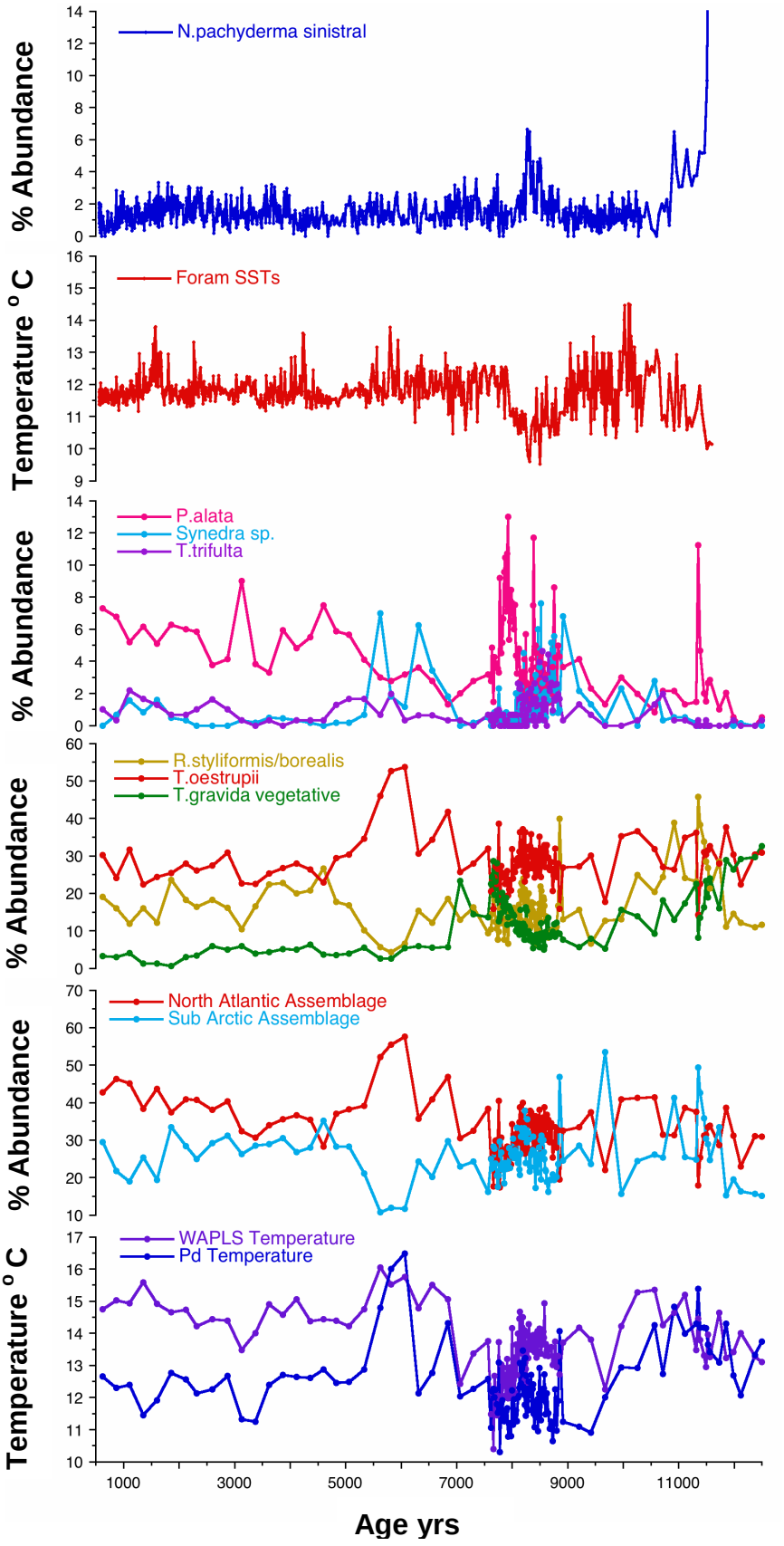

Figure 9.8 Summary plot of MD99-2251 data. Data from this study are compared to the %*N.pachyderma* sinistral and SST data of Ellison *et al.*, (2006).

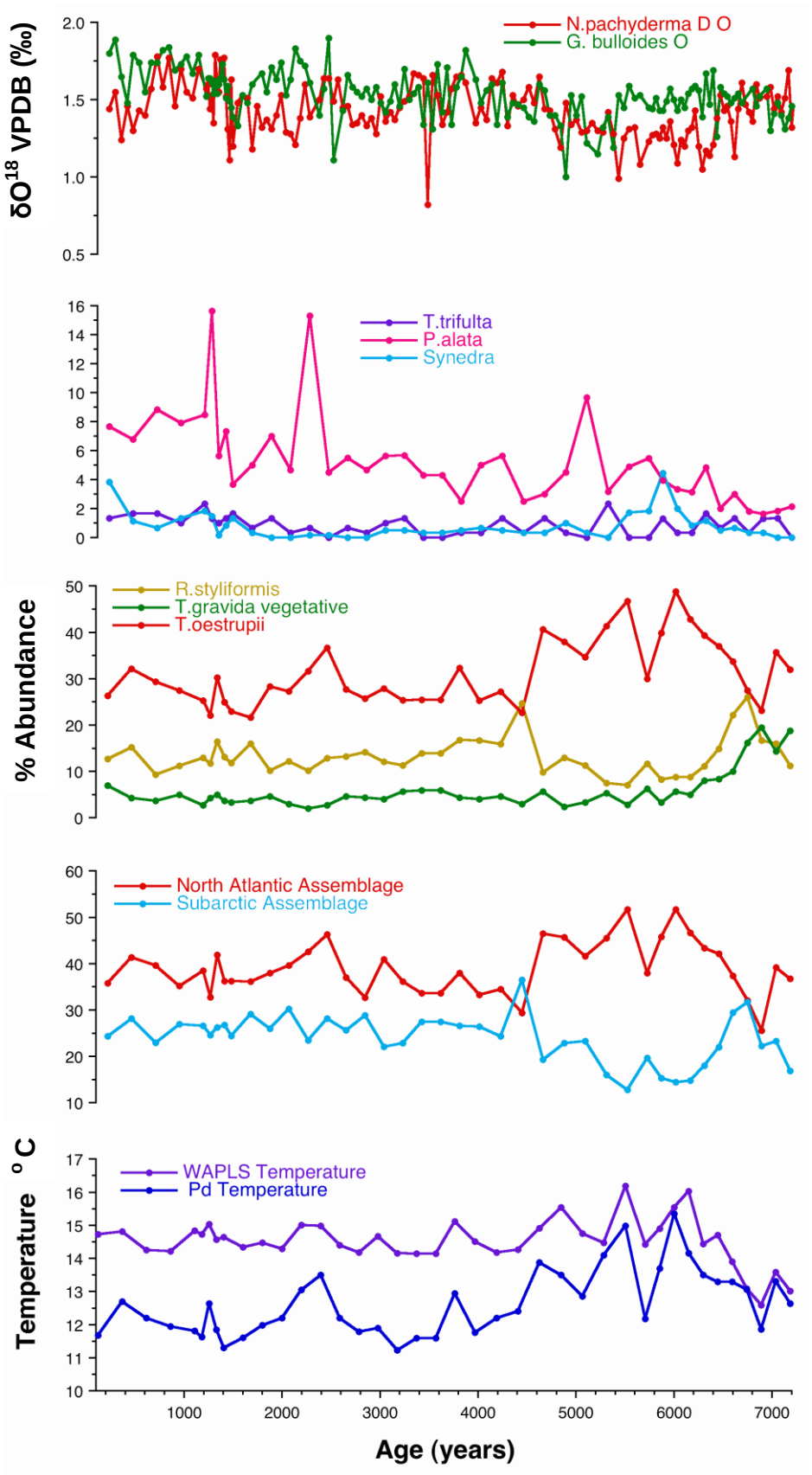

Figure 9.9 Summary plot of MD99-2252 data. Data from this study are compared to the %*N.pachyderma* sinistral and SST data of Ellison *et al.*, (2006).

Sea surface temperatures and floral assemblage data from cores MD99-2251 and MD99-2252 indicate a warming out of the Younger Dryas, an unstable early Holocene, 11.5-9kyr, a broad cooling form 9-7kyr, a warm interval 7-5kyr and a stable slightly cooler Late Holocene, 5kyr to present. Truly Arctic floras are only seen as dominant in this study during the Younger Dryas between 12.5 and 11.75kyr. Warming into the Holocene from around 12kyr sees the establishment of warmer flora by the onset of the Holocene at 11.5kyr. It is important to note that while the Younger Dryas is clearly distinguished in the the floral assemblage data, it does not appear as a prominent event in the SST record. The Arctic assemblage for the Younger Dryas is dominated by both forms of *Thalassiosira gravida* and by *Actinocyclus curvatulus,* with negligible contribution for the *Rhizosolenia hebetata* subspecies. The sea-ice assemblage also reaches its highest levels for this interval with five of the eight Younger Dryas samples showing sea-ice flora at around or exceeding five percent, levels only reached elsewhere in the core at around 8.1kyr. The explanation for the relatively high SST estimates for the Younger Dryas may lie in the fact that the North Atlantic floras still constitute around 30% of the total flora for this interval.

The Early Holocene period, from around 11.5 to 9kyr, in core MD99-2251 exhibits high variability with fluctuations between Sub Arctic and North Atlantic floras. This period is also characterised by episodes of single species dominance of the floral assemblage (section 7.6.1). In the case of this study *Rhizosolenia hebetata semispina,* and *Rhizosolenia styliformis/borealis* reach 38-45% of the total flora on five occasions around 8.9kyr, 9.9kyr, 10.9kyr and twice around11.3kyr (Figure 7.7). The 9.9kyr peak is of the species *Rhizosolenia hebetata semispina.* All other peaks are of *Rhizosolenia styliformis/borealis. Rhizosolenia styliformis/borealis* constitutes over 20% of the total flora for the entire interval 10.3-11.7kyr.

Similar peaks in *Rhizosolenia styliformis/borealis* and *Thalassiothrix longissima* have been identified for core L009-14 (Andersen *et al.,* 2004a; Berner *et al.,* 2008). The authors note that high concentrations of *Rhizosolenia* spp. have been identified at the convergence of warm and cold waters in the present day equatorial Pacific (Yoder *et al.,* 1994, Dore *et al.,* 2008). Water mass boundaries in coastal waters have long been identified as associated with increased biological activity. It is therefore suggested that these peaks in concentration of *Rhisosolenia* spp. (Yoder *et al.,* 1994; Kemp *et al.* 2006) could reflect the

presence or close proximity of an open ocean front, in this case the Sub Arctic Front. There are no records of monospecific concentrations of *Thalassiothrix longissima* in the modern oceans as identified in Andersen *et al.* (2004a). However Neogene records from the Sub Polar North Atlantic and equatorial Pacific, report monospecific diatom mats of *Thalassiothrix longissima* that have been interpreted as marking the past position of an ocean frontal system (Boden & Backman, 1996; Kemp & Baldauf, 1993). There appear to be no contemporary records of monospecific blooms of *Rhizosolenia hebetata semispina*. The highly variable early Holocene in core MD99-2251 with intervals of monospecific blooms is therefore interpreted as a period of oscillating dominance of subpolar waters and warm waters as a result of the periodic eastward incursion of cooler waters from the East Greenland Current and with changes in the proximity to the site of the Sub Polar Front.

The interval 9.5-7kyr marks the lowest sea surface temperatures for the Holocene, but is not characterised by monospecific blooms. The last *Rhizosolenia* spp. peak occurs at around 8.9kyr in MD99-2251. Andersen *et al.* (2004a) suggest that cold intervals which do not exhibit these *Rhizosolenia* sp. peaks may be best interpreted as resulting from a reduction in the strength of Irminger Current, a branch of the North Atlantic Current, rather than a southward migration of the Sub Polar Front. The subsequent warming for 7kyr to 5kyr is characterised by a corresponding increase in North Atlantic flora, especially *Thalassiosira oestrupii* which, as the dominant species of the North Atlantic assemblage, may be considered as an indicator of the strength of the Irminger Current. The Late Holocene (5kyr to present) may again be interpreted with respect to the relative strength of the Irminger Current, decreasing in this interval from the maximum strength of the 7-5kyr warming.

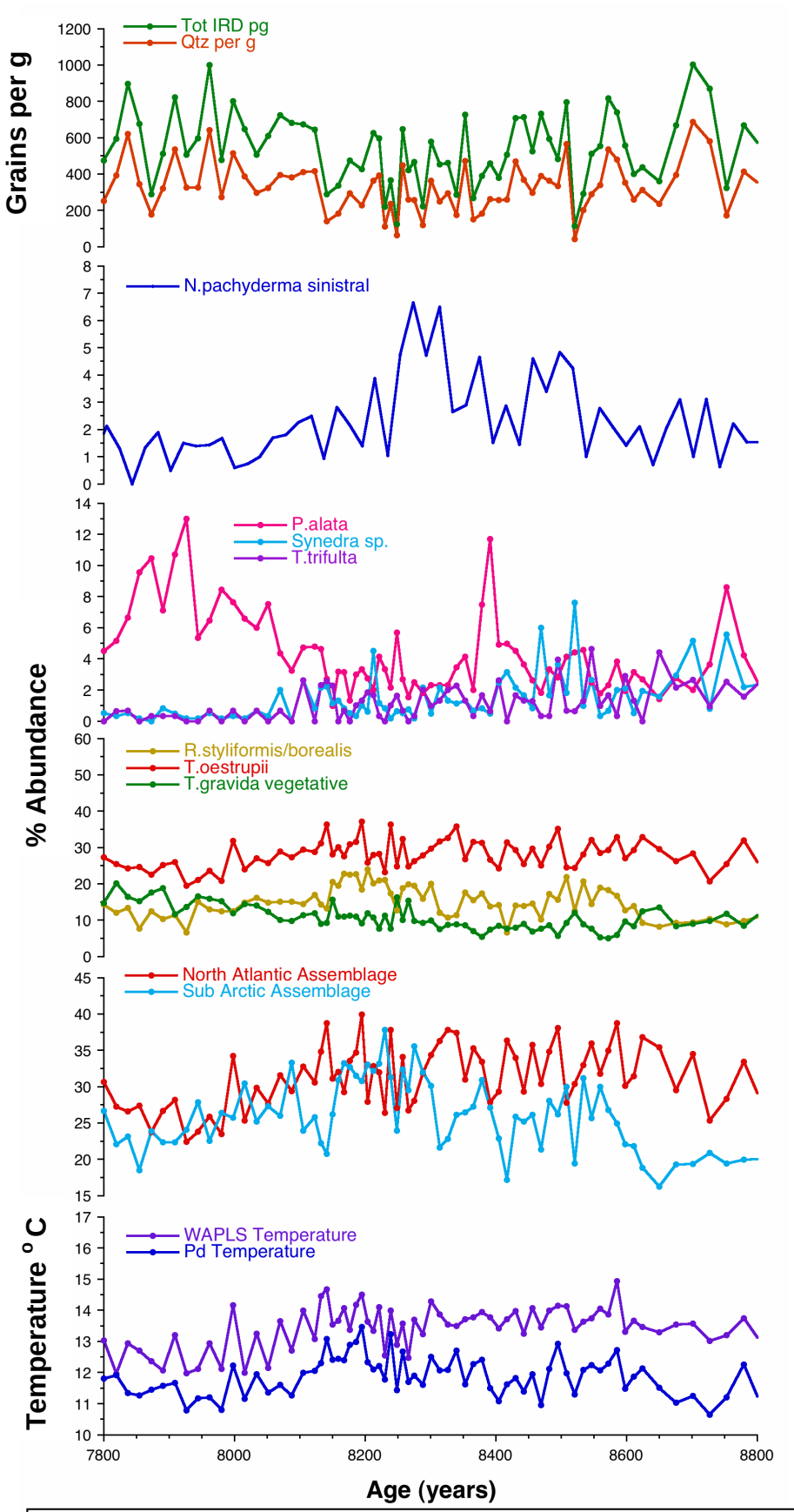

Figure 9.10 Summary plot of 8.2kyr data from MD99-2251. Percentage abundance *N.pachyderma* sinistral from Ellison *et al.* (2006)

9.2 The 8.2kyr event

A high resolution study of core MD99-2251 was undertaken for both diatom assemblage data and ice rafted debris flux. Figure 9.10 presents a synthesis of the data from this high resolution study as well as the percentage abundance of *Neogloboquadrina pachyderma* sinistral from MD99-2251 (Ellison *et al.,* 2006). The 8.2kyr is widely accepted as the most significant climate perturbation of the Holocene. However it appears not to register as a distinct event outside the range of the recorded Holocene variability in either the SST, diatom floral assemblage, or the IRD record of MD99-2251. Rather a broad cooling is recognised in the diatom flora from 9.5-7kyr.This broad cooling is also observed in L009-14 (Berner *et al.,*2008) from the Reykjanes Ridge. Rohling & Palike (2005) observe that where the 8.2kyr event is recognised in the North Atlantic it is present with a more broad cooling anomaly identified by the authors as occurring around 8.6 to 8.0kyr. Certainly this is not inconsistent with the MD99-2251 SST and floral assemblage record as 8.6 to 8.0kyr marks the centre of the broad 9.5 to 7kyr cooling already recognised. Some possible correlation may be drawn between the pattern of abundance of Sub Polar flora during the interval 8-8 to 7.8kyr and the percentage abundance of *N. pachyderma* sinistral with both records showing a general increase between 8.6 and 8.2kyr. This reflects the general cooling interval identified by Rohling & Palike (2005).

Where a discrete event may be recognised in MD99-2251 is in an examination of individual sea-ice and cold water species (Figure 9.10). It must be emphasised, however that while the percentage presence of a given species may double for the period 7.8 to 8.8kyr, these changes reflect very small numerical increases as the particular species are poorly represented in any Holocene sample of MD99-2251. For example, *Thalassiosira gravida* resting spore exhibits a background presence for the Holocene of 1-3 frustules per sample with an increase to 4-7 frustules for period 7.8 to 8.8kyr.However K-means cluster analysis of MD99-2291 also recognises a unique floral cluster for the interval 7.8-8.8kyr (Figure 6.36). As previously discussed, Ran *et al.* (2006) recognises an increase in individual sea-ice and cold water floras for the interval 8.3 to 8.1kyr in core MD99-2275 from the North Iceland shelf. .

The high resolution interval analysed for IRD in MD99-2251 should identify the fifth of the cycles of increased Holocene IRD recognised by Bond *et al*. (1997). However no IRD peak is recognised in core MD99-2251 for the period 8.8 to 7.8kyr instead a low but variable input is identified for the entire interval. Studies of Holocene IRD from the Norwegian Sea (Moros *et al.,* 2004b) and North Iceland Shelf cores (Andrews *et al.,* 2009) conclude that the prevailing oceanographic conditions have a greater influence on the IRD signal than the prevailing climate signal. IRD is found at low and fluctuating levels throughout the Holocene in these locations. Moros *et al*. (2004b) identify a peak in IRD related to the 8.2kyr event (Figure 10.8). This is not recognised in the Iceland Shelf cores (Andrews *et al.,* 2009) or this study.

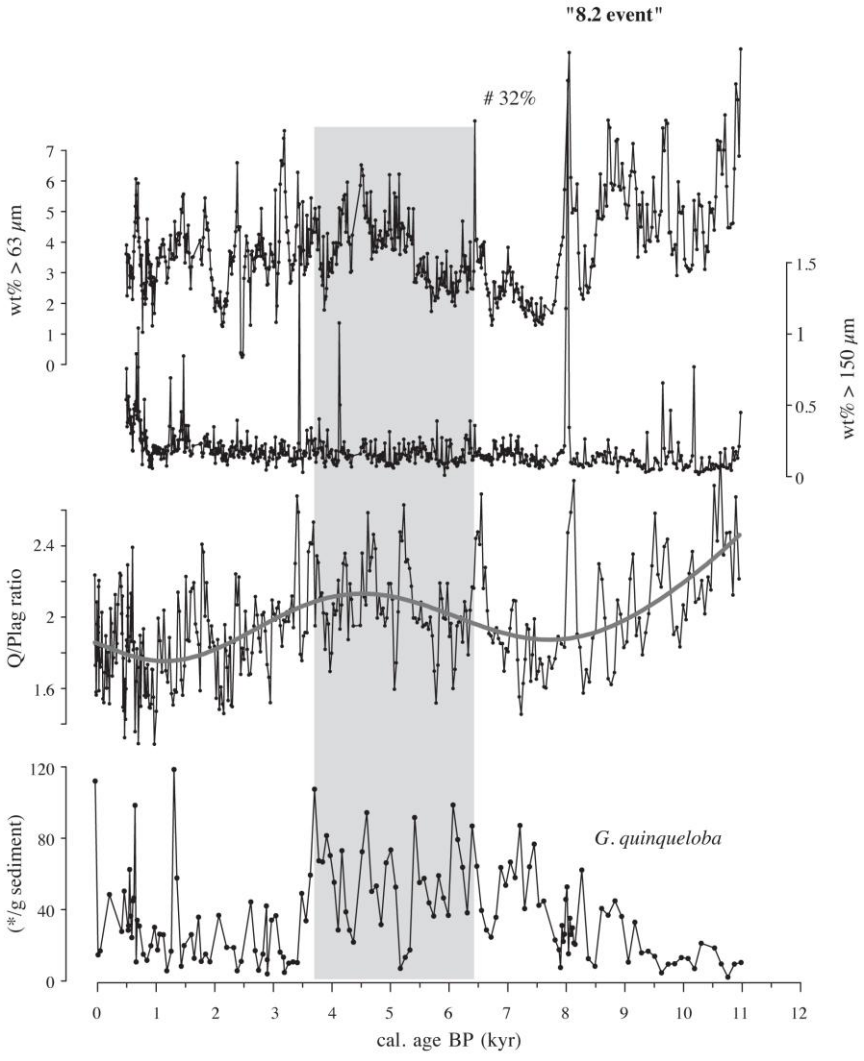

Figure 9.11 Holocene IRD variability from core MD95-2001 from the Norwegian Sea indicating an increase in terrigenous input between 6.5 and 3.7 kyr and associated with the 8.2kyr event. (Moros *et al.,* 2004b)

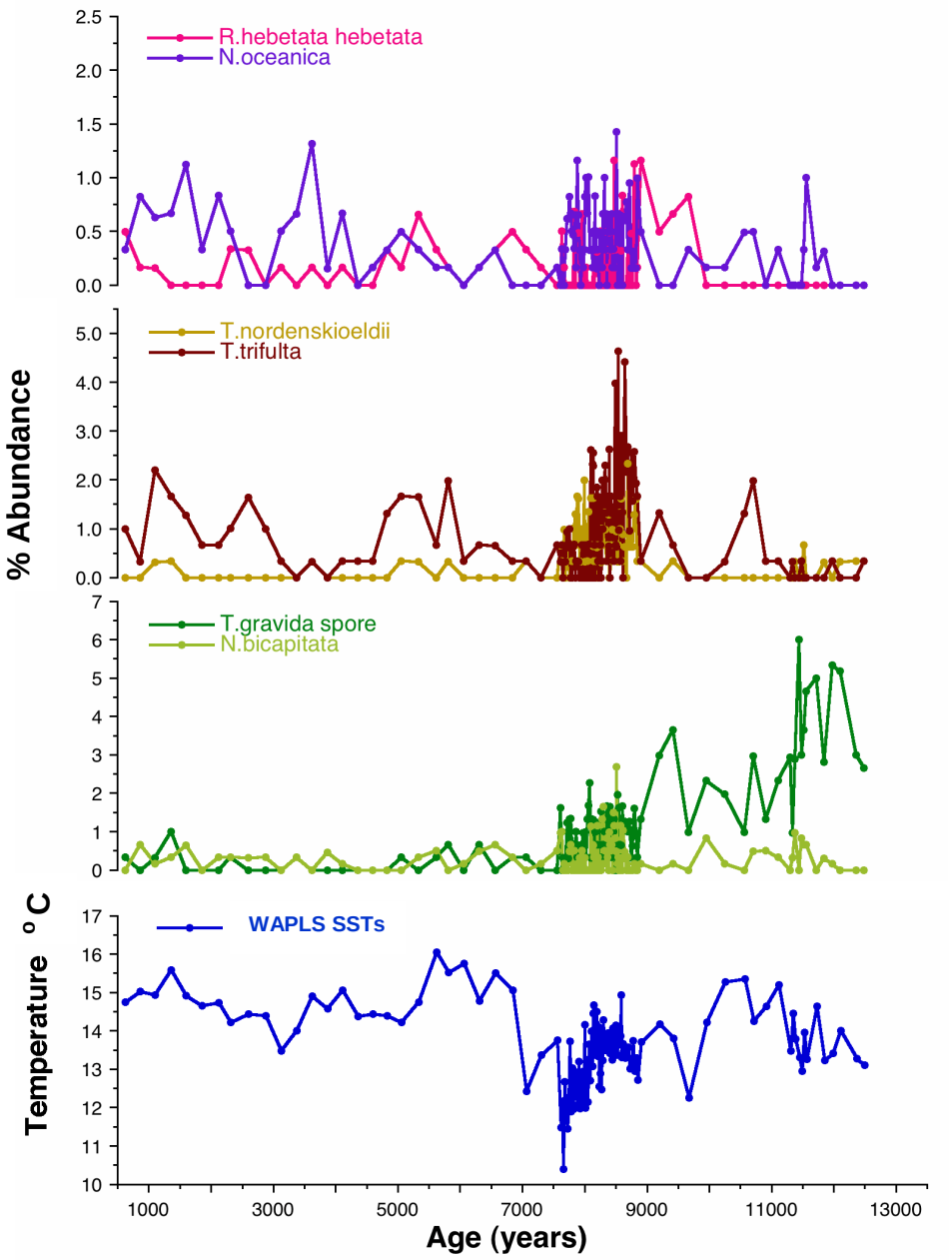

Figure 9.12 Holocene variations in sea-ice and colder water diatom species in core MD99-2251 around 7.8-8.8kyr.

The question remains as to why the 8.2kyr event is not recognised in MD99-2251 in the diatom and IRD records, but is clearly recognised in the foraminferal data. The difference in diatom and foraminifera generated SSTs may be a function of different organisms recording different climate signals. The diatom generated SSTs are widely considered to reflect summer values, whereas a winter and summer signal may be distinguished from the foraminiferal derived SSTs. It is improbable that the problem is an

issue of bioturbation blurring a discrete signal as the diatom and foraminiferal samples are taken from the same core. The sensitivity of the different transfer functions may be the key issue in the varying records. As has already been indicated, the diatom derived SSTs failed to indicate truly low values for the Younger Dryas despite high levels of Arctic and sea-ice flora. The same issues may apply to the diatom derived SSTs for the 8.2yrs event. Percentage abundances of North Atlantic flora remain high throughout the high resolution study interval 8.8 to 7.8kyr at around 20 to 35% , the same as for the Younger Dryas (which is robustly identified by the presence of the Vedde Ash).

9.3 Correlation with Holocene Variability in other records

The question arises as to whether these palaeoceanographic interpretations of the variability of diatom floras and ice rafted debris flux for MD99-2251 and MD99-2252 may be related to wider climate variability observed for the North Atlantic Holocene and what forcing mechanisms may be considered to have caused this variability.

Previous analyses of core MD99-2251 have examined the relative foraminiferal abundances, oxygen isotope ratios and mean sortable silt (Ellison *et al.,* 2006), as well as Magnesium/Calcium ratios (Farmer *et al.,* 2008). Percentage abundances of the planktonic foraminifera *Neogloboquadrina pachyderma* sinistral, a cold water indicator and $\delta^{18}O$ ratios in *Globigerina bulloides*, indicate a relatively stable Holocene climate with the exception of the 8.2kyr event (Figure 9.10). This is clearly significantly different from the results of this study. The Mg/Ca ratios in contrast show distinct temperature variations through the Holocene (Figure.9.11). An abrupt warming at the onset of the Holocene is followed by an increase in temperatures until around 9.5kyr. There is then a broad stable cool period until around 3.5kyr when temperatures show a stepped increase. While the Mg/Ca data for MD99-2251 therefore reflects the greater variability in temperatures shown in the diatom analyses, the timing and magnitude of those variations differs significantly. The onset of the broad cooling in the Mg/Ca record may be considered synchronous with the onset of the 9.5-7kyr cool period indicated in the diatom abundance data. However neither of the foraminiferal investigations for core MD99-2251 reflect the significant warming indicated in the diatom analyses from 7-5kyr.

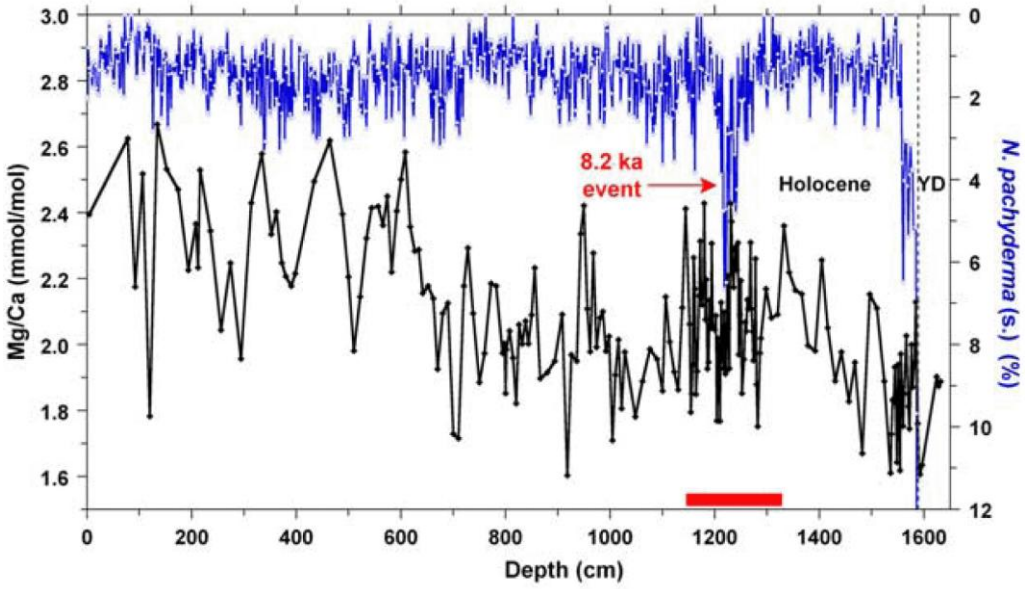

Figure 9.13 Holocene variations in the relative abundance of the planktonic foraminifera *Neogloboquadrina pachyderma* sinistral and Mg/Ca ratios measured for *Globigerina bulloides* in core MD99-2251. Lower Mg/Ca ratios reflect colder calcification temperatures. From Farmer *et al.* (2008).

The diatom temperature trends shown in this study show a greater correlation with other diatom records from adjacent cores from the Reykjanes Ridge; L009-14 (Andersen *et al.* 2004a; Berner *et al.* 2008) and DS97-2P (Witak *et al.*, 2005). However even between these records there is a notable variation in the percentage abundances of *Thalassiosira oestrupii* (the key North Atlantic Current indicator) between these Reykjanes Ridge cores. In this study the percentage abundance of *Thalassiosira oestrupii* remains consistently around 20-35% of the total flora with a mean of 28.5% in MD99-2251 and 31% for MD99-2252 and a maximum abundance of 53.7% at around 6.1kyr in the MD99-2251 record. Although no absolute percentage data are available for the abundance of *Thalassiosira oestrupii* in L009-14, the percentage abundances of the North Atlantic Assemblage, which is dominated by *Thalassiosira oestrupii*, vary from around 20 to 35% with the mid Holocene maximum in the North Atlantic assemblage for L009-14 having values approaching 80% (labelled as Factor 2 in Figure 9.6). This contrasts with the record obtained from core DS97-2P, recovered from almost exactly the same location as core L009-14, where the percentage abundance of *Thalassiosira oestrupii* varies between only 5 and 20%. These differences are interpreted as reflecting a high sensitivity of the diatom

flora to the position of the Irminger Current even across the restricted location of the Reykjanes Ridge.

Other diatom records from the Icelandic shelf and Nordic Seas (Andersen *et al.,* 2004b; Justwan *et al.,* 2008) reveal a different pattern of sea surface temperature development during the Holocene than the Reykjanes Ridge diatom records (Figure 9.3). This suggests that diatom records may be best used as regional rather than global indicators of climate variability, recording changes in diatom flora as a proxy for changes in surface water circulation patterns. In support of this argument is the fact that neither the Reykjanes Ridge cores or those from the Iceland Shelf and Nordic seas considered in this study appear to record the 8.2kyr event as a significant climate Holocene perturbation within the scale of the overall Holocene variation. While cooling is recorded in the Reykjanes Ridge cores for the period approximately 9.5 to 7kyr there is no discrete event recorded around 8.2kyr that does not fall within the range of the general Holocene variability for the cores. The Nordic Sea and Icelandic Shelf cores appear to be registering maximum Holocene temperatures for the period 10.5 to 4kyr.

The 8.2kyr event is best identified in these records in a detailed study of individual sea-ice and cold water species such as *Fragilariopsis oceanica* and *Thalassiosira gravida* resting spore. These increases are recorded in both core MD99-2275 from the Icelandic shelf (Ran *et al.,* 2006) and in MD99-2251 (Figure 9.8). The 8.2kyr has been linked to catastrophic discharges of meltwater from proglacial lakes Agassiz and Ojibway, associated with the decaying of the Laurentide Ice Sheet. These meltwater pulses caused cooling and freshening of surface water, a significant reduction in North Atlantic Deepwater formation causing a slow down of the meridional over turning circulation (Rohling & Palike, 2005, Alley & Agustsdottir, 2005; Ellison *et al.,* 2006). It is possible to hypothesise that fresher surface waters could result in the increased formation of sea-ice, as fresher water freezes at a lower temperature. This might explain the increase in sea-ice forms for this interval, although it has to be noted that the actual numerical increases are very low and in the region of less than five to less than ten frustules per sample. It would be useful to analyse the fresh water diatom species from the MD99-2251 to see if there is any significant increases in occurrence for the 8.8 to 7.8kyr interval.

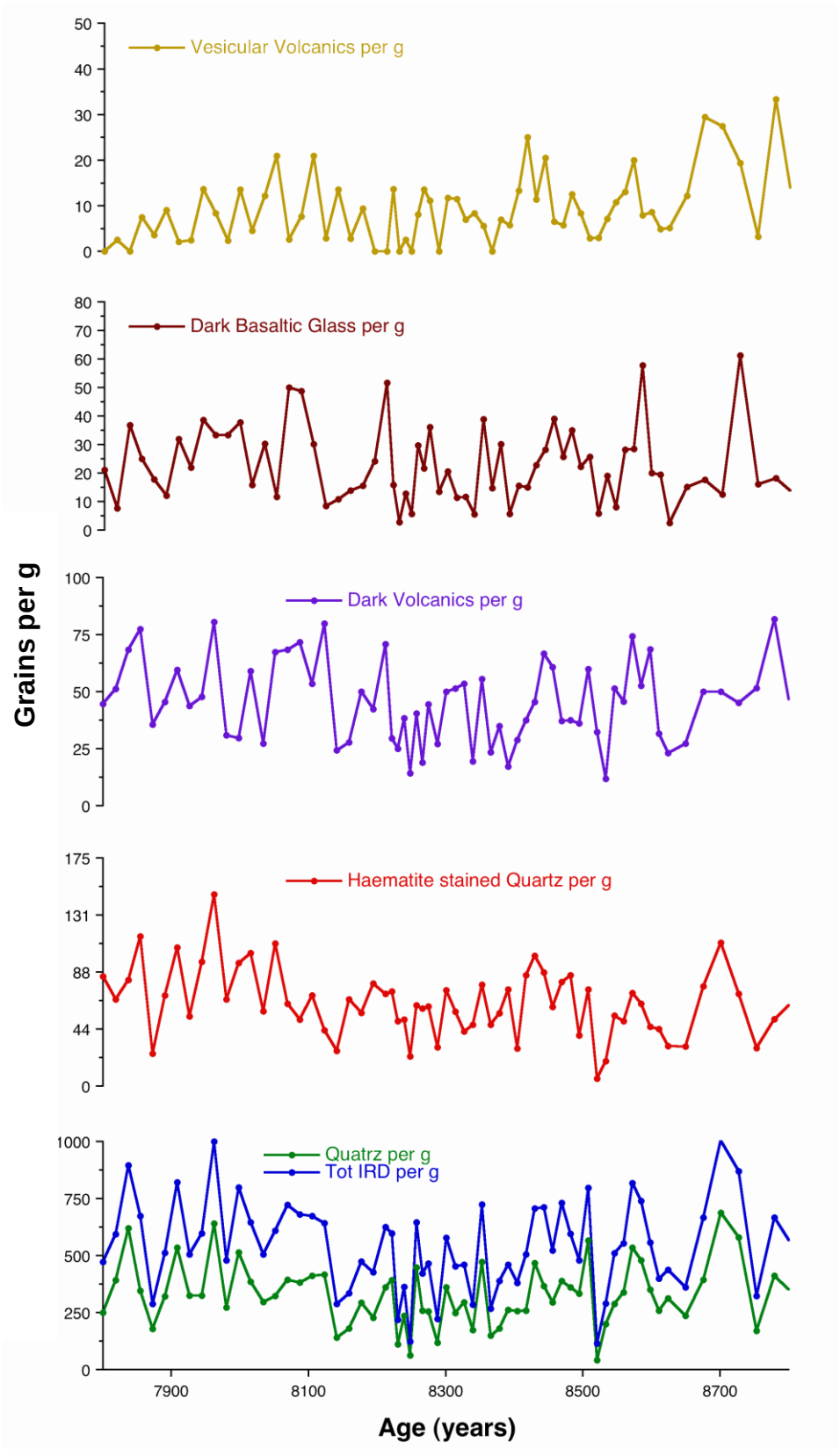

Figure 9.14 MD99-2251 7.8-8.8kyrs study. Abundance per gram of IRD lithologies and total IRD per gram. No clear peak in IRD input is identified related to the 8.1kyr IRD peak of Bond *et al.* (1997)

Berner *et al.* (2008) recognise an anticorrelation between solar radiation proxies (^{14}C production rate and ^{10}Be flux) and cooling events recorded in L009-14, indicating an underlying forcing of changes of solar insolation for the Holocene. No such correlation is observed for MD99-2251. A cycle of increased IRD input for the Holocene has also been identified (Bond *et al.* 1997) and linked to solar forcing. These IRD cycles are not recognised in this study. A high resolution investigation of the 8.8-7.8kyr interval revealed a prevailing fluctuation in IRD input, but no increase related to the 8.1kyr peak identified by Bond *et al.* (1997) (Figure 9.12). The hypothesis that IRD flux in the Holocene is the result of prevailing oceanographic conditions (Moros *et al*., 2006; Andrews *et al*., 2009) appears to best explain the data from this study. It is suggested that the dominance of warmer currents over the core site for the time period study had a stronger influence on IRD flux than the wider climate cooling. The diatom data for this interval indicates a predominance of North Atlantic Current flora.

Berner *et al.* (2008) also identify a correlation between Holocene cooling events in L009-14 and changes in North Atlantic deep-water (NADW) formation, arguing a strong coupling between the surface and deep ocean variability. As previously discussed there has not always been an exact correlation between the fluctuations of Holocene NADW as recorded by different palaeoproxies (Oppo *et al.*, 2003, Hall *et al.*, 2004), the relative strength of the North Atlantic Current over the core site appears to have the strongest influence on the diatom floras from 9.5kyr to the present. This strength of the surface currents is strongly influenced by the strength of deep water currents. Hall *et al.* (2004) recognise a strongest influence of the North Atlantic Current form around 4.8 to 8kyr which would coincide with the maximum temperatures recognised in MD99-2251 diatom generated SSTs.

9.4 Summary

This study presents a multiproxy reconstruction of the Holocene Sub Polar North Atlantic from diatom abundance data, ice rafted debris flux and stable isotope analysis of foraminifera. Two marine cores are studied, MD99-2251 which extends for the entire Holocene and MD99-2252 for the last 7.2kyr. The cores are sampled at least 250yr resolution and decadal resolution for a study of the 8.2kyr event. Diatom reconstructed sea surface temperatures indicate a highly variable early Holocene, a broad cooling from 9.5 to 7kyr, a warming from 7kyr to 5kyr and a cooler more stable late Holocene. Two transfer functions were used to analyse the diatom abundance data. The WAPLs transfer function with a Nordic sea based core top data set gave higher SST estimates than would be expected for the Holocene North Atlantic. A regionally based data set was constructed from Sub Polar and northern North Atlantic core tops and the simpler Parks Index transfer function applied. Despite the less sophisticated mathematical procedure, the Parks Index transfer function gave a better estimate of Holocene SSTs according to World Ocean Atlas values (Levitus & Boyer, 1994). This result suggests that regional constraint of a transfer function is of more importance than the complexity of the mathematical technique.

The SST estimates were robustly repeatable between the two cores and also strongly reflect diatom based SST estimate from an adjacent core, L0009-14 form the Reykjanes Ridge (Berner *et al.* 2008). Diatom derived SSTs from the northern North Atlantic and Nordic Seas however (Andersen *et al.,* 2004b; Justwan *et al.,* 2008) show different patterns of Holocene variability suggesting that the diatom derived SSTs reflect a regional rather than wider climate signal. The diatom derived SSTs from MD99-2251 also differ from the temperature estimates derived from the same core from stable isotope and Mg/Ca ratios from planktonic foraminifera (Ellison *et al.* 2006; Farmer *et al.* 2008). The most probable explanation for this is that the two groups of organisms are registering different climate signals. It is possible to derive both winter and summer SST signals from foraminiferal analysis, whereas the diatoms are considered to reflect a summer SST signal. However it must also be noted that the diatom derived SSTs for MD99-2251 fail to record truly low temperatures for the Younger Dryas, the coldest interval in the study, and so the difference in foraminfera and diatom derived estimates may be a result of difficulties with the diatom SSTs in registering very low temperatures.

Another analysis undertaken on the diatom floras was to relate assemblage groupings of floras to surface currents using factor analysis. This type of study has been undertaken by a number of authors (Koç & Schrader, 1990; Jiang *et al.*, 2001; Andersen *et al*. 2004a). Palaeoceanographic reconstructions may be made on the basis of the relative abundance of these assemblage flora. MD99-2251 may be seen to have a truly Arctic flora at the transition from the Younger Dryas to the Holocene. Sub Arctic and North Atlantic floras then remain the two dominant assemblages, with North Atlantic floras dominant during periods when SSTs are higher, such as the 7 to 5kyr interval .

The early Holocene (11.5 to 9.5kyr) in core MD99-2251 is best understood when considering the third analysis of diatom abundance data, the relative abundance of individual species. This interval is punctuated by a number of near monospecific peaks of pennate diatoms, chiefly *Rhizosolenia styliformis/borealis.* Peaks in *Rhizosolenia* spp. have been associated with open ocean fronts (Yoder *et al.,* 1994; Kemp *et al.* 2006). In this instance the peaks are interpreted as indicating the proximity of the Sub Arctic Front (SAF). The highly variable early Holocene is interpreted as responding to strong shifts in surface circulation with the continued break up of the Laurentide ice sheet and migrations of the SAF. Similarly considering the distribution of individual diatom flora best reflects the response of MD99-2251 to the 8.2kyr event. Colder species associated with the East Greenland current such as *T.gravida* vegetative are in higher abundance (Figure 9.15).

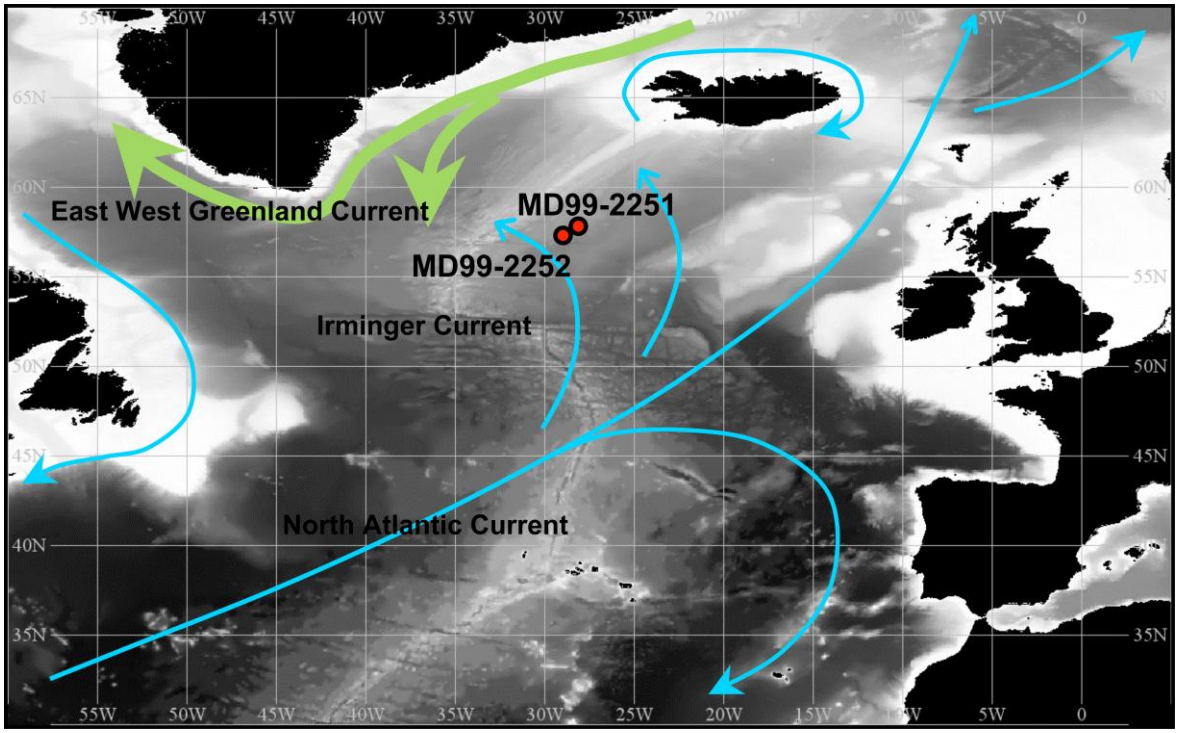

Figure 9.15 indicating the possible relative strength of surface currents influencing the core sites MD99-2251 and MD99-2252 for the early Holocene (11-5-9.5kyr) The East Greenland current is shown as stronger with thick green arrows. Diatom species abundance counts show an increase in taxa associated with the East Greenland current during this interval. Core sites MD99-2251 and MD99-2252 may also have been have been periodically adjacent to the Sub Arctic front causing stratification in the water column and parted increases in individual taxa, notably R.styliformis/borealis during the early Holocene.

The SSTs indicate a broad cooling from 9.5 to 7kyr and the floral assemblage analyses show an increase in Sub Arctic flora for the same interval. The IRD record shows no distinct peak related to the event in correspondence to the IRD peak at 8.1kyr identified in North Atlantic sediments by Bond *et al.* (1997). However analysis of the relative abundance of sea-ice and cold water forms indicates a distinct peak in abundance from 8.8 to 7.8kyr. It is hypothesised that the increase in sea-ice forms may be related to an increase in sea ice formation as a result of surface freshening from the catastrophic discharges of meltwater from proglacial lakes Agassiz and Ojibway. It is concluded therefore that the diatom palaeoproxies employed in this study best reflect variations in surface hydrography for the Holocene, particularly the strength of the Irminger Current over the core sites, the migration of the Sub Artic Front and sensitivity of diatom floras to the presence of sea ice.

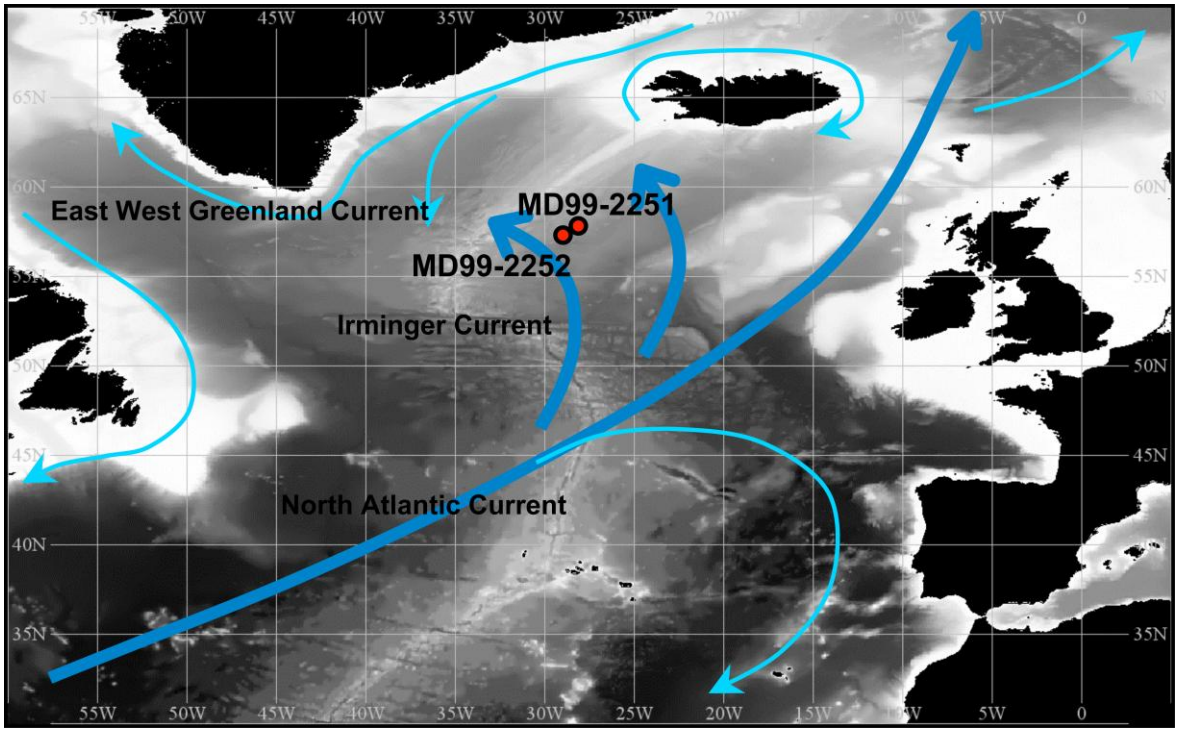

Figure 6.16 indicating the possible relative strength of surface currents influencing the core sites MD99-2251 and MD99-2252 for the mid Holocene (5-7kyr) The North Atlantic and Irminger currents are shown as stronger with thick blue arrows. Diatom species abundance counts show an increase in taxa associated with these current during this interval especially *T.oestrupii* which exhibits its highest abundances around 6kyr when sea surface temperature estimates are highest.

The mid and late Holocene for core MD99-2251 may be understood in terms of the relative abundance of the North Atlantic floras indicating the relative strength of the Irminger Current, a branch of the warm North Atlantic Current, over the core site. When the Irminger Current is strong the North Atlantic floras are dominant and SST estimates highest as in the 7-5kyr interval (Figure 6.16). When the Irminger Current is weaker Sub Arctic floras are dominant and the SSTs are lower Figure (6.17). This variation in the strength of the Irminger Current may also be correlated with variations in North Atlantic deep water (NADW) indicating a strong coupling between surface and deep water circulation.

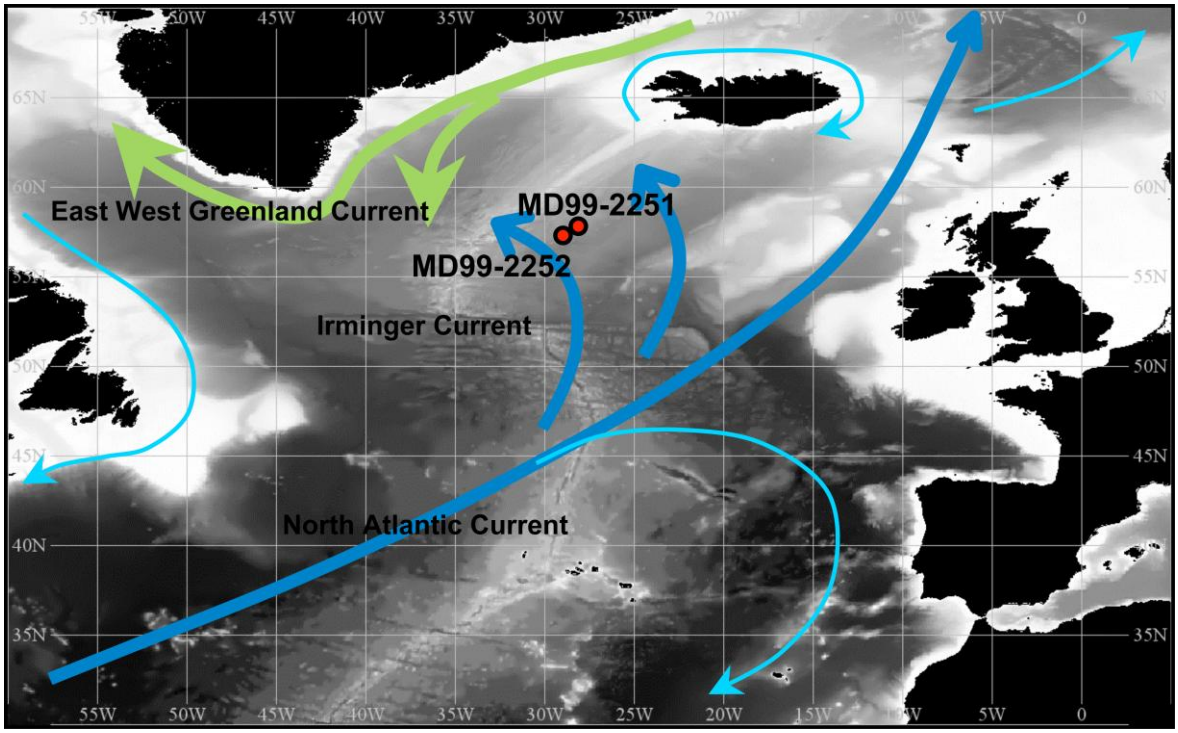

Figure 6.17 indicating the possible relative strength of surface currents influencing the core sites MD99-2251 and MD99-2252 for the late Holocene (5kyr to present) The North Atlantic, Irminger current, and East Greenland currents are shown as equally influential with thick blue and green arrows. Diatom species abundance counts show a mix of both Sub Arctic taxa in this interval

Chapter Ten

Conclusions

"We must always remember with gratitude and admiration the first sailors who steered their vessels through storms and mists, and increased our knowledge of the lands of ice...

Roald Amundsen

10.1 Chapter Ten Conclusions

Diatom assemblage data have been shown to be a powerful means of reconstructing past sea surface temperatures. In regions where they are the dominant organisms and where the foraminifera fauna become almost monospecific, with populations constituting over 95% *Neogloboquadrina pachyderma* sinistral, analysis of diatom floras can be particularly useful in constraining subtle temperature changes not recorded by the foraminifera.

However the sensitivity and accuracy of the temperature reconstructions appears to be highly dependant upon the constraints on the regional data set. The results discussed in Chapter eight of this study indicate a 2-3^{o}C difference between SST estimates derived from a Nordic Sea dataset and a regionally focused northern North Atlantic dataset. Diatom derived sea surface temperatures also appear to give a regional rather than global signal, related to regional surface hydrography.

The tendency of certain diatom flora to bloom in response to conditions of ocean stratification can cause difficulties for the reconstruction of sea surface temperatures from diatom assemblage data. A single species may constitute over 50% of the total flora. In these circumstances the diatom flora is unlikely to be responding primarily to temperature but to ocean nutrient conditions. However these monospecific floral blooms may be a useful palaeoceanographic indicator of the proximity of an open ocean front.

Perhaps a more useful form of analysis of diatom floras, other than SST reconstructions, is the identification of groups of flora strongly associated with different water masses or currents. It is then possible to reconstruct patterns of surface circulation by applying these floral grouping down core. A number of such analyses have been presented in this study. A series of issues arise with this form of analysis however; as a result of these groupings being delineated by factor analysis of different data sets the choice of species selected as representative of a particular water mass or current can be inconsistent between studies. The

identification of water masses and currents also may be inconsistent and localised, for example the East Icelandic Current assemblage of Jiang *et al.* (2001). One drawback of this is that it becomes difficult to compare assemblage based studies without close examination of the original raw data. Another problem with these analyses is that in many cases an individual species may be identified as being associated with more than one water mass or current. In such cases a review of all the assemblages can give specious results as the percentage abundances of different assemblages represented involve the recounting of certain species.

The distribution of individual diatom species may also be analysed. However the ecological constraints on individual species are sometimes poorly understood consisting usually of reports of extant forms in plankton tows and a corresponding general geographic distribution. A better understanding of the tolerance of individual species to specific temperatures and salinities would allow for more detailed palaeoreconstructions.

10.2 Future research

The development of a more regionally constrained diatom core top data set for the Sub Polar North Atlantic would allow for more accurate SST reconstructions from diatom assemblages from the region.

An understanding of how particular floral assemblages related to water masses would enable better palaeoclimate reconstructions, specifically the importance of water column structure and nutrient availability which may be of more importance than temperature under certain circumstances

A better understanding of the ecological constraints of individual diatom species and the extant floral assemblages associated with particular water masses would also greatly assist on accurate paleoreconstructions using diatoms.

Bibliography

Abrantes, F., 1988. Diatom Assemblages as Upwelling Indicators in Surface Sediments Off Portugal. Marine Geology, 85(1): 15-39.

Abrantes, F., 2000. 200 000 yr diatom records from Atlantic upwelling sites reveal maximum productivity during LGM and a shift in phytoplankton community structure at 185 000 yr. Earth and Planetary Science Letters, 176(1): 7-16.

Abrantes, F., Gil, I., Lopes, C. and Castro, M., 2005. Quantitative diatom analyses - A faster cleaning procedure. Deep-Sea Research Part I-Oceanographic Research Papers, 52(1): 189-198.

Abrantes, F., Lopes, C., Mix, A. and Pisias, N., 2007. Diatoms in Southeast Pacific surface sediments reflect environmental properties. Quaternary Science Reviews, 26(1-2): 155-169.

Alley, R.B., 2007. Wally was right: Predictive ability of the North Atlantic "Conveyor belt" hypothesis for abrupt climate change. Annual Review of Earth and Planetary Sciences, 35: 241-272.

Alley, R.B. and Agustsdottir, A.M., 2005. The 8k event: cause and consequences of a major Holocene abrupt climate change. Quaternary Science Reviews, 24(10-11): 1123-1149.

Alley, R.B. and Macayeal, D.R., 1994. Ice-Rafted Debris Associated with Binge Purge Oscillations of the Laurentide Ice-Sheet. Paleoceanography, 9(4): 503-511.

Alley, R.B. et al., 1997. Holocene climatic instability: A prominent, widespread event 8200 yr ago. Geology, 25(6): 483-486.

Alley, R.B. et al., 1993. Abrupt Increase in Greenland Snow Accumulation at the End of the Younger Dryas Event. Nature, 362(6420): 527-529.

Alverson, A.J., Manoylov, K.M. and Stevenson, R.J., 2003. Laboratory sources of error for algal community attributes during sample preparation and counting. Journal of Applied Phycology, 15(5): 357-369.

Andersen, C., Koc, N. and Moros, M., 2004. A highly unstable Holocene climate in the subpolar North Atlantic: evidence from diatoms. Quaternary Science Reviews, 23(20-22): 2155-2166.

Andersen, K.K. et al., 2004. High-resolution record of Northern Hemisphere climate extending into the last interglacial period. Nature, 431(7005): 147-151.

Andrews, J.T. et al., 2009. A robust, multisite Holocene history of drift ice off northern Iceland: implications for North Atlantic climate. Holocene, 19(1): 71-77.

Andrews, J.T. and Tedesco, K., 1992. Detrital Carbonate Rich Sediments, Northwestern Labrador Sea - Implications for Ice-Sheet Dynamics and Iceberg Rafting (Heinrich) Events in the North-Atlantic. Geology, 20(12): 1087-1090.

Arbic, B.K., Macayeal, D.R., Mitrovica, J.X. and Milne, G.A., 2004. Palaeoclimate - Ocean tides and Heinrich events. Nature, 432(7016): 460-460.

Archer, D. et al., 1997. A meeting place of great ocean currents: shipboard observations of a convergent front at 2 degrees N in the Pacific. Deep-Sea Research Part Ii-Topical Studies in Oceanography, 44(9-10): 1827-1849.

Armand, L.K. and Zielinski, U., 2001. Diatom species of the genus Rhizosolenia from Southern Ocean sediments: Distribution and taxonomic notes. Diatom Research, 16(2): 259-294.

Austin, W.E.N., Bard, E., Hunt, J.B., Kroon, D. and Peacock, J.D., 1995. The C-14 Age of the Icelandic Vedde Ash - Implications for Younger-Dryas Marine Reservoir Age Corrections. Radiocarbon, 37(1): 53-62.

Austin, W.E.N. and Kroon, D., 2001. Deep sea ventilation of the northeastern Atlantic during the last 15,000 years. Global and Planetary Change, 30(1-2): 13-31.

Bailey, J.W., 1856. Notice of microscopic forms found in the soundings of the Sea of Kamtschatka. The American Journal of Science and Arts Second Series(22): 1-6.

Barber, D.C. et al., 1999. Forcing of the cold event of 8,200 years ago by catastrophic drainage of Laurentide lakes. Nature, 400(6742): 344-348.

Barber, H.G. and Haworth, E.Y., 1981. A guide to the morphology of the diatom frustule. Freshwater Biological Association Scientific Publication(44): 1-112.

Bard, E. et al., 1994. The North-Atlantic Atmosphere-Sea Surface C-14 Gradient During the Younger Dryas Climatic Event. Earth and Planetary Science Letters, 126(4): 275-287.

Bard, E. et al., 1988. Penetration of Bomb Radiocarbon in the Tropical Indian-Ocean Measured by Means of Accelerator Mass-Spectrometry. Earth and Planetary Science Letters, 87(4): 379-389.

Bar-Matthews, M., Ayalon, A., Kaufman, A. and Wasserburg, G.J., 1999. The Eastern Mediterranean paleoclimate as a reflection of regional events: Soreq cave, Israel. Earth

and Planetary Science Letters, 166(1-2): 85-95.

Barron, J.A., 1985. Late Eocene to Holocene Diatom Biostratigraphy of the Equatorial Pacific-Ocean, Deep-Sea Drilling Project Leg-85. Initial Reports of the Deep Sea Drilling Project, 85(OCT): 413-456.

Battarbe, R.W., 1973. New Method for Estimation of Absolute Microfossil Numbers, with Reference Especially to Diatoms. Limnology and Oceanography, 18(4): 647-653.

Battarbee, R.W. et al., 2001. Evidence for Holocene climate variability from the sediments of a Scottish remote mountain lake. Journal of Quaternary Science, 16(4): 339-346.

Battarbee, R.W., Mackay, A.W., Jewson, D.H., Ryves, D.B. and Sturm, M., 2005. Differential dissolution of Lake Baikal diatoms: correction factors and implications for palaeoclimatic reconstruction. Global and Planetary Change, 46(1-4): 75-86.

Battarbee, R.W. et al., 2008. Assessing the accuracy of diatom-based transfer functions in defining reference pH conditions for acidified lakes in the United Kingdom. Holocene, 18(1): 57-67.

Bendle, J.A.P. and Rosell-Mele, A., 2007. High-resolution alkenone sea surface temperature variability on the North Icelandic Shelf: implications for Nordic Seas palaeoclimatic development during the Holocene. Holocene, 17(1): 9-24.

Bennion, H., Johnes, P., Ferrier, R., Phillips, G. and Haworth, E., 2005. A comparison of diatom phosphorus transfer functions and export coefficient models as tools for reconstructing lake nutrient histories. Freshwater Biology, 50(10): 1651-1670.

Berger, A. and Loutre, M.F., 1991. Insolation Values for the Climate of the Last 10000000 Years. Quaternary Science Reviews, 10(4): 297-317.

Berner, K.S., Koc, N., Divine, D., Godtliebsen, F. and Moros, M., 2008. A decadal-scale Holocene sea surface temperature record from the subpolar North Atlantic constructed using diatoms and statistics and its relation to other climate parameters. Paleoceanography, 23(2).

Bersch, M., 1995. On the Circulation of the Northeastern North-Atlantic. Deep-Sea Research Part I-Oceanographic Research Papers, 42(9): 1583-1607.

Bersch, M., Meincke, J. and Sy, A., 1999. Interannual thermohaline changes in the northern North Atlantic 1991-1996. Deep-Sea Research Part Ii-Topical Studies in Oceanography,

46(1-2): 55-75.

Bianchi, G.G., Hall, I.R., McCave, I.N. and Joseph, L., 1999. Measurement of the sortable silt current speed proxy using the Sedigraph 5100 and Coulter Multisizer IIe: precision and accuracy. Sedimentology, 46(6): 1001-1014.

Bianchi, G.G. and McCave, I.N., 2000. Hydrography and sedimentation under the deep western boundary current on Bjorn and Gardar Drifts, Iceland Basin. Marine Geology, 165(1-4): 137-169.

Birks, C.J.A. and Koc, N., 2002. A high-resolution diatom record of late-Quaternary sea-surface temperatures and oceanographic conditions from the eastern Norwegian Sea. Boreas, 31(4): 323-344.

Blanco, S., Alvarez, I. and Cejudo, C., 2008. A test on different aspects of diatom processing techniques. Journal of Applied Phycology, 20(4): 445-450.

Blunier, T., Chappellaz, J., Schwander, J., Stauffer, B. and Raynaud, D., 1995. Variations in Atmospheric Methane Concentration During the Holocene Epoch. Nature, 374(6517): 46-49.

Boalch, G.T., 1971. Typification of Diatom Species Coscinodiscus-Concinnun Smith,W and Coscinodiscus-Granii Gough. Journal of the Marine Biological Association of the United Kingdom, 51(3): 685-&.

Boalch, G.T., 1975. The Lauder species of the diatom genus *Bacteriastrum*. Beiheft zur Nova Hedwigia(53): 185-189.

Boden, P. and Backman, J., 1996. A laminated sediment sequence from the northern North Atlantic Ocean and its climatic record. Geology, 24(6): 507-510.

Bond, G. et al., 1993. Correlations between Climate Records from North-Atlantic Sediments and Greenland Ice. Nature, 365(6442): 143-147.

Bond, G. et al., 1992. Evidence for Massive Discharges of Icebergs into the North-Atlantic Ocean During the Last Glacial Period. Nature, 360(6401): 245-249.

Bond, G. et al., 2001. Persistent solar influence on north Atlantic climate during the Holocene. Science, 294(5549): 2130-2136.

Bond, G. et al., 1997. A pervasive millennial-scale cycle in North Atlantic Holocene and glacial climates. Science, 278(5341): 1257-1266.

Bond, G.C. and Lotti, R., 1995. Iceberg Discharges into the North-Atlantic on Millennial Time Scales During the Last Glaciation. Science, 267(5200): 1005-1010.

Brambilla, E. and Talley, L.D., 2008. Subpolar Mode Water in the northeastern Atlantic: 1. Averaged properties and mean circulation. Journal of Geophysical Research-Oceans, 113(C4).

Brambilla, E., Talley, L.D. and Robbins, P.E., 2008. Subpolar Mode Water in the northeastern Atlantic: 2. Origin and transformation. Journal of Geophysical Research-Oceans, 113(C4).

Broecker, W.S., 1987. The Biggest Chill. Natural History, 96(10): 74-&.

Brown, E. et al., 2001. Ocean Circulation. The Oceanography Series, 3. Butterworth-Heinemann, Oxford, 286 pp.

Brown, L., Sanders, R., Savidge, G. and Lucas, C.H., 2003. The uptake of silica during the spring bloom in the Northeast Atlantic Ocean. Limnology and Oceanography, 48(5): 1831-1845.

Came, R.E., Oppo, D.W. and McManus, J.F., 2007. Amplitude and timing of temperature and salinity variability in the subpolar North Atlantic over the past 10 k.y. Geology, 35(4): 315-318.

Campbell, I.D., Campbell, C., Apps, M.J., Rutter, N.W. and Bush, A.B.G., 1998. Late Holocene similar to 1500yr climatic periodicities and their implications. Geology, 26(5): 471-473.

Campeau, S., Pienitz, R. and Hequette, A., 1999. Diatoms as quantitative paleodepth indicators in coastal areas of the southeastern Beaufort Sea, Arctic Ocean. Palaeogeography Palaeoclimatology Palaeoecology, 146(1-4): 67-97.

Chapman, M.R. and Shackleton, N.J., 1998. Millennial-scale fluctuations in North Atlantic heat flux during the last 150,000 years. Earth and Planetary Science Letters, 159(1-2): 57-70.

Chapman, M.R. and Shackleton, N.J., 2000. Evidence of 550-year and 1000-year cyclicities in North Atlantic circulation patterns during the Holocene. Holocene, 10(3): 287-291.

Chapman, M.R., Shackleton, N.J., Zhao, M. and Eglinton, G., 1996. Faunal and alkenone reconstructions of subtropical North Atlantic surface hydrography and paleotemperature over the last 28 kyr. Paleoceanography, 11(3): 343-357.

Chappell, J., 2002. Sea level changes forced ice breakouts in the Last Glacial cycle: new results

from coral terraces. Quaternary Science Reviews, 21(10): 1229-1240.

Chappellaz, J. et al., 1993. Synchronous Changes in Atmospheric Ch4 and Greenland Climate between 40-Kyr and 8-Kyr Bp. Nature, 366(6454): 443-445.

Cleve, P.T., 1896. Diatoms from Baffins Bay and Davis Strait. Bihang till Kongliga Svenska Vetenskaps-Akademiens Handlingar(22 (3,4)): 1-22.

Cleve, P.T. and Moller, J.D., 1878. Diatoms. Part 3, Nos. 109-168: 1-9.

Cook, E.R., D'Arrigo, R.D. and Mann, M.E., 2002. A well-verified, multiproxy reconstruction of the winter North Atlantic Oscillation index since AD 1400. Journal of Climate, 15(13): 1754-1764.

Cortijo, E. et al., 1997. Changes in sea surface hydrology associated with Heinrich event 4 in the North Atlantic Ocean between 40 degrees and 60 degrees N. Earth and Planetary Science Letters, 146(1-2): 29-45.

Cox, E.J., 1981. Observations on the Morphology and Vegetative Cell-Division of the Diatom Donkinia-Recta. Helgolander Meeresuntersuchungen, 34(4): 497-506.

Cox, E.J. and Ross, R., 1980. The striae of pennate diatoms, Proceedings of the 6th International Diatom Symposium. Koeltz, Budapest, pp. 267-278.

Crawford, N. and Taylor, D.G., 1974. Subfraction of Platelet Membranes by Zonal Centrifugation - Identification of Surface Membranes. Febs Letters, 41(2): 317-322.

Dansgaard, W. et al., 1993. Evidence for General Instability of Past Climate from a 250-Kyr Ice-Core Record. Nature, 364(6434): 218-220.

Davis, C.O., Hollibaugh, J.T., Seibert, D.L.R., Thomas, W.H. and Harrison, P.J., 1980. Formation of Resting Spores by Leptocylindrus-Danicus (Bacillariophyceae) in a Controlled Experimental Ecosystem. Journal of Phycology, 16(2): 296-302.

De Seve, M.A., 1999. Transfer function between surface sediment diatom assemblages and sea-surface temperature and salinity of the Labrador Sea. Marine Micropaleontology, 36(4): 249-267.

deMenocal, P., Ortiz, J., Guilderson, T. and Sarnthein, M., 2000. Coherent high- and low-latitude climate variability during the holocene warm period. Science, 288(5474): 2198-2202.

Dickson, R.R. and Brown, J., 1994. The Production of North-Atlantic Deep-Water - Sources, Rates, and Pathways. Journal of Geophysical Research-Oceans, 99(C6): 12319-12341.

Dickson, R.R., Gmitrowicz, E.M. and Watson, A.J., 1990. Deep-Water Renewal in the Northern North-Atlantic. Nature, 344(6269): 848-850.

Dore, J.E., Letelier, R.M., Church, M.J., Lukas, R. and Karl, D.M., 2008. Summer phytoplankton blooms in the oligotrophic North Pacific Subtropical Gyre: Historical perspective and recent observations. Progress in Oceanography, 76(1): 2-38.

Drebes, G., 1972. The Life history of the centric diatom *Bacteriastrum hyalinum* Lauder. Beiheft zur Nova Hedwigia(39): 95-110.

Drebes, G. and Schnepf, E., 1977. Development of Marine, Parasitic Phycomycete Lagenisma-Coscinodisci (Lagenidiales). Helgolander Wissenschaftliche Meeresuntersuchungen, 29(3): 291-301.

Ducklow, H.W. and Harris, R.P., 1993. Introduction to the Jgofs North-Atlantic Bloom Experiment. Deep-Sea Research Part Ii-Topical Studies in Oceanography, 40(1-2): 1-8.

Dugdale, R.C., Wilkerson, F.P. and Minas, H.J., 1995. The Role of a Silicate Pump in Driving New Production. Deep-Sea Research Part I-Oceanographic Research Papers, 42(5): 697-719.

Duplessy, J.C. et al., 1992. Changes in Surface Salinity of the North-Atlantic Ocean During the Last Deglaciation. Nature, 358(6386): 485-488.

Ehrenberg, C.G., 1841. Uber noch jetzt zahlreich lebende Thierarten der Kreidebildung und den Organismus der Polythalamien. Abhandlungen der Koniglichen Akademie der Wissenschaften zu Berlin: 81-174.

Elderfield, H., Yu, J., Anand, P., Kiefer, T. and Nyland, B., 2006. Calibrations for benthic foraminiferal Mg/Ca paleothermometry and the carbonate ion hypothesis. Earth and Planetary Science Letters, 250(3-4): 633-649.

Elliot, M. et al., 1998. Millennial-scale iceberg discharges in the Irminger Basin during the last glacial period: Relationship with the Heinrich events and environmental settings. Paleoceanography, 13(5): 433-446.

Ellison, C.R.W., 2006. North Atlantic Holocene Palaeoceanography; Surfacea and Deep Ocean Variability in the Subpolar North Atlantic, University of East Anglia, Norwich, 341 pp.

Ellison, C.R.W., Chapman, M.R. and Hall, I.R., 2006. Surface and deep ocean interactions during the cold climate event 8200 years ago. Science, 312(5782): 1929-1932.

Farmer, E.J., Chapman, M.R. and Andrews, J.E., 2008. Centennial-scale Holocene North Atlantic surface temperatures from Mg/Ca ratios in Globigerina bulloides. Geochemistry Geophysics Geosystems, 9.

Farmer, E.J., Chapman, M.R. and Andrews, J.E., 2010. North Atlantic *Globorotalia inflata* coretop Mg/Ca Calibrations and temperature reconstructions over Termination I, 2010 IOP Conference Series: Earth Environmental Science 9 012019. IOP Publishing.

Farnham, I.M., Johannesson, K.H., Singh, A.K., Hodge, V.F. and Stetzenbach, K.J., 2003. Factor analytical approaches for evaluating groundwater trace element chemistry data. Analytica Chimica Acta, 490(1-2): 123-138.

Field, A.P., 2005. Discovering statistics using SPSS : (and sex, drugs and rock 'n' roll. ISM. Sage, London.

Flower, R.J., 1993. Diatom Preservation - Experiments and Observations on Dissolution and Breakage in Modern and Fossil Material. Hydrobiologia, 269: 473-484.

Fryxell, G.A., 2000. Nitzschia bicapitata (Bacillariophyceae) and related taxa from oceanic aggregations. Diatom Research, 15(1): 43-73.

Fryxell, G.A. and Hasle, G.R., 1972. Thalassiosira-Eccentrica (Ehrenb) Cleve, Thalassiosira-Symmetrica Sp-Nov, and Some Related Centric Diatoms. Journal of Phycology, 8(4): 297-317.

Fryxell, G.A. and Hasle, G.R., 1974. Coscinodiscaceae: Some consistent patterns in diatom morphology. Beiheft zur Nova Hedwigia(45): 69-84.

Fryxell, G.A. and Hasle, G.R., 1977. The genus *Thalassiosira*: Some species with a modified ring of central strutted processes. Beiheft zur Nova Hedwigia(54): 67-89.

Fryxell, G.A. and Hasle, G.R., 1979. Genus Thalassiosira - Species with Internal Extensions of the Strutted Processes. Phycologia, 18(4): 378-393.

Fryxell, G.A. and Hasle, G.R., 1980. The Marine Diatom Thalassiosira-Oestrupii - Structure, Taxonomy and Distribution. American Journal of Botany, 67(5): 804-814.

Fryxell, G.A. and Johansen, J.R., 1990. Family Thalassiosiraceae. Section 2: The genus *Thalassiosira* from the Antarctic. In "Polar Marine Diatoms" (L. K. Medlin & J. Priddle, eds.): 98-103.

Fryxell, G.A., Sims, P.A. and Watkins, T.P., 1986. *Azpeitia* (Bacillariophyceae): Related genera

and promorpholgy. Systematic Botany Monographs, 13: 1-74.

Ganssen, G.M. and Kroon, D., 2000. The isotopic signature of planktonic foraminifera from NE Atlantic surface sediments: implications for the reconstruction of past oceanic conditions. Journal of the Geological Society, 157: 693-699.

Gascard, J.C. and Clarke, R.A., 1983. The Formation of Labrador Sea-Water .2. Mesoscale and Smaller-Scale Processes. Journal of Physical Oceanography, 13(10): 1779-1797.

Geological Survey of Canada: 2008 Canadian Diatom Database. National Resources Canada. National Resources Canada.

Giraudeau, J., Jennings, A.E. and Andrews, J.T., 2004. Timing and mechanisms of surface and intermediate water circulation changes in the Nordic Seas over the last 10,000 cal years: a view from the North Iceland shelf. Quaternary Science Reviews, 23(20-22): 2127-2139.

Gleser, L.J., 1985. The Limitations of Models and Measurements as Revealed through Chemometric Intercomparison - Discussion. Journal of Research of the National Bureau of Standards, 90(6): 419-422.

Gombos, A.M., Jr., 1980. The early history of the diatom family Asterolampraceae. Bacillaria(3): 227-272.

Gran, H.H., 1900. Bemerkungen uber einige Planktondiatomeen, Nyt Magazin for Naturvidenskaberne, pp. 103-128.

Greville, R.K., 1860. A monograph of the genus *Asterolampra*, including *Asteromphalus* and *Spatangidium*. Transactions of the Microscopical Society of London New Series, 8: 102-125.

Grigorov, I., Pearce, R.B. and Kemp, A.E.S., 2002. Southern Ocean laminated diatom ooze: mat deposits and potential for palaeo-flux studies, ODP leg 177, Site 1093. Deep-Sea Research Part Ii-Topical Studies in Oceanography, 49(16): 3391-3407.

Grootes, P.M. and Stuiver, M., 1997. Oxygen 18/16 variability in Greenland snow and ice with 10(-3)- to 10(5)-year time resolution. Journal of Geophysical Research-Oceans, 102(C12): 26455-26470.

Grousset, F.E. et al., 1993. Patterns of Ice-Rafted Detritus in the Glacial North-Atlantic (40-Degrees-55-Degrees-N). Paleoceanography, 8(2): 175-192.

Grunow, A., 1884. Die Diatomeen von Franz Josefs-Land. Denkschriften der kaiserlichen

Akademie der Wissenschaften. Mathematisch-naturwissenschaftliche Classe, 28: 53-112.

Gwiazda, R.H., Hemming, S.R. and Broecker, W.S., 1996. Tracking the sources of icebergs with lead isotopes: The provenance of ice-rafted debris in Heinrich layer 2. Paleoceanography, 11(1): 77-93.

Hall, I.R., Bianchi, G.G. and Evans, J.R., 2004. Centennial to millennial scale Holocene climate-deep water linkage in the North Atlantic. Quaternary Science Reviews, 23(14-15): 1529-1536.

Hallegraeff, G.M., 1986. Taxomony and morphology of the marine plankton diatoms *Thalassionema* and *thalassiothrix*. Diatom Research, 1: 57-80.

Hansen, B. and Osterhus, S., 2000. North Atlantic-Nordic Seas exchanges. Progress in Oceanography, 45(2): 109-208.

Hansen, B., Osterhus, S., Hatun, H., Kristiansen, R. and Larsen, K.M.H., 2003. The Iceland-Faroe inflow of Atlantic water to the Nordic Seas. Progress in Oceanography, 59(4): 443-474.

Harvey, J., 1982. Theta-S Relationships and Water Masses in the Eastern North-Atlantic. Deep-Sea Research Part a-Oceanographic Research Papers, 29(8): 1021-1033.

Hasle, G.R., 1968. The valve processes of the centric diatom genus *Thalassiosira*. Nytt Magasin for Botanikk, 15: 193-201.

Hasle, G.R., 1972. *Fragilariopsis* as a section of the genus *Nitzschia* Hassall. Beiheft zur Nova Hedwigia, 39: 111-119.

Hasle, G.R., 1974. Validation of the names of some marine planktonic species of *Nitzschia* (Bacillariophyceae). Taxon, 23: 425-428.

Hasle, G.R., 1975. Some living marine species of the diatom family Rhizosoleniaceae. Beiheft zur Nova Hedwigia, 53: 99-140.

Hasle, G.R., 1976. Biogeography of Some Marine Planktonic Diatoms. Deep-Sea Research, 23(4): 319-338.

Hasle, G.R., 1978. Some Thalassiosira Species with One Central Process (Bacillariophyceae). Norwegian Journal of Botany, 25(2): 77-110.

Hasle, G.R., 1979. *Thalassiosira decipiens* (Grun.) Jorg. (Bacillariophyceae). Bacillaria, 2: 85-108.

Hasle, G.R. and Fryxell, G.A., 1977. The genus *Thalassiosira*: Some species with a linear arcola array. Beiheft zur Nova Hedwigia, 54: 15-66.

Hasle, G.R. and Heimdel, B.R., 1968. Morphology and distribution of the marine centric diatom *Thalassiosira antarctica* Comber. Journal of the Royal Microscopical Society, 88: 357-369.

Hasle, G.R. and Lange, C.B., 1992. Morphology and distribution of *Coacinodiscus* species from the Oslofjord, Norway and the Skagerrak, North Atlantic. Diatom Research, 7: 37-68.

Hasle, G.R., Medlin, L.K. and Syvertsen, E.E., 1994. Synedropsis Gen-Nov, a Genus of Araphid Diatoms Associated with Sea-Ice. Phycologia, 33(4): 248-270.

Hasle, G.R. and Semina, H.J., 1987. The marine planktonic diatoms *Thalassiothrix longissima* and *Thalassiothrix antarctica* with comments on *Thalassionema* spp. and *Synedra reinboldii*. Diatom Research, 2: 175-192.

Hasle, G.R. and Sims, P.A., 1986. The Diatom Genus Coscinodiscus Ehrenb - C Argus Ehrenb and C Radiatus Ehrenb. Botanica Marina, 29(4): 305-318.

Hasle, G.R. and Syvertsen, E.E., 1997. in Identifying Marine Phytoplankton by Tomas, C. R. Academic Press, San Diego, 385 pp.

Hasle, G.R., von Stosch, H.A. and Syvertsen, E.E., 1983. Cymatosiraceae, a new diatom family. Bacillaria, 6: 9-156.

Haug, G.H., Hughen, K.A., Sigman, D.M., Peterson, L.C. and Rohl, U., 2001. Southward migration of the intertropical convergence zone through the Holocene. Science, 293(5533): 1304-1308.

Heiden, H. and Kolbe, R.W., 1928. Die marinen Diatomeen der Deutschen Sudpolar-Expedition 1901-1903. Deutsche Sudpolar-Expedition 1901-1903, 8: 447-715.

Heinrich, H., 1988. Origin and Consequences of Cyclic Ice Rafting in the Northeast Atlantic-Ocean During the Past 130,000 Years. Quaternary Research, 29(2): 142-152.

Hemming, S.R. et al., 1998. Provenance of Heinrich layers in core V28-82, northeastern Atlantic: Ar-40/Ar-39 ages of ice-rafted hornblende, Pb isotopes in feldspar grains, and Nd-Sr-Pb isotopes in the fine sediment fraction. Earth and Planetary Science Letters, 164(1-2): 317-333.

Hendey, N.I., 1964. An introductory account of the smaller algae of British coastal waters. Part

5: Bacillariophyceae (Diatoms). In "Ministry of Agriculture, Fisheries and Food, Fishery Investigations Series IV. 317.

Hernandez-Becerril, D.U., 1991. The morphology and taxomony of species of the diatom genus *Asteromphalus* Ehr. . Bibliotheca Diatomologica, 23: 1-55, 33 plates.

Herth, W. and Barthlott, W., 1979. The site of □-chitin fibril formation in centric diatoms I. Pores and fibril formation. Journal of Ultrastructure Research, 68: 6-15.

Herzig, W.N. and Fryxell, G.A., 1986. The diatom genus *Thalassiosira* Cleve in the Gulf Stream core rings: Taxonomy, with *T.intrannula* and *T. lineoides,* spp. nov. Botanica Marina, 29: 11-25.

Hillaire-Marecel, C. and Turon, J.-L., 1999. IMAGES 5 on board the *Marion Dufresne*. Geological Survey of Canada open file 3782. Natural Resources Canada, 246 pp.

Holden, P.B., Mackay, A.W. and Simpson, G.L., 2008. A Bayesian palaeoenvironmental transfer function model for acidified lakes. Journal of Paleolimnology, 39(4): 551-566.

Hormes, A., Muller, B.U. and Schluchter, C., 2001. The Alps with little ice: evidence for eight Holocene phases of reduced glacier extent in the Central Swiss Alps. Holocene, 11(3): 255-265.

Hughen, K.A. et al., 1998. Deglacial changes in ocean circulation from an extended radiocarbon calibration. Nature, 391(6662): 65-68.

Hughen, K.A., Overpeck, J.T., Peterson, L.C. and Trumbore, S., 1996. Rapid climate changes in the tropical Atlantic region during the last deglaciation. Nature, 380(6569): 51-54.

Hunt, A.G. and Malin, P.E., 1998. Possible triggering of Heinrich events by ice-load-induced earthquakes. Nature, 393(6681): 155-158.

Hunter, S. et al., 2007. Deep western boundary current dynamics and associated sedimentation on the Eirik Drift, southern Greenland margin. Deep-Sea Research Part I-Oceanographic Research Papers, 54(12): 2036-2066.

Hurrell, J.W., 1995. Decadal Trends in the North-Atlantic Oscillation - Regional Temperatures and Precipitation. Science, 269(5224): 676-679.

Hurrell, J.W. et al., 2003. Studying climate effects on ecology through the use of climate indices: the North Atlantic Oscillation, El Nino Southern Oscillation and beyond. Proceedings of the Royal Society of London Series B-Biological Sciences, 270(1529): 2087-2096.

Hustedt, F., 1930. Bacillariophyta (Diatomaceae). In A. Pascher *Die Susswasser-flora Mitteleuropas*. Beiheft zur Nova Hedwigia, 10: 466.

Hustedt, F., 1958. Diatomeen aus der Antarktis und dem Sudatlantik. Deutsche Antarktische Expedition 1938/1939, 2: 103-191.

Hutson, W.H., 1980. Agulhas Current During the Late Pleistocene - Analysis of Modern Faunal Analogs. Science, 207(4426): 64-66.

Imbrie, J. and Kipp, N.G., 1971. A New Micro Paleontological Method for Quantitative Paleo Climatology Application to a Late Pleistocene Caribbean Core. Turekian, Karl K. (Edited by). the Late Cenozoic Glacial Ages. Xii + 606p. Illus. Maps. Yale University Press: New Haven, Conn., U.S.a.; London England: 71-181.

Jantschik, R. and Huon, S., 1992. Detrital Silicates in Northeast Atlantic Deep-Sea Sediments During the Late Quaternary - Mineralogical and K-Ar Isotopic Data. Eclogae Geologicae Helvetiae, 85(1): 195-212.

Jeansson, E. et al., 2008. Sources to the East Greenland Current and its contribution to the Denmark Strait Overflow. Progress in Oceanography, 78(1): 12-28.

Jennings, A.E., Knudsen, K.L., Hald, M., Hansen, C.V. and Andrews, J.T., 2002. A mid-Holocene shift in Arctic sea-ice variability on the East Greenland Shelf. Holocene, 12(1): 49-58.

Jiang, H., Ren, J., Knudsen, K.L., Eiriksson, J. and Ran, L.H., 2007. Summer sea-surface temperatures and climate events on the North Icelandic shelf through the last 3000 years. Chinese Science Bulletin, 52(6): 789-796.

Jiang, H., Seidenkrantz, M.S., Knudsen, K.L. and Eiriksson, J., 2001. Diatom surface sediment assemblages around Iceland and their relationships to oceanic environmental variables. Marine Micropaleontology, 41(1-2): 73-96.

Johnsen, S.J. et al., 1992. Irregular Glacial Interstadials Recorded in a New Greenland Ice Core. Nature, 359(6393): 311-313.

Jordan, R.W., Priddle, J., Pudsey, C.J., Barker, P.F. and Whitehouse, M.J., 1991. Unusual Diatom Layers in Upper Pleistocene Sediments from the Northern Weddell Sea. Deep-Sea Research Part a-Oceanographic Research Papers, 38(7): 829-843.

Justwan, A. and Koc, N., 2008. A diatom based transfer function for reconstructing sea ice

concentrations in the North Atlantic. Marine Micropaleontology, 66(3-4): 264-278.

Justwan, A., Koc, N. and Jennings, A.E., 2008. Evolution of the Irminger and East Icelandic Current systems through the Holocene, revealed by diatom-based sea surface temperature reconstructions. Quaternary Science Reviews, 27(15-16): 1571-1582.

Kaczmarska, I. and Fryxell, G.A., 1996. Alveus, gen nov (Bacillariaceae, bacillariophyta), a heavily silicified diatom found in warm water oceans. Microscopy Research and Technique, 33(1): 2-11.

Kaczmarska, I., Fryxell, G.A. and Watkins, T.P., 1986. Effect of two Gulf Stream warm core rings on distributional patterns of the diatom genus *Nitzschia*. Deep-Sea Research, 33: 1843-1868.

Karlen, W., 1976. Lacustrine Sediments and Tree-Limit Variations as Indicators of Holocene Climatic Fluctuations in Lappland, Northern Sweden. Geografiska Annaler Series a-Physical Geography, 58(1-2): 1-34.

Karlen, W. and Kuylenstierna, J., 1996. On solar forcing of Holocene climate: Evidence from Scandinavia. Holocene, 6(3): 359-365.

Karsten, G., 1905. Das Phytoplankton des Antarktischen Meeres nach dem Material der deutschen Tiefsee-Expedition 1898-1899. Deutsche Tiefsee-Expedition 1898-1899, 2(2): 1-136.

Keigwin, L.D. and Jones, G.A., 1995. The Marine Record of Deglaciation from the Continental-Margin Off Nova-Scotia. Paleoceanography, 10(6): 973-985.

Kemp, A.E.S. and Baldauf, J.G., 1993. Vast Neogene Laminated Diatom Mat Deposits from the Eastern Equatorial Pacific-Ocean. Nature, 362(6416): 141-144.

Kemp, A.E.S. et al., 2006. Production of giant marine diatoms and their export at oceanic frontal zones: Implications for Si and C flux from stratified oceans. Global Biogeochemical Cycles, 20(4).

Kieke, D. et al., 2006. Changes in the CFC inventories and formation rates of Upper Labrador Sea Water, 1997-2001. Journal of Physical Oceanography, 36(1): 64-86.

Kleiven, H.F. et al., 2008. Reduced North Atlantic Deep Water coeval with the glacial Lake Agassiz freshwater outburst. Science, 319(5859): 60-64.

Knudsen, K.L., Sondergaard, M.K.B., Eiriksson, J. and Jiang, H., 2008. Holocene thermal

maximum off North Iceland: Evidence from benthic and planktonic foraminifera in the 8600-5200 cal year BP time slice. Marine Micropaleontology, 67(1-2): 120-142.

Knudsen, K.L., Stabell, B., Seidenkrantz, M.S., Eiriksson, J. and Blake, W., 2008. Deglacial and Holocene conditions in northernmost Baffin Bay: sediments, foraminifera, diatoms and stable isotopes. Boreas, 37(3): 346-376.

Koc, N. and Jansen, E., 1994. Response of the High-Latitude Northern-Hemisphere to Orbital Climate Forcing - Evidence from the Nordic Seas. Geology, 22(6): 523-526.

Koc, N., Jansen, E., Hald, M. and Labeyrie, L., 1996. Late glacial Holocene sea surface temperatures and gradients between the North Atlantic and the Norwegian sea: Implications for the Nordic heat pump. Late Quaternary Palaeoceanography of the North Atlantic Margins(111): 177-185.

Kopczynska, E.E., Weber, L.H. and Elsayed, S.Z., 1986. Phytoplankton Species Composition and Abundance in the Indian Sector of the Antarctic Ocean. Polar Biology, 6(3): 161-169.

Kristoffersen, Y. et al., 2004. Seabed erosion on the Lomonosov Ridge, central Arctic Ocean: A tale of deep draft icebergs in the Eurasia Basin and the influence of Atlantic water inflow on iceberg motion? Paleoceanography, 19(3).

Kroger, N., Lorenz, S., Brunner, E. and Sumper, M., 2002. Self-assembly of highly phosphorylated silaffins and their function in biosilica morphogenesis. Science, 298(5593): 584-586.

Kuijpers, A. and Werner, F., 2007. Extremely deep-draft iceberg scouring in the glacial North Atlantic Ocean. Geo-Marine Letters, 27(6): 383-389.

Labeyrie, L. et al., 1995. Surface and Deep Hydrology of the Northern Atlantic-Ocean During the Past 150000 Years. Philosophical Transactions of the Royal Society of London Series B-Biological Sciences, 348(1324): 255-264.

Lamb, H.F. et al., 1995. Relation between Century-Scale Holocene Arid Intervals in Tropical and Temperate Zones. Nature, 373(6510): 134-137.

Landry, M.R. et al., 2002. Seasonal dynamics of phytoplankton in the Antarctic Polar Front region at 170 degrees W. Deep-Sea Research Part Ii-Topical Studies in Oceanography, 49(9-10): 1843-1865.

Lauder, H.S., 1864. On new diatoms. Transactions of the Microscopical Society of London New Series, 12: 6-8.

Lee, J.H. and Lee, J.Y., 1990. A light and electron microscopy study on the marine diatom *Roperia tesselata* (Roper) Grunow. Diatom Research, 5: 325-335.

Litvin, V.M., 1984. The morphostructure of the Atlantic Ocean floor; its development in the Meso-Cenozoic. Oceanographic sciences library. Reidel, Dordrecht; Lancaster.

Liu, Z., Brady, E. and Lynch-Stieglitz, J., 2003. Global ocean response to orbital forcing in the Holocene. Paleoceanography, 18(2).

Macayeal, D.R., 1993. Binge/Purge Oscillations of the Laurentide Ice-Sheet as a Cause of the North-Atlantics Heinrich Events. Paleoceanography, 8(6): 775-784.

Macayeal, D.R., 1993. A Low-Order Model of the Heinrich Event Cycle. Paleoceanography, 8(6): 767-773.

Makarova, I.V., 1988. Diatomaceous algae of the seas of the U.S.S.R.: the genus *Thalassiosira* Cl. Akademiya NAUK C.C.C.P.: 117.

Malmgren, B.A., Kucera, M., Nyberg, J. and Waelbroeck, C., 2001. Comparison of statistical and artificial neural network techniques for estimating past sea surface temperatures from planktonic foraminifer census data. Paleoceanography, 16(5): 520-530.

Malmgren, B.A. and Nordlund, U., 1997. Application of artificial neural networks to paleoceanographic data. Palaeogeography Palaeoclimatology Palaeoecology, 136(1-4): 359-373.

Mann, D.G., 1978. Studies in the family Nitzschiaceae (Bacillariophyta), University of Bristol, Bristol, XXXIII, 386, 146 plates pp.

Mann, D.G., 1981. Sieves and flaps: Siliceous minutiae in the pores of raphid diatoms. In: R. Ross (Editor), Proceedings of the Sixth Symposium on Recent and Fossil Diatoms. Koeltz, Budapest, pp. 279-300.

Marchal, O. et al., 2002. Apparent long-term cooling of the sea surface in the northeast Atlantic and Mediterranean during the Holocene. Quaternary Science Reviews, 21(4-6): 455-483.

Marshall, J. et al., 2001. North Atlantic climate variability: Phenomena, impacts and mechanisms. International Journal of Climatology, 21(15): 1863-1898.

Marshall, S.J. and Clark, P.U., 2002. Basal temperature evolution of North American ice sheets

and implications for the 100-kyr cycle. Geophysical Research Letters, 29(24).

Martin-Jezequel, V., Hildebrand, M. and Brzezinski, M.A., 2000. Silicon metabolism in diatoms: Implications for growth. Journal of Phycology, 36(5): 821-840.

Mauritzen, C., 1996. Production of dense overflow waters feeding the North Atlantic across the Greenland-Scotland Ridge .1. Evidence for a revised circulation scheme. Deep-Sea Research Part I-Oceanographic Research Papers, 43(6): 769-806.

Mayewski, P.A. et al., 2004. A 700 year record of Southern Hemisphere extratropical climate variability. Annals of Glaciology, Vol 39, 2005, 39: 127-132.

Mayewski, P.A. et al., 1997. Major features and forcing of high-latitude northern hemisphere atmospheric circulation using a 110,000-year-long glaciochemical series. Journal of Geophysical Research-Oceans, 102(C12): 26345-26366.

McBride, T.P., 1988. Preparing Random Distributions of Diatom Valves on Microscope Slides. Limnology and Oceanography, 33(6): 1627-1629.

McCartney, M.S., 1992. Recirculating Components to the Deep Boundary Current of the Northern North-Atlantic. Progress in Oceanography, 29(4): 283-383.

McCartney, M.S. and Talley, L.D., 1982. The Sub-Polar Mode Water of the North-Atlantic Ocean. Journal of Physical Oceanography, 12(11): 1169-1188.

McCave, I.N., 1994. Cruise Report: RRS Charles Darwin 88, University of Cambridge; Department of Earth Sciences.

McCave, I.N. and Hall, I.R., 2006. Size sorting in marine muds: Processes, pitfalls, and prospects for paleoflow-speed proxies. Geochemistry Geophysics Geosystems, 7.

McCave, I.N., Hall, I.R. and Bianchi, G.G., 2006. Laser vs. settling velocity differences in silt grainsize measurements: estimation of palaeocurrent vigour. Sedimentology, 53(4): 919-928.

McCave, I.N., Manighetti, B. and Robinson, S.G., 1995. Sortable Silt and Fine Sediment Size Composition Slicing - Parameters for Paleocurrent Speed and Paleoceanography. Paleoceanography, 10(3): 593-610.

McManus, J.F., Oppo, D.W. and Cullen, J.L., 1999. A 0.5-million-year record of millennial-scale climate variability in the North Atlantic. Science, 283(5404): 971-975.

McQuoid, M.R. and Hobson, L.A., 1996. Diatom resting stages. Journal of Phycology, 32(6):

889-902.

Medlin, L.K. and Kaczmarska, I., 2004. Evolution of the diatoms: V. Morphological and cytological support for the major clades and a taxonomic revision. Phycologia, 43(3): 245-270.

Medlin, L.K., Kooistra, W., Gersonde, R. and Wellbrock, U., 1996. Evolution of the diatoms (Bacillariophyta) .2. Nuclear-encoded small-subunit rRNA sequence comparisons confirm a paraphyletic origin for the centric diatoms. Molecular Biology and Evolution, 13(1): 67-75.

Medlin, L.K. and Sims, P.A., 1993. The transfer of *Pseudoeunotia doliolus* to *Fragilariopsis*. Beiheft zur Nova Hedwigia, 106: 323-334.

Meeker, L.D. and Mayewski, P.A., 2002. A 1400-year high-resolution record of atmospheric circulation over the North Atlantic and Asia. Holocene, 12(3): 257-266.

Mereschkowsky, C., 1902. Liste des Diatomees de la Mer Noire. Scripta Botanica horti Universitatis Petropolitanae, 19: 1-42.

Meunier, A., 1910. Microplankton des Mers de Barents et de Kara, Duc d'Orleans Campagne Arctique de 1907. 355.

Moore, G.F., Smyth, T.J., Groom, S.B., Land, P.E. and Tyrrell, T., 2002. Optical modeling and measurements of a coccolithophore bloom. Applied Optics, 41(36): 7679-7688.

Moore, J.K., Doney, S.C., Glover, D.M. and Fung, I.Y., 2002. Iron cycling and nutrient-limitation patterns in surface waters of the World Ocean. Deep-Sea Research Part Ii-Topical Studies in Oceanography, 49(1-3): 463-507.

Moore, J.K. and Villareal, T.A., 1996. Size-ascent rate relationships in positively buoyant marine diatoms. Limnology and Oceanography, 41(7): 1514-1520.

Moros, M., Andrews, J.T., Eberl, D.D. and Jansen, E., 2006. Holocene history of drift ice in the northern North Atlantic: Evidence for different spatial and temporal modes. Paleoceanography, 21(2).

Moros, M. et al., 2004. Sea surface temperatures and ice rafting in the Holocene North Atlantic: climate influences on Northern Europe and Greenland. Quaternary Science Reviews, 23(20-22): 2113-2126.

Nelson, D.M. and Treguer, P., 1992. Role of Silicon as a Limiting Nutrient to Antarctic Diatoms

- Evidence from Kinetic-Studies in the Ross Sea Ice-Edge Zone. Marine Ecology-Progress Series, 80(2-3): 255-264.

Nesje, A., Matthews, J.A., Dahl, S.O., Berrisford, M.S. and Andersson, C., 2001. Holocene glacier fluctuations of Flatebreen and winter-precipitation changes in the Jostedalsbreen region, western Norway, based on glaciolacustrine sediment records. Holocene, 11(3): 267-280.

Nikolaev, B.N., Shlyakov, A.M., Klimenko, N.A. and Karmazina, T.V., 1988. Investigation of the Conditions of the Triton X-100 Layer Sorbed from the High-Concentration Solution on Silica-Gel by the H-2 Nmr-Spectroscopy Method. Dopovidi Akademii Nauk Ukrainskoi Rsr Seriya B-Geologichni Khimichni Ta Biologichni Nauki(11): 52-55.

Obrien, S.R. et al., 1995. Complexity of Holocene Climate as Reconstructed from a Greenland Ice Core. Science, 270(5244): 1962-1964.

Olsen, S.M., Hansen, B., Quadfasel, D. and Osterhus, S., 2008. Observed and modelled stability of overflow across the Greenland-Scotland ridge. Nature, 455(7212): 519-U35.

Olsen, S.M., Shaffer, G. and Bjerrum, C.J., 2005. Ocean oxygen isotope constraints on mechanisms for millennial-scale climate variability. Paleoceanography, 20(1).

Oppo, D.W., McManus, J.F. and Cullen, J.L., 2003. Deepwater variability in the Holocene epoch (vol 422, pg 277, 2003). Nature, 423(6938): 400-400.

Paasche, E., 1961. Nores on phytopllankton from the Norwegian Sea. Botanica Marina, 2: 197-210.

Peragallo, H., 1892. Monographie du genre *Rhizosolenia* de quelques genres voisins. Le Diatomiste, 1: 79, 82, 99-117.

Pflaumann, U., Duprat, J., Pujol, C. and Labeyrie, L.D., 1996. SIMMAX: A modern analog technique to deduce Atlantic sea surface temperatures from planktonic foraminifera in deep-sea sediments. Paleoceanography, 11(1): 15-35.

Pflaumann, U. et al., 2003. Glacial North Atlantic: Sea-surface conditions reconstructed by GLAMAP 2000. Paleoceanography, 18(3).

Pichon, J.J. et al., 1992. Quantification of the Biogenic Silica Dissolution in Southern-Ocean Sediments. Quaternary Research, 37(3): 361-378.

Pickart, R.S., Spall, M.A., Ribergaard, M.H., Moore, G.W.K. and Milliff, R.F., 2003. Deep

convection in the Irminger Sea forced by the Greenland tip jet. Nature, 424(6945): 152-156.

Rahmstorf, S., 2002. Ocean circulation and climate during the past 120,000 years. Nature, 419(6903): 207-214.

Ran, L.H., Jiang, H., Knudsen, K.L., Eiriksson, J. and Gu, Z.W., 2006. Diatom response to the Holocene climatic optimum on the North Icelandic shelf. Marine Micropaleontology, 60(3): 226-241.

Raymo, M.E., Ganley, K., Carter, S., Oppo, D.W. and McManus, J., 1998. Millennial-scale climate instability during the early Pleistocene epoch. Nature, 392(6677): 699-702.

Read, J.F., 2001. CONVEX-91: water masses and circulation of the Northeast Atlantic subpolar gyre. Progress in Oceanography, 48(4): 461-510.

Reeh, N., 2004. Holocene climate and fjord glaciations in Northeast Greenland: implications for IRD deposition in the North Atlantic. Sedimentary Geology, 165(3-4): 333-342.

Revel, M., Sinko, J.A., Grousset, F.E. and Biscaye, P.E., 1996. Sr and Nd isotopes as tracers of north Atlantic lithic particles: Paleoclimatic implications. Paleoceanography, 11(1): 95-113.

Rimbu, N., Lohmann, G., Lorenz, S.J., Kim, J.H. and Schneider, R.R., 2004. Holocene climate variability as derived from alkenone sea surface temperature and coupled ocean-atmosphere model experiments. Climate Dynamics, 23(2): 215-227.

Risebrobakken, B., Jansen, E., Andersson, C., Mjelde, E. and Hevroy, K., 2003. A high-resolution study of Holocene paleoclimatic and paleoceanographic changes in the Nordic Seas. Paleoceanography, 18(1).

Rivera, P., 1981. Beitrage zur Taxonomie und Verbreitung der Gattung *Thalassiosira* Cleve. Bibliotheca Phycologica, 56: 1-220, 71 plates.

Rohling, E.J., Mayewski, P.A., Abu-Zied, R.H., Casford, J.S.L. and Hayes, A., 2002. Holocene atmosphere-ocean interactions: records from Greenland and the Aegean Sea. Climate Dynamics, 18(7): 587-593.

Rohling, E.J. and Palike, H., 2005. Centennial-scale climate cooling with a sudden cold event around 8,200 years ago. Nature, 434(7036): 975-979.

Ross, R. et al., 1979. An amended terminology for the siliceous components of the diatom cell.

Beiheft zur Nova Hedwigia, 64: 513-533.

Round, F.E. and Crawford, R.M., 1981. The lines of evolution of the Bacillariophyta. 1. Origin. Proceedings of the Royal Society London B, 211: 237-260.

Round, F.E. and Crawford, R.M., 1984. The lines of evolution of the Bacillariophyta. 2. The centric series. Proceedings of the Royal Society London B, 221: 169-188.

Round, F.E., Crawford, R.M. and Mann, D.G., 1990. The Diatoms : biology & morphology of the genera. Cambridge University Press, Cambridge [England] ; New York, 747 p. pp.

Ruddick, B., Walsh, D. and Oakey, N., 1997. Variations in apparent mixing efficiency in the North Atlantic central water. Journal of Physical Oceanography, 27(12): 2589-2605.

Ruddiman, W.F., 1977. Late Quaternary Deposition of Ice-Rafted Sand in Subpolar North-Atlantic (Lat 40-Degrees to 65-Degrees-N). Geological Society of America Bulletin, 88(12): 1813-1827.

Rudels, B. et al., 2005. The interaction between waters from the Arctic Ocean and the Nordic Seas north of Fram Strait and along the East Greenland Current: results from the Arctic Ocean-02 Oden expedition. Journal of Marine Systems, 55(1-2): 1-30.

Rudels, B., Fahrbach, E., Meincke, J., Budeus, G. and Eriksson, P., 2002. The East Greenland Current and its contribution to the Denmark Strait overflow. Ices Journal of Marine Science, 59(6): 1133-1154.

Ryves, D.B., Battarbee, R.W. and Fritz, S.C., 2009. The dilemma of disappearing diatoms: Incorporating diatom dissolution data into palaeoenvironmental modelling and reconstruction. Quaternary Science Reviews, 28(1-2): 120-136.

Sarnthein, M. and Altenbach, A.V., 1995. Late Quaternary Changes in Surface-Water and Deep-Water Masses of the Nordic Seas and North-Eastern North-Atlantic - a Review. Geologische Rundschau, 84(1): 89-107.

Sarnthein, M. et al., 2003. Centennial-to-millennial-scale periodicities of Holocene climate and sediment injections off the western Barents shelf, 75 degrees N. Boreas, 32(3): 447-461.

Sarthou, G., Timmermans, K.R., Blain, S. and Treguer, P., 2005. Growth physiology and fate of diatoms in the ocean: a review. Journal of Sea Research, 53(1-2): 25-42.

Savidge, G., Boyd, P., Pomroy, A., Harbour, D. and Joint, I., 1995. Phytoplankton Production and Biomass Estimates in the Northeast Atlantic-Ocean, May to June 1990. Deep-Sea

Research Part I-Oceanographic Research Papers, 42(5): 599-617.

Schmidt, A., 1878. Atlas der Diatomaceenkunde. Reisland, Leipzig.

Schulz, M. and Paul, A., 2002. Holocene climate variability on centennial-to-millennial time scales: 1. Climate records from the North-Atlantic realm. In: G. Wefer, W.H. Berger, K.E. Behre and E. Jansen (Editors), Climate Development and History of the North Atlantic Realm, pp. 41-54.

Schutt, F., 1896. Bacillarialies. In: A. Engler and K. Prantl (Editors), Die naturlichen Pflanzenfamilien, pp. 31-150.

Shackleton, N.J., Hall, M.A. and Vincent, E., 2000. Phase relationships between millennial-scale events 64,000-24,000 years ago. Paleoceanography, 15(6): 565-569.

Shipe, R.F., Carpenter, E.J., Govil, S.R. and Capone, D.G., 2007. Limitation of phytoplankton production by Si and N in the western Atlantic Ocean. Marine Ecology-Progress Series, 338: 33-45.

Silva, P.C. and Hasle, G.R., 1993. Proposal to conserve *Thalassiothrix* Cleve et Grunow (*Bacillariophyceae)* with a conserved type. Taxon, 42: 125-127.

Simonsen, R., 1972. uber die Diatomeengattung *Hemidiscus* Wallich und andere Angehorige der sogenannten "Hemidiscaceae". Veroffentlichungen des Instituts Fur Meeresforschung in Bremerhaven, 13: 265-273.

Simonsen, R., 1974. The diatom plankton of the Indian Ocean Expedition of RV "Meteor" 1964-1965. "Meteor" Forschungsergebnisse Reihe D, pp. 1-107.

Simonsen, R., 1975. On the pseudonodulus of the centric diatoms, or Hemidiscaceae reconsidered. Beiheft zur Nova Hedwigia, 53: 83-94.

Skinner, L.C. and McCave, I.N., 2003. Analysis and modelling of gravity- and piston coring based on soil mechanics. Marine Geology, 199(1-2): 181-204.

Smayda, T.J., 1970. Growth Potential Bioassay of Water Masses Using Diatom Cultures - Phosphorescent-Bay (Puerto-Rico) and Caribbean Waters. Helgolander Wissenschaftliche Meeresuntersuchungen, 20(1-4): 172-&.

Smetacek, V., Bathmann, U., van den Loeff, M.M.R., Strass, V.H. and Wegener, A., 2002. Mesoscale physics, biogeochemistry and ecology of the Antarctic Polar Front, Atlantic sector: an introduction to and summary of cruise ANT XIII/2 of RV Polarstern. Deep-Sea

Research Part Ii-Topical Studies in Oceanography, 49(18): 3707-3711.

Stevens, J., 2002. Applied Multivariate Statistics for the Social Sciences. Lawrence Erlbaum Associates, Mahwah.

Stocker, T.F. and Wright, D.G., 1996. Rapid changes in ocean circulation and atmospheric radiocarbon. Paleoceanography, 11(6): 773-795.

Stockner, J.G. and Lund, J.W.G., 1970. Live Algae in Postglacial Lake Deposits. Limnology and Oceanography, 15(1): 41-&.

Stosch, H.A.V., Theil, G. and Kowallik, K.V., 1973. Ontogenetic Investigations on Centric Diatoms .5. Morphology and Life-History of Chaetoceros-Didymum, with Observations on Some Other Species of Genus. Helgolander Wissenschaftliche Meeresuntersuchungen, 25(2-3): 384-445.

Stuiver, M. and Braziunas, T.F., 1993. Modeling Atmospheric C-14 Influences and C-14 Ages of Marine Samples to 10,000 Bc. Radiocarbon, 35(1): 137-189.

Stuiver, M., Grootes, P.M. and Braziunas, T.F., 1995. The GISP2 delta O-18 climate record of the past 16,500 years and the role of the sun, ocean, and volcanoes. Quaternary Research, 44(3): 341-354.

Stuiver, M. et al., 1998. INTCAL98 radiocarbon age calibration, 24,000-0 cal BP. Radiocarbon, 40(3): 1041-1083.

Sundstrom, B.G., 1986. The marine diatom genus Rhizosolenia, Lund University, Lund, 117, 39 plates pp.

Sutherland, D.A. and Pickart, R.S., 2008. The East Greenland Coastal Current: Structure, variability, and forcing. Progress in Oceanography, 78(1): 58-77.

Swift, J.H., Aagaard, K. and Malmberg, S.A., 1980. Contribution of the Denmark Strait Overflow to the Deep North-Atlantic. Deep-Sea Research Part a-Oceanographic Research Papers, 27(1): 29-42.

Sy, A., 1988. Investigation of Large-Scale Circulation Patterns in the Central North-Atlantic - the North-Atlantic Current, the Azores Current, and the Mediterranean Water Plume in the Area of the Mid-Atlantic Ridge. Deep-Sea Research Part a-Oceanographic Research Papers, 35(3): 383-413.

Sy, A., Schauer, U. and Meincke, J., 1992. The North-Atlantic Current and Its Associated

Hydrographic Structure above and Eastwards of the Mid-Atlantic Ridge. Deep-Sea Research Part a-Oceanographic Research Papers, 39(5A): 825-853.

Syvertsen, E.E., 1977. *Thalassiosira rotula* and *T. gravida*: Ecology and morphology. Beiheft zur Nova Hedwigia, 54: 99-112.

Syvertsen, E.E., 1979. Resting spore formation in clonal cutures of *Thalassiosira antarctica* Comber, *T. nordenskioeldii* Cleve and *Detonula confervacea* (Cleve) Gran. Beiheft zur Nova Hedwigia, 64: 41-63.

Talley, L.D., 1999. Simple coupled midlatitude climate models. Journal of Physical Oceanography, 29(8): 2016-2037.

Tanhua, T., Olsson, K.A. and Jeansson, E., 2005. Formation of Denmark Strait overflow water and its hydro-chemical composition. Journal of Marine Systems, 57(3-4): 264-288.

Taylor, A.H., Jordan, M.B. and Stephens, J.A., 1998. Gulf Stream shifts following ENSO events. Nature, 393(6686): 638-638.

Taylor, K.C., Mayewski, P.A., Twickler, M.S. and Whitlow, S.I., 1996. Biomass burning recorded in the GISP2 ice core: A record from eastern Canada? Holocene, 6(1): 1-6.

Telford, R.J., Andersson, C., Birks, H.J.B. and Juggins, S., 2004. Biases in the estimation of transfer function prediction errors. Paleoceanography, 19(4).

Telford, R.J. and Birks, H.J.B., 2005. The secret assumption of transfer functions: problems with spatial autocorrelation in evaluating model performance. Quaternary Science Reviews, 24(20-21): 2173-2179.

Terbraak, C.J.F., 1990. Interpreting Canonical Correlation-Analysis through Biplots of Structure Correlations and Weights. Psychometrika, 55(3): 519-531.

Terbraak, C.J.F. and Juggins, S., 1993. Weighted Averaging Partial Least-Squares Regression (Wa-Pls) - an Improved Method for Reconstructing Environmental Variables from Species Assemblages. Hydrobiologia, 269: 485-502.

Thornalley, D.J.R., Elderfield, H. and McCave, I.N., 2009. Holocene oscillations in temperature and salinity of the surface subpolar North Atlantic. Nature, 457(7230): 711-714.

Thouveny, N. et al., 2000. Rock magnetic detection of distal ice-rafted debries: clue for the identification of Heinrich layers on the Portuguese margin. Earth and Planetary Science Letters, 180(1-2): 61-75.

Tibby, J., Gell, P.A., Fluin, J. and Sluiter, I.R.K., 2007. Diatom-salinity relationships in wetlands: assessing the influence of salinity variability on the development of inference models. Hydrobiologia, 591: 207-218.

Timmermans, K.R., van der Wagt, B. and de Baar, H.J.W., 2004. Growth rates, half-saturation constants, and silicate, nitrate, and phosphate depletion in relation to iron availability of four large, open-ocean diatoms from the Southern Ocean. Limnology and Oceanography, 49(6): 2141-2151.

Vancampo, E. and Gasse, F., 1993. Pollen-Inferred and Diatom-Inferred Climatic and Hydrological Changes in Sumxi Co Basin (Western Tibet) since 13,000 Yr Bp. Quaternary Research, 39(3): 300-313.

Vanlandingham, S.L., 1968. Catalogue of the Fossil and Recent Genera and Species of Diatoms and Their Synonyms 1-8. J Cramer, Lehre, 4653 pp.

Vanlandingham, S.L., 1978. Catalogue of the Fossil and Recent Genera and Species of Diatoms and Their Synonyms 1-8. J Cramer, Lehre, 4653 pp.

Vidal, L. et al., 1997. Evidence for changes in the North Atlantic Deep Water linked to meltwater surges during the Heinrich events. Earth and Planetary Science Letters, 146(1-2): 13-27.

Visbeck, M. and Krahmann, G., 2003. Variability of the Northern Annular Mode's signature in winter sea ice concentration. Polar Research, 22(1): 51-57.

Waite, A., Gallager, S. and Dam, H.G., 1997. New measurements of phytoplankton aggregation in a flocculator using videography and image analysis. Marine Ecology-Progress Series, 155: 77-88.

Wanner, H. et al., 2001. North Atlantic Oscillation - Concepts and studies. Surveys in Geophysics, 22(4): 321-382.

Wetherbee, R., 2002. The diatom glasshouse. Science, 298(5593): 547-547.

Williams, D.M., 1985. Morphology, taxonomy and interrelationshios of the ribbed araphid diatoms from the genera *Diatoma* and *Meridion*. Bibliotheca Diatomologica, 8: 1-228, 27 plates.

Williams, D.M., 1986. Comparative morphology of some species of *Synedra* Ehrenb. witha new definition of the genus. Diatom Research, 1: 131-152.

Williams, D.M. and Round, F.E., 1986. Revision of the genus *Synedra* Ehrenb. Diatom Research, 1: 313-339.

Williams, D.M. and Round, F.E., 1988. Phylogenetic systematics of *Synedra*. In: F.E. Round (Editor), Proceedings of the 9th International Diatom Symposium. Biopress and Koeltz, Bristol, pp. 303-315.

Wimpenny, R.S., 1946. The size of diatoms II. Further observations on *Rhizosolenia styliformis* (Brightwell). Journal of the Marine Biological Association of the United Kingdom, 26: 271-284.

Witon, E., Malmgren, B., Witkowski, A. and Kuijpers, A., 2006. Holocene marine diatoms from the Faeroe Islands and their paleoceanographic implications. Palaeogeography Palaeoclimatology Palaeoecology, 239(3-4): 487-509.

Worthing, L.V., 1970. Norwegian-Sea as a Mediterranean Basin. Deep-Sea Research, 17(1): 77-&.

Wright, J.D. and Miller, K.G., 1996. Control of North Atlantic deep water circulation by the Greenland-Scotland ridge. Paleoceanography, 11(2): 157-170.

Yoder, J.A., Ackleson, S.G., Barber, R.T., Flament, P. and Balch, W.M., 1994. A Line in the Sea. Nature, 371(6499): 689-692.

Yu, S.Y., Andren, E., Barnekow, L., Berglund, B.E. and Sandgren, P., 2003. Holocene palaeoecology and shoreline displacement on the Biskopsmala Peninsula, southeastern Sweden. Boreas, 32(4): 578-589.

Zielinski, G.A., Mayewski, P.A., Meeker, L.D., Whitlow, S. and Twickler, M.S., 1996. A 110,000-yr record of explosive volcanism from the GISP2 (Greenland) ice core. Quaternary Research, 45(2): 109-118.

Zielinski, U. and Gersonde, R., 1997. Diatom distribution in Southern Ocean surface sediments (Atlantic sector): Implications for paleoenvironmental reconstructions. Palaeogeography Palaeoclimatology Palaeoecology, 129(3-4): 213-250.

Zielinski, U., Gersonde, R., Sieger, R. and Futterer, D., 1998. Quaternary surface water temperature estimations: Calibration of a diatom transfer function for the Southern Ocean. Paleoceanography, 13(4): 365-383.

Zong, Y.Q. and Horton, B.P., 1999. Diatom-based tidal-level transfer functions as an aid in

reconstructing Quaternary history of sea-level movements in the UK. Journal of Quaternary Science, 14(2): 153-167.

Appendix One

The Biology of Diatoms

Appendix One

1.1 The Biology of Diatoms

The diatoms or Bacillariophyceae are unicellular, sometimes colonial algae of the phylum *Heterkontophyta*. The majority of species are photosynthetic autotrophs and as such are primary producers. A few species of *Nitzchia* and *Handtzschia* are heterotrophs and certain authors have recognised forms living as photosynthetic symbiotes. (Schmaljohann & Rottger, 1978). The cell is contained within a silica cell wall. An organic coating covers the siliceous components. This coating is made up of two layers, an external membrane and an internal diatoteptic layer (von Stosch, 1981).

1.1.1 Silica Deposition and Frustule Structure

The diatom cell secretes a rigid, two part, box-like cell wall of hydrated amorphous silica (SiO_2 nH_2O). This is the characteristic feature of the Bacillariophyceae. The silica is deposited within separate vesicles for each wall element. These are known as silica deposition vesicles (SDVs). Silica is not absorbed by the cell at a constant rate, but at an accelerated rate during growth cycles. The shape and nature of growth from the SDVs determines the basic division of diatoms between the centric and pennate forms. In centric forms the SDV begins as a small pancake-shaped structure. Ribs radiate out from this central

ring as the diatom grows. In pennate forms the SDV begins as a thin long tube. Subsequent ribs expand out from this central rib or sternum. (Figure 1.1) While this basic distinction between pennate and centric forms has been more recently shown to be of less taxonomic significance (Medlin *et al.*, 1996a) it is still widely adopted in the literature. It is important to note therefore, that the distinction between centric and pennate forms is determined not by the outline of the mature form but by the central area of the diatom frustule (Round *et al.*, 1990).

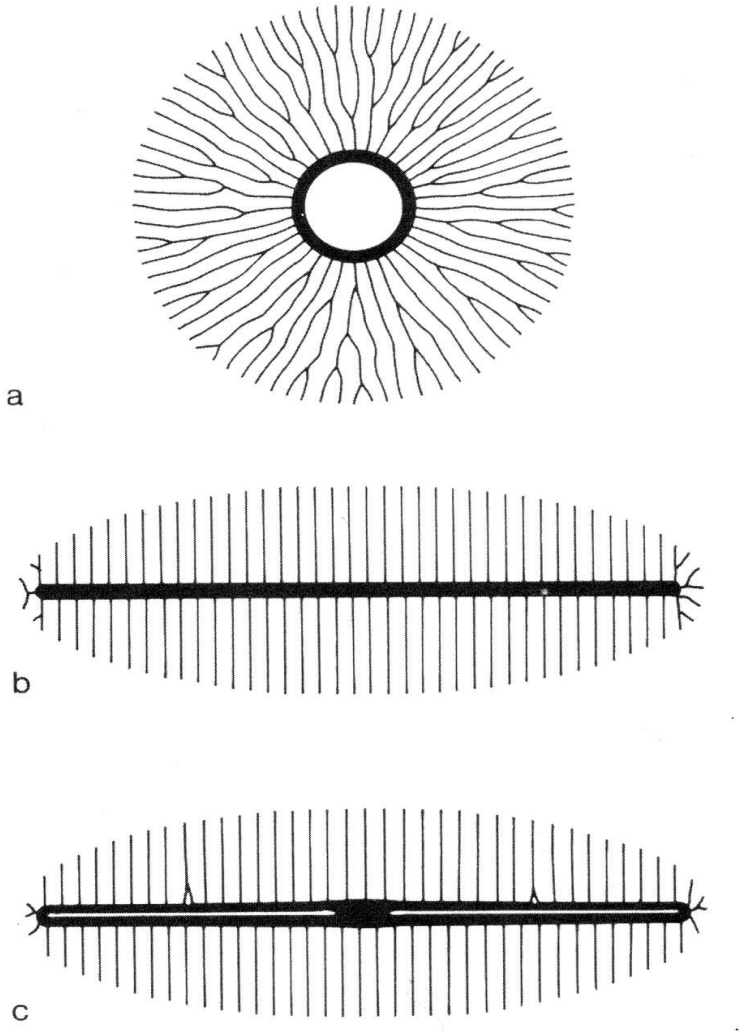

Fig 1.1 Three basic patterns of diatom growth a) centric, ribs radiating from a central ring or annulus b) simple pennate, ribs extending from both sides of a central longitudinal sternum c) raphid pennate, ribs extending from both sides of a longitudinal element that contains one or two slits (raphes). After Round *et al.* (1990)

In simpler valve forms, silica is deposited in a lattice of primary ribs, growing from the central annulus or sternum and joined by shorter lateral ribs (Cox & Ross, 1980). In more complex forms an additional layer of silica is deposited parallel or perpendicular the primary framework causing the valves to become chambered or loculate. The primary structure may form the internal or external portion of the valve. The regularly repeated perforations in the valve wall are referred to as the areolae; the patterns of these areolae across the valve, the areolation. Areolae that are restricted at one surface of the valve and occluded at the other by a thin perforated layer of silica or velum, are called loculate areolae or loculi (Figure 1.2a). Areolae that are not restricted at one surface of the valve are poroid areolae or poroids (Figure 1.2b). A velum with regular perforations is referred to as a cribia. A velum consisting of a solid disc attached by spokes is a rota. A velum consisting of flaps and bars projecting from the areola wall. The restricted opening opposite the velum in loculate areolae is the foramen (Figure 1.2a). Rows of areolae are referred to as striae, the imperforated areas between the striae as interstriae. Areas of the valve that are not perforated by areolae are known as hyaline areas (Anonymous, 1975; Hasle & Syvertsen, 1997; Round *et al.*, 1990). Recent work has shown that the species specific patterns of silica deposition are genetically determined (Kroger *et al* 2002; Wetherbee, 2002).

a) loculate areolae : loculi

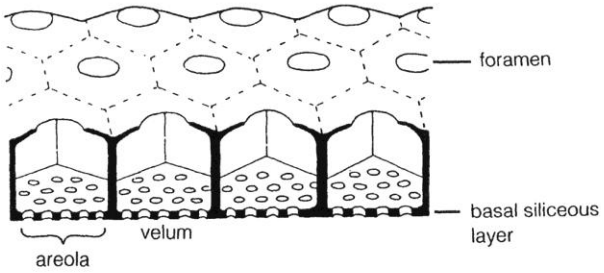

b) poroid areolae : poroids

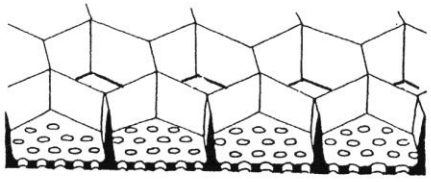

Fig 1.2 Fine structures of the diatom frustule wall: foramen, areolae, velum, loculi and poroids a) loculate areolae structure b) poroid areolae structure (Hasle & Syvertsen, 1997).

Two types of portule may also be precipitated, the fultoportula and the rimoportula (Fig 1.3). Fultoportulae or strutted processes are found only in the order Thalassiosirales. They consist of a tube passing through the silica framework of the valve which is supported by two or more buttresses internally. Externally the tube may or may not extrude above the valve surface and usually has a simple opening. Internally the opening of the fultoportula is more complex, consisting of the main tube aperture and two to five satellite slits or holes. These holes or slits are the openings to passages which connect the central tube to the inside of the cell (Fig 1.3c). Round *et al.* (1990) recognises three main types of fultoportulae: those with simple openings and buttresses, those where the satellite passages extend into tubes running parallel to the central tube and those with lobed strips of silica in the apertures. The function of the fultoportula is uncertain. Herth & Barthlott (1979) showed that it is instrumental in the secretion of β-chitin fibrils in certain species. Scmind (1984a) proposed that it may function to anchor the protoplasm (Round *et al*., 1990)

The rimoportula or labiate process is a more simple structure opening internally as one, or rarely two slits and externally as a simple aperture or raised tube. The form of the internal lipped process differs being variously raised, flush with the valve surface, having a curved, straight or crenulated slit. The arrangement of these processes is often diagnostic. In some genera, such as *Coscinodiscus*, there may be one or more larger rimoportulae, referred to as macro-rimoportulae. The rimoportulae have been considered to be important in the secretion of the mucilage used to attach cells to each other or the substratum (Round *et al*., 1990) (Figure 1.3a).

Other processes include the occluded process, a hollow tube which is occluded at one end (Figure 1.3b). Spines are closed or solid structures protruding from the valve. These may be full spines, spinules or small spines or granules, which are small rounded projections on the valve face. Setae are hollow projections of the valve extending beyond the valve margin occurring in certain genera such as *Chaetoceros*. Where the setae are used to join adjacent valves in colonial forms, terminal setae may also occur, which facilitate a break in the colonial chain (Anonymous, 1975).

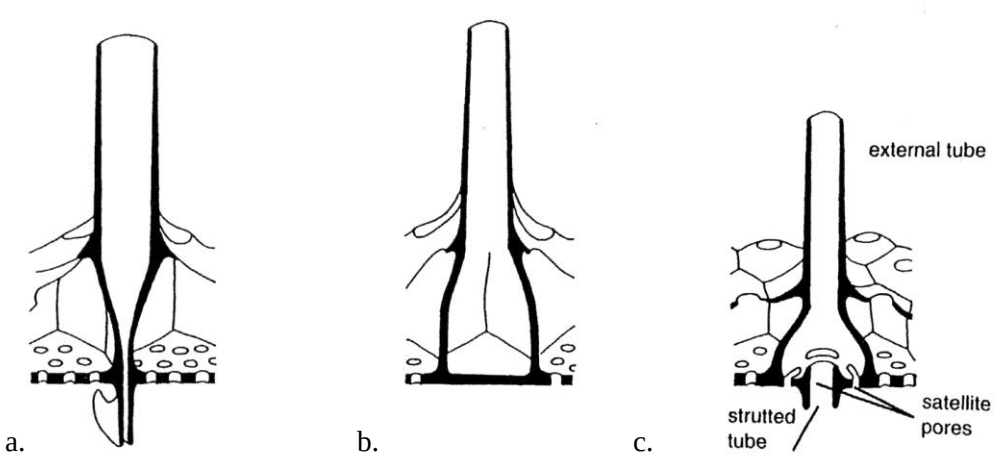

Fig 1.3 Variations in frustule portule morphology a) rimoportula or labiate process b) occluded process c) strutted process or fultoportula (Hasle & Syvertsen, 1997).

4.1.3 Colonial organisation

Colonial forms employ a number of different modes of connection between individual frustules. These include linkages by siliceous structures such as spines, linkages by mucilage pads or stalks, the inclusion of cells within mucilage tubes, envelopes or sheaths and colonies held together by threads or filaments of polysaccharide (Round *et al.*, 1990).

4.2 Frustule Morphology and Terminology

4.2.1 Introduction

With the advent of electron microscopy it became possible to identify ever more detailed morphology of the diatom frustule. Attempts were therefore made to standardise the terminology used to describe the frustule. Notable among these publications were 'Proposals for the Standardization of Diatom Terminology' (Anonymous, 1975), 'An Ammended Terminology for the Siliceous Components of the Diatom Call Wall' (Ross *et al.*, 1979), and 'A Guide to the Morphology of the Diatom Frustule' (Barber & Haworth, 1981). Further detailed terminologies have been developed specifically for both pennate (Mann, 1978, 1981;

Cox & Ross, 1981, Williams 1985, 1986) and centric diatoms (Hasle *et al* 1983; Sundstrőm, 1986; Rine & Hargraves 1988). As the majority of species in this study are centric, an emphasis is placed on describing the morphology and terminology employed for these forms rather than for pennate forms.

4.2.2 Morphology and Terminology

Valve outline varies greatly between diatom species. While pennate forms almost always exhibit bipolar symmetry, there are also tetrapolar and triradiate forms. Centric forms are predominantly circular. They may however maintain rotational symmetry with two or more poles, be semi circular, triangular and polygonal forms (Round, 1990). The diagnostic features of the diatom frustule are further defined with respect to the angle from which they are viewed (Figure 1.4a). The valve outline in valve view may be determined by the outline of the valve face or by the valve face and valve mantle. The valve mantle is the marginal area of the valve face distinguished by a slope and also in certain forms by its structure (Anonymous, 1975). The dimensions of the diatom frustule may be defined with respect to the dimensions of defined planes and axes (Figures 1.4b and 1.4c).

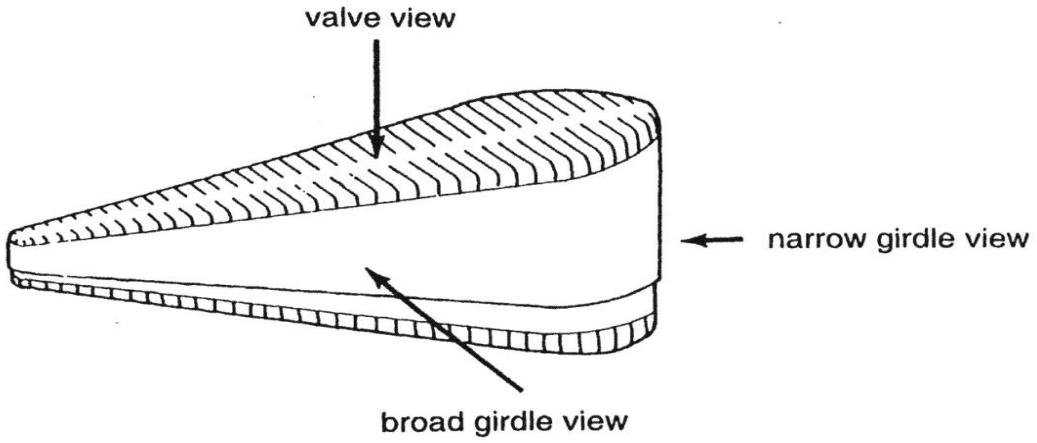

a

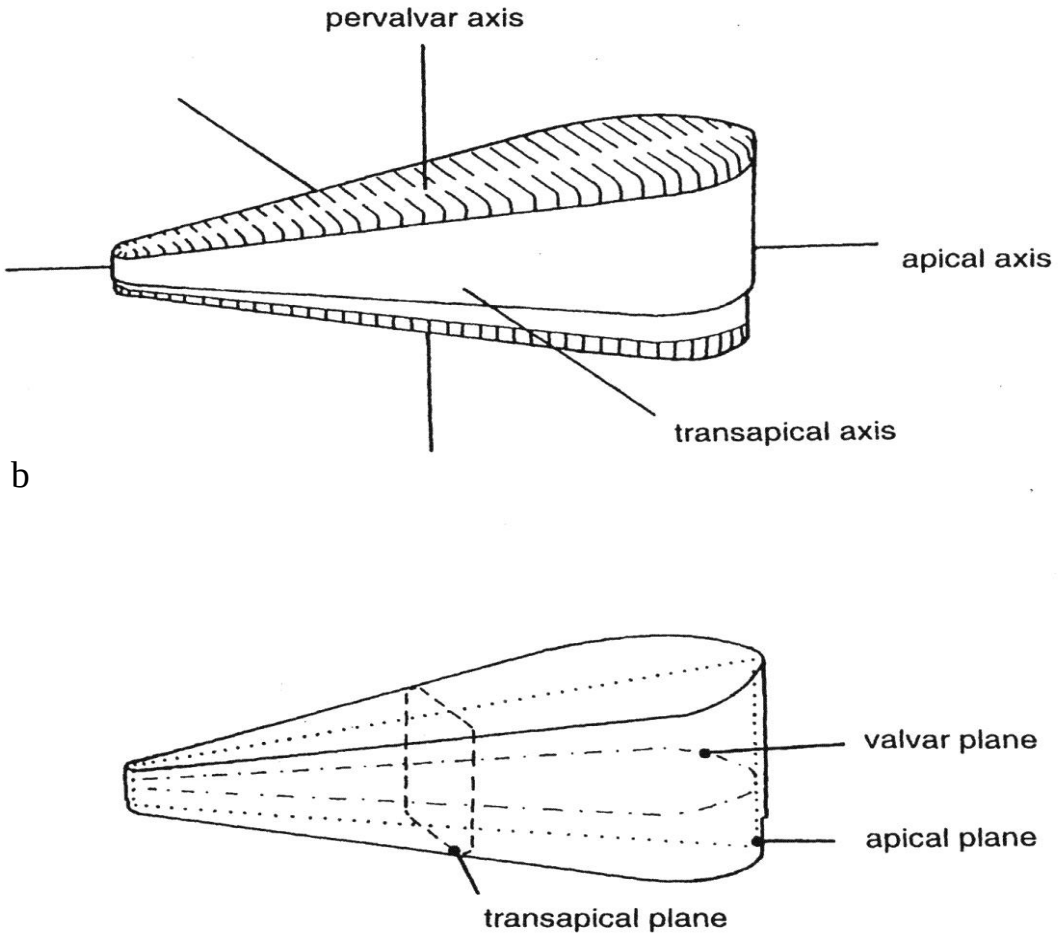

Figure 1.4 Views, axes and planes of the diatom frustule. a) views b) axes c) planes (Hasle & Syvertsen, 1997)

The two halves of the diatom cell or valves fit together in a similar manner to a pill box or petri dish (Figure 1.5). The larger of the two valves is referred to as the epitheca and the smaller the hypotheca. Attached to each of the valves are one or more connecting bands known as intercalary bands or copulae. The band immediately adjacent to the valve is referred to as the valvocopula and may have a distinct morphology from subsequent intercalary bands. The intercalary bands connected to the epivalve constitute the epicingulum and those connected to the hypovalve, the hypocingulum. The epicingulum and hypocingulum together make up the girdle. The two valves together with the girdle constitute the diatom frustule (Hasle & Silvertsen 1997).

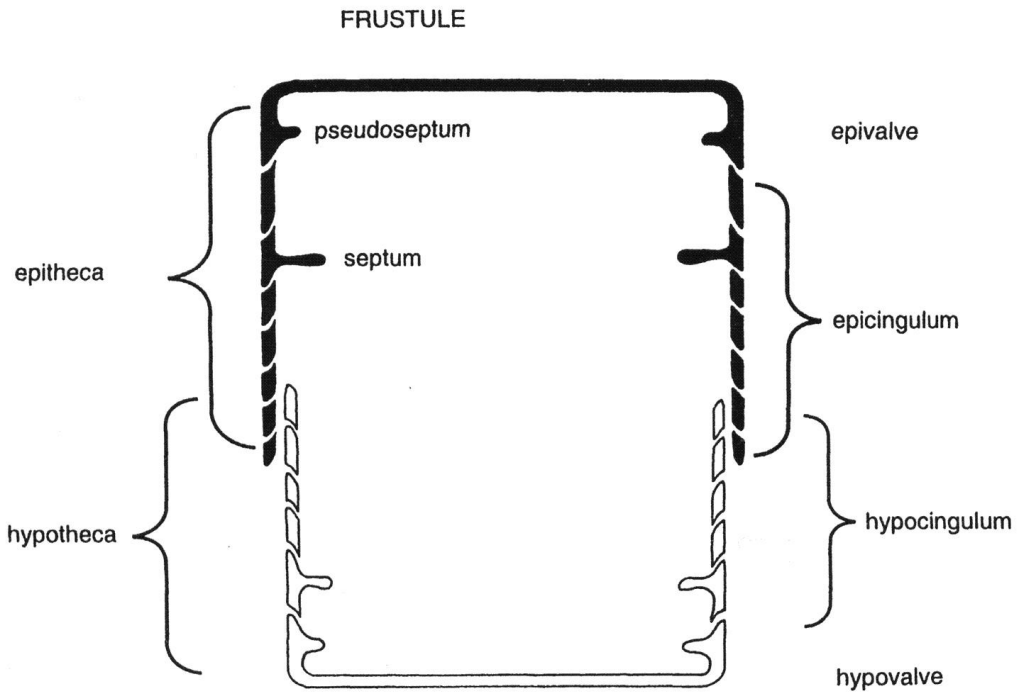

Figure 1.5 Morphology of the diatom frustule (Hasle & Syvertsen, 1997)

An important diagnostic feature of centric diatoms is the nature of their areolation. (Figure 1.6) Tangential areolation occurs where striae form lines across the valve. Where these are straight lines the areolation is referred to as linear. Where areolae run in spiralling arcs the areolation is referred to as decussate. Radial areolation occurs where the striae run from the valve centre to the margin. Fasiculate areolation is areolation that appears to be grouped into sections or bundles across the valve. This may occur with striae running parallel to the long edge of the bundle or with the longest striae running through the centre of the bundle.

Rhizosolenid centric forms have their own nomenclature which was developed largely by Sundström (1986) (Figure 1.7). The process is an elongated section of the valve fitting into a groove on the adjacent valve. The otaria are a pair of membranous costae situated near or at the base of the process. The claspers are membranous structures which clasp the otaria of the adjacent valve. The contiguous area occurs on the ventral side of the valve and joins

the otaria to the claspers, usually has a low marginal ridge and marks the area in contact with the adjacent valve (Hasle & Silvertsen, 1997).

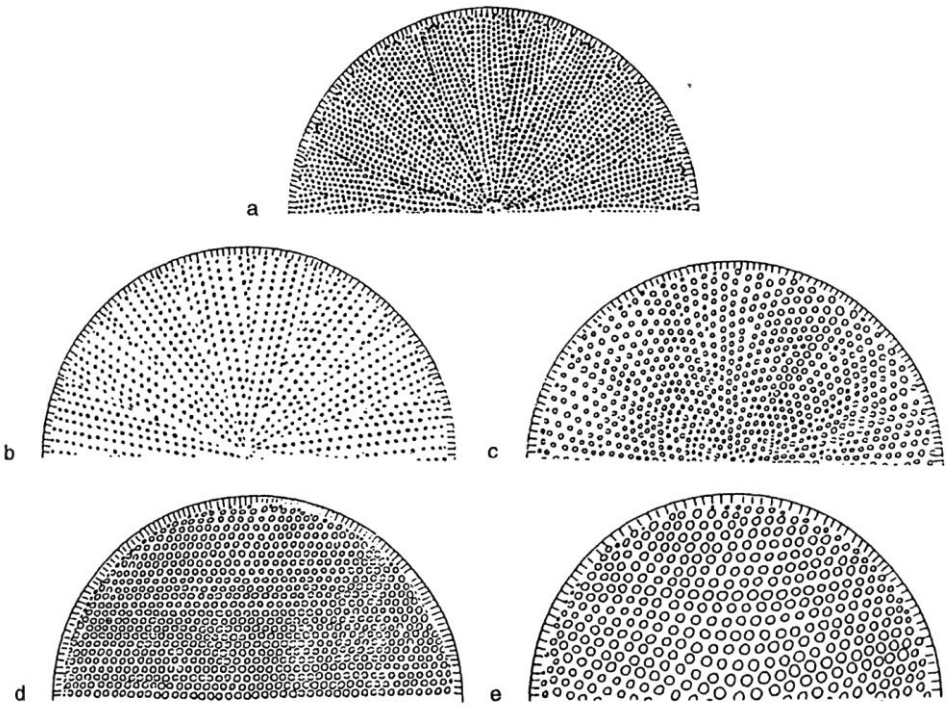

Figure 1.6 Forms of valve striation in centric diatoms a) 'curvatulus' type fasiculation: striae are parallel to the long edge of the striae bundle b) fasiculation: striae parallel to central long stria c) radial striae running from the centre to valve margin with shorter striae inserted. d) linear or tangential straight striation e) tangential curved striae. After Hasle & Syvertsen (1997).

4.3 Life cycle

The production of resting spores and the nature of the reproductive cycle, causing both an overall reduction in frustle size and the periodic production of auxospores, specialised cells developed to restore frustule size in some species, have taxonomic implications in diatoms as an individual species may exhibit different size ranges and morphologies.

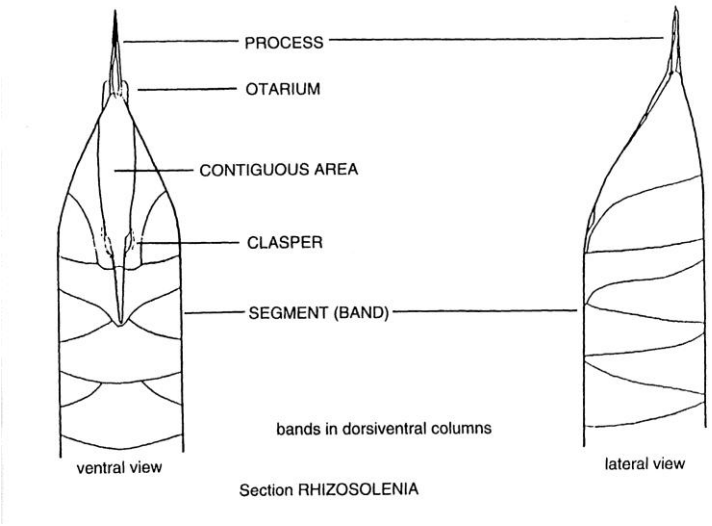

Fig 1.7 Terminology for Rhizosolenid morphology (Halse & Syvertsen, 1997)

4.3.1 Resting stages and resting spores

Diatoms are capable of exhibiting dormancy. In certain species, notably many marine centric and some few marine pennate forms, these resting stages result in the formation of a morphologically distinct resting spore (McQuoid & Hobson, 1996). In other species, predominantly subaerial and freshwater forms, the vegetative cell itself simply becomes dormant (Stockner & Lund, 1970). Some resting spores differ only marginally from their vegetative form eg *Thalassiosora nordenskioeldii* (Syvertsen, 1979). In other forms the resting spore is so morphologically distinct that it has resulted in it being classified in a different genera to the vegetative form (Hargreaves, 1986). Resting spores, like vegetative forms, have two valves. These valves are usually simpler in shape, thicker and less porous than those of the vegetative form and often exhibit spines or nodules. They rarely exhibit a well-developed girdle (Round *et al*, 1990).

There has been limited study on the longevity of resting stages and resting spores. No morphologically differentiated marine centric resting spores are known to last longer than two years. Survival rates are best in these marine forms in low temperatures and light. However, their longevity is limited by anoxic conditions (Hargreaves & French, 1983). The reasons for resting spore development are debated. It is general accepted that resting spores

are formed as a response to environmental stress. Changes in a number of environmental factors have been found to trigger the development of resting spores. These include temperature, light intensity, nutrient availability and pH (Round *et al.*, 1990). Nitrogen deficiency seems to be the key trigger in most resting spore forming species (Hargreaves & French, 1983). In marine forms, it is usually nutrient depletion that induces resting spore formation as other environmental variables such as light, temperature and salinity may be considered relatively stable (Davis *et al.*, 1980). However, resting spore formation can be considered as a response to rapid environmental change as it involves the two mitoses and the deposition of two new valves a process for example in *Chaetoceros* didymium 6-48 h (von Stosch *et al*, 1983). Two main theories prevail, that resting spore formation is employed to induce sinking at the end of a diatom bloom when nutrient levels are limited and that resting spores are formed as a predation-resistant stage to reduce grazing (Hargreaves & French, 1983). If resting spores are produced to induce sinking, it is unclear why the morphology of the resting spore cell should be so complex. Increased density and sinking rates as this could be achieved by simply thickening the vegetative cell and in many cases the resting spore cell remains encased in the parent vegetative cell (Round *et al.*, 1990). Resting spores germinate to produce vegetative cells in two ways after dormancy. Where the resting spore includes a girdle, the valves form the epitheca for two new vegetative cells eg in *Thalassiosira* (Hasle & Syvertsen, 1997). Where the resting spore has no girdle, the resting spore is shed during the production of new vegetative cells eg in *Bacteriastrum* and *Chaetoceros* (von Stosch *et al.*, 1973).

4.3.2 Reproduction

The usual method of reproduction in diatoms is asexual cell division. The valves of the parent cell become the epithecas of the daughter cells. Each daughter cell then produces a new hypotheca. As a result of this form of cell division, one daughter cell will be the same size as the parent cell and the other will be smaller (Figure 1.8). This results in an overall reduction in valve size over time (Lee, 1999). Size reduction is generally slight between generations, but over many generations can be significant. Studies on *Coscinodiscus asteromphalus* showed a decrease in valve diameter from 200 to 50μm (Werner, 1978).

As previously noted, size reduction can cause problems with classification especially when the potential size range for a particular species is unknown. Furthermore, while in centric forms the valve dimensions are little changed by size reduction; in pennate forms there can often be a significant alteration in valve outline with size reduction. In general, the width of pennate forms decreases proportionately less than the length with each successive generation. This leads to a predictable pattern of change in the valve outline of pennates. Linear forms become linear-lanceolate, then oval and even circular (Geitler, 1932; Round *et al.*, 1990). In some species of diatoms the daughter valves can also differ from the parent in their degree of silicification, also leading to difficulties with taxonomy. This has been noted to be a consideration in the genus *Thalassiosira* (Hasle *et al* 1971).

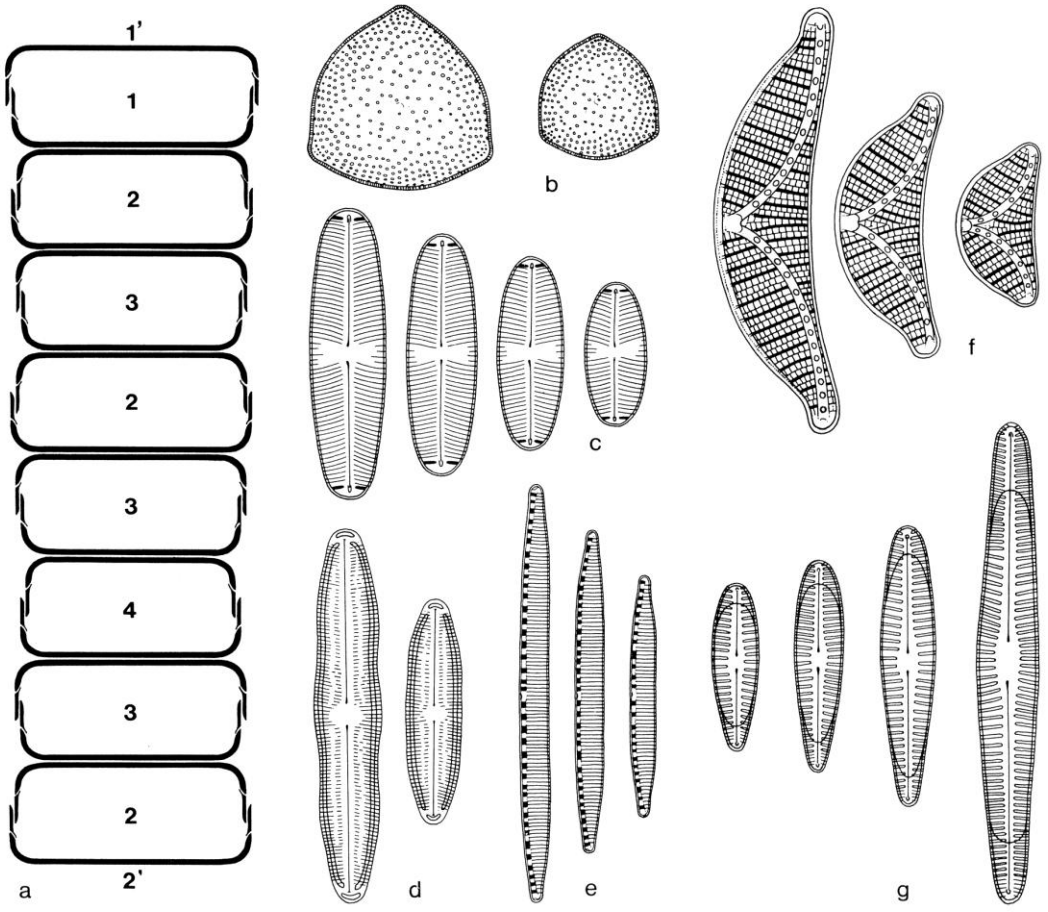

Figure 1.8 Changes in frustule morphology with reduction in cell size resulting from asexual division. a) the division of one cell to form a chain of eight. Valves 1 and 2 are the epivalve and hypovalve of the original cell. b-g show size and shape variations with cell division in a number of different forms b)*Stictodiscus* c) *Sellaphora* d) *Brachysira* e) *Nitzschia* f) *Epithemia* g) *Rhoicosphenia* A large number of cell divisions are required to form the changes from largest to the smallest forms indicated. (

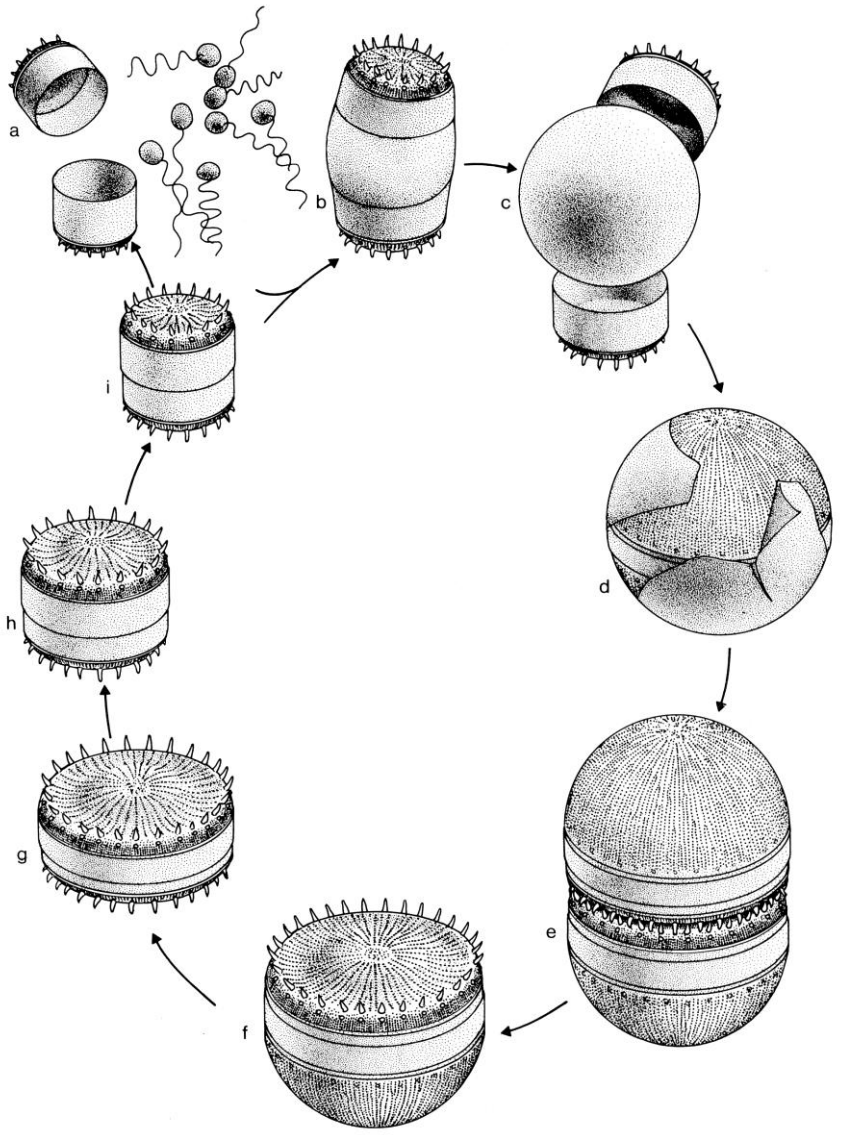

Figure 1.9 The diatom life cycle, based on the form *Stephanodiscus.* a) formation of motile gametes b) formation of auxospore c) auxospore detaches from original cell d) auxospore wall breaks open to reveal initial cell e) first division of initial cell to form two normal new hypovalves f) one of the cells produced at stage 'e' consisting of a normal valve and an initial cell valve g) a cell formed following several divisions of form 'f' h)-i) vegetative size reduction leading to the smallest cell which gives rise to male or female gametes. After Round *et al.* (1990)

Sexual reproduction and the formation of auxospores restore valve size in diatoms after a period of asexual cell division. The auxospore first forms as an organic wall. A cell sheds its silica theca, forming a sphere surrounded by an organic membrane. In some centric genera this membrane also contains siliceous scale eg *Melosira* (Crawford, 1974a). A new diatom frustule of maximum size, the initial cell, is formed within the auxpspore. This initial cell

may vary morphologically from the normal vegetative cell (Figure 1.9). Auxospores may be exogenous, semi endogenous or fully endogenous even within the same species (Figure 1.10). This has had taxonomic implications within different forms being identified as different species (Hasle & Syvertsen, 1997). Auxospore development usually occurs when the vegetative cell has reduced to around one third of its maximum size. This appears to be a threshold size beyond which the vegetative cell continues to divide and reduce in size, but can no longer create an auxospore (Drebes,1977).

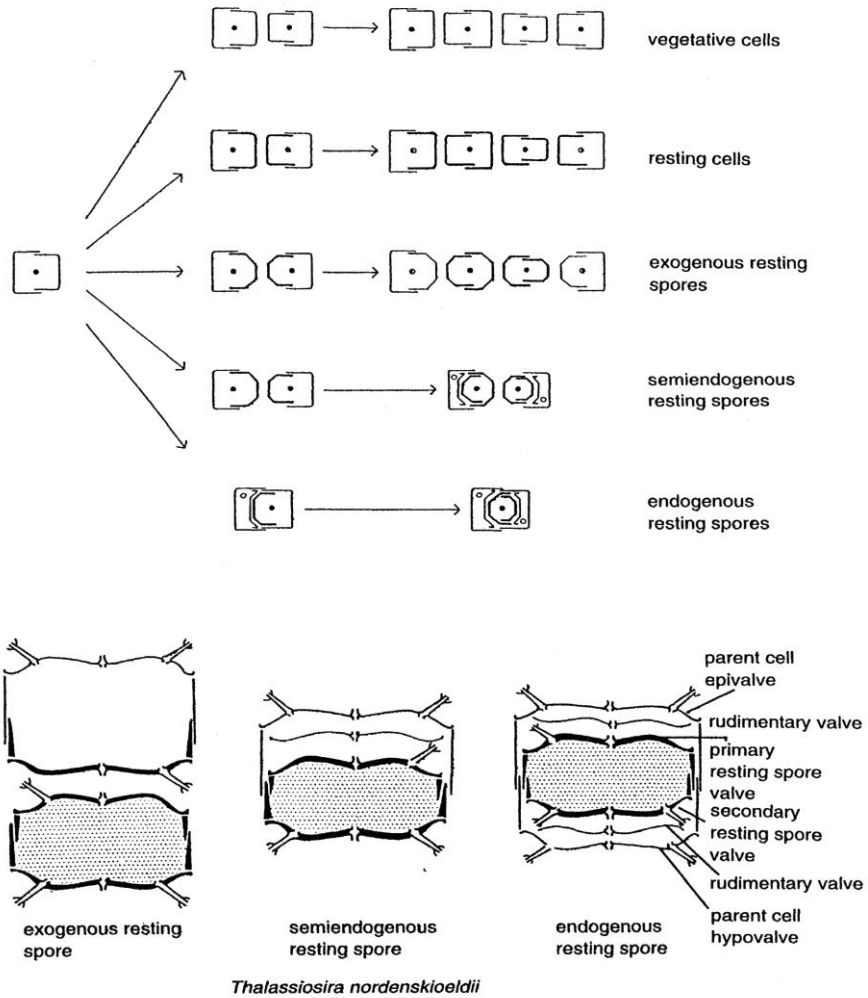

Figure 1.10 The formation of vegetative cells, resting cells and resting spores from a vegetative parent cell for *Thalassiosira nordenskioeldii.* (Hasle & Syvertesen, 1997) exogenous resting spores are formed externally from the parent cell. endogenous resting spores are formed internally from the parent cell.

Appendix Two

Diatom Taxonomic Descriptions

"That evening Nelson gave us his second biological lecture, starting with a brief reference to the scientific classification of organisms into Kingdom, Phyllum, Group, Class, Order, Genus, Species..."

Robert Falcon Scott 'Journals'

2.1 Diatom Systematics

Historic classification schemes for diatoms such as that of Schűtt (1896) were based on differences in the morphology of the silica frustule. In the late twentieth century, the advent of improved microscopy, both light and scanning electron microscopy and diatom culturing, led to a number of revised taxonomies (Ross & Sims, 1973; Simonsen, 1979; Gleser, 1985; Nikolaev, 1988; Round & Crawford, 1981; Round & Crawford, 1984). These classification systems vary with respect to the emphasis they place on different morphological features but also with respect to reproductive strategies. The fundamental division between centric and pennate forms has, until recently, remained central to diatom classification systems. Round *et al.* (1990) recognised three basic divisions, based on the morphology of the silica frustule, the type of reproduction and the plastid morphology; Coscinodiscophyceae (centric diatoms), Fragillariophyceae (araphid pennate diatoms) and Bacillariophyceae (raphid pennate diatoms).

Most recent research into RNA (Kooistra & Medlin, 1996; Medlin *et al*, 1996a; Medlin & Kacmarska 2004; Kooistra *et al.*, 2007) has lead to further taxonomic revisions based on molecular rather than morphological relationships between species. Medlin *et al*. (1996a) analysed the RNA of thirty taxa from eleven different orders and concluded that neither the historically accepted subdivision of diatoms into pennate and centric forms, nor the three classes recognised by Round *et al.* (1990) had significance on a molecular level. Instead they proposed the basic subdivision of diatoms into two clades: Clade I consisting of the centric diatoms with labiate processes located peripherally in the cell wall, Clade II consisting of the pennate diatoms, centric diatoms with central strutted processes and bipolar and multipolar centric diatoms with central labiate processes. Medlin & Kooistra (2004) proposed a revision of diatom taxonomy based on this research. This revision recognises two divisions of the diatoms (Bacillariophyta) the Coscinodiscophytina and the Bacillariophytina and three classes; the Coscinodiscophyceae the Mediophyceae and the Bacillariophyceae. They also define which orders of diatoms according to Round *et al.* (1990) should be assigned to each class. This is the taxonomy adopted in this study.

Division	Bacillariophyta
Subdivision	Coscinodiscophytina
Class	Coscinodiscophyceae
Order	Coscinodiscales, Corethrales, Rhizosoleniales, Melosirales, Orthpseirales, Aulacoseirales, Chrysanthemodiscales, Stictocyclales, Asterolamprales, Arachnoidiscales, Stictodiscales, Ethmodiscales and Leptocylindrales
Subdivision	Bacillariophytina
Class	Mediophyceae
Order	Chaetocerotales, Biddulphiales, Cymatosirales, Thalassiosirales, Triceratiales, Hemiaulales, Lithodesmiales, Toxariales and a suspected bipolar centric (= Aridissoneales)
Class	Bacillariophyceae
Order	Fragilariales, Tabellariales, Licmophorales, Raphoneidales, Thalassionematales, Rhabdonematales, Eunotiales, Lyrellales, Mastogloiales, Dictyoneidales, Cymbellales, Achnathales, Naviculales, Thalassiophysales, Bacillariales, Rhopalodiales and Surirellales

Table 5.1 Taxomic subdivisions of diatoms.
After Medlin &Kooistra (2004).

A full list of the taxa encountered in this study is provided below.

Subdivision Coscinodiscophytina
Class Coscinodiscophyceae
Orders Coscinodiscales, Rhizosoleniales, Asterolamprales

Order Coscinodiscale
Families Coscinodiscacae, Hemidiscaceae

Family Coscinodiscacae
Genera Coscinodiscus, Stellarmina

2.1.1 *Coscinodiscus*

Coscinodiscus asteromphalus
Coscinodiscus linearis
Coscinodiscus marginatus
Coscinodiscus radiatus
Coscinodiscus occulus-iridis

2.1.2 *Stellarmina*

Stellarmina stellaris

Family Hemidiscaceae
Genera *Actinocyclus, Azpeitia, Hemidiscus, Roperia*

2.1.3 *Actinocyclus*

Actinocyclus curvatulus
Actinocyclus kutzingii
Actinocyclus octinarius

2.1.4 *Azpeitia*

Azpeitia africana
Azpeitia neocrenulata
Azpeitia nodulifera

5.2.5 *Hemisdiscus*

Hemidiscus cuneiformis

5.2.6 *Roperia*

Roperia tesselata

Order Rhizosoleniales

Family Rhizosoleniaceae

Genera *Proboscia, Rhizosolenia*

5.2.7 *Proboscia*

Proboscia alata

5.2.8 *Rhizosolenia*

Rhizosolenia begonii

Rhizosolenia borealis

Rhizosolenia hebetata hebetata

Rhizosolenia hebetata semispina

Rhizosolenia styliformis

Order Asterolamprales

Family Asterolampraceae

Genera *Asteromphalus*

5.2.9 *Asteromphalus*

Asteromphalus robustus

Subdivision Bacillariophytina

Classes Mediophyceae, Bacillariophyceae

Class Mediophyceae

Orders Chaetocerotales, Thalssiosirales

Order Chaetocerotales

Family Chaetocerotaceae

Genera *Bacteriastrum*

5.2.10 *Bacteriastrum*

Bacteriastrum hyalinum

Order Thalassiosirales

Family Thalassiosiraceae

Genera *Bacteriosira, Porosira, Thalassiosira*

5.2.11 *Bacteriosira*

Bacteriosira fragilis

5.2.12 *Porosira*

Porosira glacialis

5.2.13 *Thalassiosira*

Thalassiosira angulata

Thalassiosira auguste-lineata

Thalassiosira eccentrica

Thalassiosira ferelineata

Thalassiosira gravida

Thalassiosira hyalina

Thalassiosira lineata

Thalassiosira nodulineata

Thalassiosira nordenskioeldii

Thalassiosira oestrupii

Thalassiosira pacifica

Thalassiosira trifulta

Class Bacillariophyceae

Order Bacillariales, Fragilariales, Thalassionematales

Order Bacillariales

Family Bacillariaceae

Genera *Alveus, Fragilariopsis, Nitzschia*

5.2.14 *Alveus*

Alveus marina

5.2.15 *Fragilariopsis*

Fragilariopsis atlantica

Fragilariopsis cylindrus

Fragilariopsis doliolus

Fragilariopsis rhombica

Fragilariopsis oceanica

5.2.16 *Nitzschia*

Nitzschia braarudii

Nitzschia bicapitata

Nitzschia kolazczekii

Order Fragilariales

Family Fragilariaceae

Genera *Synedra*

5.2.17 *Synedra*

Synedra sp

Order Thalassionematales

Family Thalassionemataceae

Genera *Thalassionema, Thalassiothrix*

5.2.18 *Thalassionema*

Thalassionema nitzschoides

Thalassionema nitzschoides var. *parva*

5.2.19 *Thalassiothrix*

Thalassiothrix longissima

Subdivision	Coscinodiscophytina
Class	Coscinodiscophyceae
Orders	Coscinodiscales, Rhizosoleniales, Asterolamprales

Order	Coscinodiscales
Family	Coscinodiscacae
Genera	*Coscinodiscus, Stellarmina*

2.1.1 ***Coscinodiscus*** Ehrenberg 1839 amend. Hasle & Sims 1986

Lectotype: *Coscinodiscus argus* Ehrenberg

Generic Characteristics: Cells are discoid and vary from coin to barrel shaped. In some forms the valve mantle is deeper on one side. The valves are saucer shaped to petri-dish shaped. Valve faces are flat or sometimes centrally depressed. Extant forms are round in outline, but triangular and ovoid fossil forms occur. Areolae radiate from a central annulus and may be fasiculated or grouped in decussating arcs. This type of areolation necessitates the presence of incomplete striae. Sectors of striae are separated by more or less distinct unperforated radial areas (wide interstriae, hyaline spaces or lines). The valve centre is characterised by either a hyaline area or rosette of central larger areolae. The valves are loculate, with complex external vela and internal foramina which are often rimmed and smaller on the valve mantle. There is a marginal ring of smaller labiate process and two larger marginal labiate processes (macro-rimoportule) (Round *et al.*, 1990; Hasle & Syvertsen, 1997).

Characteristics distinguishing species: The cell shape and diameter. The valve shape. The pattern and size of areolae. The height of the mantle. The shape of central the area. The presence or absence of hyaline lines. The shape of and distance between larger processes. The distance between the smaller marginal processes. The presence or absence of processes on the valve face. The chloroplast outline. Summarised from Hasle & Syvertsen (1997).

Discussion: *Coscinodiscus* has historically been one of the largest marine planktonic genera. However, recent studies have transferred many of these species to other genera especially *Thalassiosira*, *Azpeitia* and *Actinocyclus*. Hasle & Sim (1986) suggested clarification of the generic characteristics of *Coscinodiscus* based on the morphology of the type species *C.argus*. Hasle & Lange (1992) note a number of problems with the identification of *Coscinodiscus* species. They suggest that for many *Coscinodiscus* species the original descriptions are insufficient to enable accurate identification of closely related forms and that species are identified on the basis of tradition rather than strict morphological data. Many fossil species described by Ehrenberg have been based on types and illustrations of valve fragments. Holotypes have not always designated for the original descriptions. Certain authors have solved this problem by assigning lectotypes, such as Boalch (1971) for *C.concinnus* W.Smith and *C.granii* Gough. Many species have been identified from the same type localities so recollecting original material may not be helpful. Ehrenberg (1844) described fifteen different *Coscinodiscus* species from Richmond Virginia. They therefore attempt to clarify the descriptions of five *Coscinodiscus* species with respect to recognisable morphological features (Halse & Lange, 1992).

Coscinodiscus asteromphalus Ehrenberg 1844a

Description: Girdle view: valves are slightly depressed at the centre with a gently sloping mantle. There are two rows of areolae on the valve mantle. Valve view: The valves are circular, slightly convex, 80-400µm in diameter. Markov (1993) refers to the areolation pattern as radial with secondary decussate rows, Hasle & Syvertsen (1997) as decussate, with no hyaline lines. There are 3-5 areolae in 10µm near the centre of the valve and 6-7 at the valve margin. The centre of the valve has a rosette of somewhat larger areolae. The cribia have few pores with a larger ring of pores on the outside. There are two rows of areolae on the valve mantle. There is one ring of labiate processes close to valve margin, 4-6 in 10µm with 4 areolae between processes. The larger labiate processes are 120-135˚ apart. The outer opening of the larger processes is circular, the inner opening a prolonged slit coiled into spirals (Markova, 1993; Hasle & Syvertsen 1997).

Discussion: *C.asteromphalus* may be distinguished from *C.concinnus* by the distinct central rosette of areolae, smaller areolae and a deeper mantle (Hasle & Lange, 1992). *C.asteromphalus* may be distinguished from *C.argus* and *C.centralis* by having the ring of labiate processes closer to the margin (Hasle & Syvertsen, 1997).

Coscinodiscus marginatus Ehrenberg 1844a

Description: Girdle view: Valves are flat or nearly flat with a straight or deeply sloping mantle. There are two rows of large, elongated vertical pores on the mantle. Valve view: Valves are circular, 35-200µm in diameter. There is no central rosette. Areolae are coarse and in irregular radial rows with no hyaline lines, 1-3 areolae in 10µm at the centre and 2-4 near the margin. The cribia are in rings of pores with an outer ring of larger pores. There is one ring of marginal labiate processes, 2 in 10µm with 2 areolae between each process. The larger labiate processes have a circular or elongate external opening and an internal opening which is a short stalk with a strongly curved slit. Cribia resemble many pointed stars or flowers (Markova, 1993; Hasle & Syvertsen, 1997).

Discussion: *C.marginatus* is distinguished by its very coarse areolation

Coscinodiscus oculus-iridis

Description: Valves are circular with a concave centre. Areolation is radial with shorter rows near the margin. There are 3-4 areolae in 10µm at the centre and 5-6 near the margin. The centre of the valve is hyaline or has a few larger areolae. Cribia have 4-9 (usually 7-8) pores arranged in a small flower shape. There are two rows of small elongate vertical areolae on the valve mantle.

Coscinodiscus radiatus Ehrenberg 1841a

Description: Valves are circular, 30-180µm in diameter. In girdle view, valves are flat in with a concave centre and two rows of slightly elongate areolae on the valve mantle.

Areolation is characteristically regularly radial. Hasle & Syvertsen (1997) note that it may also sometimes appear indistinctly decussate. There are 3-4 areolae in 10µm at the centre and 5-6 near the margin. There are no hyaline lines. There is an indistinct central rosette of slightly larger areolae. One ring of small marginal labiate processes at the point of origin of incomplete striae 2-3 in 10µm and 3-4 areolae apart. There are two larger labiate processes 135˚ apart with large circular external openings and opening with long curves flattened tubes internally (Markova, 1993; Hasle & Syvertsen, 1997).

2.1.2 ***Stellarima*** Hasle & Sims 1986

Type: *Stellarima microtrias* (Ehrenberg) Hasle & Sims
Basionym: *Symbolophora? microtrias* Ehrenberg
Synonyms: *Cosconodiscus symbolophorus* Grunow
Coscinodiscus furcatus Karsten
Symbolophora furcata (Karsten) Nikolaev

Generic Characteristics: Valves are circular and convex. There is no distinct mantle. Areolae are small, loculate, opening internally with domed closing plates and externally simply or as cribia. Areolation is radial and fasiculate, striae are uniseriate. There are 1-15 labiate processes located in a ring at the centre of the valve, opening externally with slit like openings. There are no marginal processes (Round *et al*, 1990; Hasle & Syvertsen 1997).

Characteristics distinguishing species: The convexity of valve, whether the areolation is fasciculate or furcate, the size of the areolae and the number of areolae per sector (Hasle & Syvertsen, 1997).

Discussion: *Coscinodiscus stellaris* and *C.stellaris* var. *symbolophora* were moved to the genus *Coscinosira* on the basis of the central labiate processes. *Coscinosira* was then moved to the genus *Thalassiosira* on the basis of having strutted processes. *Stellarmina* was therefore proposed as a new genus (Hasle & Sims, 1986).

Stellarima stellaris Roper

Basionym: *Coscinodiscus stellaris* Roper

Description: Valves are lightly silicified, circular and convex, 40-115µm in diameter. Areolation is radial and fasiculate, with 18-22 striae in 10µm and 15-16 areolae in 10µm. There is a central ring of slit-like labiate processes and no marginal processes (Hasle & Syvertsen, 1997).

Ecology: warm water region to temperate, planktonic (Hasle & Syvertsen, 1997).

Family Hemidiscaceae

Genera *Actinocyclus, Azpeitia, Hemidiscus, Roperia*

2.1.3 *Actinocyclus* Ehrenberg 1837

Lectotype: *Actinocyclus octonarius* Ehrenberg

Generic Characteristics: The valve outline is circular and the valve mantle deep and straight or stepped thus forming barrel-shaped cells. The valve face is planar or concentrically waved with a corrugate surface. The areola pattern is usually fasciculate, with a marginal zone often denser in areolation and/or aereolated in a different direction to the striae. The central annulus varies in size and presence. There is a marginal ring of labiate processes, but no labiate process in the valve centre. The single marginal pseudonodulus is variable in size (Round *et al.*, 1990; Hasle & Syvertsen, 1997).

Characteristics distinguishing species: The type of fasciculation. The position of the labiate processes, whether the annulus and pseudonodulus are distinct or indistinct and the position of pseudonodulus (Hasle & Syvertsen, 1997).

Discussion: Simonsen (1975) defined the pseudonodulus as the key diagnostic feature in all *Hemidiscaceae*; all genera having a single marked pseudonodulus on each valve.

Actinocyclus being further defined as the genus in this family with a circular valve outline. As a result of this a number of species were transferred to the genus *Actinocyclus* on identification of a pseudonodulus with improved microscopy. Watkins and Fryxell (1986) however questioned the primary importance of the peseudonodulus as a diagnostic taxonomic feature in *Actinocyclus*.

Actinocyclus curvatulus Janisch 1878

Synonyms: *Coscinodiscus curvatulus* var *subocellatus* Grunow
Actinocyclus subocellatus (Grunow) Rattray

Description: Valves circular, 13-160µm in diameter. The areolation is radial and fasciculate with a marginal process at the end of each row of fascicles. Radial areola rows are parallel to edge (side) row with 8-18 areolae in 10µm. The areolae decrease in size towards the margin. There are10-12 marginal processes in 10µm. The central annulus is irregular in shape. A small irregular pseudonodulus is located close to the valve mantle. The fasiculate areolation is diagnostic in *Actinocyclus curvatulus* (Hasle & Syvertsen, 1997).

Ecology: Cosmopolitan (Hasle & Syvertsen, 1997).

Actinocylclus kutzingii A.Schmidt 1878

Basionym: *Coscinodiscus kutzingii* A.Schmidt 1878

Description: Valves are circular, 30-70µm in diameter. The areolation is fasiculated with secondary, curved rows. There are 7-8 areolae in 10µm. Radial areola rows are parallel to central row, with a marginal process at end of the central row of each fascicle. *A.kutzingii* has a fairly wide marginal zone with small areolae in two crossing systems. The central annulus is small. The pseudonodulus is very small and obscure (Hasle & Syvertsen, 1997).

Ecology: Known from North Atlantic coastal waters (Hasle & Syvertsen, 1997).

Actinocyclus octonarius Ehrenberg

Synonym: *Actinocyclus ehrenbergii* Ralfs in Pritchard

Description: Valves are circular, 50-300µm diameter with 6-8 areolae in 10µm. The areolation is distinctly fasciculate; the fascicles being separated by pronounced complete striae running from margin to central annulus. Fasiculation is further accentuated by hyaline areas adjacent to complete striae giving the appearance of the valve face being divided into distinct segments. There is a wide marginal zone with smaller areolae than on valve face. Processes positioned at the edge of end rows. The pseudonodulus is large and positioned on the junction of the valve face and mantle (Hasle & Syvertsen, 1997).

Discussion: Hustedt (1930) identifies four subspecies of *A.octinarius* based on the size and development of the central annulus, the width of the marginal zone and the amount of hyaline spaces (Hasle & Syvertsen, 1997).

Ecology: Cosmopolitan (Hasle & Syvertsen, 1997).

2.1.4 *Azpeitia* M.Peragallo in Tempére & Peragallo

Type: *Azpeitia temperi* M. Pergallo

Generic Characteristics: Valves are generally circular (although triangular and multiangular fossil forms occur) and flat. Areolae are in radiating rows. The valve mantle is shallow but distinct, (Round *et al.*, 1990) with a clear difference in areola pattern between the valve face and the mantle. A large, nearly central labiate process occurs usually on the edge of the central annulus, with a ring of large labiate processes at the edge of the valve mantle (Hasle & Syvertsen, 1997). The central labiate process often has a distinct raised external tube or nodule (Round *et al.*, 1990).

Characteristics distinguishing species: The valve face areolation, the pattern and size of areolae, the position and shape of annulus and the size of labiate processes (Hasle & Syvertsen, 1997).

Discusssion: Fryxell *et al.* (1986b) placed *Azpeitia* in the *Hemidiscaceae* on the basis of some fossil forms having a pseudonodulus.

Azpeitia africana (Janisch ex A.Schmidt) G.Fryxell & T.P. Watkins in Fryxell et al.

Basionym: *Coscinodiscus africanus* Janisch ex A.Schmidt

Description: Valves are circular to slightly elliptical, 30-90µm in diameter. Distinct external marginal slits lead to labiate processes. The central labiate process is on the edge of an eccentric circle of linearly arranged areolae. Areola rows radiate from the central annulus, in larger specimens in spiralling rows. 5-10 areolae in 10µm (Hasle & Syvertsen, 1997).

Ecology: Warm water region (Hasle & Syvertsen, 1997). Found in Indian Ocean sediments (Schrader, 1974). Tropical East Pacific (Barron, 1980b) and in Gulf Stream core rings, Central Pacific and Gulf of Mexico plankton tows (Fryxell *et al.*, 1986b).

Azpeitia nodulifera (A.Schmidt) G.Fryxell & P.A. Sims in Fryxell *et al.*

Basionym: *Coscinodiscus nodulifer* Grunow

Description: Valves are heavily silicified, flat, 20-102µm in diameter. The mantle is vertical. Areolation is radial with mixed large and small areolae. The mantle is vertical. (Halse & Syvertsen, 1997) The distinct ‘nodule’ on the valve surface is a nearly central labiate process with an external tube. The areola next to the process is notably depressed

and indicates where the process of the adjacent valve would have fitted (Fryxell *et al.,* 1986b).

Discussion: *A.nodulifera* has been confused with *A.baronii* as both species also have a distinct central nodule. (Fryxell *et al.,* 1986b)

Ecology: Warm water region (Hasle & Syvertsen, 1997). Found in plankton tows from the Central Pacific, Gulf of Mexico and Northwest Atlantic in Gulf Stream warm core rings (Fryxell *et al.,* 1986b).

Azpeitia neocrenulata (VanLandingham) G.Fryxell and T.P.Watkins in Fryxell et al.

Basionym: *Coscinodiscus neocrenulatus* Van Landingham 1968
Synonym: *Coscinodiscus crenulatus* Grunow 1884

Description: The valves are circular, 13-48µm in diameter. Areolation is fasiculate with radial rows of areolae usually parallel to an edge row, with a depression on the mantle at the edge of each row, 9-11 areolae in 10µm. Marginal labiate processes, with one large labiate process at the edge of a central annulus. The mantle is extremely fine in structure with 20 striae in 10µm (Hasle & Syvertsen, 1997). The distinct feature of *A.neocrenulata* is that the depressions on the valve margin adjacent to the labiate processes, give the valve outline a scalloped or crenulated appearance (Fryxell *et al.,* 1986b).

Ecology: Warm water region (Hasle & Syvertsen, 1997). Found in the tropical Indian Ocean (Schrader, 1974), the tropical Eastern Pacific (Barron, 1980b) and Gulf of Mexico, Central Pacific and Gulf Stream Core Ring in the North Atlantic (Fryxell *et al.,* 1986b).

2.1.5 ***Hemidiscus*** Wallich 1860

Type: *Hemidiscus cuneiformis* Wallach 1890

Generic characteristics: Girdle view: Valve face is flat with a shallow mantle with smaller areolae. Valve view: Valves are characteristically cuneiform often having a central swelling on the ventral margin. Areolation is radiate from an indistinct central annulus, irregularly fasiculate. Areolae are loculate opening externally as cribia, internally as foramina. There is a row of rimoportulae along the ventral margin which are expanded parallel to the valve margin. A single pseudonodulus is positioned slightly inward of the ventral line of rimoportulae. The copulae are more expanded dorsally then ventrally resulting in the two valves lying at an angle (Round *et al.*, 1990).

Characteristics distinguishing species: The size of the areolae. The distinction of the fasciculation and central annulus (Hasle & Syvertsen, 1997).

Discussion: *Hemidiscus* though similar in outline to *Palmeria* may be distinguished by the presence of the pseudonodulus. Simonsen (1972) recognises only two species of *Hemidiscus*, *H.kanayanus* and *H.cuneiformis* (Hasle & Syvertsen, 1997).

Hemidiscus cuneiformis Wallich 1860

Description: Valves are characteristically semi-circular, 58-288µm in length and 32.5-158µm wide. There are 6-9 areolae in 10µm at the centre of the valve and 10-13 areolae in 10µm at the margin (Hasle & Syvertsen, 1997).

Ecology: marine planktonic, warm water region (Hasle & Syvertsen, 1997). Hustedt (1930) notes that *H.cuneiformis* may be transported far north along the Norwegian coast

2.1.6 ***Roperia*** Grunow ex Pelletan 1889

Type: *Roperia tesselata* (Roper) Grunow ex Pelletan
Basionym: *Eupodiscus tesselatus* Roper

Generic Characteristics: Valves are circular. The valve face is flat with a distinct mantle. There is a characteristic large pseudonodulus near the valve rim, which is probably occluded by an organic wall or silica membrane in the living cell. The areolae are loculate, circular on the valve face to diamond-shaped on the mantle. The loculi open externally as cribria and internally as foramina. The areolation is decussate (Round *et al.*, 1990).

Discussion: Originally described by Grunow (1884), *Roperia* is closely related to *Actinocyclus* but with an asymmetrical mantle suggesting a relationship with *Hemidiscus*. (Fryxell & Hasle, 1974) Lee & Lee (1990) in their review of *Roperia tesselata* note the extent of taxonomic confusion that has been caused by the variation of external morphology at a species level and that revisions of species synonyms for *Roperia* have been made by Hustedt (1930), Hendey (1964) and Simonsen (1974). Lee & Lee (1990) recognise only three distinct species for the genus, *R.tesselata* (Roper) Grun, *R.marginata* Hanna (Hanna, 1931) and *R.excentrica* Cheng and Chin (Chin *et al.*, 1980).

Roperia tesselata (Roper) Grunow ex Pelletan

Description: The valve is circular to oval in outline, 40-70µm in diameter. There is one ring of uniform marginal processes, two processes in 10µm, and a single prominent pseudonodulus. The areolation usually differs from the centre of valve to the margin. There 6 areolae in 10µm at the centre of the valve (Hustedt, 1930; Tomas, 1997). Plate I 1-2

Ecology: Warm water zone as far north as 66^{o} N in the Norwegian Sea and 57^{o}S in the Subantarctic Pacific (Halse, 1976). Lee & Lee (1990) recognise two habitats for *Roperia tesselata*, a warm water western hemisphere habitat and a cold water North Pacific habitat. They identified different forms of *R.tesselata* with respect to these different habitats. The cold water form is larger, has rimoportulae with simple external openings (giving the valve a smooth outline) and decussate areolation. The warm water form is smaller, has rimoportulae openings with horizontal slits, slightly widened at the centre, (giving the valve a conspicuously undulate outline) and areolation that is linear at the centre and radial at the margins.

Discussion: Lee & Lee (1990) reviewed the range of morphologies reported for *Roperia tesselata*. They note varying recorded valve outline forms for the species, Fenner *et al.* (1976) state that *R.tesselata* is circular to asymmetrical in outline, while Fryxell *et al.* (1986) refer to the outline as round, oval or tear-drop shaped. A variety of areolation patterns are also reported for the species; linear (Mann, 1925; Fryxell& Hasle 1974; Fryxell et al 1986b), decussate (Roper, 1858; Van Heurck 1896) and linear at the centre with radial rows at the margin (Hustedt, 1930). Simonsen (1974) considers all variations in outline and valve edge as a series of transitional forms (Lee & Lee, 1990).

Order Rhizosoleniales
Family Rhizosoleniaceae
Genera *Proboscia, Rhizosolenia*

2.1.7 *Probosica* Sündstrom 1986

Type: ***Probisica alata*** (Brightwell) Sündstrom

Generic Characteristics: Cells are long, cylindrical and usually solitary. Valves are concoid, tapering slightly into a curved proboscis. There is a groove at base of the proboscis partially covered by two lateral flaps, in which proboscis of sister cell lies. The apex of the proboscis is obliquely truncate. Copulae are in two rows, rhomboidal in outline, giving the appearance of triangular segments (Round *et al.*, 1990).

Discussion: The genus *Proboscia* was proposed by Sündstrom (1986) as part of his revision of the genus *Rhizolsolenia*. The new genera was created for the species *Rh.alata* which was therefore renamed *Proboscia alata*, the type species of *Proboscia*. Sündstrom (1986) distinguished *Proboscia* from *Rhizolsolenia* on the basis of forms possessing a proboscis rather than a process with otaria, the presence of interlocular pores and a terminal auxospore. When *Proboscia* was first described it was a monspecific genus. Subsequently other species have been assigned to the genus, notably *Proboscia inermis* and *Proboscia truncata*, both species having been reassigned from *Rhizolsolenia* (Jordan *et al*. 1991).

Proboscia alata (Brightwell) Sündstrom

Basionym: *Rhizosolenia alata* Brightwell 1858
Synonyms: *Rhizosolenia bidens* Karsten 1905

Description: Cells are cylindrical and long, 2.5-13µm in diameter. The valve is conical and asymmetrical tapering to a slightly curved proboscis with a truncated tip with a short longitudinal slit. The claspers are of unequal length protruding slightly at their distal end. The copulae are in two columns, numerous, rhomboidal and with scattered interloculate areolae. The auxospore is terminal and may exhibit a bifurcate proboscis. The cells are usually solitary but may form chains of up to four individuals joined by the insertion of the proboscis into the claspers (Jordan *et al.*, 1991; Hasle & Syvertsen, 1997). Plate I 3-4

Discussion: A number of subspecies have been proposed for *Proboscia alata*; *P.alata* var. corpulanta Cleve *sensu* Karsten (1905), *P.alata* var. *gracillima* (Cleve) Gran *sensu* Hustedt (1905), *P.alata* var. *inermis* (Castrcane) Mangin *sensu* Mangin (1915) and *P.alata* var. *indica* (H. Peragallo) Hustedt *sensu* Kopczynska *et al.* (1986). Ferreyra & Ferrario (1983) proposed there was one Antarctic species *P.alata* which exhibits a wide range of morphologies including transitional forms between the named species *P.alata* var. *inermis*, *P.alata* var. *gracillima*, and *P.alata* var. *indica*.

Ecology: Sündstrom (1986) defined *Proboscia* from North Atlantic samples. Specimens have however been defined from the Antarctic (Jordan *et al*. 1991).

2.1.8 ***Rhizosolenia*** Brightwell 1858

Type: *Rhizosolenia styliformis* Brightwell

Generic Characteristics: Valves are cone-shaped, asymmetrical, extending into a single process or spine at the valve apex with otaria at its base. There is a single rimoportula at the base of the spine. Valves have a groove on one side to accommodate the spine of the adjacent valve. There are numerous girdle bands in two or more longitudinal columns. The

girdle bands may be scale like, trapezoid, rhomboidal or wing like in outline. Areolae are small, round to quadrate and arranged in vertical rows. *Rhizosolenia* are straight or curved, free living or form long chains (Round *et al*., 1990; Hasle & Syvertsen, 1997).

Characteristics distinguishing species: The shape of the valve and process, the number of columns in the arrangement of girdle bands, whether the bands are in dorsiventral or lateral columns, the position, extension size and shape of the otaria and the labiate structure (Hasle & Syvertsen, 1997) .

Discussion: Sündstrom (1986) emended the description of *Rhizosolenia* to only include those forms with process, otaria and claspers and copulae perforated by loculate areolae. As a consequence of this revision a number of species were excluded form the genus. Jordan *et al.* (1991) note that resting stages of *Rhizosolenia* are more heavily silicified, lack otaria and claspers and have more rows of girdle bands. The lack of linking structures and heavier silicification suggest that the resting forms do not form chains and they may experience dormancy in deeper aphotic waters or on the sea-bed in shallow waters. This dimorphism has obvious taxonomic implications. Armand & Zielinski (2001) in their review of *Rhizosolenia* from Southern Ocean sediments, attempt to clarify the taxonomic descriptions of *Rhizosolenia* species by concentrating on the morphology of the otaria.

Rhizosolenia bergonii Peragallo 1892

Description: The valves are narrow, 9-115µm in diameter and always have four columns of girdle bands. The apex is long and narrow, the process tip appears cleft. The process is 10-20µm long. There are 19-24 areolae in 10µm. The valve and the valvocopula are deeply conical. Valves are usually heavily silicified. There are no otaria (Hasle & Syvertsen, 1997).

Ecology: warm water region (Hasle & Syvertsen, 1997).

Rhizosolenia borealis Sundstrom 1986

Synonym: *Rhizosolenia styliformis* var *oceanica* Wimpenny 1946

Description: *R.borealis* has two dorsiventral columns of girdle segments, exhibits no dimorphism, is13-65µm in diameter, with a 15-28µm long process. There are 15-17 band areolae and 22-24 valve areolae in 10 µm. *R.borealis* is distinguished by the fact that the otaria extend to about half the length of the thicker basal part of the process (Hasle & Syvertsen, 1997).
Plate I 6

Discussion; Sündstrom (1986) considers *R.borealis* to be a distinct species from *R.polydactyla* on the basis of different distribution and that *R.polydactyla* is dimorphic

Ecology: Northern cold water region (Hasle & Syvertsen, 1997).

Rhizosolenia hebetata hebetata Bailey 1856

Synonym: *Rhizosolenia hebetata f. hiemalis* Gran

Description: *R. hebetata hebetata* has two columns of segments and exhibits dimorphism. It is distinguished by having a heavily silicified process and no otaria. *R. hebetata hebetata* is 15-44µm in diameter. The process is 15-25µm in length (Hasle & Syvertsen, 1997).

Ecology: Northern cold water region (Hasle & Syvertsen, 1997).

Rhizosolenia hebetata semispina (Hensen) Gran

Basionym: *Rhizosolenia semispina* Hensen

Description: *R.hebetata semispina* has two columns of girdle segments and exhibits dimorphism. Forms have a pointed otaria extending at least 3µm along the basal part of the process. Valves are 6.5-42µm in diameter. There are 28-30 band areolae in 10µm (Hasle & Syvertsen, 1997).

Discussion: Sündstrom (1986) distinguishes *R.hebetata semispina* from *R.antennnata f.semispina* on the basis of different distribution and dissimilar morphology of nominate forms.

Ecology: Northern cold water region (Hasle & Syvertsen, 1997).

Rhizosolenia styliformis

Description: *R.styliformis* has two dorsiventral columns of girdle segments and does not exhibit dimorphism. Valves are 23-90µm in diameter, with a process 15-28µm in length. There are 15-17 band areolae and 22-24 valve areolae in 10µm. The otaria are rounded usually ending at the base of the rimoportula, but may terminate below the process base and extend along the basal part of the process for a short distance (Sündstrom, 1986; Hasle & Syvertsen, 1997). Plate I 5

Discussion: Hustedt (1930) recognised three forms of *R.styliformis. R.styliformis styliformis* with classically right angled otaria passing and joining into the rimoportula, *R.styliformis* var. *longispina* with otaria that terminate at the transition of the valve and the rimoportula and *R.styliformis* var. *latissima* with more rounded and less prominent otaria. Hasle (1975) recognised two forms of *R.styliformis, R.styliformis* Brightwell var. *styliformis* where the otaria attach below the rimoportula, and *R.styliformis* var. *oceanica* Wimpenny, where the otaria attach to the rimoportula. This form was later redefined as *R.polydactyla* f. *poldactyla.* Armand & Zielinski (2001) adopt the emended description of *R.styliformis;* rounded otaria terminating below or slightly above the base of the rimoportula (Sündstrom, 1986; Priddle *et al*, 1990; Hasle & Syvertsen, 1997). They further argue that many forms of *R.styliformis* occurring in the Southern Ocean have been confused with *R. polydactyla* f. *poldactyla, R.curvata* and *R.anntenata* f. *semispina* (emend. Sündstrom, 1986).

Ecology: The Northern North Atlantic (Hasle & Syvertsen, 1997). Given the misidentification of *R.styliformis* in the Southern Ocean, there has been some debate as to whether it occurs at all in this region. Ligowski (1993) reports its presence in open ocean area of the Bellinghausen and Weddell Seas.

Order Asterolamprales
Family Asterolampraceae
Genera *Asteromphalus*

2.1.9 *Asteromphalus* Ehrenberg 1844

Lectotype: *Asteromphalus darwinii*

Generic Characteristics: Cells are discoid to slightly pear-shaped and rarely, naviculoid. The valve face is convex, without a distinct valve mantle. It is undulate in girdle view. Characteristic of *Asteromphalus*, is the pattern of hyaline rays alternating with areolate areas. One ray, the median ray, differs from the others in that it has a thinner distal section and forms a focus from which the other rays radiate. At the margin end of all but the median ray are the openings of rimoportulae. The areolae are loculate opening externally as cribia and internally as foramina (Round *et al.*, 1990).

Characteristics distinguishing species: The valve outline. The number of hyaline rays. Whether the central area is truly central or eccentric. The size of the central area as a proportion of the valve face. The shape of the separating lines and of the narrow hyaline ray within central area. The shape of the areolated sectors and the size of the areolae. (Hasle & Syvertsen, 1997)

Discussion: All *Asterolampraceae* have unique morphological features which require specific terminology. Greville (1860) was the first to formally distinguish these terms. The ray is defined as the structure corresponding to one areola occurring at regular spaced intervals around the valve surface. The ray has two openings, an interior elongate opening

or ray slit equivalent to a foramen and an exterior opening or ray-hole at the marginal end of each normal ray. Greville (1860) further defined the dark lines at the edge of rays as umbilical lines and the point where all separating lines join as the junction point. The area of the valve face where the centrally expanded rays form a circle is the central area. The portions of the valve face between the rays are referred to as the areolated segments (Gombos, 1980).

Asteromphalus robustus Castracane

Synonym: *Asteromphalus brookei* var. *robustus* (Castracane) Rattray

Description: Valve view: Cells are subcircular to elliptical in outline, 67-79μm in diameter. The central area of the valve extends to about a third of the valve diameter. There are 8-10 robust hyaline rays of similar width and length and one thinner ray. Separating lines are bent. The areolation is coarse, slightly coarser at the centre 6-7 in 10μm. The areolation pattern is quincunx with larger pores surrounding smaller poroids. Girdle view: Cells are drum shaped with slightly raised rays and a high mantle (Hernandez-Becerril, 1991a).

Discussion: *A. rombustus* is similar to *A.heptactis* but distinguished with respect to the pattern of areolation, the high mantle and pattern of separating lines (Gombos, 1980).

Subdivision	**Bacillariophytina**
Classes	**Mediophyceae, Bacillariophyceae**
Class	**Mediophyceae**
Orders	**Chaetocerotales, Thalssiosirales**
Order	**Chaetocerotales**
Family	**Chaetocerotaceae**
Genera	***Bacteriastrum***

2.1.10 ***Bacteriastrum*** G.Shadbolt 1854

Lectotype: *Bacteriastrum fulcatum* Shadbolt

Generic characteristics: Cells are cylindrical, linked to form filaments by long radiating, simple or bifurcate setae on each cell. The setae of adjacent cells are fused beyond their point of origin on the valve. Separation valves with modified setae occur at intervals. Terminal setae are not fused or branched and are often curved. Valves are centric with tiny simple areolae radiating from a central annulus, in a fan shaped pattern near the valve margin. Separation valves have one central simple rimoportula (Round *et al.*, 1990; Hasle & Syvertsen, 1997).

Characteristics distinguishing species: The morphology and position of the inner and terminal setae (Hasle & Syvertsen, 1997).

Bacteriastrum hyalinium Lauder

Description: The frustule is short in girdle view and distinctly hyaline, 13-56μm in diameter. Inner setae are bifurcate in the valvar plane, with 7-32 inner setae per valve. Terminal setae are umbrella shaped (Lauder, 1864; Hasle & Syvertsen, 1997).Plate II 1-2

Discussion: Lauder (1864) described only two species of *Bacteriastrum*; *Bacteriastrum varians* and *Bacteriastrum hyalinum*. Boalch (1975) concluded that *B.varians* was synonymous with *B.furcatum* Shadbolt but retained *B.hyalinum* as a distinct species. Boalch (1975) designated illustrations of Lauder as types for the species as none of Lauder's original material is known to survive.

Ecology: Marine planktonic, common in temperate waters (Hasle & Syvertsen, 1997). Hendey (1964) and Drebes (1972) record it as the most common species of *Bacteriatrum* in the North Atlantic and North Sea, especially in summer.

Order **Thalassiosirales**

Family **Thalassiosiraceae**

Genera ***Bacteriosira, Porosira, Thalassiosira***

2.1.11 ***Bacterosira*** Gran 1900

Type: *Bacterosira fragilis* (Gran) Gran
Correct name: *Bacterisira bathyomphala* (Cleve) Syvertsen & Hasle.

Discussion: *Bacteriosira* is a monospecific genus. Gran (1900) established *Bacteriosira* with the single species *B.fragilis*. Syvertsen & Hasle (1993) identified *Coscinodiscus bathyomphalus* (Cleve) as identical to the secondary valve of the resting spores of *B.fragilis* therefore reassigning the generic type as *Bacterisira bathyomphala* (Cleve) Syvertsen & Hasle.

Bacterosira bathyomphala Cleve 1883

Basionym: *Coscinodiscus bathyomphalus* Cleve
Synonyms: *Lauderia fragilis* Gran
Bacteriosira fragilis (Gran) Gran

Description: Valve view: The vegetative cells are cylindrical with a tall valve mantle and are 18-24µm in diameter. Valves have one marginal ring of small strutted processes, 5-7 in 10µm and one large labiate process between two strutted processes. There is a cluster of central strutted processes within a central depression each having 2-4 satellite pores. The central depression is surrounded by an irregularly silicified border. Radial striae of small areolae spread from the valve centre to valve margin. These are separated by pronounced interstriae. There are more than 30 radial ribs in 10µm.
Girdle view: The pervalvar axis is usually longer than the cell diameter. Valves form dense chains. The curved mantle and central depression of the vegetative valve lead to lense-shaped openings between sibling cells in girdle view. The cell wall is weakly silicified.

The resting spores are distinctive, semi-endogenous and heterovalvate (the resting spores were first described as *Coscinodiscus Bathyomphalus* Cleve) The primary valve has a flattened face, the secondary valve a pronounced central and conical protuberance and a horizontally flattened marginal brim. The valve mantle is shallower than that of the

vegetative cell and there are fewer central strutted processes (Hasle & Syvertsen 1993; Hasle & Syvertsen, 1997).

Ecology: Northern cold water region (Hasle & Syvertsen, 1997)

2.1.12 *Porosira* E.Jørgensen 1905

Type: *Porosira glacialis* (Grunow) Jørgensen

Generic Characteristics: Valves, discoid single or in loose chains. Areolae radiate from a central annulus. Areolae are loculate opening externally with elongate foramina, internally with cribia. There is one large labiate process in the marginal zone and many strutted processes over the valve face increasing in frequency towards the valve margin. There are numerous girdle bands with similar areolation to the valve face. Cells are single or in loose chains joined by polysaccharide threads extruding from the valve processes (Round *et al.*, 1990; Hasle & Syvertsen, 1997)

Characteristics distinguishing species: Whether the valve areolae and central annulus are distinct or indistinct, the morphology and location of labiate process, the arrangement of the marginal processes, the form of striae and areolation (Hasle & Syvertsen, 1997).

Porosira glacialis (Grunow) Jørgensen

Basionym: *Podosira hormoides* var. *glacialis* Grunow 1884
Synonyms: *Podosira glacialis* Cleve 1896
Lauderia glacialis Gran 1900
Porosira antarctica Kozlova 1963

Description: Valves are circular, moderately convex 30-40µm in diameter. The pervalvar axis is 30-40µm, with 25-26 areolae in 10µm. The labiate process is some distance from valve margin. There is no regular arrangement of strutted processes close to labiate

process. The areolae pattern is very distinctive. The radial areolae walls, which run in wavy lines from the central annulus to the valve margin, are more strongly silicified than the transverse walls. The areolae are irregular is size and outline outside the central area of the valve where they are smaller and may be surrounded by a silicified ring. (Hasle, 1974; Hasle & Syvertsen, 1997)

Ecology: Northern cold water to temperate region and Southern cold water region (Hasle & Syvertsen, 1997).

2.1.13 *Thalassiosira*

Generic Characteristics: Cells are in chains connected by organic threads which extrude from strutted process. Valves are circular, flat faced with short down turned mantles or watch-glass shaped. The mantle edge is often distinctly ribbed or rimmed. Areolae are loculate, opening externally as round foramina and internally as cribia. Areolation patterns are various. The girdle bands are numerous, the valvocopulae being more areolate than subsequent copulae (Round *et al*., 1990; Hasle & Syvertsen, 1997).

Characteristics distinguishing species: The curvature of the valve face, shape and height of the mantle. The length, thickness and location of the connecting threads and the number, length and location of processes.

Discussion: Hasle (1968a) produced the first SEM investigations of this large genus, noting that Cleve defined the genus with respect to the frustules being joined by a central fine thread of mucus to form chains. Species were identified in girdle view with respect to the shape of chains. This is a useful for some *Thalassiosira* species such as *T.nordenskioeldii* with its characteristic octagonal outline in girdle view, but unhelpful for other *Thalassiosira* species. Hasle defines species with respect to the presence, absence and position of processes and whether they have external process tubes. (Hasle 1968a) Various subsequent authors have attempted to subdivide *Thalassiosira* but have failed to agree on the most significant morphological features (Markova, 1988; Rivera, 1981; Johansen & Fryxell, 1985; Fryxell & Johansen, 1990; Hasle & Syvertsen, 1990a). No subdivision of the genus is adopted in this study.

Thalassiosira angulata (Gregory) Hasle

Basionym: *Orthosira angulata* Gregory

Description: The valve is 12-39µm in diameter, the valve face flat 8-18µm, with a smoothly curved mantle. There is a sharp distinction between the mantle and valvocopula. Areolae are hexagonal and arranged in curved tangential rows, straight rows or sectors, with 14-24 valve areolae in 10µm. There are no distinct central areolae. The marginal processes are widely spaced and have long external tubes. There is a large labiate process with a long external tube located close to a marginal strutted process. The pervalvar axis usually shorter than diameter. The connecting threads are distinctly longer than pervalvar axis (Hasle & Syvertsen, 1997).

Discussion: *T. angulata* may be distinguished from *T.decipens* by having more widely spaced marginal processes and a higher valve mantle. Hasle (1979) considers *T.decipens* to be more littoral than planktonic (Hasle & Syvertsen, 1997).

Thalassiosira auguste-lineata (A.Schmidt) Hasle and Fryxell

Basionym: *Coscinodiscus auguste-lineata* Schmidt
Synonyms: *Coscinodiscus polychordus* Gran
Thalassiosira polychorda (Gran) Jorgensen
Coscinosira polychorda (Gran) Gran

Description: Valves are circular, 14-78µm in diameter. The valve is face flat or slightly curved with a rounded mantle. The areolation varies from linear to eccentric to fasiculate with 8-18 areolae in 10µm. There are arcs of central strutted processes in a ring at some distance from valve centre, each arc having one to nine processes. The marginal strutted processes have conspicuous external tubes in one marginal ring including one radially orientated labiate process. There are many connecting threads in groups at some distance from valve centre (Fryxell & Hasle, 1977; Hasle & Syvertsen, 1997).

Discussion: The arrangement of central processes and the coarse marginal processes are diagnostic (Hasle & Syvertsen, 1997).

Ecology: Found in the North Atlantic, Canadian Arctic and North West Pacific (Fryxell& Halse, 1977).

Thalassiosira eccentrica **(**Ehrenberg) Cleve 1904

Basionym: *Coscinodiscus eccentricus* Ehrenberg 1841a

Description: Valves are circular, flat faced, 15-110µm in diameter, with a low rounded mantle. The areolation is eccentric, tending to fasciculate, with 5-11 areolae in 10µm. There is one central strutted process adjacent to central areola, surrounded by a ring of seven areolae. There are scattered strutted processes on valve face, two rings of marginal strutted processes with short external tubes and one ring of pointed spines further from valve margin. There is one marginal labiate process. Cells are joined by a single connecting thread, approximately twice the cell diameter in length (Fryxell & Hasle, 1972; Hasle & Syvertsen, 1997).

Discussion: Halse & Fryxell (1972) note that *T.eccentrica* may be distinguished from *T.angulata* and *T.pacifica*, which may also have eccentric areolation, by the presence of the central process, the arrangement of the processes across the valve and the ring of marginal spines. *T.mendiolana* has a similar pattern of processes to *T.eccentrica* but has smaller areolae with fasiculate areolation and is usually more weakly silicified (Hasle & Syvertsen, 1997).
Ecology: Cosmopolitan (Hasle & Syvertsen, 1997).

Thalassiosira ferelineata Hasle & Fryxell

Description: Valves are circular, 20-43µm in diameter. The valve face is flat with a sharp almost 90^{o} angle to the shallow rounded mantle. Areolae are hexagonal and loculate, with

6-7 areolae in 10µm on the main part of the valve. Shiono & Koizumi (2000) report much finer areolation at the valve margin, 15 areolae in 10µm. Areolation is linear to tangential. There is one central strutted process. The labiate and marginal processes are not extended externally but have long internal tubes. The one marginal labiate process is externally visible as a large oval hole, larger than an areola. There is one ring of marginal strutted processes, with processes lying approximately 6 areolae apart, 3-4 processes in 10µm. The edge of the valve mantle gives the appearance of ribbing. The mantle is areolated to the rim (Hasle & Fryxell, 1977b; Hasle & Syvertsen, 1997).

Discussion: Hasle & Fryxell (1977b) note that *T.ferelineata* has the same pattern of processes and arrangement of areolae as *T.tenera* but is larger, coarser and lacks external process tubes (Hasle & Syvertsen, 1997).

Ecology: Mainly warm water regions (Hasle & Syvertsen 1997).

Thalassiosira gravida Cleve 1896

Description: (vegetative cell) Valves are circular and flat, 17-62µm in diameter with a low and slightly curving mantle. The areolae are hexagonal and arranged in radial rows. There are numerous central strutted processes, scattered strutted processes across valve face and mantle and one large marginal labiate process. The connecting thread between valves is thick, particularly close to the valve surface (Hasle & Syvertsen, 1997).Plate II 3-4
Discussion: The diatom originally described as *Coscinodiscus subglobosus* Cleve & Grunow is a coarsely silicified, highly vaulted form found in northern waters. This form was later interpreted as the resting spore of *T.gravida* by Meunier (1910) who reassigned forms with the morphology of *Coscinodiscus subglobosus* to two new species; *T.fallax* having semi-enogenous resting spores and *T.gravida* having endogenous resting spores. Syvertsen (1979) in a series of diatom culture studies noted that the endogenous resting spore of the southern form *T.antarctica* closely corresponded to the description of *Coscinodiscus subglobosus.* He further observes that Cleve described *T.gravida* from Arctic waters at the same time as Comber described *T.antarctica* from Antarctic waters. *T.antarctica* was not at the time recorded from northern waters. Hasle & Heimdel (1968) amended the description of *T.antarctica* with samples from northern seas. A northern form

of *T.antarctica* has also been recognised *T.antarctica* var. *borealis*. Syvertsen (1979) concludes therefore that the forms corresponding to *Coscinodiscus subglobosus* should be considered as the endogenous resting spores of *T.antarctica* not of *T.gravida* and that the form designated by Meunier (1910) as *T.fallax* is in fact, the semi-endogenous resting spore of *T.antarctica*. This taxonomic confusion has resulted from the fact that *T.antarctica* can form exogenous, semi-endogenous and endogenous resting spores. The vegetative forms of *T.gravida* differ from *T.antarctica* in that *T.gravida* has numerous strutted processes scattered across the whole valve, while *T.antarctica* has 2-3 rows of marginal strutted processes. Syvertsen (1977) found no resting spores of *T.gravida* in natural samples or cultures under suitable environmental conditions for resting spore formation. However he does note that Paasche (1961) identified four morphotypes of *T.gravida* from the Norwegian Sea including a resting spore form. Syvertsen (1977) concludes that *T.gravida* may form resting spores (Syvertsen, 1977; Syvertsen, 1979: Hasle & Syvertsen, 1997). As the vegetative forms in this study are certainly *T.gravida* and not *T.antarctica*, the resting spore forms are also considered to be *T.gravida*. They are counted separately to the vegetative forms for the transfer function.

Ecology: *T.gravida* is a northern and southern cold water form. Syvertsen (1977) suggests that *T.gravida* and *T.rotala* may be temperature dependent morphotypes of the same species. *T.rotala* has a similar form to *T.gravida* except for an unevenly thickened intercalary band and that it is found in warmer waters. If these two species are simply morphotypes of the same species, that species has a cosmopolitan distribution (Syvertsen, 1977).

Thalassiosira hyalina (Grunow) Gran

Basionym: *Coscinodiscus hyalinus* Grunow in Cleve and Grunow
Description: Valves are circular, 16-45µm in diameter. Valve faces are flat or slightly convex. The mantle is low or rounded. Areolation is radial in rows or ribs, with 13-24 areolae in 10µm. The mantle is also always areolated, 5-9 areolae in 10µm. There are 2-15 central strutted processes, one ring of marginal strutted processes and one labiate process

in place of a marginal process. The pervalvar axis is about one third of cell diameter. The connecting thread is thick.
Ecology: Northern cold water form (Hasle & Syvertsen, 1997).

Thalassiosira lineata Jouse 1968

Description: Valves are circular, flat and 9-45µm in diameter with a low mantle. The areolae are hexagonal and arranged in straight rows across whole valve face, with 8-16 areolae in 10µm on the valve face, 5-6 on the mantle. Areolae are loculate opening externally as foramina and internally as round cribia. There are strutted processes over the whole valve face, two marginal rings of strutted processes and one large marginal labiate process (Hasle & Fryxell, 1977b; Hasle & Syvertsen, 1997).

Discussion: Herzig & Fryxell (1986) note that *T.lineata* may be distinguished from *T.lineoides* by the structure and location of the scattered processes (Hasle & Syvertsen, 1997).

Ecology: Warm water region (hassle & Syvertsen, 1997). Jouse, Kozlova & Mukhina (1971) record the species as subtropical or tropical, Hasle (1976a) as a warm water species.

Thalassiosira nodulineata (Hendey) Hasle & G.Fryxell comb. nov
Basionym: *Coscinodiscus nodulolineatus* Hendey 1957

Description: Valves circular, 27-58µm in diameter. The areolation is linear with 3.5-6 areolae in 10µm. There is one ring of marginal processes with 4 processes in 10µm and one labiate marginal process. Characteristic of the species is a central nodule, resembling an inverted cone, with 5-6 strutted processes, adjacent to a deep opening into the central areola. The valve mantle has 3-4 rows of tangential areolae (Hasle & Fryxell, 1977b).

Discussion: Hendey (1957) considered *T.nodulineata* to be closely related to *T.hendeyi* but distinguished primarily by the latter species lacking the modified central areola.

T.densannula has a similarly modified central areola to *T.nodulineata* but may be distinguished by the density of the marginal process and by *T.densannula* having no occluded processes Hasle & Fryxell (1977b).

Thalassiosira nordenskioeldii Cleve

Description: Valves are circular, 10-50µm in diameter, with 14-18 areolae in 10µm, centrally concave and with an oblique slanting mantle with a ribbed rim. Areolation is radiate. The valvocopula has rows of regular pores and an unperforated rim. There is a ring of prominent marginal processes with long, slender external tubes, located at the distinct bend between valve face and mantle. There are central strutted processes close to central areola and one labiate process within ring of marginal processes. The connecting thread is as long as or shorter than the pervalvar axis (Hasle, 1978a; Hasle & Syvertsen, 1997).

Discussion: *T.nordenskioeldii* may be distinguished from *T.aestivalis* by having smaller marginal processes and a narrower valve mantle (Hasle, 1978a).

Ecology: Northern cold water region to temperate (Hasle & Syvertsen, 1997).

Thalassiosira oestrupii (Ostenfeld) Hasle

Basionym: *Coscinosira oestrupii* Ostenfeld

Description: Valves are circular, 7-60µm in diameter. The valve face is flat or slightly convex, the mantle low and rounded. The valvocopula has vertical rows of pores giving the appearance of striation. Two coarse columns of pores, 9 pores in 1µm alternate with four fine columns, 14 pores in 1µm. The areolation is sublinear and usually coarser in central part of valve than closer to margin with 6-9 areolae in 10µm centrally and 9-12 at the margin. There is one ring of marginal labiate processes 0.8-1.9µm apart. There is a single central strutted process which is situated 1-3 areolae distant from a single labiate process (Fryxell & Hasle, 1980; Hasle & Syvertsen, 1997). Plate II 5-6

Discussion: Fryxell & Hasle (1980) in their overview of *T.oestrupii* from North and South Atlantic, Gulf of Mexico, Pacific Ocean, Weddell Sea and Indian Ocean samples, recognise two subspecies of *T.oestrupii; T.oestrupii* var. *oestrupii* and *T.oestrupii* var. *venrickae*. The latter form being distinguished by having more widely separated marginal processes and distinct eccentric areolation. Given the emended description of *T.oestrupiii* by Halse & Fryxell (1980), Boden (1993) noted that samples from the geological record could no longer be assigned to *T.oestrupii sensu stricto.* He establishes the new species *T. tetraoestrupii* and emends the description of *T.praeoestrupii* Dumont, Baldauf & Barron. Shiono & Koizumi (2000) in their study of Miocene, Pliocene and Pleistocene samples identify three forms of *T.oestrupii; T.oestrupii sensu stricto, T.oestrupii* early form, with an earlier geological range and a greater distance between marginal fultoportulae than *T.oestrupii sensu stricto* and *T.oestrupii* (type 1) found a Pleistocene sediments and having a smaller valve and valve areolae size than *T.oestrupii sensu stricto.* They also emend the description of *T.praeoestrupii*.

Ecology: *T.oestrupii* var. *oestrupii* is cosmopolitan and oceanic, *T.oestrupii* var. *venrickae* more often found on continental shelves and less commonly inshore and in open ocean samples (Fryxell & Hasle,1980).

Thalassiosira pacifica Angst & Gran

Description: Valves are circular, 7-46µm in diameter, flat faced or slightly concave. Areolation is eccentric or fasiculate, depending on cell diameter. The valve margin is ribbed. Areolae are loculate with 20-28 areolae in 10µm. The mantle areolae are smaller than those on valve face. There is a single central process next to the central annulus, a ring of marginal strutted process with distinct coarse external tubes and a single labiate process within the ring marginal processes. The connecting thread is approximately as long as pervalvar axis (Hasle & Syvertsen, 1997).

Discussion: *T.angulata* is distinguished from *T.decipens* by having a ribbed margin, the spacing and morphology of the marginal processes and a labiate process within the ring of marginal processes (Hasle & Syvertsen, 1997).

Ecology: Cosmopolitan, except for polar regions (Hasle & Syvertsen, 1997).

Thalassiosira trifulta G.Fryxell in Fryxell and Hasle

Synonyms: *Thalssiosira excentrica* (Ehrenberg) Cleve sensu Jouse 1971
Coscinodiscus excentricus var. *jousei* Kanaya sensu Koizumi 1973
Thalassiosira oestrupii (Ostenfeld) Hasle sensu Koizumi 1975

Description: Valves are circular, flat faced, 16-58µm in diameter, with an evenly rounded mantle. Forms are often coarsely silicified. The areolation is linear or in slightly curved tangential rows with 5-7 valve areolae in 10µm. There are 1-8 strutted processes in the centre of the valve positioned in one or two lines. The strutted processes in the marginal ring are 3-6µm apart. The strutted processes are trifultate that is, having three columnar supports connecting the process to the valve. The labiate process is usually located closer to valve mantle than centre, in larger valves 8-9 areolae from central processes. The pervalvar axis is shorter than cell diameter. The valvocopula is doubly septate and has one row of large pores next to the valve and a number of irregular rows further from the valve (Fryxell & Halse, 1979; Hasle & Syvertsen, 1997).

Discussion: Smaller specimens of *T.trifulta* may be hard to distinguish from *T.oestrupii*. This can be done however on the basis of the trifultate fultoportulae which is smaller in *T.oestrupii* (Shiono & Koizumi, 2000).

Ecology: Cold water region (Shiono & Koizumi, 2000; Hasle & Syvertsen, 1997).

Class Bacillariophyceae
Order Bacillariales, Fragilariales, Thalassionematales

Order Bacillariales
Family Bacillariaceae
Genera *Alveus, Fragilariopsis, Nitzschia*

2.1.14 *Alveus* Kaczmarska & Fryxell 1996

Discussion: *Nitschia angustata* var. *marina* was first described by Grunow in Cleve and Moller (1878) from Mediterranean samples. Grunow later distinguished this taxon as distinct in its own right and in Van Heurk (1881) it appears as *Nitschia marina*. Heiden in Heiden and Kolbe (1928) described another species, *Synedra gaussi* from southern and equatorial Atlantic samples. This species was later considered to by synonymous with *Nitschia marina*. (Kolbe, 1954) Simonsen (1974) noted that *Nitschia marina* has chambered striae similar to those in *Pinnularia*. Kaczmarska & Fryxell (1996) on further detailed study of the valve structure suggested that it was unique among nitzschoid genera and so proposed the new genus *Alveus* gen.nov.

Alveus marina (Grunow) Kaczmarska and Fryxell 1996

Basionym: *Nitzschia angustata* var. *marina* Grunow in Cleve & Moller
Synonyms: *Synedra gaussi* Heiden in Heiden & Kolbe
Pseudo-nitzschia hustedtii Meister

Description: The valve wall of *Alveus marina* is very heavily silicified and apparently double layered with the inner layer unperforated except along the non-raphe margin. The valve mantle is high and rounded. Both the valve face and mantle have biseriate striae and slightly raised interstriae. The raphe is not raised above the valve surface. The external canal wall is not perforated except for the raphe slit. Fibulae are strong and curved, 10-12 fibulae and striae in 10µm. The valve outline is linear to lanceolate with rounded apices, 53-353µm long and 8-12µm wide (Hasle & Syvertsen,1997).
Ecology: Warm water region (Hasle & Syvertsen, 1997). Equatorial and Southern Atlantic and Mediterranean occurrence (Cleve& Grunow, 1880; Heiden & Kolbe, 1928; Hustedt, 1958). Warm Core rings of the North Atlantic (Kaczmarska *et al.*, 1986). Subtropical and Indian Oceans and Arabian Sea (Cleve & Grunow1880; Simonsen, 1974). Southern Pacific (Cleve & Grunow,1880).

2.1.15 ***Fragilariopsis*** Hustedt in Schmidt emend. Hasle 1993

Type: *Fragilariopsis antarctica* (Castracane) Hustedt in Schmidt
Basionym: *Fragilaria antarctica* Castracane

Generic Characteristics: Valve faces are more or less flattened, not undulated and sharply differentiated from the mantle. Valve poles are usually bluntly rounded. Valves are linear, sublinear, linear-lanceolate, lanceolate, elliptical or subcircular in outline. They can be isopolar or heteropolar. The apical axis is often heteropolar. Striae are parallel except near the poles where they are radiate and usually consist of double rows of poroids. The raphe is strongly eccentric, positioned at the junction of the valve face and mantle. It is not raised above the valve surface. The raphe endings are simple. Cells are rectangular in girdle view, in ribbons united by the entire or greater part of the valve surface. There are approximately equal numbers of interstriae and fibulae, with fibulae often more distinct than interstriae (Round *et al.*, 1990; Hasle & Syvertsen, 1997).

Characteristics distinguishing species: The valve outline, the structure of striae, the polarity of the apical axis and whether or not the valve has a central larger interspace (Hasle & Syvertsen, 1997).
Discussion: Hasle (1972c, 1974) argued that *Fragilariopsis* should be considered as a section of the genus *Nitzschia* and so transferred *Fragilariopsis* to *Nitzschia*. This however was not widely accepted. Round *et al.* (1990) recognises *Fragilariopsis* as a distinct genus and this is the approach adopted in this study. The inclusion of *Pseudoeunotia doliolus* in *Fragilariopsis* extends the ecological boundaries of the genus to warm water regions (Medlin & Sims, 1993).

Fragilariopsis atlantica Paasche 1961
Synonym: *Nitzschia paaschei* Hasle

Description: Valve view: Valve outline varies with valve length. The largest specimens (around 40µm) are broadly linear with more or less blunted apices and a slightly heteropolar apical axis. Medium-sized valves are lanceolate with slightly pointed apices

and an isopolar apical axis. The smallest specimens broadly elliptical with broadly rounded apices. Valves are broad in relation to their length. They have a central larger interspace and central nodule. The transverse interstriae are more curved in smaller than in larger specimens. Girdle view: valves are flat, cells fairly low. The valves of sibling cells in colonial ribbons are joined along their whole length with no interspace. The interstriae are weak (Hasle & Syvertsen, 1997).

Ecology: Northern cold water region plankton (Hasle & Syvertsen, 1997).

Fragilariopsis cylindrus (Grunow) Kreiger in Helmcke & Kreiger

Basionym: *Fragalaria cylindrus* Grunow in Cleve
Synonym: *Nitzschia cylindrus* (Grunow) Hasle

Description: Valve view: Valves have straight parallel sides and broad rounded almost semicircular apices. The apical axis is 3-48μm in length, the transapical axis 2-4μm. The interstriae are transverse in rectangular portion of the valve. There are 13-17 striae and fibulae in 10μm. Oblique ribs run from the last interstria to the rounded apices. There is no central larger interspace. Girdle view: cells are rectangular. The pervalvar axis is fairly short. Valves are joined in ribbons with no interspace between adjacent valves (Hasle & Syvertsen, 1997).

Ecology: Southern and Northern cold water regions, sea ice form and as plankton (Hasle & Syvertsen, 1997).

Fragilariopsis doliolus (Wallich) Medlin & Sims

Basionym: *Synedra doliolus* Wallich
Synonym: *Pseudoeunotia doliolus* (Wallich) Grunow in Van Heurck

Description: Valve view: Valves are semi-lanceolate with bluntly rounded apices. The ventral side of the valve is straight and seldom, slightly convex. The dorsal side of the valve is more strongly convex. The apical axis is 30-70µm in length, the transapical axis 5-8µm. The transverse striae have two alternating rows of poroids. The interstriae are thickened vertically on the internal and external surfaces of valve face and mantle. The canal raphe is situated along junction of the valve face and mantle, on either the dorsal or ventral side. Girdle view: Cells are rectangular, joined in curved ribbons with no interspace between adjacent cells (Medlin & Sims, 1993; Hasle & Syvertsen, 1997). Plate III 1-2

Discussion: *Fragilariopsis doliolus* was first described by Wallich as *Synedra doliolus* but later transferred to the genus *Pseudoeunotia* by Grunow 1881 (in Van Heurck 1880-1883) *Pseudoeunotia* was established by Grunow 1881 on the basis of two species *P.doliolus* Wallach and *P.hemicyclus* Ehrenberg. Hustedt (1959) argued that the two species of *Pseudoeunotia* could not belong to the same genus on the basis of areola and striae construction and so he transferred *P.hemicyclus* to the genus *Amphicampa* thus leaving *Pseudoeunotia* as a monospecific genus. Medlin & Sims (1993) reassigned *Pseudoeunotia doliolus* to *Fragilariopsis* on the basis of it forming ribbon like colonies and having a reduced canal raphe. Hustedt (1913) established *Fragilariopsis* as an araphid genus, forming ribbon like colonies and having valve structure different to that of *Fragalaria.* He later acknowledged the presence of a a reduced canal raphe in both *Fragilariopsis* and *Pseudoeunotia.* Medlin & Sims (1993) argue that while *Fragilariopsis* forms curved ribbon like colonies, this is simply a consequence of the strongly asymmetrical cell shape and that Hasle (1965) identifies other heteropolar forms of extant *Fragilariopsis*. Therefore *Pseudoeunotia doliolus* could reasonably be considered to belong to the genus *Fragilariopsis*, there being no other morphological differences than colonies being curved (Medlin & Sims, 1993).

Ecology: Warm water region (Hasle & Syvertsen, 1997).

Fragilariopsis oceanica (Cleve) Hasle

Basionym: *Fragilaria oceanica* Cleve

Synonym: *Fragilaria arctica* Grunow in Cleve&Grunow
Nitzschia grunowii Hasle

Description: Valve view: Valve outline varies with valve length. The largest specimens are narrowly elliptical with slightly elongate ends, medium specimens are more lanceolate with rounded ends and the smallest specimens are broadly elliptical. The apical axis is 10-41µm in length, the transapical axis approximately 6µm. The interstriae on the valve face are more weakly silicified than on valve mantle, with 12-15 striae and fibulae in 10µm. The raphe is situated at the junction of the valve face and mantle, or slightly displaced onto the mantle. There is a central larger interspace. Girdle view: The cells are joined in straight or sometimes curved ribbons with no interspace between adjacent valves. The pervavlar axis often high compared with other *Fragilariopsis* species. The mantle is fairly deep and more silicified than valve face (Hasle & Syvertsen, 1997). Plate III 5-6

Ecology: Northern cold water region, sea ice form and as plankton
(Hasle & Syvertsen, 1997).

Fragilariopsis rhombica **(**O'Meara) Hustedt

Basionym: *Diatoma rhombica* O'Meara
Syonym: *Nitzschia angulata* Hasle

Description: Valve view: Valve outline varies with length. The largest and medium sized specimens are either lanceolate or linear with parallel margins tapering towards pointed apices. The smallest specimens are almost circular. The valves are broad in relation to their length with an apical axis length of 8-53µm and a transapical axis length of 7-13µm. The interstriae are straight in the central linear or convex portion of the valve and curved towards the apices. The striae have two alternate rows of poroids. There is no central larger interspace (Hasle & Syvertsen, 1997).

Ecology: Southern cold water region, plankton (Hasle & Syvertsen, 1997).

2.1.16 *Nitzschia* A.H.Hassall

Type: *Nitzschia sigmoidea* (Nitzsch) W.Smith

Generic Charateristics: Cells are solitary, form stellate or chain colonies or live in mucilage tubes. The valves are straight or sigmoid in outline; narrow, linear, lanceolate or elliptical, sometimes centrally expanded. They are broadly symmetrical in outline with respect to apical plane, but often strongly asymmetrical in structure. The apices are various, often rostrate or capitate. The striae are usually uniseriate, not interrupted by lateral sterna and consist of small round poroids occluded by hymenes and sometimes cribra. The areolae are occasionally loculate in the larger sigmoid species. In some species there are marginal ridges. The raphe is situated in a slightly to strongly asymmetrical position. There are raphes on both valves, either on the same side (hantzschoid symmetry) or opposite sides (nitzschoid symmetry). In some species the raphe extends to the poles, in others there are central raphe endings. The girdle bands often have one or more rows of transverse poroids. The number of girdle bands varies (Round *et al.*, 1990).

Nitzschia bicapitata Cleve emend. G.Fryxell

Description: Valves are 8-23μm long and 4-5μm wide, widest at the centre, smoothly curved with isopolar, bicapitate ends. Poroid areolae 3-4 in 1μm . Areole and poroids on the proximal mantle are in a double row with the largest immediately next to the raphe and aligned with the striae on the valve face. 25-30 striae in 10μm. 12-16 fibulae in 10μm. Poroids on the distal mantle form a single row (Fryxell 2000). Plate III 3-4

Discussion: First described by Cleve (1900), bicapitate forms of the diatom *Nizschia* have been widely recorded. However there have also been attempts to subdivide these forms into a number of different species, subspecies and morphotypes. *N.bicapitata* has a characteristic length in the region of 8-22.5μm. Two bicapitate forms were distinguished as distinct from *N.bicapitata* on the basis of increased length, *Nizschia capitata* 40-84 μm (Heiden & Kolbe 1928) and *Nizschia braarudii* 35-65 μm (Hasle, 1960). From a study of the literature concerning *N.bicapitata*, Kaczmarska and Fryxell defined three morphotypes of *Nitzschia bicapitata* Cleve *sensu lato* and a new species, *Nitzschia bifurcata*.

(Kaczmarska & Fryxell 1986.) From a study of archived material and new samples from plankton tows, Fryxell amended the definition of *N.bicapitata* Cleve and further defined two subspecies of *N.bicapitata*, *N.bicapitata* var *bicapitata* and *N.bicapitata* var *faeroensis* and two new species *N.leehyi* and *N.villarealii.* These distinctions were made on the basis of valve outline, length, width, number of fibulae and striae in 10µm and curvature of striae (Fryxell, 2000).

Ecology: Forms of the *N.bicapitata* group are rarely found inshore and may be considered as open ocean species. They have been considered as cosmopolitan except for polar seas (Hasle, 1976) being found abundantly in tropical waters (Lee & Fryxell 1996; Semina, 1977) but also in temperate waters (Kaczmarska & Fryxell 1986; Kaczmarska *et al.,* 1986). Studies have shown that smaller cells are found in surface waters and larger forms in deeper water (Venrick, 1990; Blain *et al.,* 1997). It need be noted that the abundance of bicapitate forms in sediment traps (Tanimura 1992, Lange *et al.,* 1994) greatly exceeds that in the sediments (Fenner, 1991; Lee & Fryxell, 1996). Hasle (1976a) reports *N. bicapitata* from 66ºN to 62ºS.

Nitzschia braarudii Heiden & Kolbe 1928

Synonym: *Nitzschia capitata* Heiden in Heiden & Kolbe

Description: Valves are 35-63µm long and 3-5µm wide, bicapitate, isopolar and lanceolate with longer forms have straight parallel sides in the central portion and in shorter forms slightly rounded margins. There is a slightly larger central interspace. Striae are in single rows of areolae with 22-30 striae and 10-15 fibulae in 10µm (Kaczmarska & Fryxell, 1986; Hasle & Syvertsen, 1997; Fryxell, 2000).

Discussion: Simonsen (1992) from an examination of the type and isotype material for *N.braarudii* and *N.capitata,* concluded that they were the same species. Fryxell (2000) does not accept this on the basis of *N.capitata* having a finer structure (15-19 fibulae in 10µm as opposed to 10-14 fibulae in 10µm in *N.braarudii*.) Both *N.braarudii* and *N.capitata* are distinctly longer forms of the bicapitate *Nitzcshia* taxa. *N.braarudii* is 35-

65µm and *N.capitata* 22-68µm. Other bicapitate Nitzschia species are within the range of 5-35µm in length. (Kaczmarska & Fryxell, 1986; Fryxell, 2000). Hasle & Syvertsen (1997) accepts that *N.braarudii* and *N.capitata* are the same species and that is also accepted in this study.

Nitzschia kolaczeckii Grunow

Description: Valves lanceolate with slightly outstretched apices. Two raphes located diagonally. Valve with three striae systems, one transverse and two oblique. Central interspace slightly larger than the rest. Apical axis 67-120µm. Transapical axis 7.5-11µm. 8-9 fibulae in 10µm. 13-16 oblique and 17-18 transverse striae in 10µm (Hasle & Syvertsen, 1997).

Ecology: warm water region (Hasle & Syvertsen 1997).

Order Fragilariales
Family Fragilariaceae
Genera *Synedra*

2.1.17 *Synedra* Ehrenberg 1830
Type: *Synedra ulna* Ehrenberg

Generic Characteristics: Valves linear, some capitate, some centrally inflated. Striae perpendicular to narrow sternum, sometimes absent or obscured from central area. Striae composed of rows of simple round or elongate areolae (Round *et al.*, 1990).
Discussion: A number of taxonomic issues have influenced the classification of *Synedra* Ehrenberg. Historically, araphid, benthic diatoms from polar waters were rarely identified beyond the generic level. Forms of the genus *Synedra* Ehrenberg were therefore not identified beyond this generic classification. This was partly due to the difficulties involved in identifying species specific distinctions in this genus without electron microscopy (Hasle *et al.*, 1994). Attempts have subsequently been made to subdivide the genus into smaller genera, based on valve striation and the presence or absence and

structure of labiate processes. These genera include *Neosynedra* Williams & Round 1986, *Tabularia* (Kűtzing) William & Round 1986, *Catacombas* Williams & Round 1986 and Hyalosynedra Williams & Round 1986 . A number of species originally assigned to *Synedra* Ehrenberg were also reassigned to other genera, notably to *Fragalaria* Lyngbye (Williams & Round 1986, 1988a,1988b). In addition, the genus, *Synedropsois* Hasle, Medlin & Syvertsen 1994 has been described as distinct from these subdivisions of *Synedra* Ehrenberg. *Synedra* is only identified to generic level in this study.

Ecology: The genus *Synedra* Ehrenberg has been identified extensively from ice assemblages (Garrison *et al.,* 1987). The generitype of the new genera *Synedropsis, Synedropsis hyperborea* (Grunow) Hasle, Medlin & Syvertsen, is an Arctic species and characteristic of sea ice. *Neosynedra* Williams & Round 1986 and and *Hyalosynedra* Williams & Round 1986 are identified as widespread marine epiphytic genera, *Tabularia* (Kűtzing) William & Round 1986 a widespread marine, brackish and occasionally freshwater epiphytic and epilithic genera and *Catacombas* Williams & Round 1986 a cosmopolitan epiphyte on seaweeds.

Order Thalassionematales
Family Thalassionemataceae
Genera *Thalassionema, Thalassiothrix*

2.1.18 *Thalassionema* Grunow ex Mereschkowsky 1902

Type: *Thalassionema nitzscoides* (Grunow) *Mereschkowsky*
Basionym: *Synedra nitzschoides* Grunow
Synonym: *Thalassiothrix nitzschoides* (Grunow) Grunow in Van Heurk

Generic Characteristics: Valve view: cell shape varying from smoothly dilated in centre (acicular, spindle shaped) to linear or distinctly dilate in the centre and at the apices; or one apex rounded and the other slightly tapering. Wide sternum. One marginal row of circular areolae. External opening of areolae larger than internal openings (foramina) and crossed

by simple silicified bar (strut) or a pattern of crossing bars. Girdle view: cells rectangular, isopolar or heteropolar (Hasle & Syvertsen, 1997). Thalassionema form stellate, zig-zag or fan-shaped colonies joined by mucilage pads (Round *et al.*, 1990).
Characteristics distinguishing species: This genera was long thought to be monospecific (*T. nitzscoides).* VanLandingham recognised two further species (VanLandingham, 1978) A detailed study of the genus supported this view of their being three distinct species, *T. nitzscoides, T.bacillaris* and *T.frauenfeldii* (Hallegraeff, 1986).

Thalassionema nitzschoides (Grunow) Grunow 1881

Basionym: *Synedra nitzschioides* Grunow 1962
Synonyms: *Thalassiothrix nitzschioides* Grunow in Van Heurck 1880-1885
Thalassiothrix curvata Castracane 1886

Description: Valve view: the two sides of the valve are usually nearly parallel but can be slightly inflated in the middle. Isopolar, usually with blunt round ends, but capitate ends also occur. Marginal areolae (10-12 in 10μ) have small internal openings. Externally they open into depressions in the valve face and mantle which are partially occluded by triradiate struts which may have side-branches. Running down the central axis of the valve is a broad axial area (pseudoraphe) with no perforations. Valve pores open externally into a large circular hole in the valve face and internally into a slit-like labiate process (Hallegraeff, 1986). Plate IV 1-4

Discussion: While *Thalassionema nitzschioides* is commonly isopolar, heteropolar forms, with an arrow-head shaped spine at one end, have been reported. Hallegraef (1986) argued that these spined forms occur in the same colonies as isopolar forms and that their fine structure and other morphological features are consistent with *T. nitzschioides*. He therefore considered them to be variants not the distinct species, *Thalassiothrix pseudonitzschioides*, as previously suggested (Schutte & Schrader, 1982). Hallegraeff noted that where the heteropolar form occurs, the corresponding spineless valve pole was associated with the mucus pad, with the spineless ends occurring centrally in stellate colonies. He also recorded forms with spines at both ends of a valve which he noted allow

stellate colonies to change to zig-zag forms (Hallegraeff, 1986). However other authors have accepted the heteropolar distinction of the species *T. pseudonitzschioides* (Hasle & Syvertsen, 1997). Moreno-Ruiz & Licea (1994) further recognised ten subspecies of *T. nitzschioides* based on whether they were heteropolar or isopolar, the fine structure of the areolae and the valve outline.

Ecology: *Thalassionema nitzschioides* is a cosmopolitan neritic species (Hallegraeff, 1986).

Thalssionema nitzschioides* var. *parva (Heiden)

Basionym: *Thalassionema nitzcshioides* var. *parva* Heiden *in* Heiden & Kolbe (*vide* Simonsen 1992)

Description: Valve view: valves are small and linear. Length 5-9.5µm, width 2.3-4.0µm, 9-12 central and terminal areolae in 10µm. Apices are rounded, isopolar, with two slit like rimoportulae at each pole, parallel or slightly oblique to the mid-line of the valve (Moreno-Ruiz & Licea, 1994).

Discussion: Different authors have given assigned different lengths to this form. Hasle (1960) and Baron (1985) note forms up to 12 µm and Fenner (1978) lengths of 21µm to 28µm. Moreno-Ruiz & Licea (1994) propose a maximum length of 10µm for this form. They further note that while *T.nitzschioides* var. *incurvata* can be of similar dimensions, it is distinguished by a concave outline (Moreno-Ruiz & Licea, 1994).

2.1.19 *Thalassiothrix* Cleve & Grunow 1880

Type: *Thalassiothrix longissima* Cleve & Grunow
Synonym: *Synedra thalassiothrix* Cleve

Generic Characteristics: Cells are solitary or in radiating colonies. Cells straight, slightly curved or sigmoid, usually strongly twisted, isopolar or heteropolar. Valves more or less inflated in the middle and at the apices. The sternum is wide and sometimes narrower near the apices. External openings of the one row of marginal areolae are elongate and larger than internal openings (foramina); covered by reticulate vela divided more or less distinctly into two compartments by a longitudinal bar running parallel to valve margins. Marginal spines located in the middle of the vela on the longitudinal bars or on the border between the vela and the imperforate margin of the valve mantle (Hasle & Syvertsen, 1997).

Thalassiothrix longissima Cleve & Grunow 1880 (conservation proposed by Silva & Halse 1993)

Description: Valves are narrow, linear and usually slightly heteropolar with a smooth rounded foot pole and a head pole with two ledge-like spines. The frustules are very long, up to 1-4mm in length and 1.5-5μm in width. Plate IV 5-6

Discussion: Hallegraeff (1986) recognised four subspecies of *Thalassiothrix longissima; Thalassiothrix longissima* Cleve & Grunow 1880 var. *longissima* Grunow ex Van Heurck 1880-5, *Thalassiothrix longissima* var. *lanceolata* (Hustedt) comb.nov, *Thalassiothrix longissima* var. *gibberula* (Hasle) comb.nov and *Thalassiothrix longissima* var. *antarctica* Grunow ex Van Heurck 1880-5. Later work by Halse and Semina (1987) on the original type material concluded that *Thalassiothrix longissima* and *Thalassiothrix antarctica* are sufficiently different to be considered separate species as originally suggested by Hustedt (1958). They argued that while both species were similar with respect to areolae structure, apical protrusions and marginal spines; only *T. antarctica* exhibited colony formation and produced both curved and straight cells. The apical spines also vary between the two species, *T.antarctica* having large winged spines at one pole and *T.longissima* serrated protrusions at both poles (Hasle & Semina 1987).

Ecology: Cold water to temperate region (Hasle & Syvertsen, 1997).

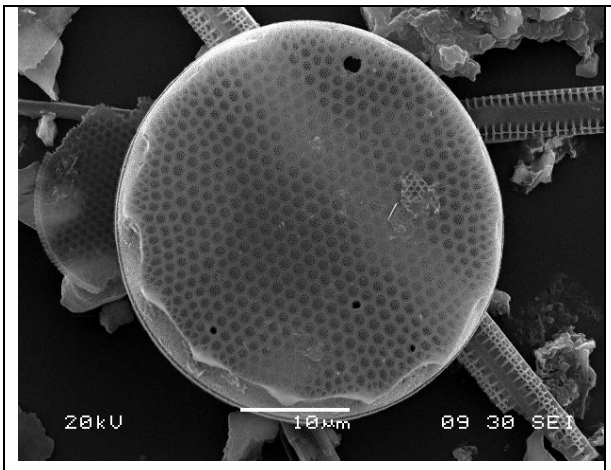	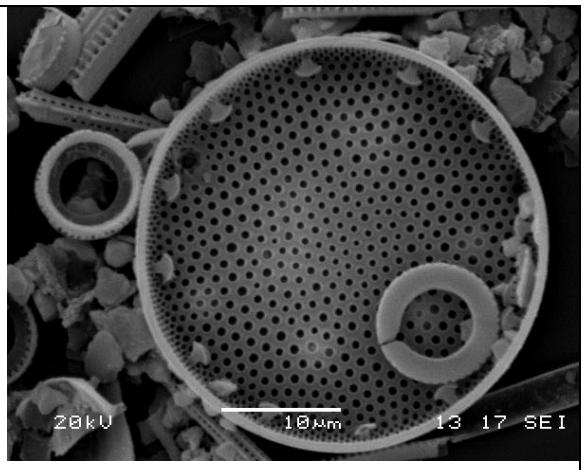
1. *Roperia tesselata* (external)	2.*Roperia tesselata* (internal)
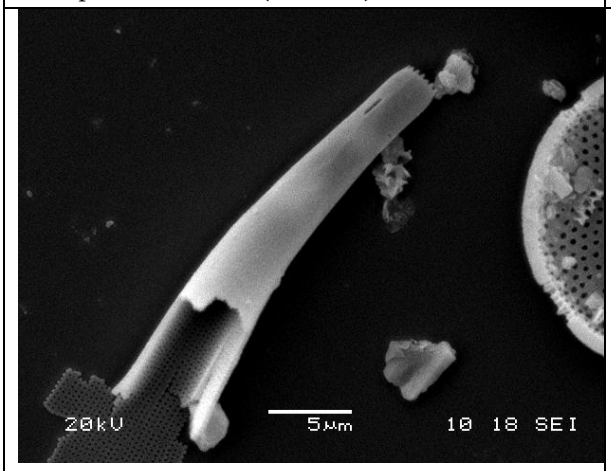	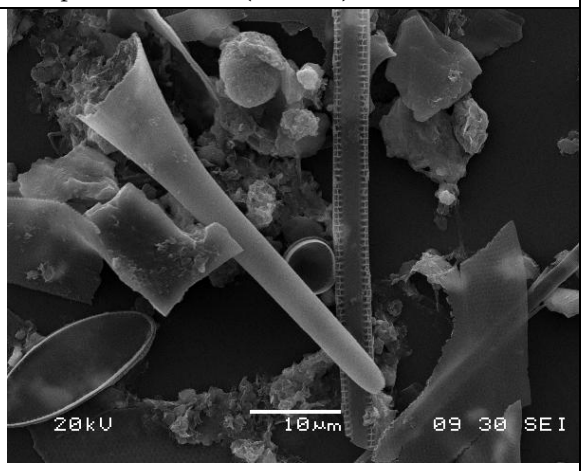
3.*Proboscia alata*	4.*Proboscia alata*
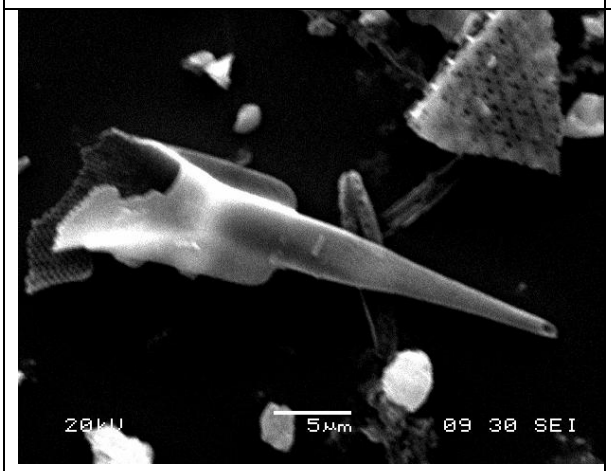	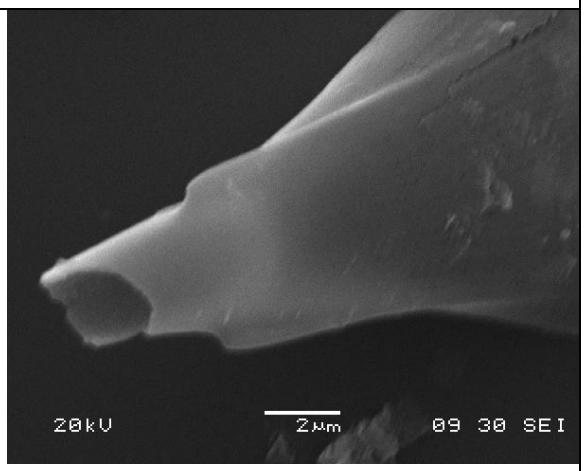
5.*Rhizosolenia styliformis*	6.*Rhizosolenia borealis*

Plate I

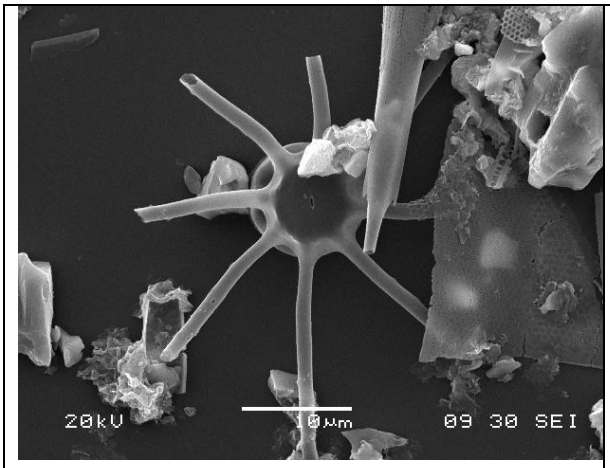	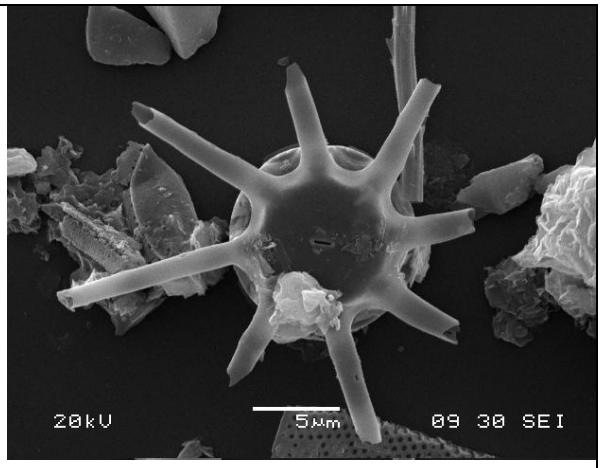
1.*Bacteriastrum hyalinum*	2.*Bacteriastrum hyalinum*
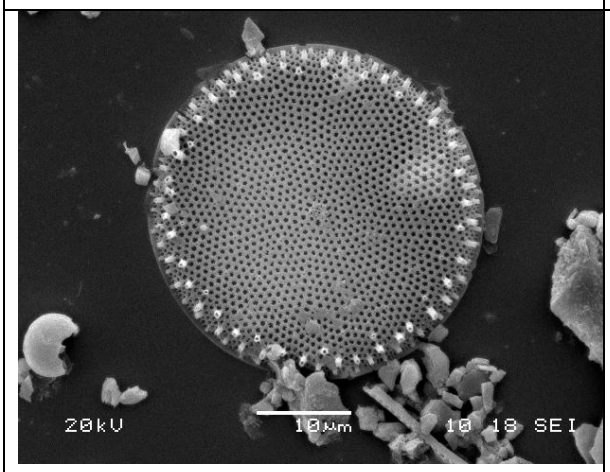	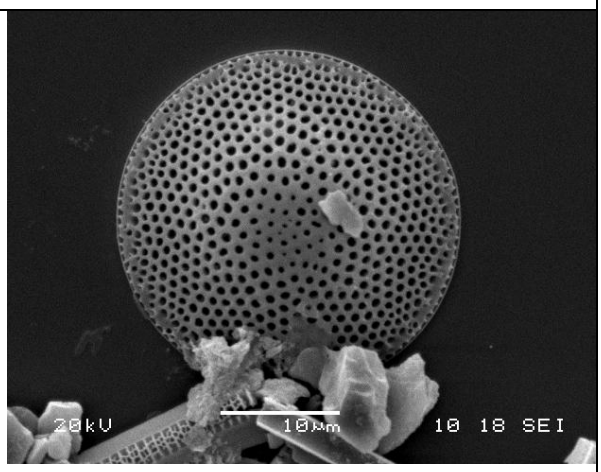
3.*Thalassiosira gravida* vegetative	4.*Thalassiosira gravida* spore
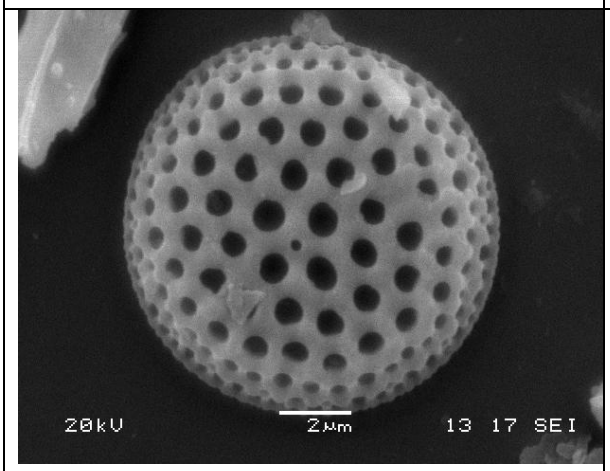	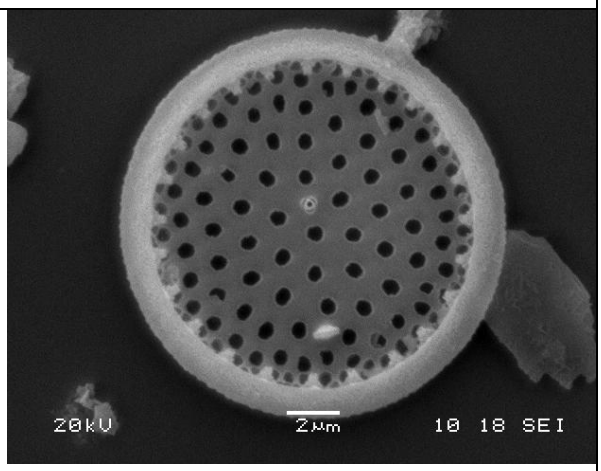
5.*Thalassiosira oestrupii* (external)	6.*Thalassiosira oestrupii* (internal)

Plate II

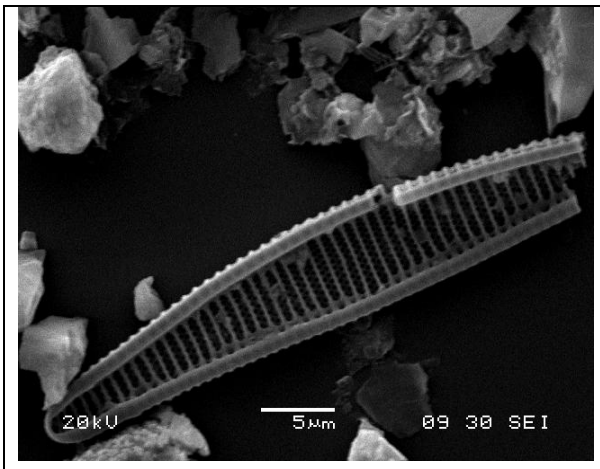	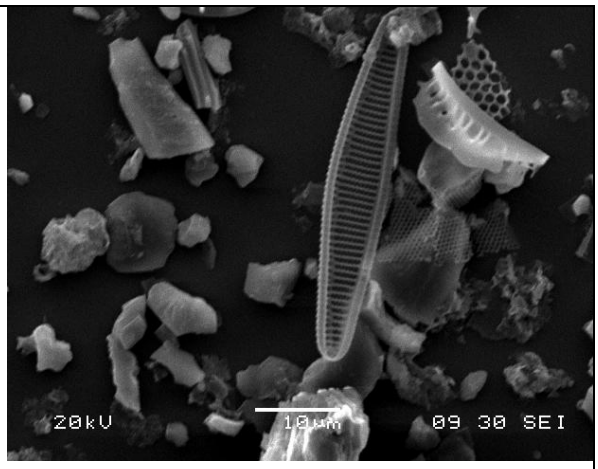
1.*Fragilariopsis doliolus*	2.*Fragilariopsis dolious*
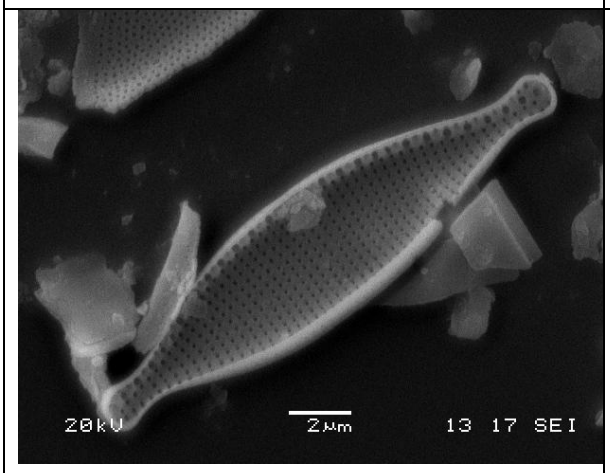	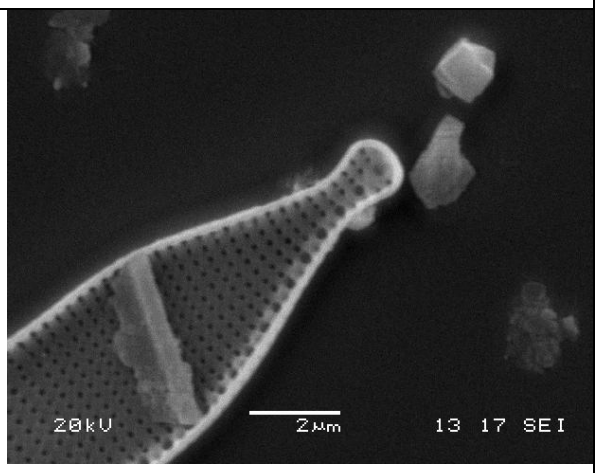
3.*Nitzschia bicapitata*	4. *Nitzschia bicapitata*
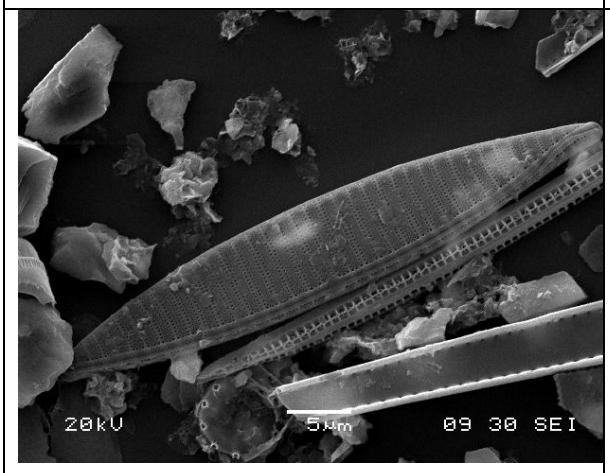	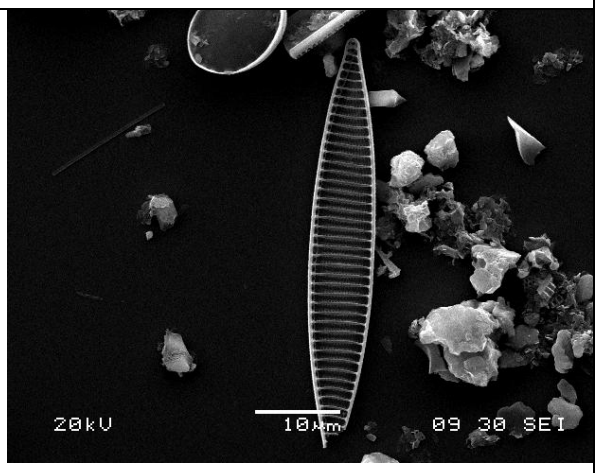
5.*Fragilariopsis oceanica*	6.*Fragilariopsis oceanica*

Plate III

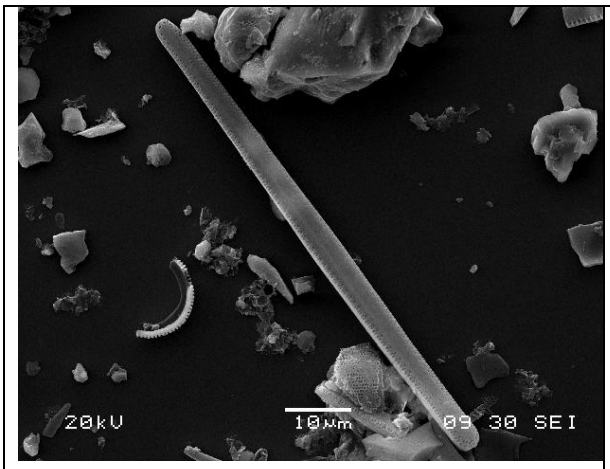	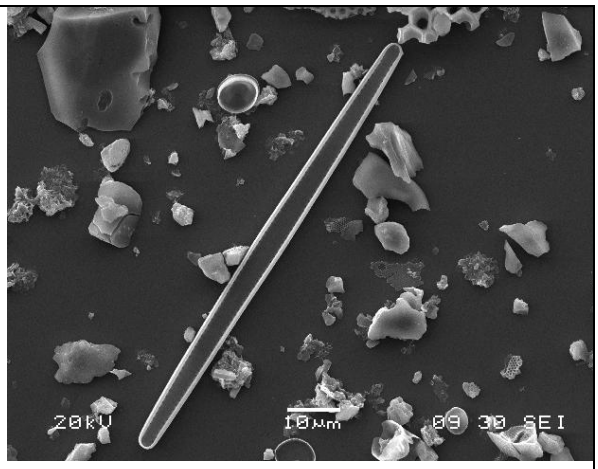
1.*Thalassionema nitzschoides*	2. *Thalassionema nitzschoides*
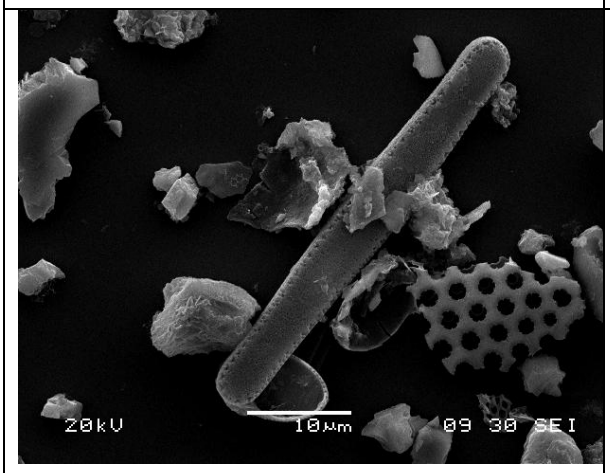	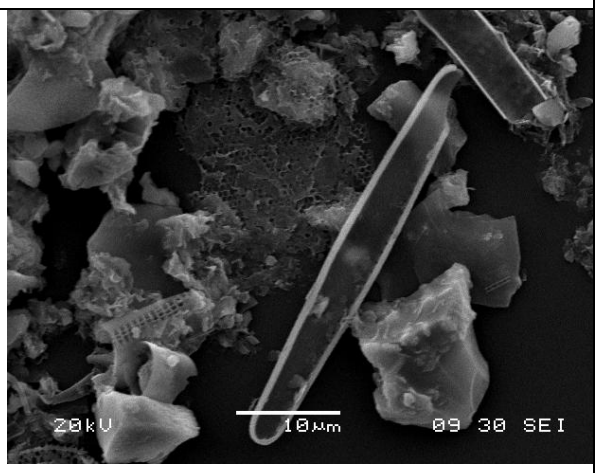
3. *Thalassionema nitzschoides* parva	4. *Thalassionema nitzschoides* parva
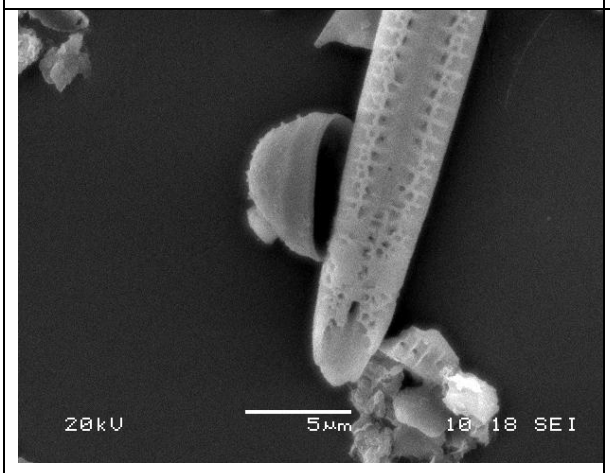	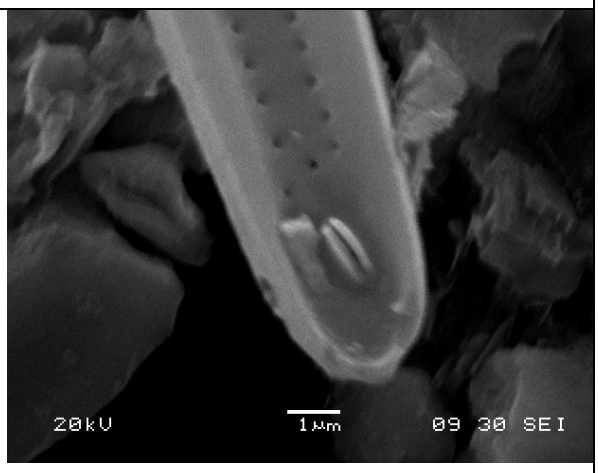
5.*Thalassiothrix longissima*	6. *Thalassiothrix longissima*

Plate IV